A Celestial Story of Supersymmetry: Inflation and Reheating in the Early Universe

Dissertation
zur
Erlangung des Doktorgrades (Dr. rer. nat.)
der
Mathematisch-Naturwissenschaftlichen Fakultät
der
Rheinischen Friedrich-Wilhelms-Universität Bonn

von
Wenbin Zhao
aus
Shanxi, China

Bonn, June 2025

Angefertigt mit Genehmigung der Mathematisch-Naturwissenschaftlichen Fakultät der Rheinischen Friedrich-Wilhelms-Universität Bonn

Gutachter/Betreuer:	Prof. Dr. Manuel Drees
Gutachter:	Priv.-Doz. Dr. Stefan Förste
Tag der Promotion:	September 3, 2025
Erscheinungsjahr:	2025

Acknowledgements

I would like to express my sincere appreciation to my supervisor, Prof. Dr. Manuel Drees, for his kind and professional guidance and support over the past five years. His sharp insights on physics are crucial in the completion of this dissertation. Since I joined his research group in August 2020, I have been continuing to learn from him on how to become a proper physicist. We had lunch and coffee almost every workday with extensive discussions not only on physics. He showed me how to ask critical questions, conduct rigorous research, and strike a balance between work and life. I sincerely hope to be as capable as he is in the future.

I'm extremely grateful to my committee members including Priv.-Doz. Dr. Stefan Förste, Prof. Dr. Klaus Desch, and Prof. Dr. Thomas Bredow, for their time and effort in reading my thesis and going through the whole process. Special thanks to Prof. Dr. Klaus Desch for chairing my committee.

I would like to extend my sincere thanks to my collaborators. It's a great pleasure to work with Prof. Dr. Gui-Jun Ding, Si-Yi Jiang, Dr. Yong Xu, and Chenhuan Wang. This dissertation could not have been completed without their help. I would also like to thank Prof. Dr. Hans Peter Nilles for writing a reference letter on my behalf this season. It is also he who drew my research interests to modular symmetry.

I thank my group members for our shared time in BCTP. It is always very delightful to talk with Prof. Dr. Xerxes Ramyar Tata, Hashika Arjun, Dr. Gerrit Bickendorf, Ojas Bhardwaj, Keshav Chaudhary, Bardia Najjari Farizhendi, Lina, Yong Koay Sheng, Rahul Mehra, Abhilash Hoskere Nagaraj, Bastian Ottensmann, Dr. Meng Shi, Dr. Cong Zhang, and Dr. Zhongyi Zhang. Special thanks to the secretaries of the theory group: Christa Boersch, Nadine Hassani, Lora Schindler, Patricia Zündorf, as well as Dr. Andreas Wißkirchen. Their assistance with daily paperwork cannot be overstated.

I leave my last thanks to my parents and sister. They gave me the total freedom to dive into physics and unwaveringly supported me throughout this journey. Without their belief in me, this work would not have been possible.

Abstract

The Standard Model of particle physics and Big Bang cosmology have been successfully used to describe the evolution and current state of the Universe. However, they are known to be incomplete as they leave several unanswered questions, including inflation, dark matter, dark energy, the baryon asymmetry of the universe, and neutrino masses. This thesis presents several models that aim to answer these questions within the framework of supersymmetry and supergravity. We begin by constructing scalar potentials that support slow roll inflation using a single chiral superfield and discuss how to satisfy cosmic microwave background constraints. We then consider how to incorporate supersymmetry breaking effects into account, which leads to a bound on the supersymmetry breaking scale and the inflation scale. After finishing this simple model, we turn to consider how to apply modular symmetry in inflation. Modular symmetry is a strong constraint as well as a useful handle in understanding the dynamics of inflation. In particular, we consider how to construct scalar potentials that resolve the flavor puzzles and simultaneously give rise to inflation. This combination naturally provides the necessary channels for reheating and predicts that the inflaton primarily decays to heavy right-handed neutrinos. By explicit calculation, we show that if the inflaton mass is high enough, this process can be used to produce the baryon asymmetry of the universe. In the end, we discuss a mechanism that produces dark matter at the end of inflation, known as gravitational particle production. We compare the relic abundance of dark matter in supergravity models and non-supersymmetric models, identifying the parameter space that generates sufficient dark matter.

List of publications

[1] M. Drees and **W. Zhao**, *Inflection Point Inflation in Supergravity*, (2025), arXiv: 2504.07769 [hep-ph].

[2] C. Wang and **W. Zhao**, *Gravitational dark matter production in supergravity α-attractor inflation*, JCAP **07** (2025) 040, DOI: 10.1088/1475-7516/2025/07/040, arXiv: 2411.15030 [hep-ph].

[3] G.-J. Ding, S.-Y. Jiang, Y. Xu and **W. Zhao**, *Modular invariant inflation, reheating and leptogenesis*, (2024), arXiv: 2411.18603 [hep-ph].

[4] G.-J. Ding, S.-Y. Jiang and **W. Zhao**, *Modular invariant slow roll inflation*, JCAP **10** (2024) 016, DOI: 10.1088/1475-7516/2024/10/016, arXiv: 2405.06497 [hep-ph].

[5] M. Drees and **W. Zhao**, *U(1)$L_\mu - L_\tau$ for light dark matter, $g_\mu - 2$, the 511 keV excess and the Hubble tension*, Phys. Lett. B **827** (2022) 136948, DOI: 10.1016/j.physletb.2022.136948, arXiv: 2107.14528 [hep-ph].

This thesis is based on [1–4], discussing inflation and reheating in the supergravity framework. A simple model of inflation and its possible connection with supersymmetry breaking is presented in [1]. Another model of inflation based on modular symmetry is presented in [4]. Reheating channels and leptogenesis based on modular symmetry approach to flavor puzzles are discussed in [3]. Production of super-heavy dark matters in supergravity is calculated in [2].

Contents

CHAPTER 1

Introduction

The rapid development of physics and astrophysics in the late 20th century has significantly changed our view of and deepened our understanding of the nature of our universe. At the microscopical scale, the fundamental particles, those not composed of other particles, were discovered in various laboratory and collider experiments. During this period, the intensive collaboration between theoretical and experimental physicists drove the development of the Standard Model (SM), which describes three of four fundamental interactions, i.e. electromagnetic, weak and strong interactions, and classifies the fundamental particles. The 17 confirmed fundamental particles are shown in Fig. 1.1. They are classified into fermions and bosons by their spin. Fermions that can interact via the strong interaction are called quarks, while the others are referred to as leptons. The last fermion, tau neutrino, was detected by the DONUT collaboration in 2000 [1]. While the last boson, the Higgs boson, was discovered by the Large Hadron Collider (LHC) in 2012 [2, 3]. In Fig. 1.2 we show the chronology of the SM from the experimental side.

On cosmological scales, astrophysical observations provide a distinct channel for advancing our understanding of physics beyond the standard model (BSM). The accidental discovery of the cosmic microwave background (CMB) in 1965 [19] and subsequent precise observations of it suggested that our universe had experienced a period of exponential expansion, known as inflation. The origin of the inflation is not identified yet. After this expansion, the universe was filled with hot, compact plasma, composed of the SM particles, such as photons and electrons, as well as other possible particles. One example is dark matter, which has a very weak interaction with SM particles, but still influences the evolution of the universe through gravitational interactions. The first evidence of dark matter was observed in the flat rotation curves of galaxies in 1970 [20]. Another important constituent is dark energy, which is responsible for the current accelerating expansion of the universe. The first observational evidence of it came from measurements of high-redshift Type Ia supernovae in 1998 [21]. Physicists are currently working on determining the nature of dark matter and dark energy.

There are two more hits for new physics worth mentioning. In the early universe, baryonic matter and antimatter should have been created equally. However, the rich structures of our universe, i.e., galaxies, stars, and the Earth, are made almost entirely of baryonic matter. All known processes in the SM, can not account for such a difference. This is called the matter-antimatter asymmetry problem. Another hit comes from the neutrinos produced in the atmosphere. In 1998, the Super-Kamiokande experiment found a zenith angle dependent deficit of muon neutrinos, which could be interpreted as oscillations between muon neutrinos and tau neutrinos [22]. Oscillation between different flavors of

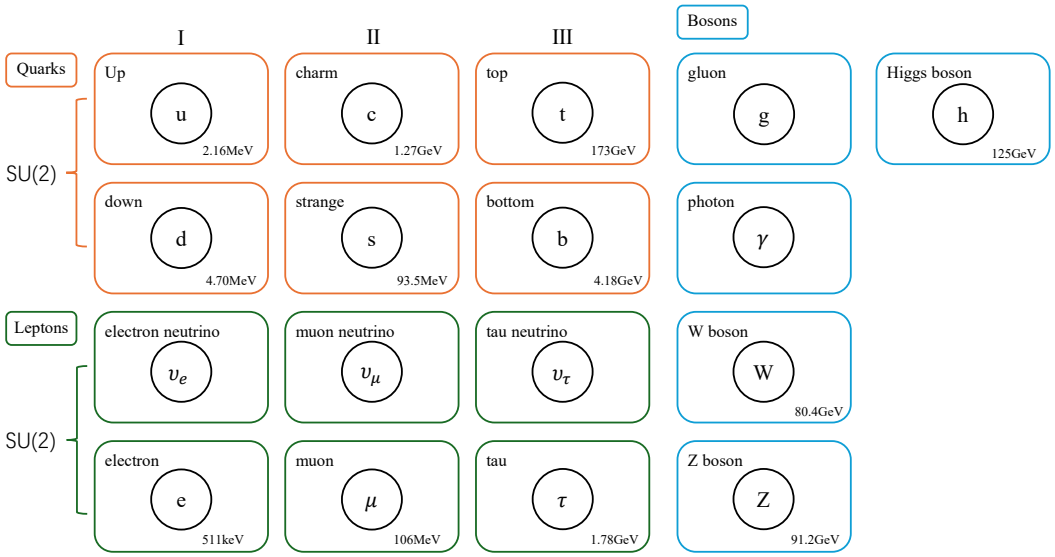

Figure 1.1: Standard model of elementary particles: the 12 fundamental fermions and 5 fundamental bosons. Particle masses are listed in the bottom right corner.

neutrinos was confirmed later in reactor neutrino measurements [23]. These neutrino oscillations are one of the evidence indicating neutrino masses, while in the SM neutrinos are precisely massless.

These incontrovertible evidences for new physics:

- dark matter;
- dark energy;
- cosmic inflation;
- the baryon asymmetry of the universe (BAU);
- neutrino masses and mixing;

are the primary motivations to extend the SM. Among the possible theoretical extensions, supersymmetry and supergravity are among the most studied ones. Even though they originated from the intrinsic structure of SM, they have motivated many models that successfully solve above cosmological problems. In this thesis, we will follow the same spirit and focus on their cosmological phenomenology, the "celestial story", instead of their well-discussed collider searches.

With the exception of dark energy, this thesis covers four out of the five aspects of new physics. We will use inflation as the core, and try to connect different topics with it. We will show that dark matter

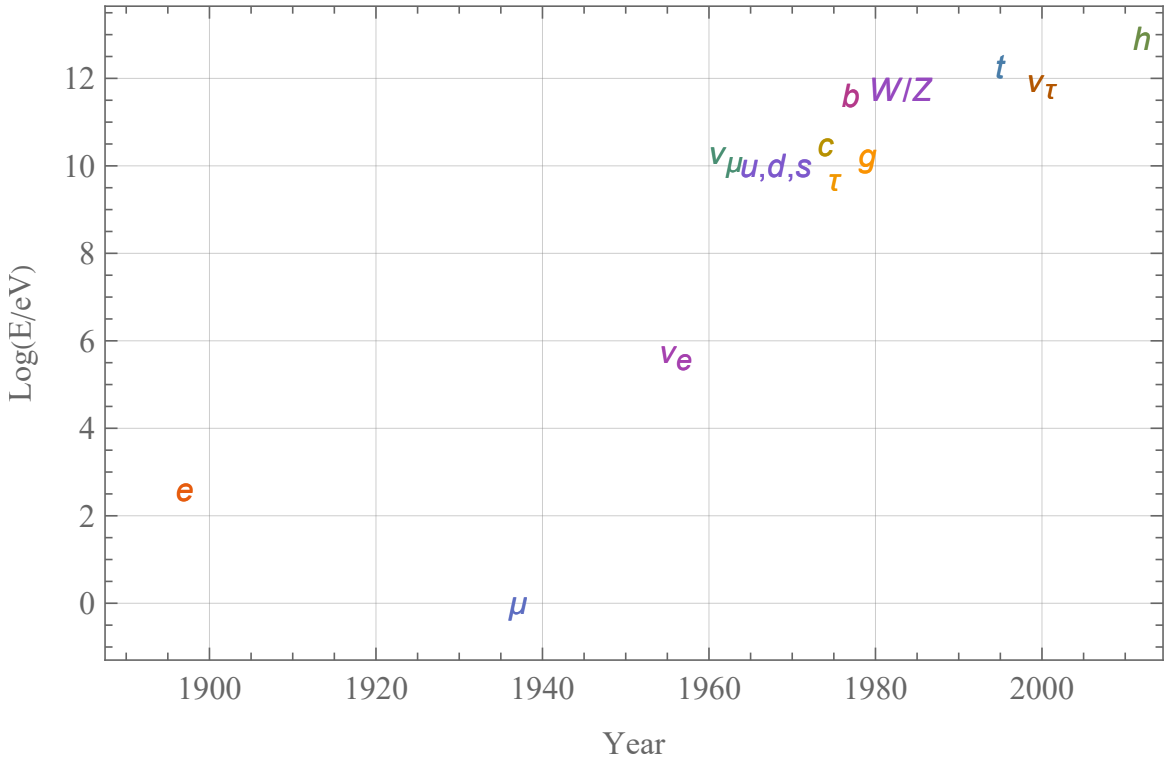

Figure 1.2: Timeline of the discoveries of SM particles. The x-axis is the time when each particle is discovered. The y-axis is the energy scale of the corresponding experiments. The electron was found in 1897 through the observation of Cathode rays by J. J. Thomson. The voltage of such a Cathode-ray tube should be around 400 eV. The muon μ was found much later in 1936 by measuring its trajectories in the cloud chambers [4, 5]. The magnetic field applied across the cloud chamber was around 10^3 Gauss, which could be roughly converted into 1 eV^2 in the natural units. Electron neutrino was confirmed at the Cowan–Reines neutrino experiment in 1956 [6], where they used 511keV photon as the signal of antineutrino-proton interactions. The rest of the SM particles are all discovered at particle accelerators and colliders, operated at different energy scales[1–3, 7–18].

and the baryon asymmetry, can be generated during a phase called reheating, when inflaton energy is supposed to transfer to radiation plasma. In some concrete models respecting additional symmetry, this process is related to neutrino masses and mixing.

This thesis is organized as follows: In chapter 2, we provide a brief introduction to the background related to this thesis, including the SM, the evolution of the early universe, canonical solutions to new physics, supersymmetry, supergravity, and modular symmetry. In chapter 3 and chapter 4 we will build two inflation potentials and compare their predictions with CMB observables. In chapter 5, we discuss reheating as well as how to generate BAU in a modular invariant theory. In chapter 6 we turn our attention to dark matter, and analyze how dark matter can be generated through gravitational interactions after inflation. In chapter 7, we summarize the findings in this thesis.

CHAPTER 2

Background Knowledge

2.1 The Standard Model

In this section we recall the basic concepts of the Standard Model (SM). Fundamental particles are described by quantum field theory, where each particle is an irreducible unitary representation of the Poincaré group. These representations are classified by a number called spin, which may take an integer or a half-integer value. In the SM, 12 particles have half-integer spin and are called fermions, while the other 5 particles have integer spin and are called bosons. In addition to the space-time symmetry group, SM particles are also representations of internal symmetry groups. For example, quarks (gluons) form fundamental (adjoint) representations of an $SU(3)$ group, which corresponds to the strong interaction. Similarly, the electro-weak interaction is associated with an $SU(2)$ group and $U(1)_Y$ group. The 12 fermions can be grouped into three generations, each with identical charges under $SU(3) \times SU(2) \times U(1)_Y$ but different masses.

The special transformation properties of SM particles under the gauge groups $SU(3) \times SU(2) \times U(1)_Y$ regulate possible forms of the SM Lagrangian, which should be invariant under the gauge transformations. As an example, the $SU(3)$ invariance requires the relevant Lagrangian to take the following form[1]:

$$\begin{aligned} \mathcal{L} &= \sum_{i=1}^{6} \bar{\psi}_i (i\gamma^\mu D_\mu - m_i)\psi_i + \sum_{a=1}^{8} F_{a,\mu\nu} F^{a,\mu\nu} \,, \\ D_\mu \psi_i &= \partial_\mu \psi_i + igG_{a,\mu} T^a \psi_i \,, \\ F_{a,\mu\nu} &= \partial_\mu G_{a,\nu} - \partial_\nu G_{a,\mu} + igf_{abc} G^b_\mu G^c_\nu \,, \end{aligned} \tag{2.1}$$

where the Greek alphabet μ, ν is used for spacetime components, which runs from 0 to 3. γ^μ is the Gamma matrices. ψ_i is the quark field, $\bar{\psi}_i = \psi^\dagger \gamma_0$ is the product of complex conjugate of ψ_i and γ_0 , $G_{a,\mu}$ is the gluon field and $F_{a,\mu\nu}$ is the corresponding energy-momentum tensor. i labels the quark species, which runs from 1 to 6 in the SM. Each quark field Ψ_i should be understood as a SU(3) triplet with 3 color indices omitted. The color indices of the gluon field a run from 1 to 8, and f_{abc} is the structure constant of the $SU(3)$ group. The difference in color indices comes from the fact that the

[1] We always use the Einstein summation convention, where repeated indices are summed.

quark field forms the fundamental representation while the gluon field forms the adjoint representation of $SU(3)$.

The $SU(3)$ symmetry is not chiral in SM, i.e., it does not distinguish left-handed and right-handed quarks. The $SU(2)$ symmetry, instead, treats them differently. The left-handed fields:

$$\begin{aligned} Q^1 = \begin{pmatrix} u_L \\ d_L \end{pmatrix}, \quad Q^2 = \begin{pmatrix} c_L \\ s_L \end{pmatrix}, \quad Q^3 = \begin{pmatrix} t_L \\ b_L \end{pmatrix}, \\ L^1 = \begin{pmatrix} \nu_{e,L} \\ e_L \end{pmatrix}, \quad L^2 = \begin{pmatrix} \nu_{\mu,L} \\ \mu_L \end{pmatrix}, \quad L^3 = \begin{pmatrix} \nu_{\tau,L} \\ \tau_L \end{pmatrix}, \end{aligned} \tag{2.2}$$

transform as the $SU(2)$ doublets while the right-handed fields:

$$u_R,\ d_R,\ c_R,\ s_R,\ t_R,\ b_R,\ e_R,\ \mu_R,\ \tau_R \tag{2.3}$$

are $SU(2)$ singlets. This difference leads to P violation in the weak sector, which was shown by the Wu experiment [24]. As a consequence, the mass term in eq.(2.1) is not gauge invariant under $SU(2)$ since it involves one left-handed field and one right-handed field. In the SM, the generation of gauge invariant mass terms requires an additional Higgs field, which transforms as an $SU(2)$ doublet :

$$H = \frac{1}{\sqrt{2}} \begin{pmatrix} \phi^+ \\ \phi_0 + i a_0 \end{pmatrix} \tag{2.4}$$

where ϕ_0 and a_0 are the CP-even and CP-odd neutral components, and ϕ^+ is the complex charged component of the Higgs doublet. Under the $SU(2)_L \times U(1)_Y$ group, the most general renormalisable scalar potential of H reads:

$$V(H) = m^2 H^\dagger H + \lambda (H^\dagger H)^2 \tag{2.5}$$

where $H^\dagger$ denotes the complex conjugate of H field. If the first parameters is negative $m^2 < 0$, then this potential is minimized at $\phi_0 = v = \sqrt{\frac{-m^2}{\lambda}}$, which is known as the vacuum expectation value of ϕ_0. This transition from $\langle \phi_0 \rangle = 0$ to $\langle \phi_0 \rangle = v$ is called spontaneous symmetry breaking. In this case, the Lagrangian is invariant under the symmetry, but the ground state of the theory is not. After spontaneous symmetry breaking, SM gauge symmetry breaks from $SU(3) \times SU(2) \times U(1)_Y$ to $SU(3) \times U(1)_{\text{em}}$, where $U(1)_{\text{em}}$ corresponds to the electromagnetic force. The vacuum expectation value induces fermion mass terms through the following Yukawa Lagrangian:

$$\mathcal{L} = -Y^e_{ij} \bar{L}^i H e^j_R - Y^d_{ij} \bar{Q}^i H d^j_R - Y^u_{ij} \bar{Q}^i \tilde{H} u^j_R + h.c. \tag{2.6}$$

where $\tilde{H} = i\sigma_2 H^*$ is defined via the second Pauli matrices σ_2. i, j are generation indices that run from 1 to 3. We collectively write $e^i_R = (e_R, \mu_R, \tau_R)$ and so on. Note that there are no right-handed neutrinos, and neutrinos are exactly massless in the SM. We will discuss a possible extension in section 2.3.3.

Before the spontaneous symmetry breaking, the boson part of the SM Lagrangian under $SU(2) \times$

$U(1)_Y$ read:

$$\begin{aligned}\mathcal{L} &= -\frac{1}{4}\left(W^a_{\mu\nu}\right)^2 - \frac{1}{4}B^2_{\mu\nu} + \left(D_\mu H\right)^\dagger \left(D_\mu H\right) + m^2 H^\dagger H - \lambda\left(H^\dagger H\right)^2, \\ D_\mu H &= \partial_\mu H - igW^a_\mu \tau^a H - \frac{1}{2}ig' B_\mu H\end{aligned} \tag{2.7}$$

where W^a_μ and B_μ are $SU(2)$ and $U(1)_Y$ gauge bosons and $W^a_{\mu\nu}$ and $B_{\mu\nu}$ are their field strength tensor. $\tau^a = \frac{1}{2}\sigma^a$ is the canonically normalized $SU(2)$ generators defined via the Pauli matrices σ^a. g and g' are the respective gauge couplings. For fermions and their interactions, we have:

$$\begin{aligned}\mathcal{L} = {} & i\bar{L}^i\left(\partial - igW^a\tau^a - ig'Y_L B\right)L^i + i\bar{Q}^i\left(\partial - igW^a\tau^a - ig'Y_Q B\right)Q^i \\ & + i\bar{e}^i_R\left(\partial - ig'Y_e B\right)e^i_R + i\bar{u}^i_R\left(\partial - ig'Y_u B\right)u^i_R + i\bar{d}^i_R\left(\partial - ig'Y_d B\right)d^i_R.\end{aligned} \tag{2.8}$$

where the Hypercharges Y_i read $Y_L = -\frac{1}{2}, Y_Q = \frac{1}{6}, Y_e = -1, Y_u = \frac{2}{3}, Y_d = -\frac{1}{3}$, respectively. This is chosen such that after symmetry breaking $SU(2)\times U(1)_Y \to U(1)_{\text{em}}$, the electric charge $Q = T^3 + Y$ is correctly reproduced. Here T^3 is the isospin charge for SM particles, which read $T^3 = \pm\frac{1}{2}$ for $SU(2)$ doublet and $T^3 = 0$ for $SU(2)$ singlets. The gauge bosons W^a_μ and B_μ become $W^\pm, Z$ bosons and photon A_μ. They are related by:

$$Z_\mu = \cos\theta_W W^3_\mu - \sin\theta_W B_\mu\,, \quad A_\mu = \sin\theta_W W^3_\mu + \cos\theta_W B_\mu\,, \quad W^\pm_\mu = \frac{1}{\sqrt{2}}W^1_\mu \mp iW^2_\mu\,. \tag{2.9}$$

where $\tan\theta_W = \frac{g'}{g}$. Their masses read:

$$M_W = \frac{gv}{2}\,, \quad M_Z = \sqrt{g^2 + g'^2}\frac{v}{2}\,, \quad M_A = 0\,. \tag{2.10}$$

The Lagrangian for fermionic particles with these bosons after symmetry breaking is:

$$\begin{aligned}\mathcal{L} = {} & \sum_i \bar{\psi}_i\left[\gamma^\mu\left(i\partial_\mu - eQ_iA_\mu - \frac{g}{2\cos\theta_W}(g^i_V - g^i_A\gamma^5)Z_\mu\right) - m_i\right]\psi_i \\ & - \frac{g}{2\sqrt{2}}\sum_i \Psi_i\gamma^\mu(1-\gamma_5)(T^+W^+_\mu + T^-W^-_\mu)\Psi_i\end{aligned} \tag{2.11}$$

where ψ_i is an arbitrary SM fermion, $e = g\sin\theta_W$ is the unit electric charge, Q_i is the electric charge of the fermion, $g^i_V = T^3_i - 2Q_i\sin{\theta_W}^2, g^i_A = T^i_3$ are the vector and axial-vector couplings. Ψ_i is an arbitrary $SU(2)$ doublet and $T^\pm = \tau_1 \pm i\tau_2$ are the weak isospin raising and lowering operators. The first line contains the electromagnetic interaction and neutral-current weak interaction, while the second line describes the charged-current weak interaction.

Before closing this section, we show the timeline of the milestones of the SM theory in Fig. 2.1. It took more than 50 years for physicists to formulate and understand the SM theory. We would expect there is another long and arduous journey to find its successor.

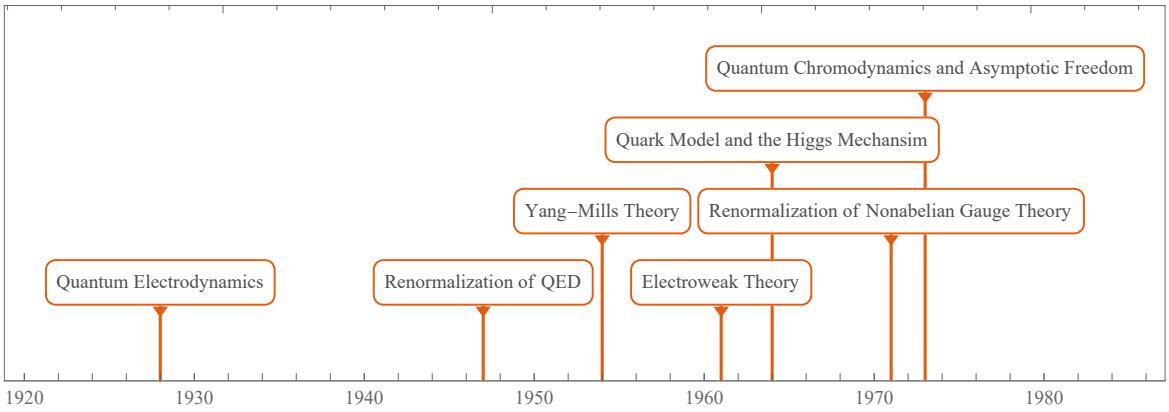

Figure 2.1: Timeline of the milestones of the SM theory. Dirac was the first person who used the term "quantum electrodynamics" (QED) to discuss the emission and absorption of radiation in quantum theory [25]. It was later realized that precise predictions of QED would require a procedure named renormalization [26–30]. In 1954, Yang-Mills theory was proposed and eventually became the basis of the understanding of strong and weak interactions [31]. Based on it, weak and electromagnetic interactions were combined into electroweak theory in 1961 [32]. The Higgs mechanism, which generates masses for most of the fundamental particles, was proposed in 1964 [33–35] and incorporated into electroweak theory in 1967 [36, 37]. The modern understanding of the strong interaction dates back to 1964, when the quark model was proposed [38, 39]. Renormalization of Yang-Mills theory and asymptotic freedom of quantum chromodynamics (QCD) were found later in the 1970s [40–42].

2.2 The Early Universe

General relativity (GR) is our cornerstone in understanding the evolution of the universe. Upon initial publication, GR manifested itself through the explanation of Mercury's anomalous perihelion shift. Since then, it has been validated through accumulated evidence from observations of gravitational time dilation, redshift, lensing, and most recently, the gravitational waves [43]. In this thesis, we will assume that GR is adequate to describe gravity. The early universe is supposed to be flat, highly isotropic and almost homogeneous, which is described by the FLRW (Friedmann–Lemaître–Robertson–Walker) metric[2]:

$$ds^2 = g_{\mu\nu}dx^\mu dx^\nu = dt^2 - a(t)^2\left(\frac{dr^2}{1-kr^2} + r^2(d\theta^2 + \sin^2\theta d\phi^2)\right). \tag{2.12}$$

where ds is the line element, $g_{\mu\nu}$ is the metric tensor with inverse $g^{\mu\nu}$, x^μ includes the cosmic time $x^0 = t$ and the polar coordinates $(x^1, x^2, x^3) = (r, \theta, \phi)$, $a(t)$ is the time dependent scale factor, k is the curvature of the space which may take $\pm 1, 0$. The FLRW metric is diagonal (We omit the t in scale factor for simplicity):

$$g_{00} = 1\,, \quad g_{11} = \frac{-a^2}{1-kr^2}\,, \quad g_{22} = -a^2r^2\,, \quad g_{33} = -a^2r^2\sin^2\theta\,. \tag{2.13}$$

[2] We use the natural units and set $c = 1$ throughout the thesis unless a unit of time and distance appears explicitly.

From the metric tensor, we can deduce the Ricci curvature $R_{\mu\nu}$ and Ricci scalar $R = g^{\mu\nu}R_{\mu\nu}$:

$$R_{00} = -3\frac{\ddot{a}}{a}\,, \quad R_{ij} = \left(a\ddot{a} + 2\dot{a}^2 + 2k\right)\frac{-g_{ij}}{a^2}\,, \quad R = 6\left(\frac{\ddot{a}}{a} + \frac{\dot{a}^2 + k}{a^2}\right)\,, \tag{2.14}$$

where a dot ($\dot{}$) refers to the derivatives with respect to cosmic time t and i, j refers the spatial indices $1, 2, 3$. Einstein's field equations governs the dynamics of the evolution:

$$R_{\mu\nu} - \frac{1}{2}Rg_{\mu\nu} + \Lambda g_{\mu\nu} = 8\pi G T_{\mu\nu}\,, \tag{2.15}$$

where Λ is the cosmological constant. We assume ingredients in the universe can be described by a perfect fluid. The energy momentum tensor $T_{\mu\nu}$ is characterized by the energy density ρ and the pressure density p:

$$T_{00} = \rho\,, \quad T_{ij} = -g_{ij}p\,, \tag{2.16}$$

The expansion of the universe under FLRW metric with perfect fluid is described by the Friedmann equations:

$$H^2 \equiv \left(\frac{\dot{a}}{a}\right)^2 = \frac{8\pi G\rho}{3} - \frac{k}{R^2} + \frac{\Lambda}{3} \equiv \frac{8\pi G}{3}(\rho_r + \rho_m + \rho_k + \rho_\Lambda) \tag{2.17}$$

where G is the Newton constant, H is the Hubble parameter which measures the expansion rate of the universe, $\rho_{r,m}$ are the matter and radiation energy density of the universe. As we will see shortly, they behave differently under the expansion of the universe. In order to treat curvature and cosmological constant on an equal footing, we have defined:

$$\rho_k = \frac{3kR^2}{8\pi G}\,, \quad \rho_\Lambda = \frac{\Lambda}{8\pi G}\,. \tag{2.18}$$

The current Hubble parameter is well constrained through CMB and Baryon Acoustic Oscillations (BAO) observations [44]:

$$H_0 = 67.66 \pm 0.42\,\mathrm{km\,s^{-1}\,Mpc^{-1}} \equiv h \times 100\,\mathrm{km\,s^{-1}\,Mpc^{-1}} \tag{2.19}$$

The right hand side of eq.(2.17) can be re-parameterized through the critical energy density ρ_0:

$$\rho_0 = \frac{3H_0^2}{8\pi G} = 1.05 \times 10^{-5} h^2 \frac{\mathrm{GeV}}{\mathrm{cm}^3}\,, \quad \Omega_i = \frac{\rho_{i,0}}{\rho_0}\,. \tag{2.20}$$

where the subscript 0 refers to their current value and Ω_i represents their relative contributions to the expansion of the universe with $\sum_i \Omega_i = 1$. Their current values read:

$$\begin{aligned} \Omega_m &= 0.3111 \pm 0.0056\,, \\ \Omega_\Lambda &= 0.6889 \pm 0.0056\,, \\ \Omega_k &= 0.0007 \pm 0.0019 \end{aligned} \tag{2.21}$$

The current energy density of radiations $\rho_{r,0}$, including photons $\rho_{\gamma,0}$ and other particles $\rho_{\nu,0}$, like neutrinos, is parameterized through the CMB temperature $T_0 = 2.7255 \pm 0.0006\,K$[3] and the effective number of relativistic neutrino species N_{eff} :

$$\rho_{\gamma,0} = \frac{\pi^2}{15} T_0^4 = 2.6 \times 10^{-10} \frac{\text{GeV}}{\text{cm}^3}\,, \quad \rho_{\nu,0} = \frac{7}{8}\left(\frac{4}{11}\right)^{\frac{4}{3}} N_{\text{eff}}\,\rho_{\gamma,0}\,, \quad \Omega_r = \frac{\rho_{\gamma,0} + \rho_{\nu,0}}{\rho_0} = 9.09 \times 10^{-5}\,. \tag{2.22}$$

where $N_{\text{eff}} \approx 3.046$ in the SM. It is not exactly 3 since neutrinos have decoupled from photon thermal bath and have a different temperature from photon temperature. The CMB and BAO constrains read $N_{\text{eff}} = 2.99^{+0.34}_{-0.33}$, which agrees with SM predictions [44].

Different energy density in eq.(2.17) has different behavior under the expansion of the universe:

$$\rho_r = \rho_{r,0}\left(\frac{a_0}{a}\right)^4\,, \quad \rho_m = \rho_{m,0}\left(\frac{a_0}{a}\right)^3\,, \quad \rho_k = \rho_{k,0}\left(\frac{a_0}{a}\right)^2\,, \quad \rho_\Lambda = \rho_{\Lambda,0}. \tag{2.23}$$

Using the central values in eq.(2.21) and eq.(2.22), we can solve the time evolution of the scale factor in eq.(2.17). Result is shown in Fig. 2.2. The evolution features three distinct epochs, where the first two of them are power-law growths and the third one is an exponential growth. This is due to the fact that different components of the energy density dominate the equation in different regions. In the earliest epoch, radiation is the major contribution to the Hubble parameter. As the energy density of radiation dilutes faster than that of matter, this epoch ends when their energy densities are equal. We will denote this time as t_{eq} which numerically reads:

$$t_{\text{eq}} \approx 5.03 \times 10^{-5}\,\text{Gyrs}\,, \quad \frac{a_{\text{eq}}}{a_0} \approx 2.92 \times 10^{-4}\,, \quad z_{\text{eq}} = \frac{a_0}{a_{\text{eq}}} - 1 \approx 3.42 \times 10^3\,. \tag{2.24}$$

where we have introduced the red shift z as an equivalently characterization of time. After the radiation-dominated epoch is the matter-dominated epoch. Again, as the energy density of matter dilutes faster than the vacuum energy, this epoch ends at t_{md} when they become comparable:

$$t_{\text{md}} = 10.18\,\text{Gyrs}\,, \quad \frac{a_{\text{md}}}{a_0} = 0.76\,, \quad z_{\text{md}} \approx 0.30\,. \tag{2.25}$$

The cosmological constant term dominates the current expansion of the universe. The total age of the universe with the chosen parameters reads:

$$t_0 = 13.74\,\text{Gyrs}\,. \tag{2.26}$$

Assuming a single component dominating the energy density in the Friedmann equation, we can analytically solve it for different epochs. The time dependence of the scale factor reads:

$$a(t) \propto \begin{cases} t^{1/2}, & \text{for radiation domination} \\ t^{2/3}, & \text{for matter domination} \\ e^{H_\Lambda t}, H_\Lambda = \sqrt{\frac{\Lambda}{3}} & \text{for cosmological constant domination} \end{cases} \tag{2.27}$$

[3] In natural units, $T_0 = (2.3486 \pm 0.0005) \times 10^{-4}\,\text{eV}$.

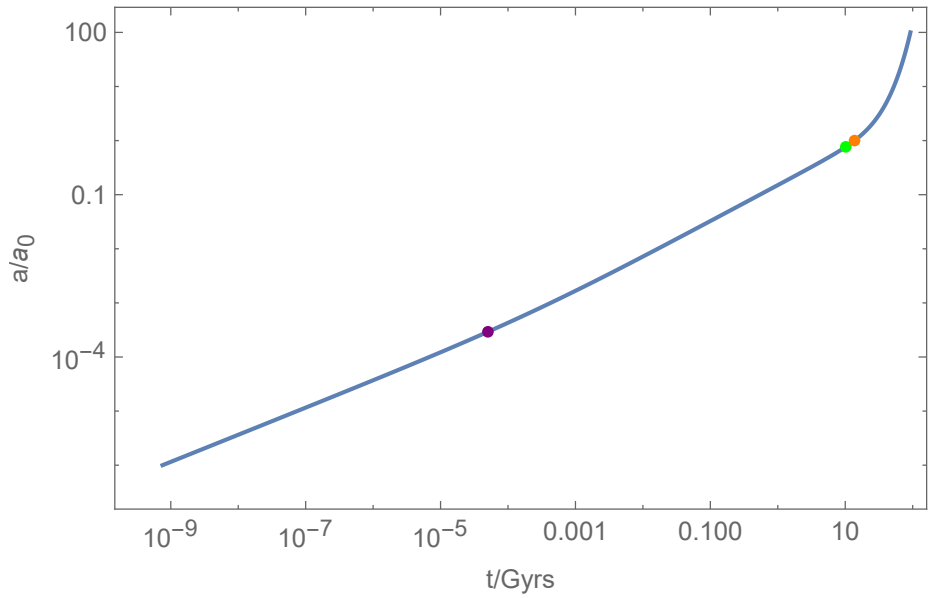

Figure 2.2: Evolution of the scale factor with current values $\Omega_m = 0.3111, \Omega_r = 9.09\times10^{-5}, \Omega_\Lambda = 1-\Omega_m-\Omega_r \approx 0.6888$ and $\Omega_k = 0$. The purple, green and yellow points refer to the time of matter-radiation equality $t_{\rm eq}$, matter-vacuum energy equality $t_{\rm md}$ and present t_0.

These different time dependencies can be clearly seen in Fig. 2.2. In this thesis, we are interested in the processes that happen well before the $t_{\rm eq}$, in the very early universe. In particular, we would like to answer how to generate a flat and radiation-dominated universe, which will be discussed in the next section.

2.3 New Physics beyond the Standard Model

2.3.1 Inflation

The CMB observation indicates that the universe is almost flat, isotropic, and homogeneous. Moreover, different regions across the sky, which seem to be causally disconnected at the time of recombination, share the same temperature. Assuming our universe started from a radiation-dominated era cannot explain its current properties.

Inflation is one of the most compelling hypotheses that addresses the above problems and generates proper initial perturbations for the universe's evolution [45–48]. Inflationary theory predicts that our universe undergoes an exponential expansion, resulting in a homogeneous, isotropic, and spatially flat universe. Due to this expansion, the different causally disconnected region at the CMB is actually connected before inflation and share the same physical properties. After inflation, the energy density responsible for the expansion is transferred into radiation, leaving us with a radiation-dominated universe. This energy transfer process is called reheating.

Currently, the simplest realization of inflation is through the dynamics of a scalar field. If the energy density of the scalar field is dominated by its potential energy, it will induce an exponential expansion of the universe. To ensure inflation happens over a sufficiently long time, this potential must be very

flat, and the scalar field should move at a very slow speed. This is the basic idea of the slow-roll inflation.

A scalar field in an FLRW universe can be described through the following action:

$$S = \int \mathrm{d}^4x\sqrt{-g}\mathcal{L} = \int \mathrm{d}^4x\sqrt{-g}\left(\frac{1}{2}\partial_\mu\phi\partial^\mu\phi - V(\phi)\right), \tag{2.28}$$

where g is the determinate of the FLRW metric in eq.(2.12). The energy-momentum tensor of the field reads:

$$T_{\mu\nu} = \frac{2}{\sqrt{-g}}\frac{\delta S}{\delta g^{\mu\nu}} = \partial_\mu\phi\partial_\nu\phi - g_{\mu\nu}\mathcal{L}\,, \tag{2.29}$$

from which we can extract the energy density and pressure:

$$\rho = \frac{1}{2}\dot{\phi}^2 + V(\phi), \quad p = \frac{1}{2}\dot{\phi}^2 - V(\phi)\,. \tag{2.30}$$

where a dot ($\dot{}$) denotes the derivative with respect to cosmic time t. The action in eq.(2.28) can also be used to derive the equation of motion of the scalar field:

$$\begin{aligned} &\ddot{\phi} + 3H\dot{\phi} + V'(\phi) = 0 \\ &H^2 = \frac{1}{3M_{\mathrm{pl}}^2}\left(\frac{1}{2}\dot{\phi}^2 + V(\phi)\right) = \frac{1}{3M_{\mathrm{pl}}^2}\rho_\phi \end{aligned} \tag{2.31}$$

where a prime ($'$) denotes the derivative with respect to ϕ and $M_{\mathrm{pl}} = \frac{1}{\sqrt{8\pi G}} \approx 2.4 \times 10^{18}$ GeV is the reduced Planck mass. The scalar field that corresponds to inflation is called an inflaton field. The slow-roll inflation occurs when the kinetic energy of the scalar field is much smaller than its potential energy, and the Hubble friction term $3H\dot{\phi}$ dominates over the acceleration term:

$$\frac{1}{2}\dot{\phi}^2 \ll V\,, \quad \left|\frac{\ddot{\phi}}{3H\dot{\phi}}\right| \ll 1\,, \tag{2.32}$$

where the first condition ensures that the inflaton field behaves like cosmological constant, and the second condition ensures that the speed of the inflaton field does not vary significantly, allowing inflation to last long enough. These conditions strongly constrain the shape of the potential. We define two slow-roll parameters:

$$\epsilon_V = \frac{M_{\mathrm{pl}}^2}{2}\left(\frac{V'}{V}\right)^2, \quad \eta_V = M_{\mathrm{pl}}^2\frac{V''}{V}\,. \tag{2.33}$$

Slow roll inflation occurs when both parameters are much smaller than 1, and terminates when they become of order one: $\epsilon_V(\phi_{\mathrm{end}}) = 1$ or $|\eta_V(\phi_{\mathrm{end}})| = 1$. The rapid expansion is reflected by the growth of the scale factor a. We define the number of e-folds as:

$$N_e(\phi_i) = \ln\left(\frac{a_{\mathrm{end}}}{a_i}\right) \approx \int_{\phi_i}^{\phi_{\mathrm{end}}} \frac{\mathrm{d}\phi}{M_{\mathrm{pl}}\sqrt{2\epsilon_V}}\,, \tag{2.34}$$

where a_i represents the initial scale factor and a_{end} is the scale factor at the end of inflation. The slow roll approximation allows us to express this growth in terms of the scalar field value during inflation,

and we use ϕ_i and ϕ_{end} as their corresponding field values respectively.

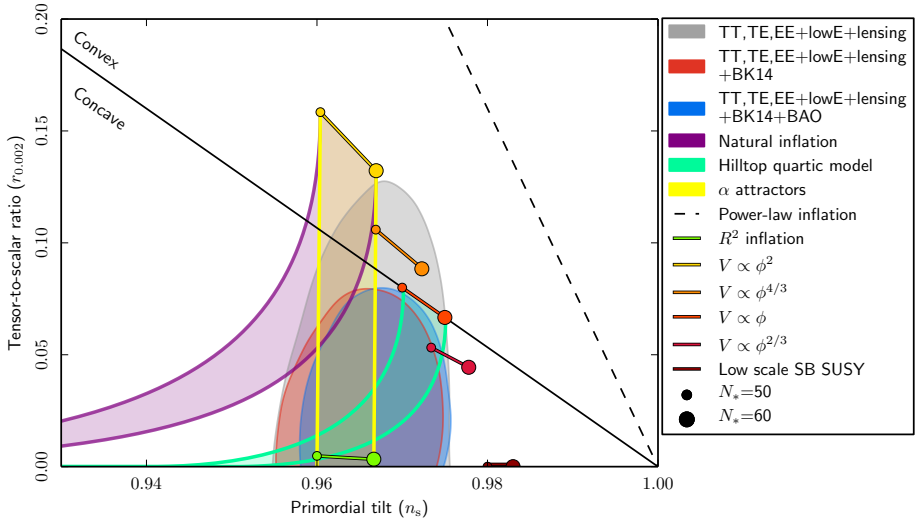

Figure 2.3: Observation constraints on the spectral index n_s and tensor to scalar ratios r compared to the theoretical predictions of selected inflationary models. For more information, see [49].

The constraints on inflation phenomenology mainly arise from the CMB. The CMB photons can be described by black body radiation such that their number density has the following distribution:

$$\frac{dn_\gamma}{dE_\gamma} = \frac{1}{\pi^2} \frac{E_\gamma^2}{e^{E_\gamma/T} - 1}, \tag{2.35}$$

where n_γ is the number density of CMB photons and E_γ is the photon energy. The photon temperature T, is a function of sphere coordinates θ and φ, and averaged to be:

$$\langle T \rangle = \frac{1}{4\pi} \int T(\theta, \varphi) \sin\theta \, \mathrm{d}\theta \mathrm{d}\varphi \approx 2.7255 \, \mathrm{K} \,. \tag{2.36}$$

with a small variation:

$$\left\langle \left(\frac{T(\theta,\varphi) - \langle T \rangle}{\langle T \rangle} \right)^2 \right\rangle^{1/2} \approx 1.1 \times 10^{-5} \,. \tag{2.37}$$

The overall isotropy of the CMB tell us that the number of e-folds must be sufficiently large. Its small anisotropy characterize the primordial cosmological perturbations $\zeta(\vec{x})$ generated by the fluctuation of the inflaton field. These perturbations translate into temperature variations in the CMB through the Sachs-Wolfe effect [50].

It is more convenient to treat space-dependent perturbations $\zeta(\vec{x})$ in the Fourier space:

$$\zeta(\vec{k}) = \int \mathrm{d}^3 x e^{i\vec{k}\cdot\vec{x}} \zeta(\vec{x}) \,. \tag{2.38}$$

where $\vec{k}$ is a 3-dimensional vector and we denote k as its norm. The two point correlations for

statistically homogeneous perturbations then read:

$$\langle \zeta^*(\vec{k}')\zeta(\vec{k})\rangle = (2\pi)^3\delta^3(\vec{k}'-\vec{k})\left(\frac{2\pi^2}{k^3}\mathcal{P}_{\mathcal{R}}(k)\right) \tag{2.39}$$

where $\delta^3(\vec{k}'-\vec{k})$ is the 3-dimensional delta function. The spectrum of curvature perturbations is usually parameterized by a power law:

$$\mathcal{P}_{\mathcal{R}}(k) = A_s\left(\frac{k}{k_0}\right)^{n_s-1}, \tag{2.40}$$

where k_0 serves as a reference scale. A_s is the amplitude n_s is the spectral index of the perturbations. When extracting information from CMB, a specific pivot scale $k_* = 0.05\text{Mpc}^{-1}$ is commonly used. This defines a scale factor a_* during inflation when such a mode leaves the horizon:

$$k_* = a_* H_{\text{inf}}\,. \tag{2.41}$$

This scale factor can be used in eq.(2.34) as a_i. When fixing the number of efolds, eq.(2.34) also fixes the field value ϕ_* through its functional dependence. For single field slow roll inflation, the spectral index is given by the slow roll parameters at ϕ_*:

$$n_s = 1 + 2\eta_V(\phi_*) - 6\epsilon_V(\phi_*) \tag{2.42}$$

The running of spectral index $\alpha = \mathrm{d}n_s/\mathrm{d}\log k$, which describes the scale dependence of spectral index, can also be calculated from derivatives of the potential: $\alpha = 16\epsilon_V(\phi_*)\eta_V(\phi_*) - 24\epsilon_V(\phi_*)^2 - 2\xi_V(\phi_*)^2$ where $\xi_V^2 = M_{\text{pl}}^4 V'V'''/V^2$.

The tensor perturbations induce primordial gravitational waves, exhibiting a similar power-law behavior:

$$\mathcal{P}_t(k) = A_t\left(\frac{k}{k_*}\right)^{n_t}. \tag{2.43}$$

In the single field slow roll inflation, the amplitude A_t and tensor spectral index n_t are related with the scalar perturbations by $r = A_t/A_s = 16\epsilon_V(\phi_*)$, $n_t = -r/8 = -2\epsilon_V(\phi_*)$. The later is know as the consistency relation. The current bounds on the spectral index and tensor-to-scalar ratio are important for constraining inflationary models [49, 51]:

$$\begin{aligned} \ln(10^{10}A_s) &= 3.044 \pm 0.014\,(68\%\text{CL})\,,\\ n_s &= 0.9649 \pm 0.0042\,(68\%\text{CL})\,,\\ \alpha &= 0.0045 \pm 0.0067\,(68\%\text{CL})\,,\\ r &< 0.036\,(95\%\text{CL})\,. \end{aligned} \tag{2.44}$$

The detailed bound on the number of e-folds depends on the post-inflationary dynamics [52, 53], and it is usually chosen to be $50 < N_e < 60$. The current limit on inflation models can be found in Fig. 2.3. Recently, the Atacama Cosmology Telescope measured a different spectral index $n_s = 0.974 \pm 0.003$ [54]. This result is not included when we build inflation models in this thesis.

After inflation, inflaton will oscillate around its minimum. A direct way to transit into a radiation

dominated universe is to assume the inflaton field decays into relativistic particles, creating a radiation thermal bath. Assuming this process does not break the isotropic and homogeneous property of the inflaton field and can be tracked perturbatively, it can be described by adding an additional friction term into the equation of motion:

$$\begin{aligned} \ddot{\phi} + (3H + \Gamma_\phi \dot{\phi} + V'(\phi) &= 0\,, \\ \dot{\rho_r} + 4H\rho_r &= \Gamma_\phi \rho_\phi\,, \\ H^2 &= \frac{1}{3M_{\rm pl}^2}(\rho_\phi + \rho_r)\,. \end{aligned} \tag{2.45}$$

where ρ_r is the energy density of the radiation bath, ρ_ϕ is the energy density of the inflaton as in eq.(2.31), Γ_ϕ is the decay width of the inflaton.

As a concrete example, we solve the eq.(2.45) with a specific α attractor models:

$$V(\phi) = V_0 \tanh^2\left(\frac{\phi}{\sqrt{6}M_{\rm pl}}\right), \tag{2.46}$$

and choose $H_{\rm inf} = \frac{V_0^2}{M_{\rm pl}^2} = 10^{15}$GeV, $\Gamma_\phi = 10^{13}$GeV as an illustration. Evolution of the energy density can be seen in Fig. 2.4. The inflaton field moves towards its minimum at $\phi = 0$ and oscillates around it. The scale factor first grows exponentially and then grows polynomially during the inflaton oscillation. When $H \ll \Gamma_\phi$, inflaton energy density decreased mainly due to the expansion of the universe. Once two scales become comparable, the friction term becomes important, causing the energy density to decay exponentially. We also see that radiation gets produced during inflation, in the level of $\rho_r = \frac{\Gamma_\phi}{4H}\rho_\phi$. Once inflation ends, its energy density also starts to decrease. However, this decrease is compensated by inflaton decay, and radiation energy density eventually exceeds the inflaton energy density. Under certain assumptions, eq.(2.45) can be solved approximately. If the mass of the inflaton field $m_\phi \gg H$, then in a Hubble patch, the inflaton field will oscillate many times and we can take an average on the inflaton energy density:

$$\rho_\phi \approx \langle \rho_\phi \rangle = \langle \frac{1}{2}\dot{\phi}^2 + V(\phi) \rangle \approx \langle \dot{\phi}^2 \rangle, \tag{2.47}$$

The eq.(2.45) can be simplified into:

$$\begin{aligned} \dot{\rho_\phi} + 3H\rho_\phi &= -\Gamma_\phi \rho_\phi\,, \\ \dot{\rho_r} + 4H\rho_r &= \Gamma_\phi \rho_\phi\,, \\ H^2 &= \frac{1}{3M_{\rm pl}^2}(\rho_\phi + \rho_r)\,. \end{aligned} \tag{2.48}$$

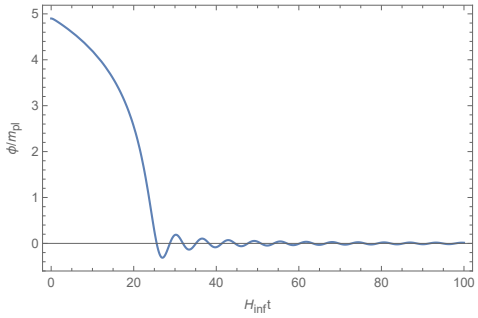

(a) Evolution of inflaton field.

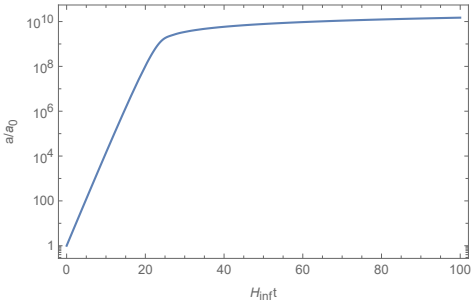

(b) Evolution of scale factor.

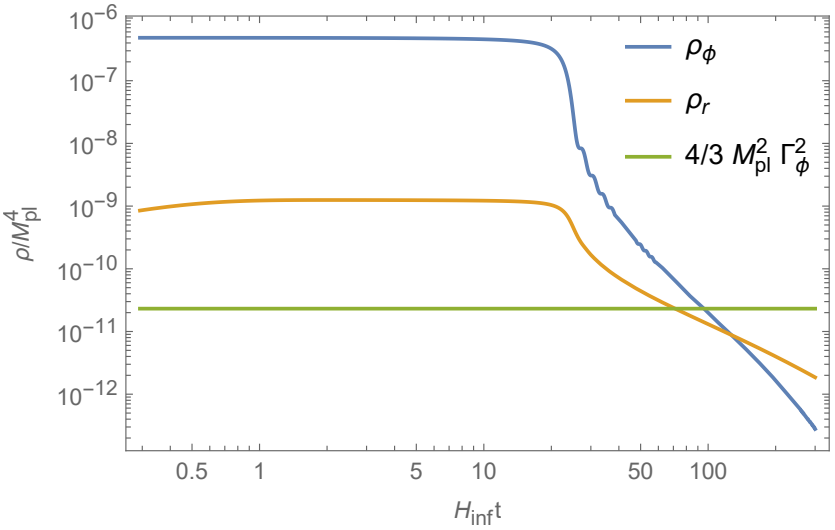

(c) Evolution of inflaton and radiation energy densities.

Figure 2.4: Evolution of inflaton field, scale factor and energy densities around the end of inflation. The time is rescaled by the inflation Hubble scale $H_{\rm inf}$.

With the following solutions [55]:

$$\begin{aligned}\rho_\phi(t) &= \rho_{\rm end}\left(\frac{a}{a_{\rm end}}\right)^{-3} e^{-\Gamma(t-t_{\rm end})}\,,\\ \rho_r(t) &= \rho_{\rm end}\left(\frac{a}{a_{\rm end}}\right)^{-4}\int_{\Gamma_\phi t_{\rm end}}^{\Gamma_\phi t}\left(\frac{a(\tilde{t})}{a_{\rm end}}\right)e^{u_{\rm end}-u}{\rm d}u\,,\quad u=\Gamma_\phi\tilde{t}\,.\end{aligned} \tag{2.49}$$

Thus, the inflaton energy density redshifts like matter, with a damping rate proportional to its decay width. One more simplification can be made if we use the instant reheating paradigm: The inflaton energy density dominates the evolution of the scale factor, and inflaton decays into radiations at a given time $t_{\rm reh}=\Gamma_\phi^{-1}$ when $H(t_{\rm reh})=\frac{2}{3}\Gamma_\phi$. Energy density of radiations at $t_{\rm reh}$ will be:

$$\rho_r(t_{\rm reh})=\frac{\pi^2 g_* T_{\rm reh}^4}{30}=\rho_\phi(t_{\rm reh})=3M_{\rm pl}^2H^2=\frac{4}{3}M_{\rm pl}^2\Gamma_\phi^2\,, \tag{2.50}$$

which determines the reheating temperature:

$$T_{\rm reh} = \left(\frac{40}{\pi^2 g_*}\right)^{1/4} \left(M_{\rm pl}\Gamma_\phi\right)^{1/2} . \tag{2.51}$$

Reheating temperature represents the initial stage when radiations start to dominate the evolution of the universe. Numerically, we can define the reheating temperature when $\rho_\phi(t_{\rm reh}) = \rho_r(t_{\rm reh})$, corresponds to the intersection of blue and orange curves in Fig. 2.4. As one can see, the actual reheating temperature is lower than the estimated ones in eq.(2.51) as reheating takes a finite time, which dilutes both inflaton and radiation energy densities.

Based on our current understanding, reheating is not only a perturbative process. During inflaton oscillations, it should be treated as a coherent oscillating homogeneous condensate. For inflaton itself, many inflatons can decay simultaneously instead of independently. For the produced particles, the Bose condensation effects can be important, which will enhance the production rates. With this in mind, we will only use eq.(2.51) as a rough estimate.

In this thesis, we will discuss different inflation models and their reheating channels in detail. Contents related with inflation can be found in chapter 3, 4, 5, 6 and contents related with reheating can be found in chapter 5.

2.3.2 Dark Matter

The current matter density Ω_m in eq.(2.21) contains two parts:

$$\begin{aligned} \Omega_m &= \Omega_b + \Omega_c \\ \Omega_b h^2 &= 0.02242 \pm 0.00014 , \\ \Omega_c h^2 &= 0.11933 \pm 0.00091 , \end{aligned} \tag{2.52}$$

where Ω_b refers to the normal, baryonic matter and Ω_c refers to the cold dark matter (DM) which interacts very weakly with the electromagnetic force. As DM barely absorbs, reflects, or emits light, it is very hard to detect through optical means. However, we can infer the existence of DM through its gravitational effects on visible matter. DM energy density contributes to the expansion of the universe, which is encoded in the CMB photon spectrum. On the other hand, DM is involved in the dynamics, evolution and formation of galaxies. One of the most well-known examples is the flat rotation curves of spiral galaxies [56]. From Newton's law, the rotation curve of the galaxy should obey:

$$v(R) = \sqrt{G\frac{M(R)}{R}} , \quad M(R) = 4\pi \int_0^R \rho(r) r^2 {\rm d}r . \tag{2.53}$$

Hence, we can infer the mass distribution of the galaxies through the distance dependence of the rotation speed. On the other hand, we can estimate the mass distribution of visible matter through optical observations. Most observations indicate that these two distributions do not agree with each other. Fig. 2.5 shows the observed rotation curve of a barred spiral galaxy NGC 3198. Without the DM contribution, the velocity should fall at large radii while the observed rotation curve is flat. Fitting of the rotation curve requires two components: a thin exponential disk, representing the distribution of visible matter and a spherical halo, representing the distribution of DM.

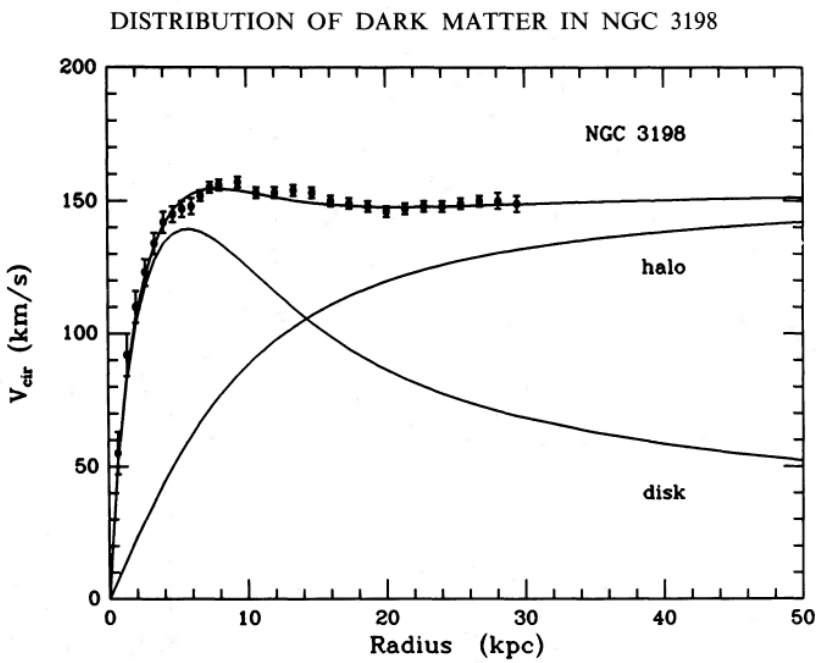

Figure 2.5: Observed rotation curve (dots with error bars) of a barred spiral galaxy NGC 3198, which can be modeled by two components: a thin disk, representing the distribution of visible matter and a spherical halo, representing the distribution of DM. This figure is taken from [57].

Rather than its observational evidence, we are more interested in understanding how DM can be produced in the early universe. If the coupling strength between DM and SM particles is large enough, DM can stay in thermal equilibrium with the SM thermal bath. Assuming the dominant interaction between DM χ and SM particle $\psi_{\rm SM}$ is a $2 \leftrightarrow 2$ scattering $\chi\bar{\chi} \leftrightarrow \psi_{\rm SM}\psi_{\rm SM}$, the DM number density n_χ obeys the following Boltzmann equations:

$$\frac{dn_\chi}{dt} + 3Hn_\chi = -\langle\sigma v\rangle(n_\chi^2 - n_{\chi,eq}^2) \tag{2.54}$$

where $\langle\sigma v\rangle$ is the thermally averaged cross section between DM and SM particles. $n_{\chi,eq}$ is the number density of DM particles in the full thermal equilibrium. The left hand side of the equation describes the time evolution and dilution of the number density by expansion of the universe. The right hand side of the equation describes the pair production and annihilation of DM particles. There are three additional assumptions we implicitly made:

- There is no asymmetry between χ and its antiparticle $\bar{\chi}$ such that $n_\chi = n_{\bar{\chi}}$.
- χ particles are in the kinetic equilibrium, their distribution follows the thermal distributions.
- CP is conserved in the $2 \leftrightarrow 2$ scattering, thus the thermally averaged cross section is the same for production and annihilation processes. The effective degrees of freedom g_* around the relevant temperature is also a constant.

Before solving the equations, we would like to get rid of the expansion term by introducing the following dimensionless quantities:

$$Y_\chi = \frac{n_\chi}{s}, \quad s = \frac{2\pi^2}{45} g_* T^3, \quad x = \frac{m_\chi}{T}. \tag{2.55}$$

where s is the entropy density of the universe. The modified Boltzmann equation reads:

$$\frac{dY_\chi}{\mathrm{d}x} = -\frac{4\pi\sqrt{g_*}}{3\sqrt{10}} \frac{m_\chi M_{\rm pl}}{x^2} \langle\sigma v\rangle (Y_\chi^2 - Y_{\chi,eq}^2) \tag{2.56}$$

Let's first consider the case that DM was in thermal equilibrium with the SM thermal bath. The number density of the χ particles in the comoving volume $n_\chi a^3$ becomes a constant when the right hand side of eq.(2.54) becomes much smaller than the friction term $3Hn_\chi$. This usually happens when DM χ is non-relativistic and the number density of χ field becomes exponentially suppressed. In this region, $n_{\chi,eq}$ follows the Boltzmann distribution:

$$n_{\chi,eq} = g_\chi \left(\frac{m_\chi T}{2\pi}\right)^{3/2} e^{-m_\chi/T}. \tag{2.57}$$

Eq.(2.56) can be solved approximately to give:

$$Y_\chi(\infty) = \frac{3\sqrt{5}}{\sqrt{\pi g_*}} \frac{1}{m_\chi M_{\rm pl} x_f \langle\sigma v\rangle}, \quad x_f = \log\left(\frac{g_\chi m_\chi M_{\rm pl}\langle\sigma v\rangle}{(2\pi^{3/2})\sqrt{g_*}}\right)^{-1}, \tag{2.58}$$

where $Y_\chi(\infty)$ refers to its current value. The current energy density reads:

$$\Omega_\chi h^2 = \frac{2m_\chi s_0 Y_\chi(\infty)}{\rho_0} = 1.8\times10^{-10}\,\frac{\mathrm{GeV}^{-2}}{\langle\sigma v\rangle}\frac{1}{\sqrt{g_*}}\log\left(\frac{g_\chi m_\chi M_{\rm pl}\langle\sigma v\rangle}{(2\pi^{3/2})\sqrt{g_*}}\right). \tag{2.59}$$

We can see from eq.(2.59) that DM energy density is mostly sensitive to the inverse of the thermally averaged cross-section. One of the typical solutions that gives the correct DM abundance is called a weakly interacting massive particle (WIMP):

$$m_\chi \approx 100\,\mathrm{GeV}, \quad \langle\sigma v\rangle \approx 10^{-8}\,\mathrm{GeV}^{-2}, \tag{2.60}$$

as the averaged cross-section is comparable to weak interaction cross-sections at energies of order 100 GeV. Numerical solutions of eq.(2.54) can be found in Fig. 2.6. We fixed the DM mass and varied $\langle\sigma v\rangle$ for illustration purposes. As we expected, higher $\langle\sigma v\rangle$ keeps DM in the thermal bath longer and suppresses its final abundance.

In contrast, if the coupling between DM and SM particles is small, DM may never reach thermal equilibrium with the SM thermal bath. Solution of the Boltzmann equation eq.(2.54) in this case can be found in Fig. 2.7. This is known as the freeze-in mechanism, where DM final abundance scales proportional to the cross-section.

We would like to point out that DM does not need to be produced from the SM thermal bath. Another interesting case is that DM is directly produced from inflaton decays, such that DM gets

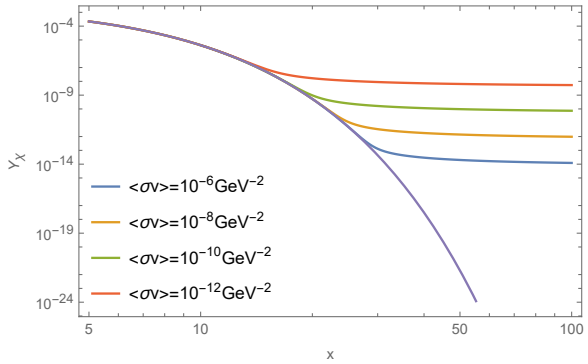

Figure 2.6: DM abundance for different choices of the thermally averaged cross-sections via freeze-out mechanism. We have fixed $m_\chi = 100\text{GeV}$, $g_\chi = 1$ and $g_* = 100$. The purple line represents the DM abundance in the thermal equilibrium.

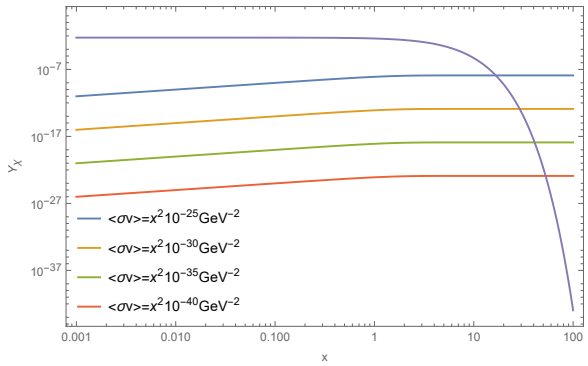

Figure 2.7: DM abundance for different choices of the thermally averaged cross-sections via freeze-in mechanism. We have fixed $m_\chi = 100\text{GeV}$, $g_\chi = 1$ and $g_* = 100$. The purple line represents the DM abundance in the thermal equilibrium.

populated at the end of inflation. In this thesis, we will focus on a similar but slightly different case. As a non-perturbative effect, DM can be produced from the oscillation of the space-time background at the end of inflation [58]. This is known as gravitational particle production, which we will present in chapter 6.

2.3.3 Neutrino Mass

As we already mentioned, neutrinos appear to have very tiny but non-zero masses. Currently, we only know the mass difference among three mass eigenstates and the sum of three neutrino masses with a slight preference for normal ordering($m_1^2 < m_2^2 < m_3^2$) [44, 59]:

$$\Delta m_{21}^2 = 7.49^{+0.19}_{-0.19} \times 10^{-5}\text{eV}^2\,, \quad \Delta m_{31}^2 = 2.534^{+0.025}_{-0.023} \times 10^{-3}\text{eV}^2\,, \quad \sum m_\nu < 0.12\text{eV} \tag{2.61}$$

where $\Delta m_{ij}^2 = \left|m_i^2 - m_j^2\right|$, the first two constraints come from neutrino oscillation experiments while the third one is a cosmological constraint.

However, neutrinos are precisely massless in the SM. At the tree level, due to the absence of right-handed neutrinos, there are no Yukawa mass terms for left-handed neutrinos. In principle, one may expect that the neutrino mass term could be generated from loop corrections. However, in the SM, the neutrino mass term can only arise from $\bar{L}_L L_L^c$:

$$L_i = \begin{pmatrix} \nu_i \\ l_i \end{pmatrix}_L , \quad L_L^c = C\,\bar{L}_L^T . \tag{2.62}$$

This term would violate the accidental symmetry of the SM, both the total lepton symmetry and $B-L$ symmetry. If they are exact, loop corrections will not break them, and they will not be able to generate such a mass term.

We can make an analogy to introduce three additional right-handed neutrinos ν_R, and simply write down their Yukawa interactions:

$$\mathcal{L} = Y_\nu \bar{L}_L^i \tilde{H} \nu_R^j , \tag{2.63}$$

If this single term corresponds to the neutrino mass, the neutrino Yukawa couplings would range from 10^{-14} to 10^{-13}, which are much smaller than other Yukawa couplings, which vary from 10^{-6} to 1 in the SM. One of the possible ways to avoid the small Yukawa couplings is called the "see-saw mechanism", where two types of mass terms determine the neutrino masses:

$$-\mathcal{L}_\nu = M_{Dij} \bar{\nu}_{Ri} \nu_{Lj} + \frac{1}{2} M_{Nij} \bar{\nu}_{Ri} \nu_{Rj}^c + \text{ h.c.} \tag{2.64}$$

where the first term, arising from Yukawa interactions, is called a Dirac mass term. The second term, including the charge conjugated matrix C and charge conjugated field $\nu_R^c = C\bar{\nu}_R^T$, is called a Majorana mass term. In the matrix form, both terms can be described as:

$$-\mathcal{L}_\nu = \bar{\nu}^c \begin{pmatrix} 0 & M_D^T \\ M_D & M_N \end{pmatrix} \nu, \quad \nu = (\nu_L, \nu_R^c)^T . \tag{2.65}$$

If the Majorana mass matrix M_N are much larger than the Dirac mass matrix M_D, then the diagonalization of the mass matrix in eq.(2.65) leads to three light neutrinos ν_l and three heavy neutrinos N with:

$$M^l \simeq -V_l^T M_D^T M_N^{-1} M_D V_l, \quad M^h \simeq V_h^T M_N V_h \tag{2.66}$$

where V_l and V_h diagonalize $M_D^T M_N^{-1} M_D$ and M_N, respectively. In this case, the masses of heavy neutrinos are proportional to M_N while the light ones are suppressed by the ratio of Majorana and Dirac mass terms $M_D^T M_N^{-1}$. This suppression offers an elegant answer to the smallness of the observed neutrino masses. This mechanism will be used in chapter 5.

2.3.4 Baryon Asymmetry

Our world is made from matter, outnumbering antimatter by many orders of magnitude. In the baryon sector, this asymmetry is parameterized by the baryon-to-photon ratio [60]:

$$\eta_B = \frac{n_{B,0}}{n_{\gamma,0}} = \frac{n_B - n_{\bar{B}}}{n_\gamma} \approx 6.05 \times 10^{-10} . \tag{2.67}$$

This ratio remains constant at the hot stage of cosmological evolution, up to $T \approx 100\,\text{GeV}$ in the SM, as there are no physical processes that violate baryon numbers. This ratio is mostly constrained by the Big Bang Nucleosynthesis(BBN), where the light elements including D,^{3} He,^{4} He,^{7} Li are produced through nuclear reactions. The rates of these reactions depend on the density of baryons, which gives the constraint we listed above.

We take the point of view that such a ratio must come from a physical process, referred to as baryogenesis. It could happen either at the radiation dominated stage or even at the reheating epoch. To generate a baryon asymmetry, three physical conditions, known as the Sakharov conditions, have to be satisfied [61]:

- Baryon number violation.
- C- and CP-violation.
- Departure from thermal equilibrium.

The first condition is necessary for a baryon-symmetric universe with $\eta_B = 0$ to evolve into a universe with $\eta_B \neq 0$. The second condition ensures that for any given process that produces net baryons, there is no process that produces net anti-baryons at the same rate. The third condition ensures that the inverse process does not wash out the generated baryon number.

The first two conditions exist in the SM. Non-perturbative effects in the electroweak sector could violate the combination $B + L$ but preserve $B - L$ [62]. Such a process could play a significant role in the early universe [63], it is refereed to as sphaleron process [64]. One of the possible mechanisms to generate baryon asymmetry, leptogenesis, where lepton asymmetry is produced first and transferred into baryon asymmetry, relies on the sphaleron process.

CP violation also exists in the quark sector of the SM. The Yukawa interaction term in eq.(2.6) is not invariant under CP transformations if the Yukawa matrices Y^u, Y^d, Y^e are not real. In the SM, there are no right-handed neutrinos, and we can always make Y^e real. However, it is impossible to make both Y^u and Y^d real. The CP-violation of quark sector can be parameterized through the Cabibbo–Kobayashi–Maskawa (CKM) matrix:

$$M_{ckm} = \begin{pmatrix} c_{12}c_{13} & s_{12}c_{13} & s_{13}e^{-i\delta} \\ -s_{12}c_{23} - c_{12}s_{23}s_{13}e^{i\delta_{13}} & c_{12}c_{23} - s_{12}s_{23}s_{13}e^{i\delta} & s_{23}c_{13} \\ s_{12}s_{23} - c_{12}c_{23}s_{13}e^{i\delta_{13}} & -c_{12}s_{23} - s_{12}c_{23}s_{13}e^{i\delta} & c_{23}c_{13} \end{pmatrix} \tag{2.68}$$

where $c_{ij} = \cos\theta_{ij}$ and $s_{ij} = \sin\theta_{ij}$. δ is known as the CP-violating phase. The CKM matrix relates the flavor eigenstates of down-type quarks to the mass eigenstates:

$$\begin{pmatrix} d_f \\ s_f \\ b_f \end{pmatrix} = M_{ckm} \begin{pmatrix} d_m \\ s_m \\ b_m \end{pmatrix}, \tag{2.69}$$

where the subscript f refers to the flavor eigenstates and m refers to the mass eigenstates. CKM matrix is mostly constrained by meson decays, the parameters in eq.(2.68) read [60]:

$$\begin{aligned} &\sin\theta_{12} = 0.22501 \pm 0.00068\,, \quad &&\sin\theta_{13} = 0.003732^{+0.000090}_{-0.000085}\,, \\ &\sin\theta_{23} = 0.04183^{+0.00079}_{-0.00069}, &&\delta = 1.147 \pm 0.026\,. \end{aligned} \tag{2.70}$$

Once we introduce nonzero neutrino masses through right-handed neutrinos, lepton mixing will also break CP. This leads to the Pontecorvo–Maki–Nakagawa–Sakata (PMNS) matrix, which relates the flavor eigenstates of neutrinos to their mass eigenstates:

$$\begin{pmatrix} \nu_e \\ \nu_\mu \\ \nu_\tau \end{pmatrix} = M_{PMNS} \begin{pmatrix} \nu_1 \\ \nu_2 \\ \nu_3 \end{pmatrix}. \tag{2.71}$$

The PMNS can be parameterized in the same way as the CKM matrix, with different parameters [59]:

$$\begin{aligned} \sin^2\theta_{12} &= 0.307^{+0.012}_{-0.011}, & \sin^2\theta_{23} &= 0.561^{+0.012}_{-0.015}, \\ \sin^2\theta_{23} &= 0.02195^{+0.00054}_{-0.00058}, & \delta &= 177^{+19\circ}_{-20}. \end{aligned} \tag{2.72}$$

Out of thermal equilibrium process doesn't exist in the cosmology history with pure SM. Electroweak and QCD sectors experience a smooth crossover rather than a phase transition in the early universe [65]. Electroweak phase transition can be a first-order phase transition only after adding new fields. Hence in this thesis, we will consider another scenario rather than phase transitions. If the right-handed neutrino has a mass higher than the reheating temperature, its decay naturally happens out of thermal equilibrium. When CP is violated in this process, it will generate lepton asymmetry, which can be transferred into the baryon sector through the sphaleron process. This will be discussed in chapter 5.

2.4 Supersymmetry

Supersymmetry (SUSY) is one of the frameworks that systematically extend the SM. It is based on space-time symmetries which relate fermions with bosons and vice versa. In this section, we will give a brief introduction to the basics of SUSY. For detailed instructions, we refer to [66].

Given the success of using symmetry groups to describe fundamental physics in the SM. One would wonder how non-trivial the symmetry group could be from a theoretical point of view. Historically, there was a no-go theorem indicating that for any physical theory, the symmetry group of the theory is necessarily locally isomorphic to the direct product of an internal symmetry group and the Poincaré group [67]. Later people found that a non-trivial extension of the Poincaré group is only possible if we introduce spinorial generators [68]. Recall the Poincaré algebra reads:

$$\begin{aligned} \left[P^\mu, P^\nu\right] = 0 \qquad & \left[M^{\mu\nu}, P^\sigma\right] = i\left(P^\mu \eta^{\nu\sigma} - P^\nu \eta^{\mu\sigma}\right) \\ \left[M^{\mu\nu}, M^{\rho\sigma}\right] = i\left(\eta^{\nu\rho} M^{\mu\sigma} - \eta^{\nu\sigma} M^{\mu\rho} + \eta^{\mu\sigma} M^{\nu\rho} - \eta^{\mu\rho} M^{\nu\sigma}\right) & \end{aligned} \tag{2.73}$$

where P^μ is the generator for space translation and $M^{\mu\nu}$ is the generator for space time rotations. Adding this spinorial generator Q leads to the following extensions:

$$\begin{aligned} &\left\{Q_\alpha, \bar{Q}_{\dot{\alpha}}\right\} = 2\sigma^\mu_{\alpha\dot{\alpha}} P_\mu, \quad \left[M^{\mu\nu}, Q_\alpha\right] = \left(\sigma^{\mu\nu}\right)^\beta_{\ \alpha} Q_\beta, \qquad \left[M^{\mu\nu}, \bar{Q}^{\dot{\alpha}}\right] = \left(\bar{\sigma}^{\mu\nu}\right)^{\dot{\alpha}}_{\ \ \dot{\beta}} \bar{Q}^{\dot{\beta}}, \\ &\left[Q_\alpha, P^\mu\right] = \left\{Q_\alpha, Q_\beta\right\} = 0. \end{aligned} \tag{2.74}$$

where σ^μ is the Pauli matrix. The combination of eqs.(2.73, 2.74) is the SUSY algebra we are interested in [69]. Several consequences are related to this algebra:

- Energies are necessarily positive definite.
- The supercharges change the spin of the particle by $1/2$:

$$Q|\text{boson}\rangle = |\text{fermion}\rangle, \quad Q|\text{fermion}\rangle = |\text{boson}\rangle\,. \tag{2.75}$$

- If SUSY is exact, the masses of symmetry partners would be the same.

In the SM, particles are described as representations of the both gauge groups and Poincaré groups. In the supersymmetric theories, this means particles are representations of gauge groups and extended Poincaré group. The basic objects we would like to study have hence changed. Instead of a single particle of definite spin, we will start from the superfield which contains particles with different spins:

$$\begin{aligned}\mathcal{F}(x,\theta,\bar{\theta}) =& f(x) + \sqrt{2}\theta\xi(x) + \sqrt{2}\bar{\theta}\bar{\chi}(x) + \theta\theta M(x) + \bar{\theta}\bar{\theta}N(x)\,,\\ &+ \theta\sigma^{\mu}\bar{\theta}A_{\mu}(x) + \theta\theta\bar{\theta}\bar{\lambda}(x) + \bar{\theta}\bar{\theta}\theta\zeta(x) + \frac{1}{2}\theta\theta\bar{\theta}\bar{\theta}D(x)\,,\end{aligned} \tag{2.76}$$

where $(x,\theta,\bar{\theta})$ is the superspace coordinates, an extension to regular 4-dimensional coordinates. $\theta,\bar{\theta}$ are complex grassmann variables conjugating to each other. $f(x), M(x), N(x), D(x)$ are scalar fields, $\xi(x), \bar{\chi}(x), \bar{\lambda}(x), \zeta(x)$ are Weyl spinor fields and $A_{\mu}(x)$ is a vector field. Eq.(2.76) forms a linear and reducible representation of the SUSY group. Some fields are redundant and do not contribute to actual physics. In practice, two of the irreducible representations, chiral superfield Φ and vector superfield V, will be used to construct the physical Lagrangian. They read:

$$\begin{aligned}\Phi(y^{\mu},\theta) = \Phi(x^{\mu} - i\theta\sigma^{\mu}\bar{\theta},\theta) =& \phi(x) - i\theta\sigma^{\mu}\bar{\theta}\partial_{\mu}\phi(x) - \frac{1}{4}\theta\theta\bar{\theta}\bar{\theta}\partial^{\mu}\partial_{\mu}\phi(x) + \sqrt{2}\theta\xi(x)\\ &+ \frac{i}{\sqrt{2}}\theta\theta\partial_{\mu}\xi\sigma^{\mu}\bar{\theta} + \theta\theta F(x)\\ V_{WZ}(z) = V_{WZ}(x,\theta,\bar{\theta}) =& \theta\sigma^{\mu}\bar{\theta}A_{\mu}(x) + \theta\theta\bar{\theta}\bar{\lambda}(x) + \bar{\theta}\bar{\theta}\theta\lambda(x) + \frac{1}{2}\theta\theta\bar{\theta}\bar{\theta}D(x)\end{aligned} \tag{2.77}$$

where we have used the Wess-Zumino gauge to simplify the expression for the vector field. Note that the chiral superfield contains a scalar field $\phi(x)$ and a spinor field $\xi(x)$. The vector superfield contains a vector field $A_{\mu}(x)$ and a spinor field $\lambda(x)$. We can obtain a supersymmetric Lagrangian through the product of left chiral superfields Φ_i:

$$\begin{aligned}\mathcal{L} =& \left[\Phi_i^{\dagger}\Phi_i\right]_D + \left[\mathcal{W}\left(\Phi_i\right) + h.c.\right]_F\\ \mathcal{W}\left(\Phi_i\right) =& h_i\Phi_i + \frac{1}{2}m_{ij}\Phi_i\Phi_j + \frac{1}{3!}f_{ijk}\Phi_i\Phi_j\Phi_k\end{aligned} \tag{2.78}$$

where $\Phi_i^{\dagger}\Phi_i$ is a vector superfield and $\mathcal{W}\left(\Phi_i\right)$ is a chiral superfield called superpotential. The sub-indices refer to the D field and F field in eq.(2.77). In terms of the component fields, the Lagrangian reads:

$$\begin{aligned}\mathcal{L} =& i\xi_i\sigma^{\mu}\left[\partial_{\mu}\right]\bar{\xi}_i + \partial^{\mu}\phi_i^{\star}\partial_{\mu}\phi_i + F_i^{\star}F_i\\ &+ \left[\left(h_k + m_{ik}\phi_i + \frac{1}{2}f_{ijk}\phi_i\phi_j\right)F_k - \frac{1}{2}\xi_i\xi_j\left(m_{ij} + f_{ijk}\phi_k\right) + h.c.\right].\end{aligned} \tag{2.79}$$

As the $F(x)$ field has no derivatives, it has no dynamics and can be integrated out by using its equation of motion. This leads to our final expression:

$$\begin{aligned} \mathcal{L} &= i\xi_i\sigma^\mu\left[\partial_\mu\right]\bar{\xi}_i + \partial^\mu\phi_i^\star\partial_\mu\phi_i - \left(\frac{1}{2}\xi_i\xi_j\mathcal{W}_{ij}(\phi) + h.c.\right) - V\left(\phi_i,\phi_j^\star\right) \\ V\left(\phi_i,\phi_j^\star\right) &= \mathcal{W}_i(\phi)\overline{\mathcal{W}}^i(\bar{\phi}) = F_i^* F_i\,, \end{aligned} \tag{2.80}$$

The subscript of the superpotential $W_i(\phi), W_{ij}(\phi)$ refers to the derivative respective to the superfield Φ_i and picking the scalar field ϕ, i.e.

$$W_i(\phi) = \left.\frac{\partial W}{\partial\Phi_i}\right|_{\Phi\to\phi}, \quad W_{ij}(\phi) = \left.\frac{\partial^2 W}{\partial\Phi_i\partial\Phi_j}\right|_{\Phi\to\phi}. \tag{2.81}$$

The first two terms in eq.(2.80) are the kinetic term for spinor fields and scalar fields, respectively. The third term contains the mass term of spinor fields as well as the Yukawa interaction terms. Note that gauge interactions are not included in eq.(2.80). As we are mostly interested in gauge invariant scalar fields in this thesis, we will not discuss how to include gauge interactions here.

The simplest realization of SM with SUSY is known as the Minimal Supersymmetric Standard Model (MSSM). For each particle in the SM, it predicts a superpartner associated with that particle. If SUSY is exact, the electron and its superpartner should have degenerate masses. However, collider experiments haven't found any scalar with the electron mass. This means SUSY must be broken in specific ways. With some algebra, one can show that spontaneous SUSY breaking means the global minimum of the scalar potential in eq.(2.74) has a non-zero value. One example is SUSY breaking from the O'Raifeartaigh model [70]:

$$\mathcal{W}\left(\Phi_1,\Phi_2,\Phi_3\right) = m\Phi_2\Phi_3 + \lambda\Phi_1\left(\Phi_3^2 - \mu^2\right). \tag{2.82}$$

The equation of motion of F_i fields reads:

$$\begin{aligned} F_1^\star &= -\lambda\left(\phi_3^2 - \mu^2\right), \\ F_2^\star &= -m\phi_3, \\ F_3^\star &= -m\phi_2 - 2\lambda\phi_1\phi_3. \end{aligned} \tag{2.83}$$

One can see from above that it is impossible to set all three terms to zero. The minimum of the scalar potential would be non-zero and breaks the SUSY. Breaking of the SUSY will induce a mass splitting between SM particles and their superpartners, making superpartners much heavier.

2.5 Supergravity

Just like gauging internal symmetry groups leads to strong and electroweak interactions in the SM. SUSY can also be gauged, which leads to gravitational interaction. Such a field theory with gauged SUSY is referred to as supergravity (SUGRA). For a detailed introduction, please consult [71]. As we are primarily interested in the scalar potential in this thesis, we will briefly discuss how to describe

spin-0 and spin-1/2 fields in SUGRA.

In SUGRA, the scalar potential is generated by the Kähler potential $\mathcal{K}$ and the holomorphic Superpotential $\mathcal{W}$. Both of them are supposed to be functions of the superfield Φ^α. We define the Kähler covariant derivative and Kähler metric as:

$$D_\alpha \mathcal{W} = \frac{\partial \mathcal{W}}{\partial \Phi^\alpha} + \frac{1}{M_{\rm pl}^2}\frac{\partial \mathcal{K}}{\partial \Phi^\alpha}\mathcal{W}\,, \quad \mathcal{K}_{\alpha\bar{\beta}} = \frac{\partial^2 \mathcal{K}}{\partial \Phi^\alpha \partial \overline{\Phi^\beta}} = \partial_\alpha \partial_{\bar{\beta}} \mathcal{K} \tag{2.84}$$

For a given Kähler potential $\mathcal{K}$ and superpotential $\mathcal{W}$, interaction Lagrangian with scalar and spinor field reads [72]:

$$\begin{aligned} e^{-1}\mathcal{L} \;=\; & -\mathcal{K}_{\alpha\bar{\beta}}(\partial_\mu \phi^\alpha \partial^\mu \bar{\phi}^{\bar{\beta}} + i\bar{\chi}^{\bar{\beta}}\bar{\sigma}^\mu \partial_\mu \chi^\alpha) - e^{\mathcal{K}}\left(\mathcal{K}^{\alpha\bar{\beta}} D_\alpha \mathcal{W}\overline{D_\beta \mathcal{W}} - \frac{3}{M_{\rm pl}^2}|\mathcal{W}|^2\right) \\ & -\frac{1}{2}e^{\mathcal{K}/(2M_{\rm pl}^2)}\left[(D_\alpha D_\beta \mathcal{W})\chi^\alpha \chi^\beta + \text{h.c.}\right], \end{aligned} \tag{2.85}$$

where we denote the scalar field as ϕ^α and the 2 component spinor field as χ^α, where α runs over all the chiral supermultiplets in the theory. $e = \sqrt{-\det g}$ is the determinant of frame field. $\mathcal{K}^{\alpha\bar{\beta}}$ is the inverse of the Kähler metric. The scalar potential:

$$V(\Phi) = e^{\mathcal{K}/M_{\rm pl}^2}\left(\mathcal{K}^{\alpha\bar{\beta}} D_\alpha \mathcal{W}\overline{D_\beta \mathcal{W}} - \frac{3}{M_{\rm pl}^2}|\mathcal{W}|^2\right). \tag{2.86}$$

is known as the F-term potential. One can see that if we take the limit $M_{\rm pl} \to \infty$, the scalar potential reduces to the global supersymmetric case in eq.(2.80).

Like the global SUSY, gauged SUSY can also be broken spontaneously. This requires $D_\Phi \mathcal{W} \neq 0$ at the minimum of the scalar potential. Let us focus on the case where SUSY is broken by a Polonyi field spontaneously. This can be done by considering the following superpotential [73]:

$$\mathcal{W}_h = \mu M_{\rm pl}(z+\beta)\,, \mathcal{K} = z\bar{z}\,, \tag{2.87}$$

where z is a chiral superfield, μ is an energy scale in $O(\text{TeV})$ and β is of order $M_{\rm pl}$. From now on, in the SUGRA part (including the following chapters), we will set $M_{\rm pl} = 1$ for simplicity. The scalar potential and its derivative generated from this superpotential read:

$$\begin{aligned} V_{\rm h} &= \mu^2 \mathrm{e}^{z\bar{z}}\left(|1+\bar{z}(z+\beta)|^2 - 3|z+\beta|^2\right), \\ \partial_{\bar{z}} V_{\rm h} &= zV + \mu^2 \mathrm{e}^{z\bar{z}}\{(z+\beta)[-2+z(\bar{z}+\beta)] + z[1+\bar{z}(z+\beta)]\}. \end{aligned} \tag{2.88}$$

One of the solutions satisfying $V_h = \partial_{\bar{z}} V_{\rm h} = 0$ is:

$$\beta = 2-\sqrt{3}\,, \quad z_0 = \sqrt{3}-1\,. \tag{2.89}$$

It leads to a SUSY breaking vacuum with the SUSY breaking scale $m_{3/2} = \mu e^{2-\sqrt{3}}$. We will study the role of Polonyi field during inflation in chapter 3.

2.6 Modular symmetry

Modular symmetry is another symmetry that BSM physics could have, which naturally arises in the string theories. If the extra dimensions of any string model are compactified on the torus, one would expect the 4-dimensional theory to respect modular symmetry. It is an internal, global symmetry that acts on the SM particles. It can be used as a flavor symmetry [74], which tries to answer the "flavor puzzle" of the SM, namely:

- Why are the mixing angles in lepton fields and quark fields so different? In the lepton sector, we have two large mixing angles and one small mixing angle, while in the quark sector, three mixing angles are all small.
- Why are there mass hierarchies for the three generations of lepton and quark fields?
- Why are neutrino masses so small?

One possible approach to answering these questions is to use fewer parameters to build models that can reproduce SM masses and mixing angles, with the hope that this will help us understand the relationships among them. This will be used in this thesis.

We start by introducing the basics of the modular symmetry. The homogeneous modular group Γ is the group of linear fraction transformations:

$$\tau \to \gamma\tau = \frac{a\tau + b}{c\tau + d}, \qquad \mathtt{Im}(\tau) > 0\,, \tag{2.90}$$

where a, b, c and d are integers satisfying $ad - bc = 1$. It acts on the complex number τ in the upper-half complex plane. Each linear fractional transformation can be associated with a two-dimensional integer matrix:

$$\gamma = \begin{pmatrix} a & b \\ c & d \end{pmatrix} \tag{2.91}$$

with unit determinant. Since γ and $-\gamma$ lead to the same linear fraction transformation, the homogeneous modular group Γ can be reduced into inhomogeneous modular group $\overline{\Gamma}$, which is isomorphic to the projective special linear group $PSL(2,\mathbb{Z}) \equiv SL(2,\mathbb{Z})/\{\pm\mathbb{1}\}$. It has two generators: the duality transformation $\mathcal{S} : \tau \to -1/\tau$ and the shift transformation $\mathcal{T} : \tau \to \tau + 1$. In the matrix form, they read:

$$\mathcal{S} = \begin{pmatrix} 0 & 1 \\ -1 & 0 \end{pmatrix}, \quad \mathcal{T} = \begin{pmatrix} 1 & 1 \\ 0 & 1 \end{pmatrix}. \tag{2.92}$$

These linear fraction transformations can map the upper half complex plane into the fundamental domain for which two interior points are not related to each other under Eq. (2.90). The standard fundamental domain $\mathcal{D}$ denotes the set

$$\mathcal{D} = \left\{ \tau \,\middle|\, |\tau| \geq 1, |\mathtt{Re}(\tau)| \leq 1/2 \text{ and } \mathtt{Im}(\tau) > 0 \right\}. \tag{2.93}$$

with three fixed points which are invariant under $\mathcal{S}$ or $\mathcal{T}$ or their combinations:

$$i, \omega = e^{\frac{2\pi i}{3}}, i\infty\,.$$

In this thesis, we will intensively study functions that transform specially under modular transformations:

$$f(\gamma\tau) = (c\tau + d)^k f(\tau)\,, \quad \gamma \in \Gamma\,, \tag{2.94}$$

which are called modular forms. k is the weight of the modular form. When $k = 0$, we refer to it as a modular function. There is an important recursion relationship of modular forms, which indicates how derivatives of modular forms transform:

$$f'(\gamma\tau) = (c\tau + d)^{k+2} f'(\tau) + \frac{k}{2\pi i} c(c\tau + d)^{k+1} f(\tau), \quad \gamma \in \Gamma\,, \tag{2.95}$$

Especially, for a weight 0 modular form, its derivative is a weight 2 modular form. Eq.(2.95) then tells us that for a modular function, its derivative vanishes at the fixed points of modular symmetry. This plays a crucial role in our construction of inflation potentials, as the first slow-roll conditions require its first derivative to be small. In this sense, modular symmetry does half of the job for inflation model buildings.

Applying modular symmetry to SM not only requires our scalar potentials to be modular functions, but it also adds new structures to the Yukawa sector. We require the matter multiplets to be representations of finite modular groups $\Gamma_N = SL(2,\mathbb{Z})/\pm\Gamma(N)$, where $\Gamma(N)$ is a principal congruence subgroup of $SL(2,\mathbb{Z})$ and N is an integer:

$$\Gamma(N) = \left\{ \begin{pmatrix} a & b \\ c & d \end{pmatrix} \in SL(2,\mathbb{Z}), \quad \left| \begin{pmatrix} a & b \\ c & d \end{pmatrix} = \begin{pmatrix} 1 & 0 \\ 0 & 1 \end{pmatrix} \pmod N \right\}. \tag{2.96}$$

Finite modular groups Γ_N are generated by $\mathcal{S}, \mathcal{T}$ transformations with the following constraint:

$$\mathcal{T}^N = \mathbb{1}\,. \tag{2.97}$$

When $N = 2, 3, 4, 5$, Γ_N are isomorphic to the permutation groups S_3, A_3, S_4, A_4.

Formally, this means under the action of $\gamma \in \Gamma$, the chiral supermultiplets Φ_I (matter fields) should transform as

$$\Phi^I \xrightarrow{\gamma} (c\tau + d)^{-k_I} \rho^{IJ}(\gamma)\Phi^J\,, \tag{2.98}$$

where k_I is the modular weight of Φ_I, and ρ is a unitary representation of the finite modular group. We can write the superpotential as follows:

$$\mathcal{W}(\Phi) = \sum_n Y_{I_1\ldots I_n}(\tau)\Phi^{(I_1)}\ldots\Phi^{(I_n)} \tag{2.99}$$

For the n-th order term to be modular invariant the functions $Y_{I_1\ldots I_n}(\tau)$ should be modular forms of weight $k_Y(n)$ transforming in the representation ρ of Γ_N :

$$Y_{I_1\ldots I_n}(\gamma\tau) = (c\tau + d)^{k_Y(n)} \rho(\gamma) Y_{I_1\ldots I_n}(\tau) \tag{2.100}$$

with $k_Y(n)$ and ρ such that:

- The weight $k_Y(n)$ should compensate the overall weight of the product $\varphi^{(I_1)}\ldots\varphi^{(I_n)}$:

$$k_Y(n) = k_{I_1} + \ldots. + k_{I_n} \tag{2.101}$$

- The product $\rho \times \rho^{I_1} \times \ldots \times \rho^{I_n}$ contains an invariant singlet.

Eq.(2.99) will reduce to eq.(2.78) when the modulus field acquires a vacuum expectation value.

When working in the framework of SUGRA, we also need to include the transformations of the Kähler potential. This depends on the field content present in the Kähler potential. In this thesis, we will consider the following supermultiplets:

- The Kähler modulus τ, which transforms as eq.(2.90).
- The dilaton field S, which is invariant under modular transformations.
- The matter fields Φ_I which transforms as eq.(2.98).

The modular invariance of the SUGRA theory requires the combined function $\mathcal{G}$:

$$\mathcal{G}(\tau, \bar{\tau}; S, \bar{S}; \Phi_I, \bar{\Phi}_I) = \mathcal{K}(\tau, \bar{\tau}; S, \bar{S}; \Phi_I, \bar{\Phi}_I) + \ln \left|\mathcal{W}(\tau, S, \Phi_I)\right|^2 . \tag{2.102}$$

to be invariant under modular transformations. They can be separately invariant, or the modular transformations of $\mathcal{K}$ and $\mathcal{W}$ compensate each other so that the function $\mathcal{G}$ is modular invariant. We will deal with the second option in this thesis. We consider the following form of the Kähler potential $\mathcal{K}$:

$$\mathcal{K}(\tau, \bar{\tau}; S, \bar{S}; \Phi_I, \bar{\Phi}_I) \quad = \quad K(S, \bar{S}) - 3 \ln \left[-i(\tau - \bar{\tau})\right] + \sum_I (-i\tau + i\bar{\tau})^{-k_I} |\Phi_I|^2 . \tag{2.103}$$

The Kähler potential for the dilaton field will be omitted here as it does not transform under modular transformation. Since $(-i\tau + i\bar{\tau}) \xrightarrow{\gamma} |c\tau + d|^{-2}(-i\tau + i\bar{\tau})$, the modular transformation of the Kähler potential $\mathcal{K}$ is

$$\mathcal{K} \xrightarrow{\gamma} \mathcal{K} + 3 \ln(c\tau + d) + 3 \ln(c\bar{\tau} + d) . \tag{2.104}$$

The superpotential $\mathcal{W}$ is a holomorphic function of τ, S and Φ_I. For our interest, we will decompose it as

$$\mathcal{W}(\tau, S, \Phi_I) \quad = \quad \mathcal{W}_{\text{moduli}}(\tau, S) + \mathcal{W}_{\text{matter}}(\tau, \Phi_I) . \tag{2.105}$$

where the first term generates the inflaton scalar potential and the second term generates the Yukawa term of the SM. It is required that $\mathcal{W}$ has to be a modular function of weight -3, i.e.,

$$\mathcal{W} \xrightarrow{\gamma} e^{i\delta(\gamma)}(c\tau + d)^{-3}\mathcal{W} , \tag{2.106}$$

up to a phase $\delta(\gamma)$ factor.

The matter superpotential $\mathcal{W}_{\text{matter}}$ can be expanded in power series of the supermultiplets Φ_I as before,

$$\mathcal{W}_{\text{matter}}(\tau, \Phi_I) = \sum_n Y_{I_1 \ldots I_n}(\tau) \Phi_{I_1} \ldots \Phi_{I_n} , \tag{2.107}$$

where $Y_{I_1 \ldots I_n}(\tau)$ is a modular form multiplet and it should transform as,

$$Y_{I_1 \ldots I_n}(\tau) \xrightarrow{\gamma} Y_{I_1 \ldots I_n}(\gamma\tau) = e^{i\delta(\gamma)}(c\tau + d)^{k_Y} \rho_Y(\gamma) Y_{I_1 \ldots I_n}(\tau) , \tag{2.108}$$

with

$$\begin{cases} k_Y = k_{I_1} + \ldots + k_{I_n} - 3\,, \\ \rho_Y \bigotimes \rho_{I_1} \bigotimes \ldots \bigotimes \rho_{I_n} \ni \mathbf{1}\,, \end{cases} \tag{2.109}$$

where $\mathbf{1}$ refers to the trivial singlet of Γ_N. Note that the first condition is changed compared with the SUSY case in eq.(2.101). We will show some concrete examples of modular invariant inflation with a specific choice of $\mathcal{W}_{\text{moduli}}(\tau, S)$ in chapter 4,5.

CHAPTER 3

Inflection Point Inflation in SUGRA

As we mentioned in chapter 2, recent observations of the cosmic microwave background (CMB) by the Planck and BICEP/Keck experiments strongly favor an exponentially expanding period of the early universe [49, 51], which is called inflation [45–48]. The simplest implementation, slow roll inflation, needs a single scalar field "inflaton" ϕ rolls over a flat region in the potential.

Power law potentials $V \propto \phi^n$ offer one of the most elegant and simplest realizations of inflation. However, such potentials with $n > 1$ have been ruled out by the CMB observations, due to the large tensor-to-scalar ratio predicted by these models. Given this fact, a broad program has been pursed to investigate alternative models for inflation. Among them are the so-called inflection point inflation models, where different ϕ^n terms collectively provide an inflection point in the potential and accommodate inflation around it. Inflection point models have attracted much attention in recent years [75–87]. They have been well studied both during and after inflation [88–92].

Loop corrections can easily spoil the flatness of the inflaton potential, while supersymmetry (SUSY) provides a convenient way to protect it. For this reason, different inflation models have often been considered in a supergravity (SUGRA) framework [93–110]. This chapter will follow the same spirit to consider a supersymmetric inflection point inflaton model. We want to present a systematic study allowing us to scan over the possible parameter space. We will focus on the similarities and differences between the previously studied non-supersymmetric, renormalizable models and SUGRA models.

SUSY must be broken since no superpartner of a Standard Model particle has as yet been detected. Once SUSY breaking terms are included, they may modify the form of the inflaton potential, thereby breaking the slow-roll conditions. Thus, the SUSY breaking scale must be bounded from above for successful inflation. To investigate this effect, we will focus on the case where SUSY is broken by the Polonyi model [73]. We find two limiting cases by comparing the relative strength of the inflation sector and the SUSY breaking sector. They lead to very different bounds on the SUSY breaking scale.

To be more precise, we consider a SUSY-preserving inflaton field ϕ, which accommodates a near inflection point in the scalar potential at $\phi = \phi_0$. We find that the Hubble parameter and the inflaton mass both increase with ϕ_0 when $\phi_0 < 1$. They reach a maximum around $\phi_0 \sim 1$, then start to decrease because of the exponential factor in the potential. Thus, in such a model, the Hubble parameter can not exceed $O(10^{10})$GeV. The tensor-to-scalar ratio r is much smaller than the current upper bound. The model also predicts a near constant running $\alpha \sim -0.003$, a unique feature that the next generation of observations might be able to test [111–116].

The remainder of this chapter is organized as follows. In section 3.1 we recap basic results obtained

in the non-supersymmetric, renormalizable version of the model and argue why it is interesting to consider this scenario in the SUGRA framework. In section 3.2 we present our model's analytic and numerical results. We further discuss the SUSY breaking effects in our model. In section 3.3 we summarize and draw some conclusions.

3.1 Renormalizable Inflection Point Model and Beyond

3.1.1 Potential setup and CMB observables

We start from the most general renormalizable potential of a single real scalar inflaton field ϕ:

$$V(\phi) = b\phi^2 + c\phi^3 + d\phi^4\,, \tag{3.1}$$

where we have removed the constant and linear terms, so that the minimum of the potential is defined to be at $\phi = 0$ with vanishing vacuum energy[1]. Requiring an inflection point, $V'(\phi_0) = V''(\phi_0) = 0$, then leads to:

$$b = \frac{9c^2}{32d}\,, \quad \phi_0 = -\frac{3c}{8d}\,. \tag{3.2}$$

CMB observations indicate the potential is not exactly flat, but rather concave. One way to realize this is to introduce a small deviation from the inflection point conditions in the cubic term. For our purpose it is more convenient to write the coefficients in terms of the inflection point position ϕ_0. The modified potential then reads:

$$V(\phi) = d\left(\phi^4 - \frac{8}{3}\phi_0(1-\beta)\phi^3 + 2\phi_0^2\phi^2\right)\,. \tag{3.3}$$

There are three free parameters in the potential, d, ϕ_0 and β. In eq.(3.3), d determines the overall normalization of the potential, which can be matched to the power spectrum of curvature perturbation P_ζ once the other parameters are fixed. The other two parameters govern the shape the potential and hence determine the CMB observables, such as the number of e-folds when the CMB pivot scale left the horizon, $N_{\rm cmb}$, and the spectral index n_s. In a "small field" set–up, i.e. for sub-Planckian field values, $\phi_0 < 1$, fixing $N_{\rm cmb} = 65$ and eq.(2.44) require [88]:

$$\begin{aligned} d &= 6.61\times 10^{-16}\phi_0^2\,; \\ \beta &= 9.73\times 10^{-7}\phi_0^4\,. \end{aligned} \tag{3.4}$$

This leads to the following predictions:

$$\begin{aligned} b &= 1.3\times 10^{-15}\,\phi_0^4\,; \quad & c &= 1.8\times 10^{-15}\,\phi_0^3\,; \\ H_{\rm inf} &= 8.6\times 10^{-9}\,\phi_0^3\,; \quad & m_\phi &= 5.2\times 10^{-8}\,\phi_0^2\,; \\ r &= 7.1\times 10^{-9}\,\phi_0^6\,; \quad & \alpha &= -1.4\times 10^{-3}\,. \end{aligned} \tag{3.5}$$

The same ansatz for the potential can also describe "large field" scenarios, where $\phi_0 > 1$. However, in this case no analytical treatment is known. Numerical studies showed that this model can cover the

[1] A tiny cosmological constant can be added.

whole allowed parameter space in the $n_s - r$ plane and may even lead to double eternal inflation [89].

3.1.2 Possible Realization in SUGRA and Associated Problem

As we mentioned in chapter 2, in SUGRA the scalar potential is generated by the Kähler potential K and the holomorphic Superpotential W. A canonically normalized field requires $K = -\Phi\Phi^*$ and we will use this Kähler potential throughout this chapter. For simplicity we choose the superpotential to be a polynomial function of the complex field Φ:

$$W(\Phi) = B\Phi^2 + C\Phi^3 + D\Phi^4\,, \tag{3.6}$$

where we neglect the constant and linear terms as in the renormalizable case. The ansatz (3.6) ensures that $V(0) = W(0) = 0$, i.e. the potential has a supersymmetric stationary point at $\Phi = 0$. The three coefficients B, C, D are chosen to be real. The complex Φ can in general be written as $\Phi = (\phi + i\chi)/\sqrt{2}$, where ϕ and χ are real fields. We want to identify ϕ with the inflaton field. By choosing the coefficients in eq.(3.6) to be real we make sure that the potential $V(\phi, \chi)$ depends only on even powers of χ. Moreover, we make sure that $\partial^2 V(\phi,\chi)/\partial\chi^2 > 0$ for $\chi = 0$ and $\phi \in [0, \phi_0]$. We therefore can assume that $\chi = 0$ throughout, so that we can ignore this imaginary component when computing the inflationary dynamics. It is not hard to write down the scalar potential $V(\phi) \equiv V(\phi, \chi = 0)$ in this setup:

$$\begin{aligned} V(\phi) = \mathrm{e}^{\frac{\phi^2}{2}}\Bigg[&2B^2\phi^2 + 3\sqrt{2}BC\phi^3 + \frac{1}{4}\phi^4\left(B^2 + 16BD + 9C^2\right) + \frac{1}{2}\phi^5\left(\sqrt{2}BC + 6\sqrt{2}CD\right) \\ &+ \frac{1}{8}\phi^6\left(B^2 + 6BD + 3C^2 + 16D^2\right) + \frac{1}{8}\phi^7\left(\sqrt{2}BC + 4\sqrt{2}CD\right) \\ &+ \frac{1}{16}\phi^8\left(2BD + C^2 + 5D^2\right) + \frac{CD\phi^9}{8\sqrt{2}} + \frac{D^2\phi^{10}}{32}\Bigg], \end{aligned} \tag{3.7}$$

In order to try to match to the renormalizable case, we expand V up to the fourth order:

$$V(\phi) \approx 2B^2\phi^2 + 3\sqrt{2}BC\phi^3 + \frac{1}{4}(5B^2 + 9C^2 + 16BD)\phi^4\,. \tag{3.8}$$

Matching eq.(3.8) to eq.(3.1) and using eqs.(3.4) and (3.5) implies:

$$\begin{aligned} B &= 2.571 \times 10^{-8}\phi_0^2\,, \\ C &= 1.615 \times 10^{-8}\phi_0 \times (1-\beta)\,, \\ D &= 7.210 \times 10^{-10} - 8.034 \times 10^{-9}\phi_0^2 - 5.7 \times 10^{-8}(2\beta - \beta^2)\,. \end{aligned} \tag{3.9}$$

Hence for $\phi_0 \ll 1$ the coefficients of the superpotential would have to scale as $B \propto \phi_0^2$, $C \propto \phi_0^1$, $D \propto \phi_0^0$. The problem emerges when we substitute these matching conditions back into the full potential eq.(3.7). Writing the latter as:

$$V(\phi) = e^{\frac{1}{2}\phi^2}\sum_{n=2}^{10} a_n\phi^n\,, \tag{3.10}$$

the coefficients a_n have the following scaling behavior for $\phi_0 \ll 1$:

$$\begin{aligned} &a_2 \propto \phi_0^4; \quad a_3 \propto \phi_0^3; \quad a_4 \propto \phi_0^2; \quad a_5 \propto \phi_0^1; \quad a_6 \propto \phi_0^0; \\ &a_7 \propto \phi_0^1; \quad a_8 \propto \phi_0^0; \quad a_9 \propto \phi_0^1; \quad a_{10} \propto \phi_0^0. \end{aligned} \tag{3.11}$$

Thus, when we evaluate the value of the potential and its first and second derivatives at $\phi \sim \phi_0$, the first five terms (from ϕ^2 to ϕ^6) would contribute with comparable magnitude. Therefore the terms $\propto \phi^5$ and ϕ^6 can easily spoil the flatness of the potential, i.e. the expansion only to order ϕ^4 is not self–consistent. For this reason, it is necessary to consider an inflection point model in the full potential eq.(3.7) (or at least up to ϕ^6) rather than trying to directly match the renormalizable, non-supersymmetric potential.

3.2 Inflection Point Model in SUGRA

3.2.1 Analytic Analysis of the Model

Requiring that the full potential eq.(3.7) has an inflection point at $\phi = \phi_0$, i.e. $V'(\phi_0) = V''(\phi_0) = 0$, leads to the following solutions[2]:

$$\begin{aligned} B =& D \frac{\phi_0^2 \left(1152 + 480\phi_0^2 + 72\phi_0^4 + 12\phi_0^6 + \phi_0^8\right)}{2\left(192 + 96\phi_0^2 + 4\phi_0^6 + \phi_0^8\right)} \\ C =& -D \frac{\sqrt{2}\phi_0 \left(384 + 192\phi_0^2 + 24\phi_0^4 + 8\phi_0^6 + \phi_0^8\right)}{192 + 96\phi_0^2 + 4\phi_0^6 + \phi_0^8} \end{aligned} \tag{3.12}$$

For $\phi_0 \ll 1$ we can approximate the above solutions by their leading order results:

$$B \approx D \times 3\phi_0^2, \quad C \approx D \times (-2\sqrt{2}\phi_0)\,.$$

The full potential at $\phi \leq \phi_0$ can be further simplified if we only include terms up to ϕ_0^6:

$$V(\phi) \approx 2D^2\phi^2(\phi^2 - 3\phi\phi_0 + 3\phi_0^2)^2\,. \tag{3.13}$$

This expansion now *is* self-consistent, i.e. the higher order terms, starting at $O(\phi^7)$, are indeed suppressed. At the inflection point ϕ_0, the potential reads:

$$V(\phi_0) \approx 2D^2\phi_0^6\,. \tag{3.14}$$

The potential (3.13) has a minimum at $\phi = 0$ and is positive semi-definite, i.e. $V(\phi) \geq 0\ \forall\phi$. As in the non-supersymmetric case, in the small field scenario $\phi_0 \ll 1$ we can get semi-analytic results for inflationary observables by expanding the slow-roll parameter around the inflection point via the ansatz

[2] Since we are dealing with high-order polynomial equations there often are several solutions. However, we find that the others usually have $V < 0$ at the minimum, leading to a very large and negative cosmological constant.

$\phi = \phi_0(1-\delta\phi)$, and adding a deviation from the strict inflection point condition via $B \longrightarrow B + D \times \delta B$:

$$\begin{aligned}
\epsilon &= \frac{1}{2}\left(\frac{V'}{V}\right)^2 = \frac{1}{2}\left(\frac{2\delta B + 6\phi_0^2\delta\phi^2}{\phi_0^3}\right)^2 , \\
\eta &= \frac{V''}{V} = \frac{10.5\,\delta B - 24\,\delta\phi}{2\phi_0^2} , \\
\xi^2 &= \frac{V'V'''}{V^2} = \frac{24\delta B + 72\phi_0^2\delta\phi^2}{\phi_0^6} .
\end{aligned} \tag{3.15}$$

We only keep terms up to linear order in δB and quadratic in $\delta\phi$; this will turn out to be sufficient.

We are now ready to discuss which $\delta\phi$ and δB reproduce the CMB observations. In our model the duration of inflation is controlled by η since $\epsilon \ll \eta$. The beginning (when the pivot scale $k_* = 0.05\,\mathrm{Mpc}^{-1}$ crossed out of the horizon) and end of observable inflation are given by:

$$\eta_{\rm cmb} = \frac{n_s - 1}{2} , \quad \eta_{\rm end} = -1 , \tag{3.16}$$

Solving the second eq.(3.15) for $\delta\phi$, we get:

$$\delta\phi = -\frac{2\phi_0^2\eta - 10.5\delta B}{24} . \tag{3.17}$$

The number of e-folds $N_{\rm cmb}$ is given by:

$$\begin{aligned}
N_{\rm cmb} &= \int_{\phi_{\rm cmb}}^{\phi_{\rm end}} \frac{1}{\sqrt{2\epsilon}} d\phi \\
&= \int_{\phi_{\rm cmb}}^{\phi_{\rm end}} \frac{\phi_0^3}{2\delta B + 6\phi_0^2\delta\phi^2} d\phi \\
&= -\int_{\delta\phi_c}^{\delta\phi_e} \frac{\phi_0^4}{2\delta B + 6\phi_0^2\delta\phi^2} d\delta\phi \\
&= \frac{\phi_0^2}{6\sqrt{\beta}}\left(\arctan\left(\frac{\delta\phi_{\rm end}}{\sqrt{\beta}}\right) - \arctan\left(\frac{\delta\phi_{\rm cmb}}{\sqrt{\beta}}\right)\right) .
\end{aligned} \tag{3.18}$$

In the last step we have switched from the absolute deviation δB to the relative one $\beta = D \times \delta B/B = \delta B/(3\phi_0^2)$ in order to factor out ϕ_0 in the denominator; except for the first line, eq.(3.18) also only holds for $\phi_0 \ll 1$. Recall that the arc-tangent functions can be at most $\pi/2$. Numerically, requiring $N_{\rm cmb} = 50$ yields $\beta = 2.7 \times 10^{-5}\phi_0^4$ and $\delta B = 8.2 \times 10^{-5}\phi_0^6$. From the second eq.(2.44) and remembering $|\epsilon| \ll |\eta|$ we see that $|\eta| \geq 0.015$ when and after CMB scales crossed out of the horizon. Hence we can neglect the second term in eq.(3.17) for $\phi_0 \ll 1$, and determine the inflation period by:

$$\delta\phi = -\frac{\phi_0^2}{12}\eta . \tag{3.19}$$

Inserting this into the last line of eq.(3.18) yields

$$N_{\rm cmb} = \frac{\phi_0^2}{6\sqrt{\beta}}\left(\arctan\left(\frac{-\phi_0^2\eta_{\rm end}}{12\sqrt{\beta}}\right) - \arctan\left(\frac{-\phi_0^2\eta_{\rm cmb}}{12\sqrt{\beta}}\right)\right), \tag{3.20}$$

which can be solved numerically. For example, setting $n_s = 0.9659\,, N_{\rm cmb} = 45$ would result in $\delta B = 6.1\times10^{-5}\phi_0^6$.

Having fixed δB and the initial $\delta\phi$, the overall scale of inflation, and hence D, is determined by the power of Gaussian curvature perturbations. To this end we first calculate ϵ at $\phi_{\rm cmb}$:

$$\epsilon_{\rm cmb} = 8.88\times10^{-9}\phi_0^6\,, \tag{3.21}$$

Using eqs.(2.44) and (3.14) we find that the normalization factor is independent of ϕ_0:

$$D^{-2} = \frac{2\phi_0^6}{P_\zeta 24\pi^2\epsilon_{\rm cmb}} = 4.52\times10^{14}\,. \tag{3.22}$$

It is then straightforward to evaluate the value of the Hubble parameter during inflation and the physical mass of the inflaton after inflation:

$$H_{\rm inf} = \sqrt{\frac{V(\phi_0)}{3}} = 3.84\times10^{-8}\phi_0^3\,, \quad m_\phi = \sqrt{4B^2} = 2.81\times10^{-7}\phi_0^2\,. \tag{3.23}$$

The running of the spectral index α can also be determined:

$$\alpha = 16\epsilon\eta - 24\epsilon^2 - 2\xi^2 \approx -2\xi^2 = -2\frac{24\delta B + 72\phi_0^2\delta\phi^2}{\phi_0^6} \approx -0.0030\,. \tag{3.24}$$

This running of the spectral index is a feature of our model, since it does not depend on ϕ_0.

However, our numerical results do depend on $N_{\rm cmb}$. Taking as second example the rather large value $N_{\rm cmb} = 65$ while keeping $n_s = 0.9659$, we get:

$$\begin{aligned} \delta B &= 2.60\times10^{-5}\phi_0^6\,, & \epsilon_{\rm cmb} &= 1.59\times10^{-9}\phi_0^6\,,\\ D^{-2} &= 2.53\times10^{15}\,, & H_{\rm inf} &= 1.62\times10^{-8}\phi_0^3\,,\\ m_\phi &= 1.19\times10^{-7}\phi_0^2\,, & \alpha &= -0.0015\,. \end{aligned} \tag{3.25}$$

The tensor-to-scalar ratio $r = 16\epsilon$ is always too small to reach the sensitivity of any currently conceivable observation. However, the S4CMB experiment, together with small-scale structure information (e.g. on the Lyman-α forest) could achieve 10^{-3} sensitivity for α, which would test our model [111–116].

By comparing with the predictions of the renormalizable model given in eqs.(3.5), we see that of $H_{\rm inf}$ and m_ϕ scale with ϕ_0 in the same way in both cases, with roughly a factor 2 difference in coefficients. Even though the SUGRA potential is more complicated and scales as ϕ^6 in the simplest limit, they thus make very similar predictions for the inflationary observables. In particular, the overall coefficient D of the sixth order SUGRA potential is independent of ϕ_0, while in the non-SUSY case

the coefficient of the quartic potential $d \propto \phi_0^2$; hence in both cases $V(\phi \simeq \phi_0) \propto \phi_0^6$.

We also note that the curvature of the potential is negative for an extended range of ϕ below ϕ_0. In the non-SUSY case, this holds for $\phi/\phi_0 \in [1/3, 1]$, independently of the value of ϕ_0; in the SUGRA case with $\phi_0 \ll 1$, this region extends to $\phi/\phi_0 \in [1/4, 1]$. The minimum of the curvature occurs at $\phi \simeq 0.54\phi_0$, closer to the origin than in the non-SUSY case, with a value just below $-0.23\, m_\phi^2$, smaller in magnitude than in the non-SUSY case. The latter reduces the tachyonic instability while the former increases it. Hence, we expect the non-perturbative effects after inflation studied in [92] for the non-SUSY case would be similar in the SUGRA version of the model.

When ϕ_0 is larger than unity, it is hard to make a comprehensive analytic analysis, but we can still understand the model qualitatively. To this end we first formally rewrite the potential as:

$$V(\phi) = e^{\frac{1}{2}\phi^2} P(\phi)\,. \tag{3.26}$$

The slow roll parameter then scales like $\eta \propto \phi^2 \times f(\delta\phi)$ with $f(0) \approx 0$. The duration of inflation is still controlled by $\delta\eta = \eta_{\rm cmb} - \eta_{\rm end} \approx 1$, the larger ϕ_0, the smaller $\delta\phi$ should be. The resulting decrease in the integration range in eq.(3.18) has to be compensated by increasing the integrand, by a reduction of ϵ. Since the ratio between the potential $V(\phi_0)$ and ϵ is fixed by the power of curvature perturbations, an increase of ϕ_0 would eventually lead to a decrease of the potential and hence of the Hubble parameter. Moreover, the potential near ϕ_0 is increased by the exponential factor, which becomes unity at the origin. Hence, the mass of inflaton should be suppressed by $e^{-\frac{1}{2}\phi_0^2}$.

As a brief summary, by fixing n_s and $N_{\rm cmb}$, we find the inflection point model would always give a tiny tensor-to-scalar ratio r and a constant running of spectral index α. The Hubble scale of inflation first increases with increasing inflection point position ϕ_0, and then decreases once ϕ_0 exceeds 1. The inflaton mass follows the same pattern but drops much faster in the second phase. In the next section, we confirm these expectations by showing some numerical results.

3.2.2 Numerical Results of the Model

In this section, we present our numerical results. We introduce three steps to scan the allowed parameter space of our model, following the same spirit as our analytic treatment:

- We choose ϕ_0 as a free parameter and solve the inflection point equations $V' = V'' = 0$ to find corresponding values of B/D and C/D. We pick the solution that will generate a positive semi-definite potential, see eqs.(3.12).
- We slightly deform the potential by $B \to B + \delta B$. CMB scales start to leave the horizon at $\phi_{\rm cmb}$, which is determined by $1 + 2\eta = n_s$ since still $\epsilon \ll |\eta|$ in all cases. Inflation ends at $\phi_{\rm end}$, which is determined by $\eta = -1$. We find that both the start point and the end point mildly depend on δB. The correct δB is given by fixing $N_{\rm cmb}$, for which we consider the range from 45 to 65.
- Having fixed δB, we can recalculate the slow roll parameters at the pivot scale $\eta_{\rm cmb}$ and $\epsilon_{\rm cmb}$. We then determine the correct normalization D of the potential by requiring $P_\zeta = 2.1 \times 10^{-9}$. This allows us to compute the Hubble value and the inflaton mass.

We begin by showing four inflaton potentials with different choices of ϕ_0 in Fig. 3.1. For comparison, these potentials are rescaled by their values at the inflection point. When $\phi_0 < 1$, the shape of the

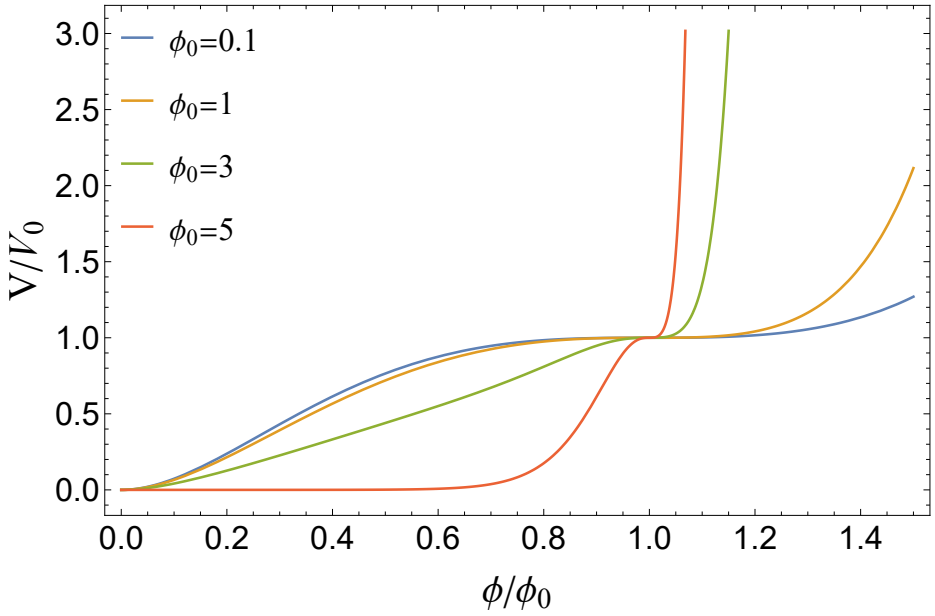

Figure 3.1: Resealed inflation potential for different choices of the location of the inflection point ϕ_0. Here $V_0 = V(\phi_0)$ is the value of the potential at the inflection point. Blue, orange, green, and red curves corresponding to $\phi_0 = 0.1,\ 1,\ 3$ and 5, respectively.

potential becomes independent of ϕ_0 for $\phi \leq \phi_0$. Increasing ϕ_0 beyond 1 shortens the flat plateau; it also makes it even flatter, which is difficult to see in this figure.

The corresponding values of the Hubble parameter during inflation can be found in the top left frame of Fig. 3.2, where we use blue and orange lines to represent different values of $N_{\rm cmb}$. As expected the Hubble scale first increases with increasing ϕ_0, then drops once $\phi_0 > 1$. There is no lower bound on $H_{\rm inf}$ from the pure model perspective. However, the maximum value is determined by the special shape of the potential and can never exceed 10^{11} GeV. It obeys a power law when ϕ_0 is small, which agrees with our analytic estimation.

The relation between inflaton mass m_ϕ and inflection point ϕ_0, shown in the top right frame, follows the same pattern as the Hubble scale when ϕ_0 is small. However, the inflaton mass drops dramatically for $\phi_0 > 1$, due to the exponential suppression discussed at the end of the previous section. When $\phi_0 \approx 10$, the inflaton mass could be as low as 1 GeV. This tiny value differs from the Hubble scale by more than nine orders of magnitude. Thus our model offers a way to separate the Hubble and inflaton mass scales.

The running of spectral index α is shown in the bottom right frame. It remains independent of ϕ_0 even for $\phi_0 \geq 1$. In contrast to the non-SUSY version of the model, α strongly depends on $N_{\rm cmb}$. When $N_{\rm cmb} = 45$ $\alpha \approx -0.0032$. Increasing $N_{\rm cmb}$ reduces the absolute value of α, reaching $\alpha \approx -0.0013$ for $N_{\rm cmb} = 65$.

Finally, the bottom left frame of Fig. 3.2 shows the relationship between the tensor-to-scalar ratio r and ϕ_0. It follows the same pattern as the Hubble scale. However, since we find $r < 10^{-7}$, a positive detection of tensor modes by current or near-future experiments would exclude our model.

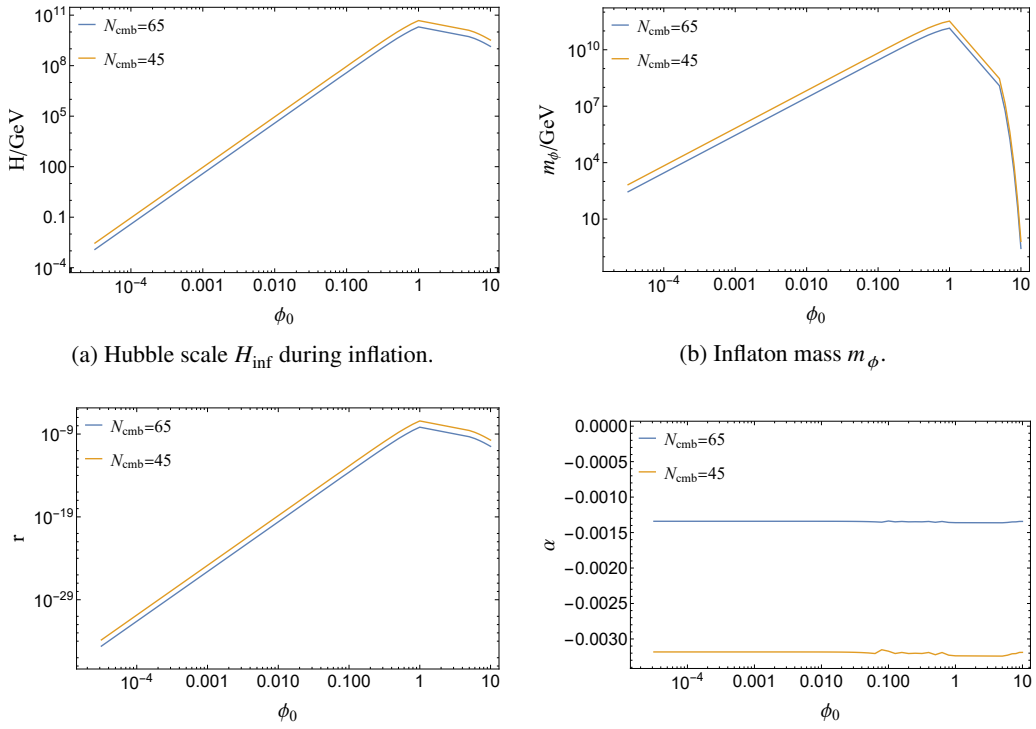

(a) Hubble scale $H_{\rm inf}$ during inflation.

(b) Inflaton mass m_ϕ.

(c) Tensor to scale ratio r.

(d) Running of spectral index α.

Figure 3.2: The dependence of the Hubble parameter $H_{\rm inf}$ during inflation, the inflaton mass m_ϕ, tensor-to-scalar ratio r, and the running of spectral index α on the position ϕ_0 of the inflection point. Different lines represent different choices of the number of e-folds: $N_{\rm cmb} = 65$ (blue) and $N_{\rm cmb} = 45$ (orange). We fixed $n_s = 0.9659$ and $P_\zeta = 2.1 \times 10^{-9}$.

3.2.3 SUSY Breaking by a Polonyi Field

Clearly SUSY must be broken in any realistic model. In this subsection we investigate if the existence of a SUSY breaking sector would change the inflation potential significantly. For simplicity we consider the classical Polonyi ansatz [73], where a single chiral superfield Z with a linear superpotential is introduced to break SUSY:

$$\begin{aligned} W &= B\Phi^2 + C\Phi^3 + D\Phi^4 + \mu M_{\rm pl}(Z + \beta_{\rm P}) \\ &= W_{\rm I} + W_{\rm P} \end{aligned} \tag{3.27}$$

where μ essentially sets the SUSY breaking scale; we explicitly include a factor $M_{\rm pl}$ here to ensure the correct dimension of μ. Both Φ and Z are complex fields. As before, we want the real part of Φ to be the inflaton field ϕ. Z is the Polonyi field whose vacuum expectation value $\langle Z\rangle$ is the only source of SUSY breaking after inflation, when $\langle\phi\rangle = 0$. The SUSY breaking with vanishing vacuum energy requires $\beta_{\rm P} = 2 - \sqrt{3}$, which gives the gravitino mass $m_{3/2} = \mu e^{2-\sqrt{3}}$ when Z stays at the SUSY breaking minimum at $Z = \langle Z\rangle = (\sqrt{3} - 1)M_{\rm pl}$.

Let's first consider the case where the Polonyi sector gives a small perturbation to the inflation

potential. For $\phi_0 < 1$ our previous results suggest:

$$\begin{aligned} \tilde{B} &= \frac{B}{D} \approx 3\phi_0^2 \,, \\ \tilde{C} &= \frac{C}{D} \approx -2\sqrt{2}\phi_0 \,, \\ D &\approx 4.7 \times 10^{-8} \,. \end{aligned} \tag{3.28}$$

We require that the Polonyi field does not change the inflation potential significantly, which means $|W_{\rm I}| \gg |W_{\rm P}|$. The existence of the SUSY breaking term will not alter the slow roll parameters significantly if

$$\epsilon_\mu \ll \epsilon_{\rm cmb} \quad \text{and} \quad \eta_\mu \ll \eta_{\rm cmb} \,, \tag{3.29}$$

where the subscript μ means the additional contribution to the slow roll parameter due to the SUSY breaking term.

We assume that during inflation the Polonyi field stays at the origin, $Z = 0$, which will be verified later. Under this assumption, the additional contribution to the inflaton potential reads:

$$V_\mu(\phi) = \frac{e^{\frac{1}{2}\phi^2}}{4}\mu\left((-4\beta_{\rm P}B\phi^2 + 2\beta_{\rm P}(B+D)\phi^4 + \sqrt{2}\beta_{\rm P}C\phi^5 + \beta_{\rm P}D\phi^6) + \mu(4 - 12\beta_{\rm P}^2 + 2\beta_{\rm P}^2\phi^2)\right) . \tag{3.30}$$

After substituting $\beta_{\rm P} = 2 - \sqrt{3}$, the additional contributions to slow roll parameters are:

$$\begin{aligned} \epsilon_\mu \approx& \sqrt{2\epsilon_{\rm cmb}}\frac{\left(8\sqrt{3}-13\right)\tilde{\mu}^2\phi_0 + \left(4\sqrt{3}-8\right)\tilde{\mu}\phi_0^3}{2\phi_0^6} \,, \\ \eta_\mu \approx& \frac{(8\sqrt{3}-13)\tilde{\mu}^2 + (5\sqrt{3}-10)\tilde{\mu}\phi_0^4}{2\phi_0^6} \,, \end{aligned} \tag{3.31}$$

where we have introduced the rescaled parameter $\tilde{\mu} = \mu/D$ to simplify the expression. The first term in eq.(3.31) is the cross term between the original and SUSY breaking induced derivatives of the potential in $(V')^2$. Using $\epsilon_{\rm cmb} = 8.88 \times 10^{-9}\phi_0^6$ and requiring $\epsilon_\mu < 0.05\,\epsilon_{\rm cmb}$, which ensures $\eta_\mu \ll \eta_{cmb}$ as well, we get an upper bound on SUSY breaking scale μ:

$$\mu < 3.4 \times 10^6 \left(\frac{\phi_0}{M_{\rm pl}}\right)^6 \text{ GeV} \,. \tag{3.32}$$

Since we have not found any SUSY particle in collider searches, we conservatively require $\mu > 1$TeV. From eq.(3.32) this implies $\phi_0 > 0.3$, corresponding to $H > 10^8$ GeV.

If we increase the SUSY breaking scale while keeping the inflation scale fixed, the Polonyi field will move from the origin to its present minimum at $\sqrt{3} - 1$. In Fig. 3.3 we show the position of the Polonyi field during inflation, by minimizing $V(\phi, z)$ with respect to z for fixed $\phi = \phi_0$; here we only consider the real part z of Z, fixing the imaginary part to the origin throughout. We see that z tends to stay near the origin when $\tilde{\mu} \ll \phi_0^2$, and slowly moves to its own vacuum at $\sqrt{3} - 1$ as $\tilde{\mu}$ becomes comparable to ϕ_0^2.

On the other hand, if $W_{\rm P} \gg W_{\rm I}$, the Polonyi field will stay at $Z = \sqrt{3} - 1$. In this case, the inflection

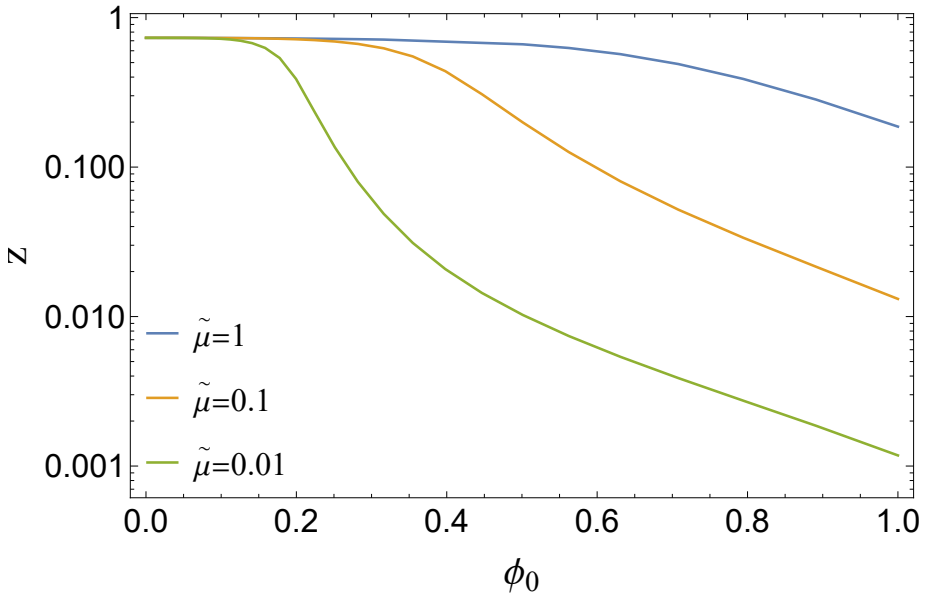

Figure 3.3: Position of the Polonyi field z during inflation. Different colors represent different choices of the relative SUSY breaking scale $\tilde{\mu}$. When $\tilde{\mu} \gg \phi_0^2$, the Polonyi field stays at $\sqrt{3}-1$, whereas for $\tilde{\mu} \ll \phi_0^2$ the Polonyi field stays close to the origin.

point conditions $V'(\phi_0) = V''(\phi_0) = 0$ up to ϕ_0^2 read:

$$\begin{aligned} V' = 0 &\Rightarrow 8\tilde{B}^2 + 18\sqrt{2}\tilde{B}\tilde{C}\phi_0 - 4\left(\sqrt{3}-2\right)\tilde{B}\tilde{\mu} + 18\tilde{C}^2\phi_0^2 - 3\sqrt{2}\left(\sqrt{3}-3\right)\tilde{C}\tilde{\mu}\phi_0 + 2\tilde{\mu}^2 = 0\,, \\ V'' = 0 &\Rightarrow 4\tilde{B}^2 + 18\sqrt{2}\tilde{B}\tilde{C}\phi_0 - 2\left(\sqrt{3}-2\right)\tilde{B}\tilde{\mu} + 27\tilde{C}^2\phi_0^2 - 3\sqrt{2}\left(\sqrt{3}-3\right)\tilde{C}\tilde{\mu}\phi_0 + \tilde{\mu}^2 = 0 \end{aligned} \tag{3.33}$$

with the following solutions:

$$\tilde{B} \approx 0.4952\tilde{\mu}\,, \quad \tilde{C} \approx -\frac{0.4996\tilde{\mu}}{\phi_0}\,. \tag{3.34}$$

The potential at the inflection point is then:

$$V(\phi_0) \approx 0.1872\,\mu^2\phi_0^2\,. \tag{3.35}$$

By Taylor expanding around the inflection point and substituting $\tilde{B} \to \tilde{B}(1-\delta B), \phi \to \phi_0(1-\delta\phi)$, we find:

$$\begin{aligned} \epsilon &\approx \frac{12.1\left(\delta B + 2.44\delta\phi^2\right)^2}{\phi_0^2}\,, \\ \eta &\approx \frac{21.6\delta B - 24.0\delta\phi}{\phi_0^2}\,. \end{aligned} \tag{3.36}$$

This expansion is similar in structure from the previous cases. Following the same procedure and

using $n_s = 0.9659$, $N_{\rm cmb} = 65$, we have:

$$\delta B = 4.45 \times 10^{-6} \phi_0^4 , \quad \epsilon_{\rm cmb} = 3.92 \times 10^{-10} \phi_0^6, \quad \alpha \approx -0.0013 . \tag{3.37}$$

We can further deduce the scales of SUSY breaking scale and inflation:

$$\mu = \tilde{\mu} D = 4.82 \times 10^{-8} \phi_0^2 , \quad H_{\rm inf} = 4.57 \times 10^{-9} \phi_0^3 , \quad m_\phi \approx 2\mu . \tag{3.38}$$

If the Polonyi field already sits in its SUSY breaking minimum during inflation, all relevant energy scales, i.e., Hubble scale $H_{\rm inf}$, the SUSY breaking scale μ, and inflaton mass m_ϕ, are completely determined by the position of inflection point ϕ_0. The scaling of $H_{\rm inf}$ and m_ϕ with ϕ_0 is also as in the non-SUSY version of the model, or as in the SUGRA model without Polonyi sector. The new feature is that ϕ_0, or $H_{\rm inf}$, also determines μ; again demanding $\mu > 1$ TeV therefore implies $\phi_0 > 2 \times 10^{-4}$ in this set-up. This strong correlation can only be relaxed by lifting the Polonyi field away from the SUSY breaking point $\sqrt{3} - 1$.

In Fig. 3.4, we show how different quantities depend on ϕ_0. For $\phi_0 \ll 1$ this is described by eqs.(3.38) and (3.37), while $\phi_0 \geq 1$ can again only be treated numerically. As before, we fix the spectral index n_s and the number of e-folds $N_{\rm cmb}$, and additionally $\tilde{\mu}$ for better illustration.

The Hubble parameter $H_{\rm inf}$ and the tensor-to-scalar ratio r have the same scaling with ϕ_0 as before. They both increase as ϕ_0 approaches unity, and start to decrease for $\phi_0 > 1$. The running of the spectral index is again almost independent of ϕ_0 and of the order of 10^{-3}. The scaling of the SUSY breaking scale μ is rather different. When $\phi_0 < 0.1$, the Polonyi field stays around the SUSY breaking point, and increases with ϕ_0 as eq.(3.38) suggested. When $\phi_0 > 0.1$, the Polonyi field is shifted away from the SUSY breaking point during inflation. This also leads to a milder increase of μ along ϕ_0. Once ϕ_0 exceeds 1, the SUSY breaking scale drops dramatically, which is similar to the behavior of m_ϕ in the previous case. Requiring $\mu \geq 1$ TeV therefore implies $\phi_0 \leq 5$ for this value of $\tilde{\mu}$.

So far we fixed $\tilde{\mu} = 0.01$. For $\phi_0 \ll 1$ this choice is in fact irrelevant, since the physical parameters B, δB, C and μ are all fixed uniquely for given ϕ_0, see eqs.(3.34), (3.37) and (3.38). However, we see in Fig. 3.5, which shows the relation between μ and $H_{\rm inf}$, that this is no longer true for $\phi_0 \geq 0.1$. Nevertheless, for a given Hubble scale during inflation there will be a maximum SUSY breaking scale it can host, corresponding to the case where SUSY is already broken by the Polonyi field:

$$\mu < \frac{4}{\phi_0} H_{\rm inf} \approx 3 \times 10^4 \left(\frac{H_{\rm inf}}{\rm GeV} \right)^{2/3} \text{GeV} . \tag{3.39}$$

Once the Polonyi field moves away from the SUSY breaking point, one will have more freedom to set the SUSY breaking value, depending on the position of the Polonyi field during inflation. If the Polonyi field stays at the origin and only perturbs the potential, the SUSY breaking scale would simply be $\mu = \tilde{\mu} \times D$, where D can be treated as a constant. This explains why the relative ratio of three different cases when they deviate from the straight line in Fig. 3.5 is almost a constant.

We conclude that only the light cyan region below the topmost line in Fig. 3.5 is accessible in our model. Different choices of $\tilde{\mu}$ will leave the straight line at different Hubble scales, and can thus populate this region, always keeping in mind that $\mu > 1$ TeV is needed for phenomenological reasons. The resulting lower bound on the Hubble scale during inflation is around 1 GeV. This bound is much smaller than the naive estimate of 10^8 GeV we derived below eq.(3.32) from the requirement that the Polonyi sector can be treated as a small perturbation.

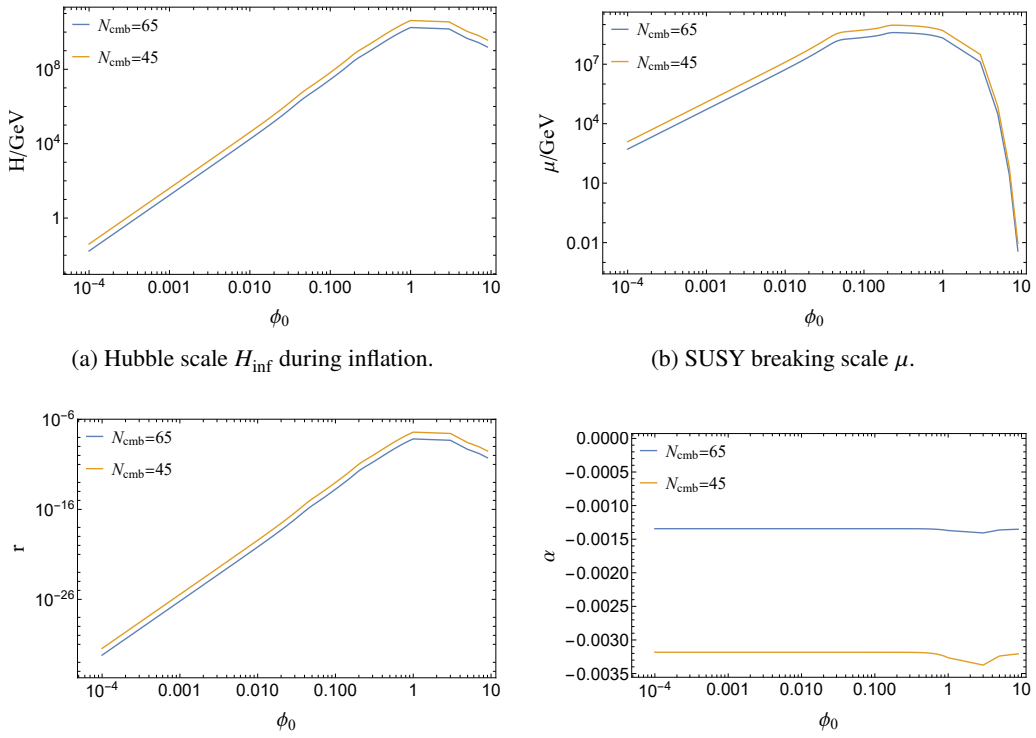

(a) Hubble scale $H_{\rm inf}$ during inflation.

(b) SUSY breaking scale μ.

(c) Tensor to scale ratio r.

(d) Running of spectral index α.

Figure 3.4: The dependence of the Hubble parameter during inflation $H_{\rm inf}$ (top left), the SUSY breaking scale μ (top right), the tensor-to-scalar ratio r (bottom left), and the running of spectral index α (bottom right) on ϕ_0. Different lines represent different choices for the number of e-folds: $N_{\rm cmb} = 65$ (blue) and $N_{\rm cmb} = 45$ (orange). We fixed $\tilde{\mu} = 0.01$, $n_s = 0.9659$ and $P_\zeta = 2.1 \times 10^{-9}$ in this graph.

3.3 Summary and Conclusions

In this chapter we revisited the renormalizable inflection point inflation model in the SUGRA framework. We adopted the minimal assumption that only one canonical field drives inflation. While SUSY protects the flatness of the potential from radiative corrections, local SUSY or SUGRA also modifies the potential through non-renormalizable terms. These new terms contribute to slow roll parameters on an equal footing. As in the non-supersymmetric case the shape of the potential is determined by the position ϕ_0 of the inflection point, which is a free parameter of our model. When fixing the well-constrained power spectrum of curvature perturbations and its spectral index, we find ϕ_0 controls the tensor-to-scalar ratio r, the running of the spectral index α, the Hubble scale during inflation $H_{\rm inf}$, and the physical inflaton mass m_ϕ.

For $\phi_0 \ll 1$ a perturbative treatment is possible. In this case, r, $H_{\rm inf}$ and m_ϕ are monomial functions of ϕ_0 and reach their maximum around $\phi_0 \approx 1$. The running of the spectral index α is almost independent of ϕ_0 but depends more strongly on $N_{\rm cmb}$ than in the non-supersymmetric, renormalizable version of the model. The tensor-to-scalar ratio r is always smaller than 10^{-7}, which is below the sensitivity of any current or planned experiments. The running of the spectral index, which lies in order of $O(-10^{-3})$, might be probed by the next generation of CMB experiments. The predictions of

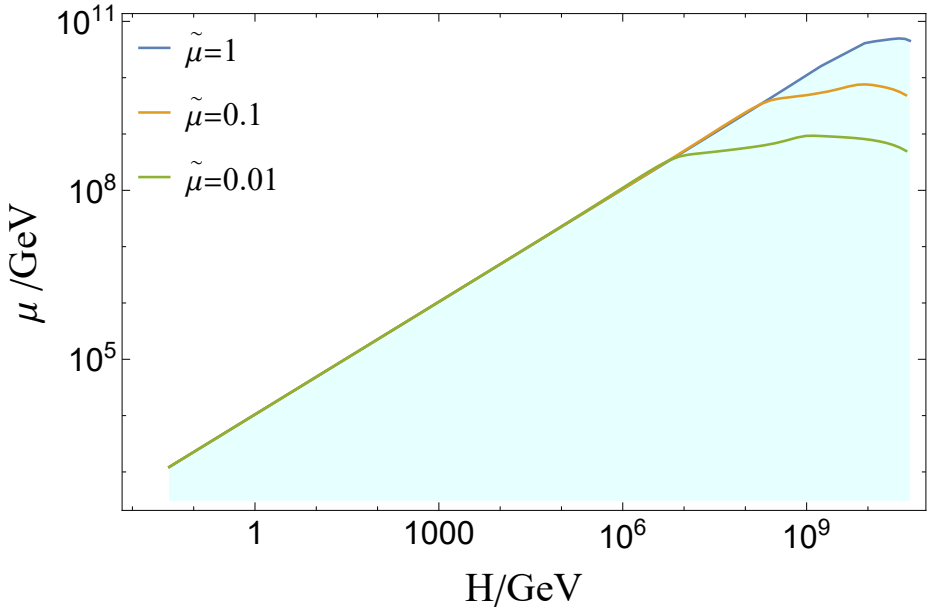

Figure 3.5: The scale of SUSY breaking μ vs. the inflationary Hubble scale H_{inf} on a log-log scale. Different colors represent different choices of relative scale $\tilde{\mu}$. The straight line is the Polonyi field dominated case, where the SUSY breaking scale only depends on the inflection point positions. The right, flat region is an inflation field-dominated region, where the SUSY breaking scale depends linearly on the relative scale $\tilde{\mu}$.

this SUGRA model are quite similar to those from the renormalizable model. All observables have the same scaling with respect to ϕ_0. Thus, even though the SUGRA potential contains terms up to ϕ^6 while the renormalizable potential only has terms up to ϕ^4, it still provides a relatively reliable estimate of inflationary quantities.

The main difference between the SUGRA case and the renormalizable case appears when ϕ_0 exceeds 1. In this region the exponential factor $e^{1/2\phi^2}$ in the SUGRA case becomes large, which suppresses r, H_{inf} and m_ϕ. The energy scales are therefore bounded from above: $H_{\text{inf}} < 10^{11}$ GeV and $m_\phi < 10^{12}$ GeV. The renormalizable potential is not able to capture this behavior, which leads to a very different prediction of inflationary observables in this large field scenario.

We further added a SUSY breaking Polonyi sector to the model. If the SUSY breaking scale is much smaller than the Hubble scale, the Polonyi field will stay at the origin and serve as a perturbation to the field. When these two energy scales become comparable, the Polonyi field will move away from the origin and modify the inflation potential. These effects lead to a nontrivial bound between the SUSY breaking scale and the inflation scale. We find that for a TeV scale SUSY breaking, we need the Hubble scale to be larger than 1 GeV.

It has been pointed out that in the KKLT model, the Hubble scale is always smaller than the gravitino mass $m_{3/2}$ (or SUSY breaking scale μ) [117]. In our model, we find a slightly different conclusion: in some regions, the Hubble scale can be larger than the gravitino mass. In such a scenario SUSY will protect the inflaton potential from loop corrections. This should allow larger couplings of the inflaton to Standard Model (super)fields, and thus larger reheat temperature than in the non–supersymmetric version.

In this chapter, we tried to be as simple as possible to relaize inflation in SUGRA. We have to pay

the price that our model parameters become finetuned and there is no symmetry which can protect them. In the next chapter, we will consider a slightly complicated model, but the flatness of the potential is linked with a certain symmetry.

CHAPTER 4

Modular Invariant Inflation

Modular symmetry and moduli fields (modulus) are ubiquitous in higher dimensional theory such as superstring theory [118–120]. The modulus generally denote the scalar degrees of freedom in the effective action of the four dimensional spacetime and describe low energy excitations in the extra dimensions such as the shape and size of the extra compact space. In the torus or orbifold compactification, the shape of the torus is determined by the complex modulus τ. The Yukawa couplings arise from the overlap integral of the zero mode profiles of the matter fields, and they are functions of τ transforming nontrivially under the modular symmetry group. The modulus τ and modular flavor symmetry are used to explain the flavor structure of quarks and leptons [74], see Refs. [121, 122] for reviews.

The modulus and modular symmetry could have phenomenological implications in cosmology, and the modulus can be a candidate for the inflaton to realize inflation in the early Universe [123]. It has been showed that successful inflation can not be realized with a single moduli field for the logarithmic Kähler potential [103, 124, 125]. A stabilizer field X besides the modulus τ was introduced in Refs. [126, 127] to build an inflation potential, and the Kähler potential modified by X was considered to flatten the scalar potential in the whole complex plane. Higher powers of τ are included in the logarithm of the Kähler potential to realize modular inflation in [128]. The modular invariance puts strong constraints on the scalar potential of the modulus [129–131], and the Starobinsky like model can arise in the context of modular symmetry [132].

The modular symmetry is broken by the vacuum expectation value (VEV) of the modulus field τ, and there is no VEV of τ which preserves the full modular symmetry group. Only after the complex modulus τ obtains a VEV, the modular forms and the Yukawa couplings get fixed. Hence the VEV of the complex modulus τ has to be dynamically stabilized. The extrema of the modular invariant scalar potentials tend to be close to the boundary of fundamental domain or the imaginary axis [133–142]. Particularly the fixed points $\tau = i, \omega$ are preferred extrema. Recently it is shown that either Minkowski minima or De Sitter (dS) minima at the fixed points can be achieved by considering non-perturbative corrections to the dilaton Kähler potential [133, 138, 140]. The scalar potential of the modulus can not only dynamically fix its VEV, but can also possibly accommodate inflation. It has been noticed that realizing slow roll inflation in the moduli sector is closely related to admitting metastable dS vacua [125].

The purpose of this chapter is to investigate whether the supergravity motivated potential [133] for modular stabilization, including dilation and non-perturbative effects, could also realize slow roll

inflation driven by the modulus τ. Motivated by the vacuum structure of τ and the special properties of the fixed points $i, \omega = e^{i2\pi/3}, i\infty$ under modular transformation, we shall consider inflationary trajectories along the boundary of fundamental domain, moving from one fixed point to another. After inflation, the modulus stays around the fixed point, which can be used to address the flavor mixing and fermion mass hierarchy in the SM [143–153]. We find that the scalar potential is strongly constrained by modular symmetry and a class of inflation potentials can be generated in this approach. The resulting predictions are all compatible with current cosmological observations. It is promising that the modular symmetry approach can help to explain the flavour puzzle and cosmic inflation in a coherent way.

The remainder of this chapter is organised as follows. In section 4.1, we introduce the setup of our model. The explicit form of the scalar potential is presented, and we emphasize its special features due to modular invariance. We study the slow roll inflation of the modulus τ rolling along the boundary of the fundamental domain in section 4.2. For the case that inflationary trajectory lies on the unit arc in the τ plane, the quadratic polynomial function $\mathcal{P}(j(\tau)) = 1 + \beta\left(1 - \frac{j(\tau)}{1728}\right) + \gamma\left(1 - \frac{j(\tau)}{1728}\right)^2$ is considered. Either of β or γ should be non-zero in order to reproduce the observed value of the spectral index. The ultra slow roll inflation could be realized if the inflaton τ rolls along the vertical boundary of fundamental domain. Section 4.3 contains a summary of our result and discussions of some possible further developments. We present the basic aspects of relevant modular forms in Appendix A.1. We present the numerical results for some examples of modular inflation models in Appendix A.2. Finally, we briefly discuss the stabilization of dilaton in Appendix A.3.

4.1 The Framework

Supergravity is the low-energy limit of superstring theory which is a promising candidate of quantum gravity, and it is predictive framework allowing to address both inflation and beyond standard model physics. Consequently we adopt the framework of supergravity in this thesis. In order to be more general, we do not use any concrete models of string theory and any specific compactification mechanism. In the following, we present the superpotential and Kähler potential from which the modular invariant scalar potential is derived. Then the properties of the scalar potential and the constraints on the parameter space of the scalar potential are explored.

4.1.1 Modular Invariant Scalar Potential in SUGRA

As an effective theory of superstring theory, the spectrum of a $N = 1$ supergravitry theory normally contains the dilaton, Kähler moduli, complex structure moduli, gauge fields, and twisted and untwisted matter fields after heterotic orbifold compactifications. Given the fact that a single Kähler moduli is not enough to realise inflation [103, 125], we find it is natural to include dilaton field into our analysis. This choice has been adopted in existing literature to study different phenomenon [133, 138]. In this chapter, the Kähler modulus field τ plays the role of inflaton field. The Kähler potential $\mathcal{K}$ can be expressed as

$$\kappa^2\mathcal{K}(\tau, \bar{\tau}, S, \bar{S}) = K(\tau, \bar{\tau}, S, \bar{S}) - h \ln\left[-i(\tau - \bar{\tau})\right] , \tag{4.1}$$

where $K(\tau, \bar{\tau}, S, \bar{S})$ is the Kähler potential for the dilaton, the parameter h is a dimensionless constant which depends on the choice of the number of compactified complex dimensions [126]. The effective

SUGRA description of the low-energy limit of superstring theory gives $h = 3$ [1]. At the tree level, there is no τ-dependence in the dilaton Kähler potential, hence $K(\tau, \bar{\tau}, S, \bar{S}) = -\ln(S + \bar{S})$. When we consider the non-perturbative contributions, the corresponding dilaton Kähler potential is given by

$$K(\tau, \bar{\tau}, S, \bar{S}) = -\ln(S + \bar{S}) + \delta k_{np}(S, \bar{S}) \equiv K(S, \bar{S}) \,, \tag{4.3}$$

where the additional term δk_{np} denotes the non-perturbative contribution from Shenker-like effects in heterotic string theories [154]. It provides non-perturbative corrections to Kähler potential within the $4D$ low-energy effective field theory, of the order of $O(e^{-1/g_s^2})$, where g_s^2 represents the closed string coupling constant. A general parametrization of δk_{np} is provided by [155, 156]:

$$\delta k_{np} = d \left(\frac{S + \bar{S}}{2} \right)^{p/2} \exp\left(-b \sqrt{\frac{S + \bar{S}}{2}} \right) , \tag{4.4}$$

where $p\,, b > 0$ and d is a real constant. The Shenker-term δk_{np} is crucial to stabilize the dilaton and realize heterotic de Sitter vacua [138].

The most general non-perturbative superpotential invariant under the modular symmetry reads [133]:

$$\mathcal{W}(S, \tau) = \Lambda_W^3 \frac{\Omega(S) H(\tau)}{\eta^6(\tau)} \,, \tag{4.5}$$

where Λ_W is the characteristic energy scale for this interaction. The function $\Omega(S)$ is technically arbitrary. It could take the form $\Omega(S) = c + e^{-S/b_a}$ [157], which arises from gaugino condensation. Here c is a constant and b_a is related to the beta function of gauge group factor. We will assume the dilation field is stabilized as a premise. We leave a short discussion on dilation stabilization in Appendix A.3. The modulus field τ would serve as the inflaton. The modular function $H(\tau)$ is regular in the fundamental domain without singularities, and its most general form is [133]:

$$H(\tau) = (j(\tau) - 1728)^{m/2} j(\tau)^{n/3} \mathcal{P}(j(\tau)) \,, \tag{4.6}$$

where $j(\tau)$ is the modular invariant j function given in eq.(A.20), $\mathcal{P}(j(\tau))$ is an arbitrary polynomial function of $j(\tau)$, and both m and n are non-negative integers. To simplify the analysis, we choose the polynomial to be second order in $j(\tau)$:

$$\mathcal{P}(j(\tau)) = 1 + \beta \left(1 - \frac{j(\tau)}{1728} \right) + \gamma \left(1 - \frac{j(\tau)}{1728} \right)^2 , \tag{4.7}$$

where β, γ are free real parameters. An equivalent parameterization of the H function is given by [133,

[1] In corresponding theory, the compactification of six dimensions will bring about three moduli τ_i $(i = 1, 2, 3)$ that corresponds to the radii of the three two-tori of the internal space and its standard form of Kähler potential [133]

$$\mathcal{K} = -\ln(S + \bar{S}) + \sum_{i=1}^{3} \ln\left[-i(\tau_i - \bar{\tau}_i) \right] , \tag{4.2}$$

for which $\mathcal{K}$ is completely symmetric under the exchange of the three τ_i. We consider the minimal case, the symmetric point with $\tau_1 = \tau_2 = \tau_3 = \tau$ that freezes all moduli fields except the single modulus τ. This gives $h = 3$.

138]:

$$H(\tau) = \left(\frac{G_4(\tau)}{\eta^8(\tau)}\right)^n \left(\frac{G_6(\tau)}{\eta^{12}(\tau)}\right)^m \mathcal{P}(j(\tau))\,, \tag{4.8}$$

where G_4 and G_6 are Eisenstein series of weight 4 and 6 respectively and their definition of G_4 and G_6 is given in eq.(A.4). From eqs. (A.20) and (A.21), one can see that the two expressions of the H function in eq.(4.6) and eq.(4.8) are equivalent up to a normalization constant. Notice that $H(\omega) = 0$ for $n \geq 1$ and $H(i) = 0$ for $m \geq 1$, as shown in eq.(A.28).

The scalar potential for dilaton field and modulus field with the Kähler potential in Eqs. (4.2,4.1) and the superpotential in eq.(4.5) is:

$$V(\tau, S) = \Lambda^4 Z(\tau, \bar{\tau}) \left[(A(S, \bar{S}) - 3)|H(\tau)|^2 + \hat{V}(\tau, \bar{\tau})\right]\,, \tag{4.9}$$

where we have defined $\Lambda = (\Lambda_W^6 \kappa^2 e^{K(S,\bar{S})} |\Omega(S)|^2)^{1/4}$ with

$$\begin{aligned} A(S, \bar{S}) &= \frac{K^{S\bar{S}} D_S W D_{\bar{S}} \bar{W}}{|W|^2} = \frac{K^{S\bar{S}} |\Omega_S + K_S \Omega|^2}{|\Omega|^2}\,, \\ \hat{V}(\tau, \bar{\tau}) &= \frac{-(\tau - \bar{\tau})^2}{3} \left| H_\tau(\tau) - \frac{3i}{2\pi} H(\tau) \widehat{G}_2(\tau, \bar{\tau}) \right|^2\,, \\ Z(\tau, \bar{\tau}) &= \frac{1}{i(\tau - \bar{\tau})^3 |\eta(\tau)|^{12}}\,, \end{aligned} \tag{4.10}$$

where the subscript in $\Omega_S = \partial\Omega/\partial S$ and $H_\tau = \partial H/\partial\tau$ denotes the derivative with respect to the specific field. $\widehat{G}_2$ is the non-holomorphic modular form of weight 2, and its definition can be found in the Appendix A.1. In addition, we see both the functions $\hat{V}$ and Z are modular functions with weight 0. We have assumed that the dilaton sector is stabilized, thus $A(S, \bar{S})$ is treated as a free parameter in the model. The $A(S, \bar{S})$ term is crucial for uplifting the potential. Once $A(S, \bar{S}) > 3$, we can guarantee that the potential in eq.(4.9) is positive semi-definite.

4.1.2 The Properties of the Modular Invariant Scalar Potential

The vacuum structure of this potential at $\tau = i$ and at $\tau = \omega = e^{i2\pi/3}$ has been extensively studied in [138], where they find the following results based on the choice of (m, n) in eq.(4.6):

- If $m = n = 0$, then both fixed points can have a de Sitter (dS) vacuum.
- If $m > 1, n = 0$, then $\tau = \omega$ is a dS minimum, while $\tau = i$ is Minkowski minimum.
- If $m = 0, n > 1$, then $\tau = i$ is a conditional dS minimum, which depends on the value of $A(S, \bar{S})$. $\tau = \omega$ is always a Minkowski minimum.
- If $m = 1, n > 0$ or $n = 1, m > 0$, the vacuum is unstable.
- If $m > 1, n > 1$, then we always have Minkowski extrema in these two fixed points.

The scalar potential in eq.(4.9) is modular invariant. Consequently the derivatives $\partial_\tau V$ and $\partial_{\bar{\tau}} V$ are weights (2,0) and (0,2) non-holomorphic modular functions respectively. Hence, they vanish at the

fixed points:

$$\left.\frac{\partial V}{\partial \tau}\right|_{\tau=i,\omega} = \left.\frac{\partial V}{\partial \bar{\tau}}\right|_{\bar{\tau}=i,\omega} = 0\,. \tag{4.11}$$

Moreover, the scalar potential is also invariant under $\tau \to -\bar{\tau}$. This can be proven by noticing the following transformation properties[2]:

$$\begin{aligned} \eta(\tau) &\to \eta(\tau)^*\,, \quad H(\tau) \to H(\tau)^*\,, \\ H_\tau &\to -H_\tau^*\,, \quad \hat{G}_2 \to \hat{G}_2^*\,. \end{aligned} \tag{4.12}$$

This fact comes from the reality of the scalar potential. Together with the modular transformations $\tau \to \tau + 1$ and $\tau \to -1/\tau$, they ensure the first derivative along certain directions at the boundary of the fundamental domain vanishes [133][3]:

$$\left.\frac{\partial V}{\partial Re(\tau)}\right|_{Re(\tau)=\pm 1/2,0} = 0\,, \qquad \left.\frac{\partial V}{\partial \rho}\right|_{\rho=1} = 0\,, \tag{4.13}$$

where we have used $\tau = \mathrm{Re}(\tau) + i\mathrm{Im}(\tau)$ in the first equality and $\tau = \rho e^{i\theta}$ in the second equality. If $\mathrm{Re}(\tau)$ or ρ sits in a local minimum, we can neglect the motion of them at the corresponding boundaries. In this case, we have a single field inflation. One explicit example can be find in section 4.2. Thus the modular symmetry provides a good reason to separate the modulus field to one inflaton field and another one perpendicular to inflation direction.

Motivated by the vacuum structure of modulus [138] and the special properties of fixed points $\tau = i, \omega = e^{i2\pi/3}$ under modular transformation, we shall consider two different trajectories of inflation along the boundary of fundamental domain:

- $m = 0, n \geq 2$, we consider slow roll along the lower boundary (arc) from one fixed point i to another fixed point ω.
- $m \geq 2, n \geq 2$, we consider slow roll along the left boundary from $i\infty$ to the fixed point ω.

We illustrate these two trajectories in Fig. 4.1. We will show some concrete examples below where the scalar potential is flat enough to accommodate inflation.

[2] We have assumed that the coefficients of the polynomial $\mathcal{P}(j)$ to be real.

[3] Let's write $\tau = x + iy$, where x and y are the real and imaginary parts of τ, respectively. The combined modular symmetry $\tau \to \tau + 1$ and reality condition $\tau \to -\bar{\tau}$ tell us that the potential is invariant under $x \to -x - 1$, $y \to y$ and $x = -1/2$ is a fixed point of the symmetry. Hence we have $V(x) = V(-x-1)$. Taking derivative with respect to x on both sides yields:

$$\left.\frac{\partial V(x)}{\partial x}\right|_{x=-1/2} = \left.\frac{\partial V(-x-1)}{\partial x}\right|_{x=-1/2} = -\left.\frac{\partial V(u)}{\partial u}\right|_{u=-1/2}\,,$$

where we have defined $u = -x - 1$. Hence, the derivative vanishes at the fixed points $x = \pm 1/2$. For the second case, we can express $\tau = \rho e^{i\theta}$. The combined transformations of $\tau \to -1/\tau$ and $\tau \to -\bar{\tau}$ indicate that the potential is invariant under $\rho \to 1/\rho, \theta \to \theta$. Hence $V(\rho)$=$V(1/\rho)$ and $\rho = 1$ is a fixed point of this transformation, and consequently we get

$$\left.\frac{\partial V(\rho)}{\partial \rho}\right|_{\rho=1} = \left.\frac{\partial V(1/\rho)}{\partial \rho}\right|_{\rho=1} = -u^2\left.\frac{\partial V(u)}{\partial u}\right|_{u=1} = -\left.\frac{\partial V(u)}{\partial u}\right|_{u=1}\,,$$

with $u = 1/\rho$. Thus the identiy $\left.\frac{\partial V(\rho)}{\partial \rho}\right|_{\rho=1} = 0$ is satisfied.

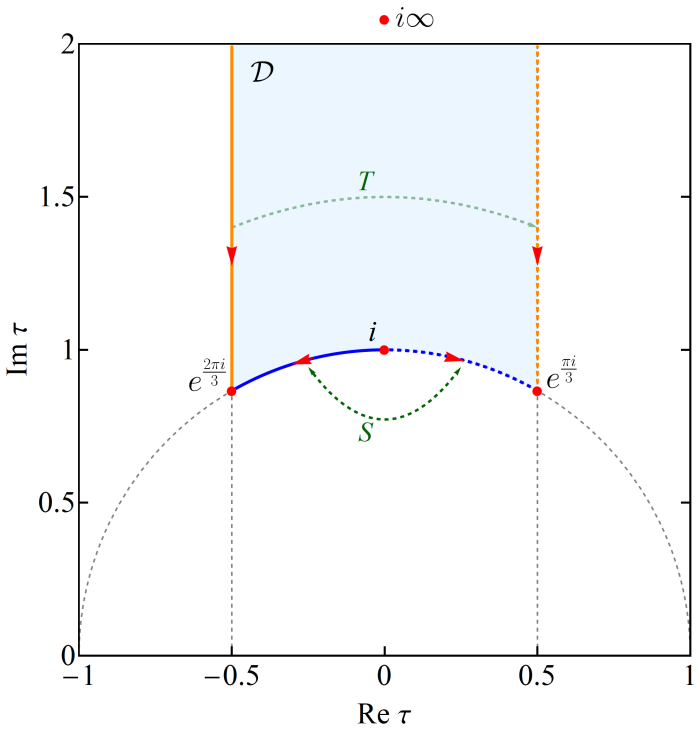

Figure 4.1: The light blue region represents the fundamental domain $\mathcal{D}$ of the modular group, while the blue line denotes the inflationary trajectory from maxima $\tau = i$ to minima $\tau = \omega = e^{i2\pi/3}$. Additionally, the blue dashed line depicts the inflaton slowly rolls from i to $-\omega^2 = e^{i\pi/3}$. Meanwhile, the orange line signifies the occurrence of accidental inflation to the point ω.

4.1.3 Constraints on the Scalar Potential from Inflation and Modular Stabilization

Let's first focus on the case where inflation occurs at the lower boundary. The modular symmetry fixed points $\tau = i, \omega$ play a special role in moduli stabilization, where they are separately considered to be a minimum [133, 138]. For inflation, we would like to have one of them to be the minimum of the scalar potential and another one to be the saddle point. We are interested in how they are connected. The saddle point of the potential could serve as the starting point for inflation. The minimum of the potential has to be stable, hence the possibility of $m = 1$ or $n = 1$ is excluded. The whole potential has to be non-negative in the fundamental domain, consequently we always require $A(S, \bar{S}) \geq 3$.

In the following, we explore the constraints on the parameters of the scalar potential from modular inflation. As mentioned earlier, in order to realize the slow roll inflation drived by τ, we would like one of the fixed points to be a saddle point and the other to be the minimum. This can not be achieved for $m \geq 2$ and $n = 0$, as both fixed points are local minima of the scalar potential. In principle, there exists a parameter space for $m = 0$ and $n = 0$ where $\tau = i$ is a saddle point and $\tau = \omega$ is a dS minimum. We may refer to $V(i)$ as the inflation scale and $V(\omega) \approx 10^{-122}$ as the cosmological constant today. However, the ratio of their value reads:

$$\frac{V(i)}{V(\omega)} = \frac{\Gamma^{18}(1/3)}{\Gamma^{12}(1/4)} \frac{|\mathcal{P}(1728)|^2}{|\mathcal{P}(0)|^2} \,. \tag{4.14}$$

Thus for a TeV scale inflation where $V(i) \approx 10^{-30}$, we need $|\mathcal{P}(1728)|^2/|\mathcal{P}(0)|^2 \approx 10^{90}$. Given that $j(\tau)$ varies by only 10^3 from $\tau = i$ to $\tau = \omega$, it seems very unnatural to consider such a huge difference in the polynomial $\mathcal{P}(j)$. Hence we do not consider the choice $m = n = 0$ in this chapter.

Another possibility is $n \geq 2$ and $m = 0$ where $\tau = i$ is a saddle point and $\tau = \omega$ is a global minimum with $V(\omega) = 0$. To explicitly discuss this possibility, we should calculate the Hessian matrix at the fix points. The first derivative of the scalar potential vanishes and the second derivatives at $\tau = i$ read:

$$\partial_\tau^2 V\Big|_{\tau=i} = -C_n(A-1)\mathcal{B}_n\,, \quad \partial_\tau\partial_{\bar{\tau}} V\Big|_{\tau=i} = C_n(A-2+|\mathcal{B}_n|^2)\,. \tag{4.15}$$

where the functions $\mathcal{B}_n$ and C_n are:

$$\begin{aligned} \mathcal{B}_n &\equiv \frac{\Gamma^8(1/4)}{192\pi^4}\left(1+8n+41472\frac{\mathcal{P}'(1728)}{\mathcal{P}(1728)}\right)\,, \\ C_n &\equiv \frac{(2\pi)^9 4^{2n-1}3^{2n+1}}{\Gamma^{12}(1/4)}\,|\mathcal{P}(1728)|^2\,, \end{aligned} \tag{4.16}$$

where $\mathcal{P}'(j) \equiv d\mathcal{P}/dj$ is the derivative of the polynomial function $\mathcal{P}(j)$ with respect to j. For inflation along the unit arc in the complex τ plane, it is convenient to calculate the Hessian matrix in the polar coordinates $\tau = \rho e^{i\theta}$, and the elements of the Hessian matrix at the starting point $\tau = i$ are determined to be:

$$\begin{aligned} \frac{\partial^2 V}{\partial\rho^2} &= 2C_n\left[A-2+|\mathcal{B}_n|^2+(A-1)\mathrm{Re}(\mathcal{B}_n)\right]\,, \\ \frac{\partial^2 V}{\partial\theta^2} &= 2C_n\left[A-2+|\mathcal{B}_n|^2-(A-1)\mathrm{Re}(\mathcal{B}_n)\right]\,, \\ \frac{\partial^2 V}{\partial\theta\,\partial\rho} &= -2C_n(A-1)\mathrm{Im}(\mathcal{B}_n)\,. \end{aligned} \tag{4.17}$$

From eq.(4.16), we see that C_n is a positive number and the imaginary part of $\mathcal{B}_n$ vanishes at $\tau = i$, since the coefficients of the polynomial $\mathcal{P}(j)$ are real in our setting and thus $\mathcal{P}$ is real at $\tau = i$. Consequently the cross derivative $\frac{\partial^2 V}{\partial\theta\,\partial\rho}$ is exactly zero at $\tau = i$. In fact, this cross derivative is always vanishing anywhere at the boundary $|\tau| = 1$ of the fundamental domain, as can be seen from the footnote 3. For the inflaton τ rolling along the unit arc, the scalar potential at the starting point $\tau = i$ should reach a maximum along angular direction θ while it gets a minimum along the radial direction ρ. As a consequence, the following conditions should be satisfied [4]

$$\frac{\partial^2 V}{\partial\rho^2}\Big|_{\tau=i} > 0\,, \quad \frac{\partial^2 V}{\partial\theta^2}\Big|_{\tau=i} < 0\,, \quad V(i) > 0, \tag{4.19}$$

[4] The scalar potential at $\tau = i$ is

$$V(i) = \Lambda^4(A-3)12^{2n}\frac{(2\pi)^9}{\Gamma^{12}(1/4)}\,|\mathcal{P}(1728)|^2\,. \tag{4.18}$$

which leads to

$$A > 2 + \mathcal{B}_n\,, \qquad \mathcal{B}_n > 1\,. \tag{4.20}$$

The condition $\mathcal{B}_n > 1$ restricts the polynomial parameter in eq.(4.7) as follow,

$$\beta < \frac{1}{24}\left(8n + 1 - \frac{192\pi^4}{\Gamma^8(1/4)}\right)\,. \tag{4.21}$$

Moreove, another condition $A > 2 + \mathcal{B}_n$ can be written into a more suggestive form:

$$A > \frac{\Gamma^8(1/4)}{192\pi^4}\,(1 + 8n - 24\beta) + 2\,. \tag{4.22}$$

In particular, when $\beta = 0$ and $n = 2$, the parameter A should be greater than 29.132. Besides the local properties of the scalar potential at the fix points, we would also like to impose an additional constraint along the inflationary trajectory $\pi/2 < \theta < 2\pi/3$:

$$\left.\frac{\partial V}{\partial \theta}\right|_{\rho=1} < 0\,, \quad \left.\frac{\partial^2 V}{\partial \rho^2}\right|_{\rho=1} > 0\,, \tag{4.23}$$

where the first condition ensures that the inflaton smoothly rolls down to the minimum at $\tau = \omega$, and the second one ensures $\rho = 1$ is a local minimum along the inflation trajectories. The algebraic expression for this condition is rather complicated and we solve it numerically. The first constraint is demonstrated in Fig. 4.2 and the second one is verified for each inflation potentials.

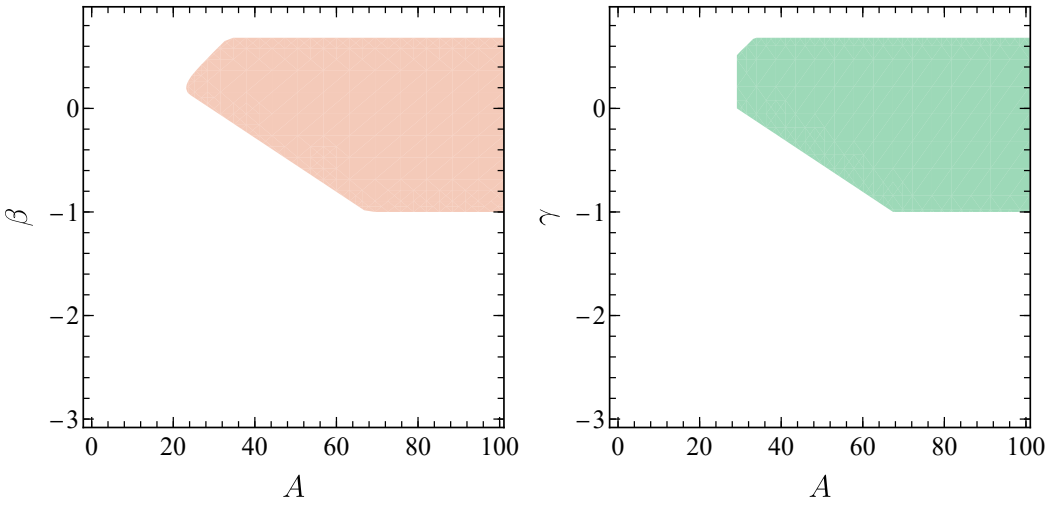

Figure 4.2: In the left panel, we examine the parameter space (A, β) with $\gamma = 0$, constrained by the condition $\partial V/\partial\theta < 0$. Similarly, the right panel explores the parameter space (A, γ) with $\beta = 0$. Here, we illustrate this concept using the example $n = 2$.

The potential at the fixed point $\tau = \omega$ or $\tau = -\omega^2$ is much simpler, we have:

$$V(\omega) = 0\,, \quad \partial_\tau^2 V(\omega) = 0\,, \quad \partial_\tau \partial_{\bar{\tau}} V(\omega) \geq 0\,. \tag{4.24}$$

From eq.(4.9), as long as $A \geq 3$ the potential is non-negative in the whole complex space. Hence, $V(\omega) = 0$ is enough to ensure $\tau = \omega$ is a global minimum of the scalar potential.

4.2 Modular Invariant Inflation

In this section, we shall show that the scalar potential in eq.(4.9), which has been used to address the modulus stabilization [133, 138], can also naturally realize the slow roll inflation. We are concerned with the inflationary trajectories along the boundary of fundamental domain in the following.

4.2.1 Slow Roll along the Unit Arc

In this scenario, it might be useful to rewrite the scalar potential in terms of the radial and angular components, $\tau = \rho e^{i\theta}$. The kinetic term of the modulus reads as,

$$\mathcal{L}_{\rm kin} = \frac{\partial^2 \mathcal{K}}{\partial\tau\partial\bar{\tau}}\partial_\mu\tau\partial^\mu\bar{\tau} = \frac{3}{(-i\tau + i\bar{\tau})^2}\partial_\mu\tau\partial^\mu\bar{\tau} = \frac{3}{4\sin^2\theta}\left(\frac{1}{\rho^2}\partial_\mu\rho\partial^\mu\rho + \partial_\mu\theta\partial^\mu\theta\right) . \tag{4.25}$$

As shown in eq.(4.13), the modular invariance of the scalar potential requires $\partial V/\partial\rho|_{\rho=1} = 0$. Here and hereafter, we will always set $\rho = 1$ and keep θ as the only degree of freedom. To normalize the kinetic term of θ, we further introduce the canonical field $\phi = \sqrt{3/2}\ln(\tan(\theta/2))$. As an example, we have $\phi = 0$ when $\theta = \pi/2$.

In this section, we consider the case where $m = 0, n \geq 2$ in eq.(4.6). This potential has a local maximum at $\tau = i$ and a local Minkowski minimum at $\tau = \omega$. As mentioned earlier, the modular symmetry ensures that the first derivative of the potential vanishes at $\tau = i$, which motivates us to investigate the inflation near this point. The inflation trajectory is shown in Fig. 4.1. The inflation phenomenology can be approximated by its Taylor expansion near $\tau = i$ ($\phi = 0$). The full potential in eq.(4.9) can be approximated by the following term during inflation:

$$V(\phi) = V_0(1 - \sum_{k=1}^{\infty} C_{2k}\phi^{2k}) , \tag{4.26}$$

where each coefficient depends on the choice of $A(S, \bar{S}), (m, n)$ and the parameterzation of the polynomial function $\mathcal{P}(j)$. Note that the potential is an even function of ϕ, which arises from the $\mathcal{S}$ symmetry of the modular group. Along the arc, the $\mathcal{S}$ symmetry $\tau \to -1/\tau$ indicates a Z_2 symmetry in terms of the canonically normalised field $\phi \to -\phi$. We will focus on the case where $\phi > 0$. During inflation, we find the potential is mostly dominated by the terms $C_2\phi^2$ and $C_{2p}\phi^{2p}$, where p is a specific integer. This implies that $0 < |C_{2p'}| \ll C_{2p}$ for all $p' < p$. Let's first investigate this simplified potential:

$$V(\phi) = V_0(1 - C_2\phi^2 - C_{2p}\phi^{2p}) , \tag{4.27}$$

The slow-roll parameters read:

$$\begin{aligned}\varepsilon_V &= \frac{1}{2}\left(\frac{V'}{V}\right)^2 = \frac{1}{2}\left(\frac{-2C_2\phi - 2pC_{2p}\phi^{2p-1}}{1 - C_2\phi^2 - C_{2p}\phi^{2p}}\right)^2 , \\ \eta_V &= \frac{V''}{V} = \frac{-2C_2 - 2p(2p-1)C_{2p}\phi^{2p-2}}{1 - C_2\phi^2 - C_{2p}\phi^{2p}} ,\end{aligned} \tag{4.28}$$

where $C_2 \ll C_{2p}$ and $C_{2p} \gg 1$. We are interested in the region where $\phi \ll 1$, which means $\varepsilon_V \approx (\eta_V\phi)^2 \ll \eta_V$. Note the starting point of the observable inflation, ϕ_*, can be calculated from:

$$n_s = 1 - 6\epsilon(\phi_*) + 2\eta(\phi_*) \approx 1 + 2\eta(\phi_*) \approx 1 - 4C_2 - O(\phi_*^2) , \tag{4.29}$$

and the CMB observation suggests $n_s \approx 0.9649$ [49]. For our setup, we would require $1 - 4C_2 > n_s$; otherwise, the spectral index will be smaller than the observed value of CMB. This approximately implies $0 < C_2 < 0.008$.

The starting point ϕ_* and end point ϕ_e of observable inflation are controlled by η and corresponding field values are given by,

$$\begin{aligned}\phi_* &\approx \left(-\frac{\eta_* + 2C_2}{2p(2p-1)C_{2p}}\right)^{\frac{1}{2p-2}} , \\ \phi_e &\approx \left(-\frac{\eta_e + 2C_2}{2p(2p-1)C_{2p}}\right)^{\frac{1}{2p-2}} ,\end{aligned} \tag{4.30}$$

where we have defined $\eta_* = (n_s - 1)/2$, $\eta_e = -1$, and used approximation $1 - C_2\phi^2 - C_{2p}\phi^{2p} \approx 1$. This can be verified by substituting the above solution into the expression, which is suppressed by large C_{2p}. The number of e-folds is given by,

$$\begin{aligned}N_e &= \int_{\phi_*}^{\phi_e} \frac{1}{\sqrt{2\varepsilon_V(\phi)}} d\phi \\ &\approx \int_{\phi_*}^{\phi_e} \frac{1}{2C_2\phi + 2pC_{2p}\phi^{2p-1}} d\phi \\ &= \frac{\ln\left(2pC_{2p} + 2C_2\phi^{2-2p}\right)}{2C_2(2p-2)}\Bigg|_{\phi_*}^{\phi_e} \\ &= \frac{1}{2C_2(2p-2)}\left(\ln\frac{\eta_e + (4-4p)C_2}{\eta_e + 2C_2} - \ln\frac{\eta_* + (4-4p)C_2}{\eta_* + 2C_2}\right) ,\end{aligned} \tag{4.31}$$

which initially decrease with C_2 and then increases with it in the region where $0 < C_2 < 0.008$. The minimum of e-folds, $N_{e,\min}$, is approximately 77 for $n_s = 0.9649$ and $p = 2$, and approximately 50 for $n_s = 0.9649$ and $p = 3$. Thus $p = 2$ always generates too many e-folds, while $p \geq 3$ could be consistent with our current observations. It is therefore necessary to ensure C_2 and C_4 are much smaller than C_6 in the expansion.

We will address the coefficients C_{2n} in the following section. To do this, we need the local expansion of the j-invariant and η functions in terms of the canonically normalized field ϕ:

$$\begin{aligned} j(\phi) &\approx 1728(1 - 9.579\phi^2 + 40.142\phi^4 - 102.618\phi^6) + \mathcal{O}\left(\phi^8\right) , \\ |\eta(\phi)| &\approx 0.768 + 0.083\phi^2 - 0.028\phi^4 + 0.005\phi^6 + \mathcal{O}\left(\phi^8\right) , \end{aligned} \tag{4.32}$$

and the explicit form of the polynomial $\mathcal{P}(j)$. For illustration, we will consider the quadratic form of $\mathcal{P}(j)$ parameterized as:

$$\mathcal{P}\left(j(\tau)\right) = 1 + \beta\left(1 - \frac{j}{1728}\right) + \gamma\left(1 - \frac{j}{1728}\right)^2 + \dots . \tag{4.33}$$

As one can see from eq.(4.32), the parameter β controls the ϕ^2 term, while γ governs the ϕ^4 term in the polynomial $\mathcal{P}(j)$. The overall factor V_0 of the scalar potential is determined to be

$$V_0 = \frac{12^{2n}(2\pi)^9}{\Gamma^{12}(1/4)}\Lambda^4\left[A(S,\bar{S}) - 3\right] . \tag{4.34}$$

We start our study by considering the simplest case, $P(j) = 1$. In this scenario, the shape of the potential is entirely determined by the dilaton contribution $A(S,\bar{S})$. The potential can then be approximated by:

$$\begin{aligned} C_2 =& 0.298 + 6.386n - \frac{0.178 + (7.617 + 81.554n)n}{A - 3} , \\ C_4 =& -0.438 + 1.917n - 20.389n^2 + \frac{0.992 + 14.387n - 122.250n^2 + 520.779n^3}{A - 3} , \\ C_6 =& 0.234 + 9.024n - 18.321n^2 + 43.398n^3 \\ &+ \frac{-1.998 - 23.195n - 718.051n^2 + 1247.593n^3 - 1662.767n^4}{A - 3} . \end{aligned} \tag{4.35}$$

The requirement for $0 < C_2 < 0.008$ imposes an algebraic constraint on A:

$$3.596 + 12.771n < A < 3.612 + 12.771n , \tag{4.36}$$

which suggests that A is tightly constrained. In this case, the corresponding C_4 and C_6 are given by:

$$\begin{aligned} C_4 &\approx 1.228 + n(-9.571 + 20.389n) , \\ C_6 &\approx 1.289 - \frac{0.206}{0.047 + n} + n\left[-52.076 + (85.482 - 86.797n)n\right] . \end{aligned} \tag{4.37}$$

For $n = 2$, this roughly means $A \approx 29.142$, $C_4 \approx 63.640$ and $C_6 \approx -455.408$. One can extend these results easily for general n. Even though $\left|C_6\right| > C_4$, we have verified that the ϕ^4 contribution is larger than the ϕ^6 contribution during inflation, and the end of the inflation is controlled by the ϕ^4 term. It is also interesting to consider the cases with large n. Note C_4 scales as n^2 while C_6 scales as n^3, which might raise concerns that the later term will eventually outgrows the former. However, this is not the

case. We can examine their relative contributions at the end of inflation, where the $C_6\phi^6$ contributes the most. Using eq.(4.30) with $p = 2$ and maintaining the assumption that $C_4\phi^4$ is much larger than $C_6\phi^6$, we have:

$$\phi_e^2 = \frac{1}{12C_4}, \qquad \frac{C_6\phi^6}{C_4\phi^4} = \frac{C_6}{12C_4^2} \propto \frac{1}{n}, \tag{4.38}$$

which tells us that the relative contribution of the $C_6\phi^6$ term is suppressed by large n. These results perfectly align with our assumption, confirming that higher-order terms never dominate the potential. Meanwhile, the relative large coefficient C_4 leads to an overproduction of the number of e-folds if we choose n_s to be around its central value. i.e. To achieve $50 < N_e < 60$, n_s must be smaller than the CMB measurement. Theoretical prediction for this case can be found in Fig. 4.3. We use solid and dashed lines to represent the results for $N_e = 50$ and $N_e = 60$, respectively, with different colors labeling different choices of n. Increasing n does not change the preferred region of the spectral index but does decrease the tensor to scalar ratio. However, the spectral index lies between 0.942 and 0.955, which is excluded by the Planck 2018 results. Thus, we conclude that while the simplest choice of $\mathcal{P}(j)$ can support inflation, it does not fit our observational constraints within this framework.

The next simplest choice would be $\beta \neq 0$. In this case, we have two free parameters: A and β, with two algebraic constraints: $0 < C_2 < 0.008$ and $0 < C_4 \ll C_6$. The additional β dependent terms in C_2, C_4, C_6 are given by:

$$\begin{aligned}
C_2 =& C_2|_{\beta=0} + C_{2,\beta} \\
=& C_2|_{\beta=0} - 19.157\beta + \frac{-733.987\beta^2 + 22.851\beta + 489.325\beta n}{A-3}, \\
C_4 =& C_4|_{\beta=0} + C_{4,\beta} \\
=& C_4|_{\beta=0} - 91.748\beta^2 + \beta(85.997 + 122.331n) \\
&+ \frac{\beta^2(12741.904 + 9374.025n) + \beta(-262.043 - 3953.512n - 4687.013n^2)}{A-3}, \\
C_6 =& C_6|_{\beta=0} + C_{6,\beta} \\
=& C_6|_{\beta=0} + \beta^2(796.369 + 585.877n) - \beta(237.566 + 475.949n + 390.584n^2) \\
&+ \frac{\beta^2(106147.206 + 133975.980n + 52377.172n^2)}{A-3} \\
&- \frac{\beta(1383.980 + 16226.188n + 26183.928n^2 + 19953.208n^3)}{A-3},
\end{aligned} \tag{4.39}$$

where we have separated the coefficients into β dependent and independent terms. The $C_{2,4,6}|_{\beta=0}$ are the same as those given in eqs. (4.35). The solution for $0 < C_2 < 0.008$ is:

$$3.596 - 38.314\beta + 12.771n < A < 3.612 - 38.314\beta + 12.771n\,. \tag{4.40}$$

We further choose $-2 < C_4 < 5$, such that $|C_4| \ll C_6$. If $C_4 \gg 1$, the inflation potential will be dominated by the ϕ^4 term. We have argued such a case is ruled out by the small spectral index n_s.

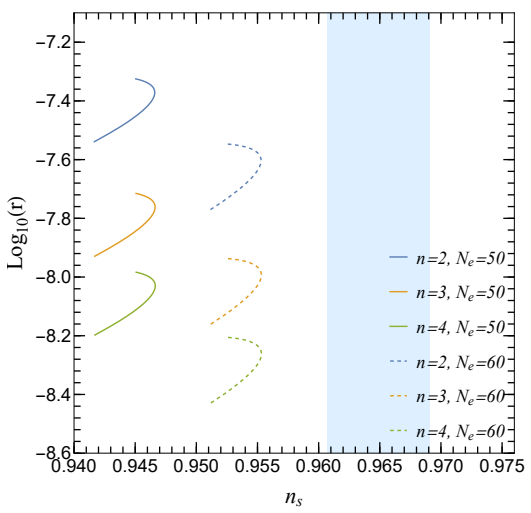

(a) $\mathcal{P}(j) = 1$.

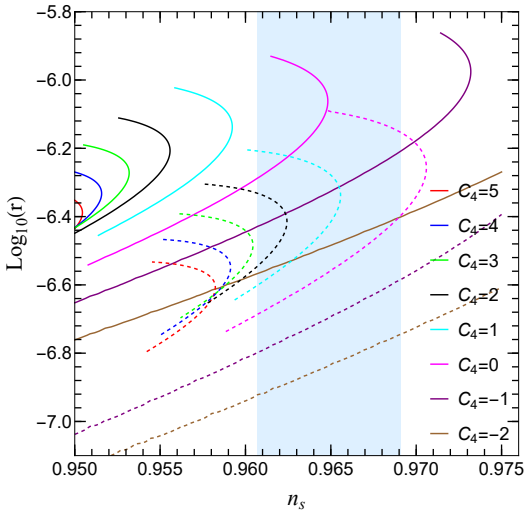

(b) $\mathcal{P}(j) = 1 + \beta(1 - j/1728)$.

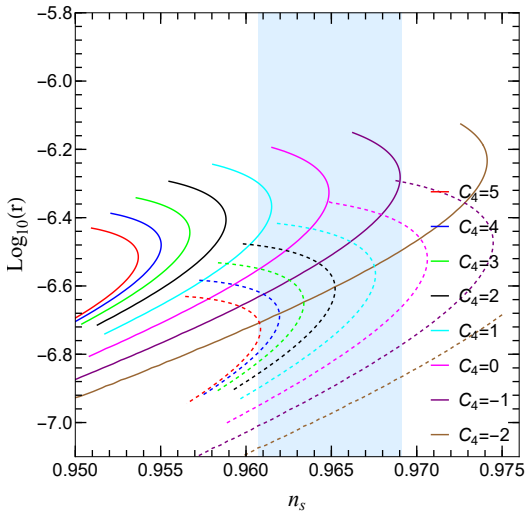

(c) $\mathcal{P}(j) = 1 + \gamma\,(1 - j/1728)^2$.

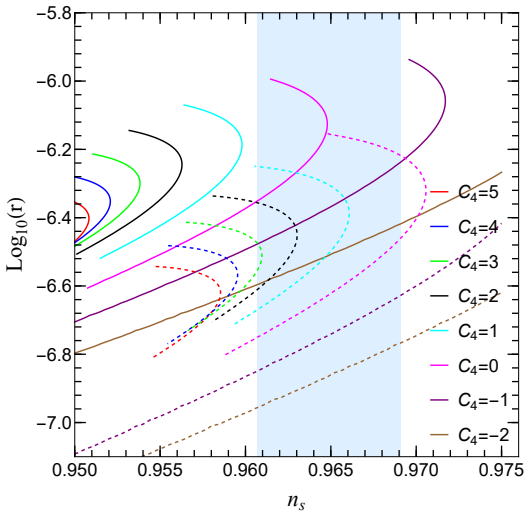

(d) $\mathcal{P}(j) = 1 + \beta(1 - j/1728) + \gamma\,(1 - j/1728)^2$.

Figure 4.3: We present theoretical predictions of modular invariant inflation with different choices of the polynomial $\mathcal{P}(j)$. When $\mathcal{P}(j) = 1$, the parameter A varies within the region $3.596 + 12.771n < A < 3.612 + 12.771n$ given by eq.(4.36). Conversely, when $\mathcal{P}(j) \neq 1$, we fix $n = 2$ for plotting purposes. Additionally, we select C_2 and C_4 as the physical parameters and plot the lines by varying C_2 while holding C_4 constant. In the last panel, we set $A(S, \bar{S}) = 25$. The x-axis represents the spectral index of the CMB power spectrum n_S, while the y axis is the tensor-to-scalar ratio r on a logarithm scale. Solid lines indicate predictions for $N_e = 50$, whereas dashed lines are the predictions for $N_e = 60$. Different colors denotes varying choices of C_4.

When $C_4 < -2$, it will create additional maximum along the inflation trajectory. The solution reads [5]:

$$\begin{aligned} n &= 2, \quad 0.1261 < \beta < 0.1268\,, \\ n &= 3, \quad 0.2450 < \beta < 0.2454\,, \\ n &= 4, \quad 0.3752 < \beta < 0.3755\,. \end{aligned} \tag{4.41}$$

[5] There are other solutions; however, they introduce additional barriers between the inflation point and the minimum of the potential. Thus we will ignore them in this chapter.

Plugging the above solution into C_6, we find $C_6 \approx 350$ for $n = 2$. As in this case $C_2, C_4 \ll C_6$, we find that this setup can generate inflation potential that agrees with CMB observations. We show a possible shape of the potential and its cross-section in Fig. 4.4. Theoretical predictions for this case can be found in Fig. 4.3 where $n = 2$ is used as an example. It is straightforward to extend our results to $n > 2$. We use different colors to label different choice of C_4. Solid and dashed lines represent results for $N_e = 50$ and $N_e = 60$, respectively. The latter cases are slightly shifted towards a smaller tensor-to-scalar ratio and lager spectral index. Increasing C_4 will decrease the spectral index and vice versa, as expected. As one can see from the figures, the spectral index n_s can be in the 1σ region constrained by the CMB observation, while the tensor-to-scalar ratio r is of order $O(10^{-6})$. This is well below the current sensitivity. The running of spectral index α is of order $O(-10^{-4})$, which might be testable in the CMB S4 mission [112, 113] and future observations of 21 cm fluctuations [111, 114]. We also show the parameter space spanned by $A(S, \bar{S})$ and β in Fig. 4.5. The left and right segments are results for $N_e = 50$ and $N_e = 60$, respectively. We use different color to represent different values of spectral index n_s.

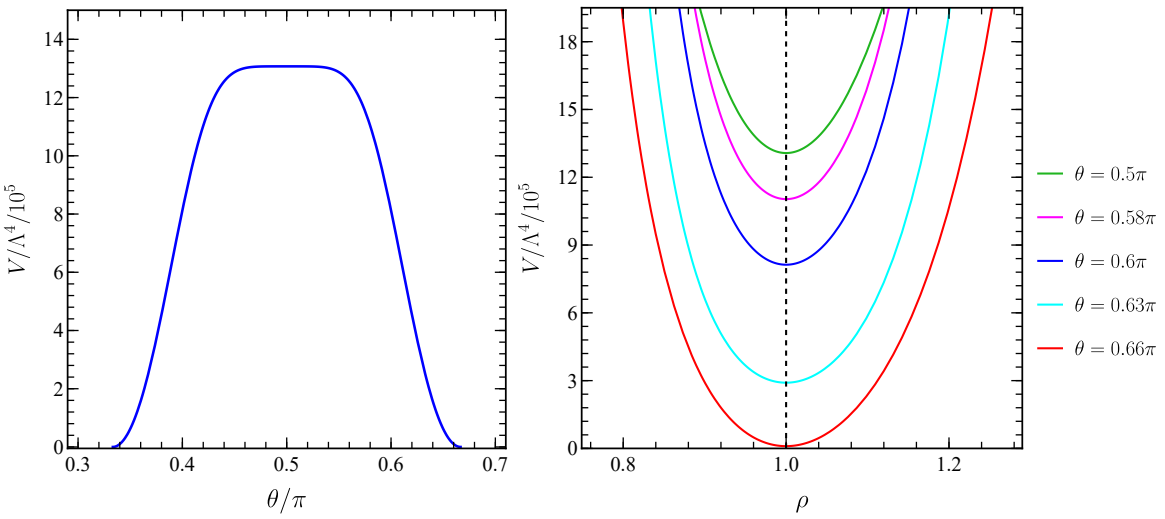

Figure 4.4: When the potential has parameters $m = 0$, $n = 2$, $A = 24.3091$, and $\beta = 0.126425$, the left panel demonstrates the cross-section of the scalar potential via $\rho = 1$ during inflation. Similarly, the right panel displays the cross-sections of scalar potential via various θ values throughout the inflationary process.

The next simple choice would be to turning on the ϕ^4 contribution in $\mathcal{P}(j)$ by introducing a non-zero value of γ. In this case, C_2 remains unchanged while C_4 and C_6 get additional contribution, which we

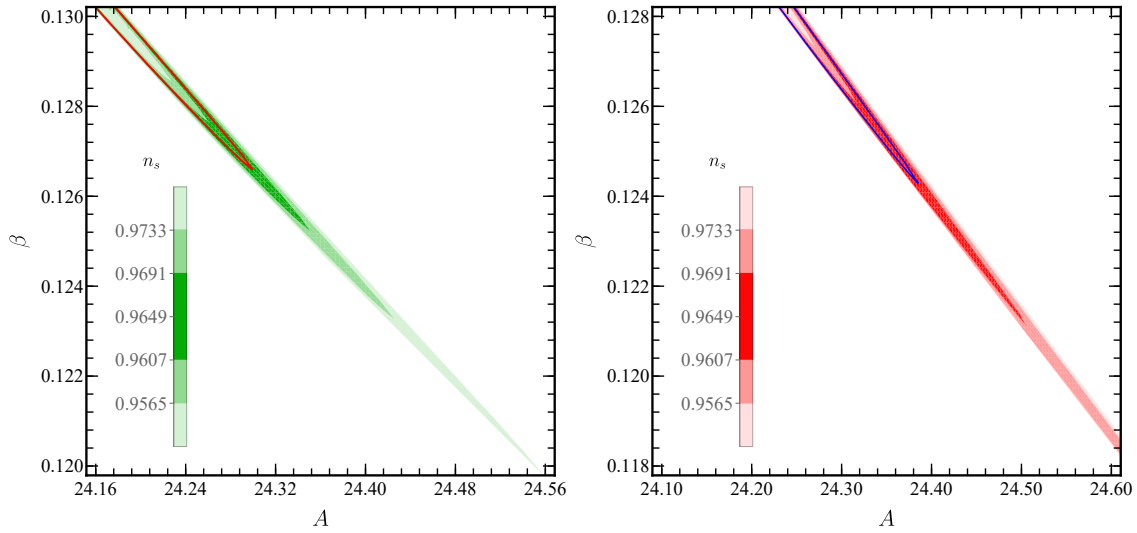

(a) $\mathcal{P}(j) = 1 + \beta(1 - j/1728)$,

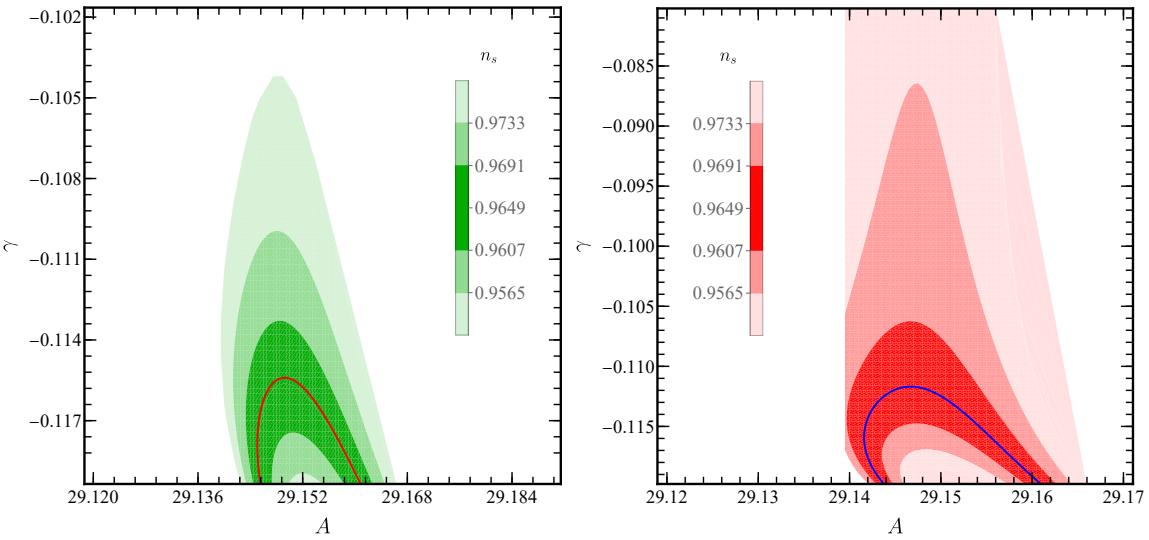

(b) $\mathcal{P}(j) = 1 + \gamma\,(1 - j/1728)^2$.

Figure 4.5: These panels illustrate contour plot of the spectral index n_s across the parameter planes (A, β)(upper sector) and (A, γ)(lower sector). In the left segment, the deep green region displays the 68% CL region, with the red line indicating the contour of central value of n_s for 50 e-folds. The right segment demonstrates the distribution of n_s, with the deep red region and blue line representing 68% CL region and its isopleth of central value for 60 e-folds, as documented in [49]. Furthermore, it's important to note that these panels adhere entirely to the constraint specified in eq.(4.22).

denote by $C_{4,\gamma}$ and $C_{6,\gamma}$:

$$\begin{aligned} C_2 =& C_2|_{\gamma=0}\,, \\ C_4 =& C_4|_{\gamma=0} + C_{4,\gamma} \\ =& C_4|_{\gamma=0} - 183.497\gamma + \frac{(437.766 + 9374.025n)\gamma}{A-3}\,, \\ C_6 =& C_6|_{\gamma=0} + C_{6,\gamma} \\ =& C_6|_{\gamma=0} + \gamma(1171.753n + 1592.738) \\ &+ \frac{-269368.311\gamma^2 - 6821.952\gamma - 113625.201n\gamma - 74824.531n^2\gamma}{A-3}\,. \end{aligned} \tag{4.42}$$

Since C_2 is unchanged, the solution for $0 < C_2 < 0.008$ remains the same as in the $\mathcal{P}(j) = 1$ case:

$$3.596 + 12.771n < A < 3.612 + 12.771n\,. \tag{4.43}$$

Again requiring $-2 < C_4 < 5$, γ is constrained to be:

$$\begin{aligned} n =&2, \quad -0.119 < \gamma < -0.106\,, \\ n =&3, \quad -0.287 < \gamma < -0.274\,, \\ n =&4, \quad -0.529 < \gamma < -0.516\,. \end{aligned} \tag{4.44}$$

These conditions ensure C_2 and C_4 are much smaller than C_6, so that the ϕ^2 and ϕ^6 terms dominate during inflation. We demonstrate the theoretical prediction for $n = 2$ in Fig. 4.3. There is no surprise that the prediction is similar to the previous case where we choose $\beta \neq 0$. Both cases have similar local expansion and inflation trajectory. The spectral index n_s can again lie in the 1σ region constrained by the CMB observation, while the tensor-to-scalar ratio r is of order $O(10^{-6})$ and the running of spectral index α is of order $O(-10^{-4})$. We also show the parameter space spanned by $A(S, \bar{S}), \gamma$ in Fig. 4.5. The left and right segments represent results for $N_e = 50$ and $N_e = 60$, respectively. We use different color to represent different values of spectral index n_s.

In the last example, we can choose A as a free parameter and deduce the value for β and γ accordingly. The expression for C_{2n} now include the mixing terms between β and γ, and they read:

$$\begin{aligned} C_2 =& C_2|_{\beta=\gamma=0} + C_{2,\beta}\,, \\ C_4 =& C_4|_{\beta=\gamma=0} + C_{4,\beta} + C_{4,\gamma} - \beta\gamma\frac{28122.076}{A-3}\,, \\ C_6 =& C_6|_{\beta=\gamma=0} + C_{4,\beta} + C_{4,\gamma} + \beta\gamma\left(-1757.630 + \frac{314263.030n + 603954.174}{A-3}\right)\,. \end{aligned} \tag{4.45}$$

For any arbitrary A there are always two possible values of β that ensure the quadratic coefficient C_2 sufficiently small:

$$\begin{aligned} \beta_1 &\approx 0.016 + 0.333n\,, \\ \beta_2 &\approx 0.094 - 0.026A + 0.333n\,. \end{aligned} \tag{4.46}$$

The second solution encompasses the previous case with $n = 2$, $\beta = 0$ and $A = 29.142$. One can then determine the appropriate γ value to ensure $C_4 \ll C_6$. We find that the most favored region is $C_2 \approx 0.004$, $C_4 < 2$ and $C_6 \approx 900$. The theoretical prediction for $A = 25$ and $n = 2$ is shown in Fig. 4.3. The physics of inflation remains nearly identical to the previous cases, yielding a similar prediction. The tensor-to-scalar ratio r and the running of spectral index α are very small, while the spectral index n_s remains within the 1σ region of the observational constraints. We use $A = 25$ and $n = 2$ as an example, some typical values of β, γ and the corresponding predictions for inflation parameters are listed in table A.1.

One may wonder if it is possible to achieve successful inflation in the opposite direction, where the modular field slowly roll from $\tau = \omega$ to $\tau = i$. This scenario requires the potential to have a maximum at $\tau = \omega$ and a minimum at $\tau = i$. The latter condition can be easily fulfilled by choosing $m \neq 0$. However, satisfying the former condition necessitates $n = 0$. In this case, $\tau = \omega$ is always a local

minimum of the potential if $A > 3$, regardless of the form of $\mathcal{P}(j)$. This behavior can be seen from their local expansion:

$$\begin{aligned} j(\phi) &\approx 1728\left[-9.36(\phi-\phi_\omega)^3 - 1.56(\theta-\phi_\omega)^5\right] + \mathcal{O}\left((\phi-\phi_\omega)^6\right), \\ V(\phi) &\approx V_0\left[1 + \frac{1}{2}\frac{A-2}{A-3}(\phi-\phi_\omega)^2 + C_3(\phi-\phi_\omega)^3\right] + \mathcal{O}\left((\phi-\phi_\omega)^4\right), \end{aligned} \tag{4.47}$$

where $V_0 = \frac{1728^m \Lambda^4 \left[A(S,\bar{S})-3\right]}{8\sin^3(2\pi/3)|\eta(\omega)|^{12}}|\mathcal{P}(0)|^2$ and $\phi_\omega = \sqrt{3/8}\ln 3$ is the value of canonical field when $\tau = \omega$. Thus, as long as $A(S,\bar{S}) > 3$ (a condition necessary to ensure the potential remains positive during inflation), $\tau = \omega$ is always a local minimum of the potential. Consequently, we will not consider slow-roll inflation in this case.

4.2.2 Slow Roll along the Left (or Right) Boundary

We would extend our discussion to the case where $m, n \geq 2$. In this case, $\tau = i, \omega$ are both minima of the potential and we consider an inflation trajectory at the left boundary (or the imaginary axis) of the fundamental domain. Unlike the previous case where we have good understanding of both inflation point and minimum of the potential, we can not make any assumption where inflation will happen. Thus it is generally difficult to give analytic expressions so we will only show an example here. However, the treatment here is using the rich vacuum structure of the modular potential and it should be very generic.

Let's first find the canonical field at the left boundary. The kinetic term for imaginary part of τ reads:

$$\mathcal{L}_{\text{kin}} = \frac{1}{2}\frac{3}{2(\text{Im}\tau)^2}\left(\partial_\mu \text{Im}\tau\right)^2 . \tag{4.48}$$

One can make a field redefinition, $\text{Im}\tau = \exp\left(\sqrt{2/3}\,\phi\right)$, to introduce the canonical field ϕ. The minimum of $\text{Im}\tau$ is $\sqrt{3}/2$, which corresponds to $\phi = \sqrt{3/2}\ln(\sqrt{3}/2) \approx -0.17$.

It has been noticed that there exist multiple local minima along the left boundary of the fundamental domain [138]. In the specific case where $m = 2$, $n = 2$, $A(S,\bar{S}) = 0$, $\mathcal{P}(j) = 1 + 10^{-3}j$, they find an additional AdS minimum at the left boundary. This minimum can be uplifted into a dS minimum by turning on the $A(S,\bar{S})$ term. This was called Accidental Inflation in String Theory [158], where the up-lifting of adjacent minimum leads to inflation.

We exploit this idea and show how the potential are shaped by different $A(S,\bar{S})$ values. One can see from the Fig. 4.6, when A is small, this additional minimum located at $\phi \approx 0.13$ is a (A)dS minimum, which is separated from the minimum at $\phi = \phi_\omega$ by a barrier. If one increases the value of A, the potential becomes flat and an inflection point will emerge. This very flat region in the potential may break up the normal slow roll inflation approximation and lead to so called ultra slow roll (USR) inflation [159–161]. It might enhance the curvature perturbation and leads to production of primordial black holes [162–164].

We find a narrow region where a SR-USR-SR transition occurs:

$$357.85 < A < 358.75\,. \tag{4.49}$$

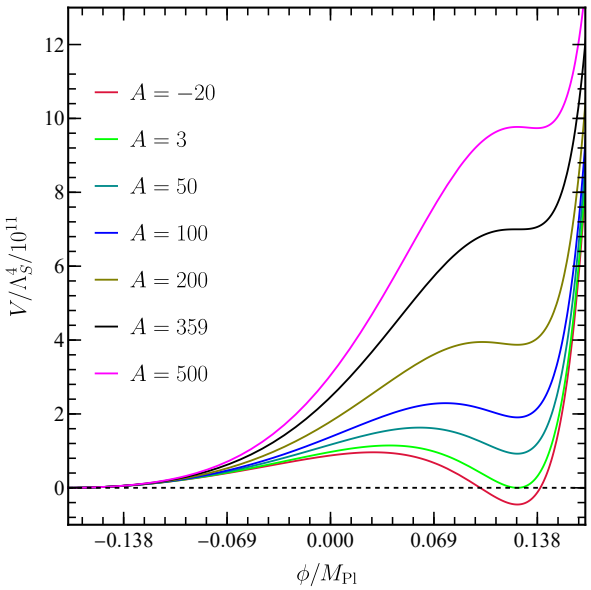

Figure 4.6: When $m = 2$, $n = 2$ and $\beta = -0.633431$, we show the scalar potential at the left boundary of the fundamental domain across different values of the parameter A. Notably, we observe the emergence of almost flat potential when $A \sim O(100)$. The flat plateau occurs around $\tau_I \approx 1.11$ or $\phi \approx 0.13$. In addition, the corresponding potential attains its minimum at $\tau = \omega$ when $A > 3$. Particularly noteworthy is the case when $A = 3$, where the vacuum becomes degenerate. Conversely, for $A < 3$, such as $A = -20$, the AdS global minimum is located at $\tau = 1.10714i$, while the fixed point $\tau = \omega$ serves as a Minkowski local minimum.

This case needs a very careful treatment and we leave it for further works.

4.3 Summary and Conclusions

In this chapter, we try to combine the ideas of modular stabilization and modular inflation. Inspired by the vacuum structure of the modular potential, we successfully find two different trajectories that can accommodate inflation phenomenology and agree with CMB observations. Those trajectories follow the boundaries of the fundamental domain and the property of modular symmetry plays a significant role in our construction. Modular symmetry ensures the flatness of the potential in the inflationary domain and the stabilization of the perpendicular field during inflation. We also find that modular symmetry is a very strong constraint that prevents us from approximating it as a simple hilltop inflation.

We have three different sets of parameters in our model. The first one is $A(S, \bar{S})$ in eq.(4.10), which determines the relative contribution from the dilaton sector. It has to be non-zero for successful inflation to happen. It is also the reason why we could evade some no-go theorem stated in previous studies on logarithmic Kähler potential inflation [103, 124, 125]. The second set of parameters is a pair of integers (m, n) from the H function in eq.(4.6), which determines the vacuum structure of the inflation potentials. We have constructed different trajectories based on that. We keep (m, n) as free parameters. They are relevant to the reheating process after inflation as they also affect how the inflaton oscillates at the minimum. This is not discussed in this chapter, we leave it for further

exploration. The third set of parameters (β, γ) is coefficient of the j-invariant polynomial in eq.(4.7). These coefficients actually shape the potential and are essential for constructing inflation potentials.

In summary, the special properties of fixed points under modular symmetry motivate us to consider the following inflation scenario: when $n \geq 2,\ m = 0$, we find the scalar potential near the fixed point i can be flat enough to accommodate inflation. In this scenario, inflation occurs along the unit arc of the fundamental domain. It is necessary to include one of the parameters in (β, γ), otherwise, the predicted spectral index n_s is smaller than observed. When $n = 2, m = 2$, we find the possibility of realizing (ultra) slow-roll inflation by uplifting the adjacent minima of the potential. In this scenario, inflation occurs along the left boundary of the fundamental domain. The contribution from the dilaton sector $A(S, \bar{S})$ is important for such an uplifting. We do not consider the case when $m \geq 2,\ n = 0$, as both fixed points are local minima.

The fine-tuning problem still exists in our model. Once we fix the parameter (m, n), $A(S, \bar{S})$ and (β, γ) have to be fixed accordingly. There is no theoretical evidence, besides the argument for accidental inflation, suggesting that they should take these specific values. In this sense, we can only answer the question how a modular invariant inflation would look like. We can not ensure that modular stabilization naturally leads to inflation. In particular, we have followed a bottom-up approach to inflation instead of a top-down approach. Here we have assumed that the dilaton is stabilized. The stabilization of dilaton field during inflation could be achieved if the stabilization happens at a much higher energy scale than the inflation scale. The stabilization of the dilaton sector and its dynamics deserve further research. It is also interesting to consider a scenario in which the dilaton field serves as the inflaton field.

In this chapter, we have only considered inflation driven by modulus field and leave reheating part untouched. In the next chapter, we will treate the reheating dynamics more concretely. As we mentioned, modular symmetry has been applied in the flavor sector. We will show in the next chapter that the same Lagrangian can be used to reheat our universe.

CHAPTER 5

Modular Invariant Inflation, Reheating and Leptogenesis

We continue our study on modular invariant inflation theories in this chapter, focusing more on the post-inflationary histories. Due to the exponential expansion, the Universe at the end of inflation is non-thermal. Any viable inflationary scenario must also explain how the Universe reheats and achieves thermal equilibrium with a temperature above the MeV scale, necessary for Big Bang Nucleosynthesis (BBN) [165–168]. In this chapter, we revisit modular slow-roll hilltop inflation [169] with a particular focus on the postinflationary reheating process. Notably, we find that inflaton-matter coupling required for reheating naturally arises from the modular symmetry approach to solve the flavor puzzles [74]. In the framework of using modular symmetry to explain lepton masses and mixing angles, it is required that the Yukawa couplings be modular forms which are holomorphic functions of the complex modulus τ; see Refs. [121, 122] for recent reviews. This naturally gives rise to couplings between the inflaton field and SM particles, which facilitate the production of these particles and reheat the universe following inflation. Analyzing reheating after modular slow-roll inflation is one of the main objectives of this chapter.

We briefly outline our approach. Since the modular forms and Yukawa couplings are determined by the vacuum expectation value (VEV) of the modulus field, our primary objective is to construct a scalar potential that supports inflation and has a minimum at the required VEV, which also fits the lepton data. The process of dynamically fixing the VEV of the modulus field is referred to as modulus stabilization. It has been shown that the extrema of modular invariant scalar potentials are typically located near the boundary of the fundamental domain or along the imaginary axis [133–142]. Flavor models with VEV around the fixed points $\tau = i$, $\tau = \omega = e^{i2\pi/3}$ are particularly interesting to us, as a small deviation from the fixed point can be used to naturally explain the lepton mass hierarchy and CP violation [143, 144, 153, 170, 171]. Inspired by this, we investigate the possibility that the inflaton slowly rolls from i and oscillates around a point near ω.

To provide a concrete example, we construct a model with A_4 modular symmetry. In this model, light neutrino masses are generated via the Type-I seesaw mechanism. Modular symmetry requires the mass terms for the right-handed neutrinos (RHNs) to be modular forms, which also induce couplings between the inflaton and RHNs. We find that inflaton dominantly decays into RHNs after inflation. Although the corresponding inflaton decay rates are suppressed by the Planck scale, the reheating temperature can still be high enough to ensure successful Big Bang nucleosynthesis (BBN). We also

find that the reheating temperature is lower than the RHN mass scale, which gives the possibility to generate the baryon asymmetry in the universe via non-thermal leptogenesis [90, 172–177].

Our results suggest that modular symmetry can be a good organising principle to solve flavor puzzle, inflation as well as postinflationary reheating. Modular invariant models for flavor problems are hard to distinguish from each other since they give more or less the same predictions in lepton masses and mixing patterns. However, their cosmology implications might be different and offer another window to probe modular symmetry.

The chapter is organized as follows. A specific lepton flavor model A_4 is presented in section 5.1. We focus on a modified modular slow-roll inflation in section 5.2 and the post-inflationary reheating in section 5.3. Our main results are summarized in section 5.4. We give a short introduction to modular group Γ_3 in Appendix A.4. The vacuum structure of the scalar potential at the fixed point $\tau = \omega$ and global minimum $\tau = \tau_0$ are investigated in Appendix A.5. The two-body and three-body decays of the inflaton are studied in Appendix A.7.

5.1 Lepton Flavor Model with $\Gamma_3 \cong A_4$ Symmetry

In the following, we focus primarily on a specific model with A_4 symmetry, and the light neutrino masses are generated by the Type-I seesaw mechanism. We will present the lepton sector and omit the quark sector, since the modulus τ has the largest couplings with the right-handed neutrinos because of their heavy masses. The quark sector contributes sub-dominantly to reheating process. The model is specified by the following representation assignments and modular weights of the lepton fields:

$$\begin{aligned} &L \sim \mathbf{3}\,,\quad e^c \sim \mathbf{1}'\,,\quad \mu^c \sim \mathbf{1}'\,,\quad \tau^c \sim \mathbf{1}''\,,\quad N^c \equiv \{N_1^c, N_2^c, N_3^c\} \sim \mathbf{3}\,,\\ &k_L = 1\,,\quad k_{e^c} = 1\,,\quad k_{\mu^c} = 5\,,\quad k_{\tau^c} = 5\,,\quad k_N = 1\,. \end{aligned} \tag{5.1}$$

The two Higgs superfields H_u and H_d transform trivially under modular symmetry. The modular invariant superpotentials responsible for the mass of lepton are

$$\mathcal{W}_{\rm matter} = \mathcal{W}_E + \mathcal{W}_\nu\,, \tag{5.2}$$

where[1]

$$\begin{aligned} \eta^6\mathcal{W}_E &= y_1 e^c (LY_{\mathbf{3}}^{(2)})_{\mathbf{1}''} H_d + y_2 \mu^c (LY_{\mathbf{3}I}^{(6)})_{\mathbf{1}''} H_d + y_3 \mu^c (LY_{\mathbf{3}II}^{(6)})_{\mathbf{1}''} H_d \\ &\quad + y_4 \tau^c (LY_{\mathbf{3}I}^{(6)})_{\mathbf{1}'} H_d + y_5 \tau^c (LY_{\mathbf{3}II}^{(6)})_{\mathbf{1}'} H_d\,, \\ \eta^6\mathcal{W}_\nu &= g_1 \left((N^c L)_{\mathbf{3}_S} Y_{\mathbf{3}}^{(2)}\right)_{\mathbf{1}} H_u + g_2 \left((N^c L)_{\mathbf{3}_A} Y_{\mathbf{3}}^{(2)}\right)_{\mathbf{1}} H_u + \frac{1}{2}\Lambda_N \left((N^c N^c)_{\mathbf{3}_S} Y_{\mathbf{3}}^{(2)}\right)_{\mathbf{1}}\,. \end{aligned} \tag{5.3}$$

Here, the couplings y_1, y_2, y_4 and Λ_N can be taken to be real since their phases can be absorbed by field redefinition, while the phases of y_3, y_5 and g_2 can not be removed. The definitions of modular forms $Y_{\mathbf{3}}^{(2)}, Y_{\mathbf{3}I}^{(6)}, Y_{\mathbf{3}II}^{(6)}$ and group contractions can be found in Appendix A.4. The Yukawa term for leptons and neutrinos, expressed in the flavor basis, can be written as

$$\mathcal{L} = \mathcal{Y}_E^{ij}(\tau) L_i^c L_j H_d + \mathcal{Y}_D^{ij}(\tau) N_i^c L_j H_u + \frac{1}{2}\mathcal{Y}_N^{ij}(\tau) N_i^c N_j^c + \text{h.c.}\,, \tag{5.4}$$

[1] In this case, the superpotential $\mathcal{W}_{\rm matter}$ should have the same modular transformation property as $\mathcal{W}_{\rm moduli}$. Thus unlike the global SUSY scenario, we introduce an extra function η^{-6} in the matter superpotential.

where the $\mathcal{Y}_E^{ij}$, $\mathcal{Y}_D^{ij}$ and $\mathcal{Y}_N^{ij}$ are some linear combinations of modular forms, and $i, j = 1, 2, 3$ are indices of generation. The corresponding charged lepton and neutrino mass matrices read as

$$\begin{aligned}
M_E &= v_d \mathcal{Y}_E(\tau) = \begin{pmatrix} y_1 Y^{(2)}_{\mathbf{3},3} & y_1 Y^{(2)}_{\mathbf{3},2} & y_1 Y^{(2)}_{\mathbf{3},1} \\ y_2 Y^{(6)}_{\mathbf{3}I,3} + y_3 Y^{(6)}_{\mathbf{3}II,3} & y_2 Y^{(6)}_{\mathbf{3}I,2} + y_3 Y^{(6)}_{\mathbf{3}II,2} & y_2 Y^{(6)}_{\mathbf{3}I,1} + y_3 Y^{(6)}_{\mathbf{3}II,1} \\ y_4 Y^{(6)}_{\mathbf{3}I,2} + y_5 Y^{(6)}_{\mathbf{3}II,2} & y_4 Y^{(6)}_{\mathbf{3}I,1} + y_5 Y^{(6)}_{\mathbf{3}II,1} & y_4 Y^{(6)}_{\mathbf{3}I,3} + y_5 Y^{(6)}_{\mathbf{3}II,3} \end{pmatrix} \frac{v_d \eta_0^6}{\eta^6}, \\
M_D &= v_u \mathcal{Y}_D(\tau) = \begin{pmatrix} 2g_1 Y^{(2)}_{\mathbf{3},1} & -g_1 Y^{(2)}_{\mathbf{3},3} - g_2 Y^{(2)}_{\mathbf{3},3} & -g_1 Y^{(2)}_{\mathbf{3},2} + g_2 Y^{(2)}_{\mathbf{3},2} \\ -g_1 Y^{(2)}_{\mathbf{3},3} + g_2 Y^{(2)}_{\mathbf{3},3} & 2g_1 Y^{(2)}_{\mathbf{3},2} & -g_1 Y^{(2)}_{\mathbf{3},1} - g_2 Y^{(2)}_{\mathbf{3},1} \\ -g_1 Y^{(2)}_{\mathbf{3},2} - g_2 Y^{(2)}_{\mathbf{3},2} & -g_1 Y^{(2)}_{\mathbf{3},1} + g_2 Y^{(2)}_{\mathbf{3},1} & 2g_1 Y^{(2)}_{\mathbf{3},3} \end{pmatrix} \frac{v_u \eta_0^6}{\eta^6}, \\
M_N &= \Lambda_N \mathcal{Y}_N(\tau) = \begin{pmatrix} 2Y^{(2)}_{\mathbf{3},1} & -Y^{(2)}_{\mathbf{3},3} & -Y^{(2)}_{\mathbf{3},2} \\ -Y^{(2)}_{\mathbf{3},3} & 2Y^{(2)}_{\mathbf{3},2} & -Y^{(2)}_{\mathbf{3},1} \\ -Y^{(2)}_{\mathbf{3},2} & -Y^{(2)}_{\mathbf{3},1} & 2Y^{(2)}_{\mathbf{3},3} \end{pmatrix} \frac{\Lambda_N \eta_0^6}{\eta^6}, \end{aligned} \tag{5.5}$$

where we have rescaled parameters y_1, g_1, Λ_N by η_0^6 to compensate the existence of η^6, and η_0 is defined at the benchmark point $\eta_0 = \eta(\tau_0)$. Fitting results will be the same as the global SUSY case. The light Majorana neutrino mass matrix is obtained through the Type-I seesaw as follows:

$$m_\nu = -M_D^T M_N^{-1} M_D \,. \tag{5.6}$$

We can perform the transformation from the flavor basis to the mass basis by

$$\begin{aligned}
U_R^{e\,T} M_E U_L^e &= \mathrm{diag}(m_e, m_\mu, m_\tau)\,, \\
U_L^{\nu\,T} m_\nu U_L^\nu &= \mathrm{diag}(m_1, m_2, m_3)\,, \\
U_N^T M_N U_N &= \mathrm{diag}(M_1, M_2, M_3)\,,
\end{aligned} \tag{5.7}$$

where U_L^e, U_R^e, U_L^ν and U_N are unitary matrices; m_i and M_i denote the masses for active neutrinos and right handed neutrinos, respectively. We consider $\langle\tau\rangle$ to stay at the arc, i.e. $|\tau| = 1$. We use the following benchmark values of the free parameters:

$$\begin{gathered}
\tau_0 = \langle\tau\rangle = -0.4847 + 0.8747i\,, \\
y_2/y_1 = 5.1844 \times 10^2\,, \quad y_3/y_1 = 1.4659 e^{-2.4143i} \times 10^2\,, \\
y_4/y_1 = 2.3952 \times 10^4\,, \quad y_5/y_1 = 1.2117 e^{-0.5024i} \times 10^3\,, \\
g_2/g_1 = 0.2465\,, \quad y_1 v_d = 0.2499\ \mathrm{MeV}\,, \quad \frac{(g_1 v_u)^2}{\Lambda_N} = 19.9673\ \mathrm{meV}\,.
\end{gathered} \tag{5.8}$$

Notice that τ_0 is close to the modular symmetry fixed point $\omega \equiv e^{2\pi i/3}$. The corresponding observables for mixing parameters of leptons and masses are given by

$$\begin{aligned}
&\sin^2\theta_{12} = 0.307\,, \quad \sin^2\theta_{13} = 0.022\,, \quad \sin^2\theta_{23} = 0.454\,,\\
&\delta_{CP}/\pi = 0.855\,, \quad \alpha_{21}/\pi = 0.939\,, \quad \alpha_{31}/\pi = 0.271\,,\\
&m_e/m_\mu = 0.00474\,, \quad m_\mu/m_\tau = 0.0588\,, \quad \frac{\Delta m^2_{21}}{\Delta m^2_{31}} = 0.0296\,,\\
&m_1 = 25.725\ \text{meV}\,, \quad m_2 = 27.127\ \text{meV}\,, \quad m_3 = 56.274\ \text{meV}\,,\\
&m_{\beta\beta} = 9.615\ \text{meV}\,, \quad (M_1, M_2, M_3) = \Lambda_N(1.372, 1.447, 2.818)\,,
\end{aligned} \tag{5.9}$$

where $m_{\beta\beta}$ is the effective mass in neutrinoless double beta decay, $M_{1,2,3}$ are the masses of heavy right-handed neutrinos. All the above lepton masses and mixing angles are within 1σ region of the experimental data [59, 60]. Remarkably, M_1 and M_2 are quasi-degenerate, which plays a crucial role for leptogenesis.

5.2 Modular Invariant Inflation with Shifted Minimum

In the last chapter, we have discussed the modular invariant inflation model, where the inflationary trajectory follows the lower boundary of the fundamental domain between the two fixed points, $\tau = i$ and $\tau = \omega = e^{i2\pi/3}$. In this setup, modular symmetry plays a crucial role in ensuring the flatness of the inflationary potential and justifying the single-field approximation.

Although the fixed point ω is a promising candidate for the potential vacuum, the residual symmetry preserved at this point complicates addressing the lepton flavor problem within this framework. It has been noted that a slight deviation from this fixed point can naturally account for the lepton mass hierarchy and CP violation [143, 144, 153, 170, 171].

In this chapter we will construct an inflationary potential with a minimum located at $\tau = \tau_0$ (cf. eq.(5.8)). Inflation occurs around the fixed point $\tau = i$ and then oscillates around the minimum of $\tau = \tau_0$ after inflation, during the reheating process. Building on the previous chapter 4, we continue to analyse the most general superpotential in eq.(4.5). As before, we treat $A(S, \bar{S})$ as a free parameter and use a special form of $H(\tau)$ to realize inflation:

$$H(\tau) = (j(\tau) - j(\tau_0))^2 \left[1 + \beta\left(1 - \frac{j(\tau)}{1728}\right) + \gamma\left(1 - \frac{j(\tau)}{1728}\right)^2\right], \tag{5.10}$$

where the first part $(j(\tau) - j(\tau_0))^2$ is used to determine the vacuum position of the potential. In this setup, the scalar potential vanishes at $\tau = \tau_0$, as both $H(\tau_0) = H_\tau(\tau_0) = 0$. Since we can ensure the potential is non-negative by setting $A(S, \bar{S}) > 3$, τ_0 is a Minkowski minimum of the potential. The rest ensures the flatness of the potential during inflation (around $\tau = i$). As we demonstrated in Appendix A.5, $\tau = \omega$ becomes a local minimum, while $\tau = \tau_0$ is the global minimum of the potential.

The analyze of inflation dynamics does not differ from the previous chapter. To show some representative examples for the inflationary predictions, we consider two benchmark parameters below. The first one is the minimal case with model parameters

$$\text{BP1:} \quad A = 55.2783\,, \quad \beta = 0.6516\,, \quad \gamma = 0\,. \tag{5.11}$$

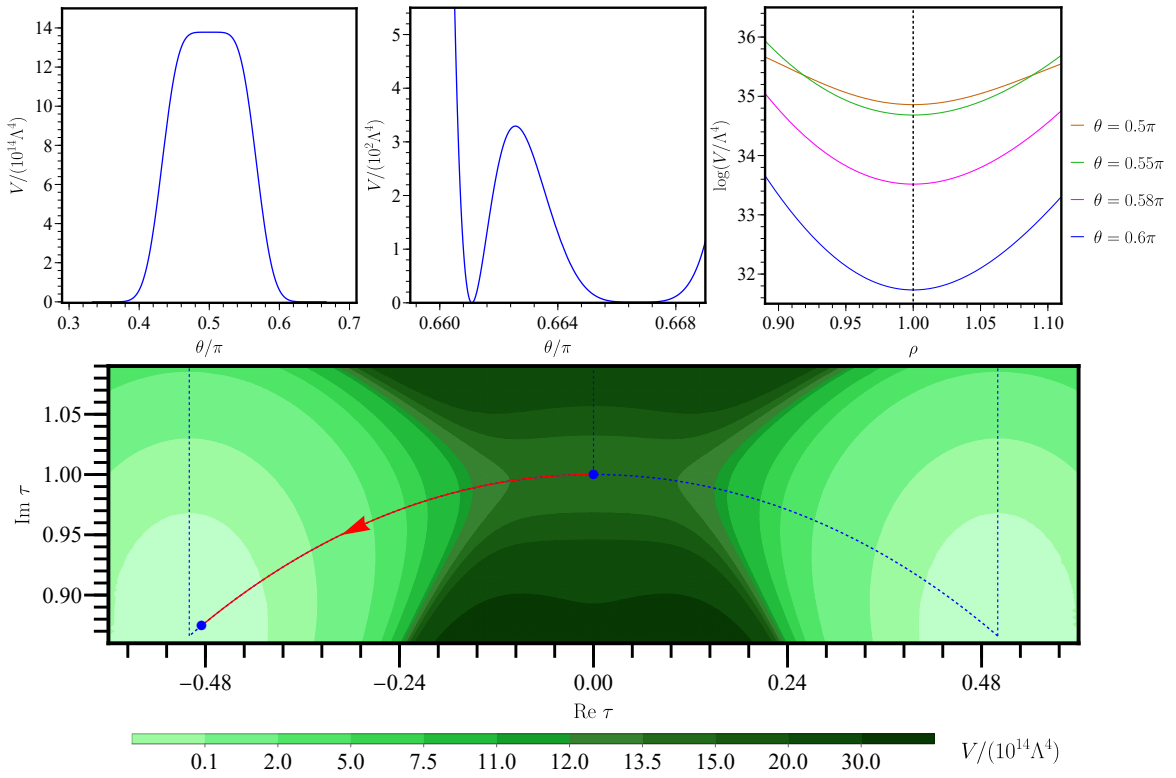

Figure 5.1: Shape of the potential along the angular and radial directions with $A = 55.2783$, $\beta = 0.6516$ and $\gamma = 0$. The top-left panel depicts the inflation potential with $\rho = 1$, where $\theta = \pi/2$ marks the starting point of inflation. The top-middle panel provides a zoomed-in view of the inflation potential around the desired minimum at $\tau = \tau_0$. Note that $\theta = 2\pi/3$ corresponds to a local minimum, whose potential energy does not vanish, while $\theta \approx 0.661\pi$ represents the global minimum. The top-right panel shows the radial potential with a fixed angular coordinate, where the inflationary trajectory remains at the minimum in this direction. Finally, the bottom panel is a contour plot of the inflation potential, with the red arrow indicating the trajectory of inflation.

We show the shape of this potential along the radial and angular direction in Fig. 5.1. Note $\tau = i$ is a saddle point of the potential. Its a local maximum in θ direction and a minimum in ρ direction. Our inflation trajectory lies in the valley of radial direction. The prediction for (n_s, r) is depicted by the black solid line in Fig. 5.2, along with constraints from Planck 2018, BICEP/Keck 2018, and BAO data [51]. The two red dots correspond to $N_e = 50$ and $N_e = 60$, respectively. The predicted value of r is of order $O(10^{-7})$, a typical feature for small-field inflation models [79, 88]. The prediction for n_s lies within the 2σ region of the Planck 2018 results. Note that a larger N_e implies that the inflaton field is closer to the saddle point, where the potential is flatter, resulting in a smaller r and a more scale-invariant spectrum with a larger n_s. Consequently, r decreases with increasing n_s as N_e increases, as shown by the black lines in Fig. 5.2. The second benchmark example corresponds to

$$\text{BP2:} \quad A = 80.2435\,, \quad \beta = 0\,, \quad \gamma = -1.2314\,. \tag{5.12}$$

The corresponding prediction is shown by the black dotted line in Fig. 5.2 with a slightly smaller r. In both cases, we find α is of order $-O(10^{-3})$, and the predictions for n_s, as shown in Fig. 5.2, can lie

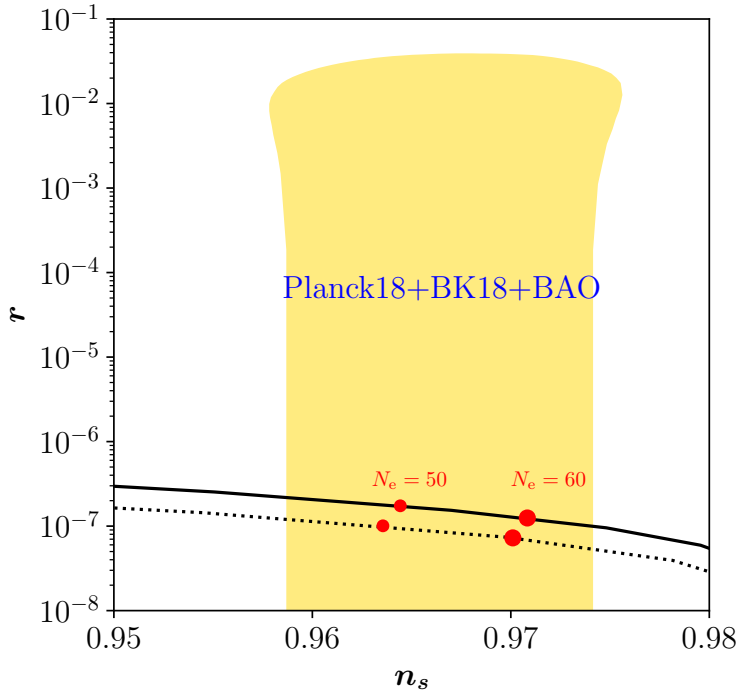

Figure 5.2: The black lines represent the predictions for (n_s, r) with model parameters: $A = 55.2783$, $\beta = 0.6516$, $\gamma = 0$ (solid line) and $A = 80.2435$, $\beta = 0$, $\gamma = -1.2314$ (dotted line). The yellow shaded region corresponds to constraints from the combined results of Planck 2018, BICEP/Keck 2018, and BAO data [51]. The small and large red dots indicate $N_e = 50$ and $N_e = 60$, respectively.

within the 2σ range of the Planck 2018 results presented in eq.(2.44). To illustrate the difference, we consider the central value of the spectral index $n_s = 0.9659$. This corresponds to

$$r \approx 1.6 \times 10^{-7}\,, \quad \alpha \approx -7.078 \times 10^{-4}\,, \tag{5.13}$$

for BP1, and

$$r \approx 9.0 \times 10^{-8}\,, \quad \alpha \approx -7.083 \times 10^{-4}\,, \tag{5.14}$$

for BP2. For the number of e-folds, we find that $N_e \simeq 52$ and $N_e \simeq 53$ for BP1 and BP2, respectively. Note that both BP1 and BP2 correspond to $C_2 = 0.004$ and $C_4 = 0$. The difference for the inflationary prediction for r and α arises from higher order terms in the inflaton potential eq.(4.9). Note that the two sets of benchmark parameters under consideration are representative of those that fit the CMB observables.

As in the last chapter, the prediction for r is far below the sensitivity of next-generation CMB experiments, such as CMB-S4, which has a sensitivity of $r \sim O(10^{-3})$ [178]. However, the prediction for a negative running $\alpha \sim -O(10^{-3})$ could be tested within the sensitivity range of future CMB measurements, especially when combined with significantly improved investigations of structures at smaller scales, in particular the so-called Lyman-α forest [113].

Before closing this section, we note that the total energy scale of the inflaton potential depends on the overall pre-factor Λ in eq.(4.9), which is a function of the value of A. Larger A corresponds

to smaller Λ, implying a smaller inflaton mass parameter. For example, for BP1 and BP2, we find $m_\phi = 4.5 \times 10^7$ GeV and $m_\phi = 3.9 \times 10^6$ GeV, respectively. This suggests that the inflaton mass changes with the value of A. If we insist on the monotonic inflation potential between $\tau = i$ and $\tau = \tau_0$, A should be larger than 43, which gives us an upper bound on inflaton mass $m_\phi < 1.5 \times 10^8$ GeV. This bound only applies to the special form of H function in eq.(5.10). We note that the inflaton mass could be larger in other inflationary scenarios based on modular symmetry [132, 179, 180]. We give a toy model of large field inflations in the appendix.

5.3 Reheating from Modulus Decay

After inflation, the inflaton field generally oscillates around its minimum of the potential and eventually decays into other particles in the Standard Model, which then thermalize, leading to a thermal bath. This process is called reheating [181–184]. The temperature at the end of reheating is referred to as the reheating temperature, which is the highest temperature[2] of the radiation dominated era, can be defined via $H(T_{\rm rh}) = \frac{2}{3}\Gamma_\phi$, where Γ_ϕ denotes the inflaton decay rate and $H(T_{\rm rh})$ denotes the Hubble parameter at $T = T_{\rm rh}$. This gives [90]

$$T_{\rm rh} = \sqrt{\frac{2}{\pi}} \left(\frac{10}{g_\star}\right)^{1/4} \sqrt{M_{\rm pl}\,\Gamma_\phi}\,, \tag{5.15}$$

where $g_\star$ is the number of relativistic degrees of freedom contribution to the total radiation energy density. It reads $g_\star = 106.75$ in the Standard model and roughly doubles in the MSSM, $g_\star = 228.75$.

After inflation, the Hubble scale of the universe decreases significantly during the oscillation of the inflaton field. Specifically, the relevant energy scale becomes much smaller than the Planck scale. Therefore, in the next section, it is sufficient to work in the global SUSY limit and neglect SUSY breaking effects. On one hand, SUSY breaking is highly model-dependent; on the other hand, for the canonical choice of a SUSY breaking scale around $O(1)$ TeV, the mass splitting between particles and sparticles is not expected to significantly affect our results. Additionally, the expansion of the universe can also break SUSY, at the scale of the Hubble parameter [97, 187–190]. As mentioned above, the Hubble scale during reheating is approximately equal to the decay width of the inflaton and does not exceed $O(1)$ GeV, provided the reheating temperature remains below 10^9 GeV. SUSY can also be broken by thermal effects, see [191] for a possible application in cosmology. This effects will also be small due to small Yukawa coupling in the neutrino sector. Hence, we will perform the calculation using the same mass for particles and the corresponding sparticles.

Decay Channels and Reheating Temperature

In this section we analyse the possible inflaton decay channels within the current setup, with which we aim to compute the reheating temperature.

We first evaluate the couplings in the SM sectors, where one can obtain the three point and four point vertices by expanding the mass matrices and Yukawa terms around the minimum of the canonically

[2] We note that the maximum temperature can exceed $T_{\rm rh}$ in non-instantaneous reheating scenarios [185]. It has also been shown that if reheating occurs via inflaton decays to heavy neutrinos, the temperature approaches a constant, causing the maximum temperature to be close to the reheating temperature [186].

normalized field ϕ. Three point vertices arise from inflaton-(s)neutrino-(s)neutrino interaction, and their Lagrangian reads[3]:

$$\mathcal{L} = \frac{1}{2}\frac{\Lambda_N}{M_{\rm pl}}\lambda_1^{ij}\phi N_i^c N_j^c + \frac{1}{2}\frac{\Lambda_N^2}{M_{\rm pl}}\lambda_2^{ij}\phi\widetilde{N}_i^{c*}\widetilde{N}_j^c + \text{h.c.}\,, \tag{5.16}$$

where N_i^c is the right handed neutrino and $\tilde{N}_i^c$ is the right handed sneutrino. We work in the basis where right handed neutrinos mass matrix is diagonal, and the coefficient matrices $\lambda_{1,2}^{ij}$ for benchmark values of the free parameters in eq.(5.8) read:

$$\lambda_1^{ij} = \left[U_N^T\frac{d\boldsymbol{y}_N}{d\phi}U_N\right]^{ij}\Bigg|_{\phi=\phi_0} = \begin{pmatrix} 1.248+0.490i & 1.420i & -1.017 \\ 1.420i & -1.863+0.517i & 1.080i \\ -1.017 & 1.080i & -0.616+1.006i \end{pmatrix}, \tag{5.17}$$

and

$$\lambda_2^{ij} = \left[U_N^\dagger\frac{d(\boldsymbol{y}_N^\dagger\boldsymbol{y}_N)}{d\phi}U_N\right]^{ij}\Bigg|_{\phi=\phi_0} = \begin{pmatrix} 3.423 & -0.106i & -4.262 \\ 0.106i & -5.390 & -1.481i \\ -4.262 & 1.481i & -3.470 \end{pmatrix}. \tag{5.18}$$

The relevant two-body decay widths are given by

$$\Gamma(\phi\to N_i^c N_j^c) = \frac{m_\phi}{8(1+\delta_{ij})\pi}\left(\frac{\Lambda_N}{M_{\rm pl}}\right)^2\left(\left|\lambda_1^{ij}\right|^2\left(1-\frac{M_i^2+M_j^2}{m_\phi^2}\right) - 2\text{Re}[(\lambda_1^{ij})^2]\frac{M_iM_j}{m_\phi^2}\right) \times\sqrt{\left(1-\frac{(M_j-M_i)^2}{m_\phi^2}\right)\left(1-\frac{(M_j+M_i)^2}{m_\phi^2}\right)}, \tag{5.19}$$

$$\Gamma(\phi\to\widetilde{N}_i^c\widetilde{N}_j^{c*}) = \left|\frac{\Lambda_N^2\lambda_2^{ij}}{M_{\rm pl}}\right|^2\frac{1}{16\pi m_\phi}\sqrt{\left(1-\frac{(M_i-M_j)^2}{m_\phi^2}\right)\left(1-\frac{(M_i+M_j)^2}{m_\phi^2}\right)}, \tag{5.20}$$

where M_i and M_j denote the right handed neutrino masses. We note when $M_i + M_j \to m_\phi$ the two-body rates vanish, as expected due to the kinematic threshold.

Analogously the Lagrangian relevant to the three body decay of inflaton is given by

$$\begin{aligned}\mathcal{L} =& \frac{\lambda_3^{ij}}{M_{\rm pl}}\phi N_i^c(L_j\cdot H_u) + \frac{\lambda_3^{ij}}{M_{\rm pl}}\phi\widetilde{N}_i^c(L_j\cdot\widetilde{H}_u) + \frac{\lambda_3^{ij}}{M_{\rm pl}}\phi N_i^c(\widetilde{L}_j\cdot\tilde{H}_u) \\ &+ \frac{\lambda_4^{ij}\Lambda_N}{M_{\rm pl}}\phi\widetilde{N}_i^{c*}(\widetilde{L}_j\cdot H_u) + \text{h.c.}\,,\end{aligned} \tag{5.21}$$

where $L_j = \left(\nu_j, l_j\right)^T$, $H_u = \left(H_u^+, H_u^0\right)^T$ are $SU(2)$ doublet and $(L_j\cdot H_u) = \nu_j H_u^0 - l_j H_u^+$. The

[3] We refer to Ref. [192] for a detailed discussion on sneutrino mass matrix and Ref. [193] for Feynman rules in 2 component notation.

contraction is the same for slepton $\tilde{L}$ and higgsino $\tilde{H}$.

The coefficients matrices in eq.(5.21) read:

$$\lambda_3^{ij} = \left[U_N^T \frac{d\mathcal{Y}_D}{d\phi} U_L^\nu\right]^{ij}\Bigg|_{\phi=\phi_0} = \begin{pmatrix} -0.490 + 1.248i & -1.347 - 0.124i & -0.003 + 0.748i \\ -1.492 + 0.124i & -0.517 - 1.864i & 0.830 \\ -0.003 - 1.288i & -1.328 - 0.001i & 1.006 + 0.616i \end{pmatrix} g_1 \,, \tag{5.22}$$

$$\lambda_4^{ij} = \left[U_N^\dagger \frac{d(\mathcal{Y}_N^\dagger \mathcal{Y}_D)}{d\phi} U_L^\nu\right]^{ij}\Bigg|_{\phi=\phi_0} = \begin{pmatrix} 2.921i & -0.225 & 3.902i \\ -0.849 & -4.896i & -1.831 \\ -5.404i & -1.827 & 3.462i \end{pmatrix} g_1 \,. \tag{5.23}$$

The decay width reads (see Appendix A.7 for details):

$$\begin{aligned}\Gamma(\phi \to N_i^c (L_j \cdot H)) &= \Gamma(\phi \to N_i^c (\widetilde{L}_j \cdot \widetilde{H})) \\ &= 2 \times \left|\frac{\lambda_3^{ij}}{M_{\rm pl}}\right|^2 \frac{m_\phi^3}{768\pi^3}\left[1 - 6\mu_N + 3\mu_N^2 + 2\mu_N^3 - 6\mu_N^2 \log(\mu_N)\right] \,,\end{aligned} \tag{5.24}$$

where we use $(L_j \cdot H)$ to indicate there are two possible final states $\nu_j H_u^0$ or $l_j H_u^+$. The factor 2 accounts for two terms in $SU(2)$ contraction. It is also possible that inflaton decays into sneutrino, and the rates are

$$\begin{aligned}\Gamma(\phi \to \widetilde{N}_i^c (L_j \cdot \widetilde{H})) &= 2 \times \left|\frac{\lambda_3^{ij}}{M_{\rm pl}}\right|^2 \\ &\times \frac{m_\phi^3}{768\pi^3}\left[1 + 9\mu_N - 9\mu_N^2 - \mu_N^3 + 6\mu_N \log(\mu_N) + 6\mu_N^2 \log(\mu_N)\right] \,;\end{aligned} \tag{5.25}$$

$$\Gamma(\phi \to \widetilde{N}_i^c (\widetilde{L}_j \cdot H)) = 2 \times \left|\frac{\lambda_4^{ij} \Lambda_N}{M_{\rm pl}}\right|^2 \times \frac{m_\phi}{512\pi^3}\left[1 - \mu_N^2 + 2\mu_N \log(\mu_N)\right] \,, \tag{5.26}$$

where $\mu_N = M_i^2/m_\phi^2$. The three-body decay rate approaches zero when $\mu_N \to 1$, which is expected, as the decay channel becomes kinematically blocked in this case.

By comparing the decay rates, we find that the channel in which the inflaton decays into two right-handed neutrinos (i.e. eq.(5.19)) dominates in the regime $O(10^2)\left(\frac{m_\phi}{10^{10}\,\text{GeV}}\right)^2$ GeV $< M_1 < m_\phi/2$. For $M_1 < O(10^2)\left(\frac{m_\phi}{10^{10}\,\text{GeV}}\right)^2$ GeV and $m_\phi/2 < M_1 < m_\phi$, the three-body channels eq.(5.24) and eq.(5.25) dominate. The decay widths discussed above are suppressed by the ratio of the inflaton mass to the Planck mass. Consequently, if the inflaton decays only into Standard Model particles, the reheating temperature remains relatively low.

In Fig. 5.3, we show the reheating temperature as a function of the lightest right-handed neutrino mass, M_1, for various inflaton masses: $m_\phi = 10^{12}$ GeV (solid red), $m_\phi = 10^{10}$ GeV (dashed red), $m_\phi = 10^8$ GeV (dash-dotted red), and $m_\phi = 3 \times 10^5$ GeV (dotted red). These results are obtained by summing over 54 channels from the two- and three-body decays discussed earlier. Larger inflaton

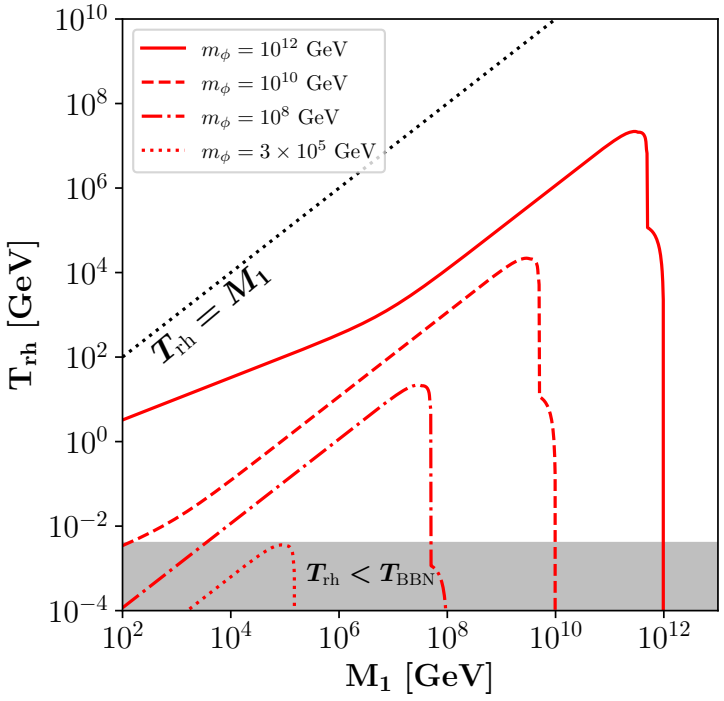

Figure 5.3: Reheating temperature as function of the lightest right handed neutrino mass M_1 and inflaton mass m_ϕ by considering inflaton two and three body decays.

masses correspond to higher decay rates, resulting in larger reheating temperatures (cf. eq.(5.15)). This explains why the solid red line with $m_\phi = 10^{12}$ GeV lies above the lines for smaller inflaton masses.

As mentioned above, in the regime $M_1 < O(10^2)\left(\frac{m_\phi}{10^{10}\,\text{GeV}}\right)^2$ GeV, the three-body channels, eqs. (5.24) and (5.25), dominate, resulting in $T_{\rm rh} \propto \sqrt{M_1}$. Beyond this regime, $T_{\rm rh} \propto M_1$ due to the dominance of the two-body rate, eq.(5.19). This explains the change in slope of the red lines when $M_1 \simeq O(10^2)\left(\frac{m_\phi}{10^{10}\,\text{GeV}}\right)^2$ GeV. The change in slopes is evident when compared to the reference black dotted line, where $T_{\rm rh} = M_1$. It is also evident that within the current setup, the reheating temperature remains below the mass of the lightest right handed neutrino. We also note that the red lines feature a kink as $M_1 \to m_\phi/2$, where the three-body decay becomes dominant in this region.

To preserve the successful predictions of Big Bang Nucleosynthesis (BBN), it is required that $T_{\rm rh} > 4\,\text{MeV}$ [165–168]. Therefore, $T_{\rm rh} < 4\,\text{MeV}$ is disallowed, as indicated by the gray region in Fig. 5.3. For the current model setup, we find that the inflaton mass must satisfy $m_\phi \gtrsim 3 \times 10^5$ GeV to be consistent with BBN constraints. We note that our inflationary setup satisfies this condition as discussed at the section 5.2.

Given that the inflaton dominantly decays to right-handed neutrinos, we also investigate the possibility of realizing baryogenesis via non-thermal leptogenesis in the next section 5.3.1. We find that achieving this within the current small-field hilltop inflationary framework is highly challenging due to the suppressed inflaton mass and low reheating temperature. A large-field inflationary scenario may provide a more viable solution. We leave this for a future work.

5.3.1 Baryon Asymmetry from Non-thermal Leptogenesis

In this section, we discuss baryogenesis via leptogenesis [194, 195]. There are two possible scenarios depending on the relative magnitudes of the reheating temperature, $T_{\rm rh}$, and the right-handed neutrino masses. If the reheating temperature is high enough for the thermal production of right-handed neutrinos to be efficient, the subsequent out-of-equilibrium decay of these neutrinos can generate a baryon asymmetry through the sphaleron process. This mechanism is known as thermal leptogenesis [196]. In thermal leptogenesis, inverse processes act as washout effects that suppress the resulting asymmetry. Consequently, thermal leptogenesis typically requires a high reheating temperature, which can lead to the gravitino problem [197–199]. On the other hand, if the reheating temperature is low, the thermal production of right-handed neutrinos will be Boltzmann suppressed. However, it has been noted that the inflaton's non-thermal two-body decay into pairs of right-handed neutrinos can still account for the baryon asymmetry of the universe [173, 174, 200]. More recently, it was shown that the inflaton's non-thermal three-body decay can also successfully lead to leptogenesis [90].

For baryogenesis via leptogenesis, it is typically required that the reheating temperature be higher than the electroweak scale to ensure the sphaleron process is efficient. In the current inflationary setup, the inflaton mass has been shown to be smaller than $O(10^8)$ GeV, as discussed at the end of section 5.2. Consequently, the reheating temperature remains below $O(100)$GeV, assuming the inflaton decays into neutrino channels (cf. Fig. 5.3). Nevertheless, given the novel feature of the current lepton flavor model, which not only resolves the lepton flavor puzzle but also naturally provides channels for reheating, it remains interesting to investigate the lower bound on the inflaton mass that would lead to the observed baryon asymmetry of the universe (BAU). To this end, we treat the inflaton mass as a free parameter.

As discussed in the previous section, in our scenario reheating temperature is lower than the lightest right-handed neutrino mass, which implies that the thermal leptogenesis is suppressed in our scenario. In this section, we will focus on the non-thermal case, the produced baryon asymmetry from right handed neutrino decay can be estimated as [90, 173]:

$$Y_B \equiv \frac{n_B}{s} \simeq -\frac{8}{23} \times \frac{3}{4}\frac{T_{\rm rh}}{m_\phi} \sum_i \epsilon_i \times \left[2\mathrm{Br}\big(\phi \to N_i + N_i\big) + \mathrm{Br}\big(\phi \to N_i + \text{others}\big)\right] , \tag{5.27}$$

where i sums over all the right handed neutrinos produced from inflaton decays. The first factor $-8/23$ is the conversion factor which transfer lepton asymmetry to baryon asymmetry [201, 202]. The ϵ_i measures the asymmetry in the right handed neutrino decays:

$$\epsilon_i = \frac{\Gamma(N_i \to H_u + L) - \Gamma(N_i \to \overline{H}_u + \overline{L})}{\Gamma(N_i \to H_u + L) + \Gamma(N_i \to \overline{H}_u + \overline{L})} , \tag{5.28}$$

where the decay process should also include SUSY channels. i.e. $N_i \to \tilde{H}_u + \tilde{L}$. In our model, we have two semi-degenerate right handed neutrinos $M_i = \Lambda_N(1.372, 1.447, 2.818)$. This leads to an enhancement of ϵ_i, which should be evaluated as [203]:

$$\epsilon_i = \frac{\mathrm{Im}\left\{(hh^\dagger)^2_{ij}\right\}}{(hh^\dagger)_{ii}(hh^\dagger)_{jj}} \frac{(M_i^2 - M_j^2)M_i\,\Gamma_{N_j}}{(M_i^2 - M_j^2)^2 + M_i^2\,\Gamma^2_{N_j}} , \tag{5.29}$$

where i, j runs over 1, 2 in our model. When $i = 1$, one should take $j = 2$ and vice versa. h is the Yukawa coupling between right handed neutrino, lepton and higgs field. In the bases where right handed neutrinos are diagonal, it reads:

$$h = U_N^T \mathcal{Y}_D U_L^\nu = \begin{pmatrix} 1.372i & -0.347 & 0.009i \\ 0.347 & 1.447i & 0.001 \\ 0.009i & -0.001 & -2.818i \end{pmatrix} g_1 \,. \tag{5.30}$$

Γ_{N_i} is the decay width of right handed neutrinos. At tree level, it reads:

$$\Gamma_{N_i} = \frac{(hh^\dagger)_{ii}}{4\pi} M_i \,. \tag{5.31}$$

We note that the decay of sneutrinos can also generate a CP asymmetry, analogous to eq.(5.28). However, their contribution to the BAU is small due to the domination of the branching ratio into heavy neutrinos from inflaton decays (cf. eq.(5.19) and eq.(5.20)). The BAU at present is given by [204]

$$\eta_B \equiv \frac{n_B}{n_\gamma} = \left(\frac{s}{n_\gamma}\right)_0 \left(\frac{n_B}{s}\right) \simeq 7.02 \times Y_B \,, \tag{5.32}$$

where $n_\gamma = \frac{2\zeta(3)T^3}{\pi^2}$ is the photon number density and $s = \frac{2\pi^2}{45} g_{\star s} T^3$ corresponding to the entropy density. The subscript 0 refers to the current time, where $T = T_0 \simeq 2.73$ K and $g_{\star s} \simeq 3.9$. Using the baryon asymmetry of the Universe (BAU) value based on Planck 2018 [205],

$$\eta_B^{\rm exp} \simeq (6.143 \pm 0.190) \times 10^{-10} \,, \tag{5.33}$$

we can obtain the required Y_B to match the observation, which is $Y_B^{\rm exp} = \frac{6.143}{7.02} \times \eta_B^{\rm exp} \simeq 8.75 \times 10^{-11}$.

5.3.2 Parameter Space

Now we have all the relevant ingredients to calculate the baryon asymmetry in this model. The results are shown in Fig. 5.4. As an example, in the left panel, we consider an inflaton mass of $m_\phi = 10^{12}$ GeV. The blue line represents the parameter space for $T_{\rm rh}$ as a function of M_1, required to yield $Y_B = 8.75 \times 10^{-11}$. Note the branching ratios change with reheating temperature. To achieve this, we treat $T_{\rm rh}$ as a free parameter. When considering inflaton two-body and three-body decays account for reheating, the corresponding reheating temperature is shown as the red line. It intersects the blue curve at $M_1 \simeq 5.3 \times 10^{10}$ GeV and $T_{\rm rh} \simeq 6.1 \times 10^6$ GeV, as indicated by the blue dot, which represents the allowed parameter space in our scenario when $m_\phi = 10^{12}$ GeV. Varying the inflaton mass shifts the intersection point of the red and blue lines. Moreover, we note that as $M_1 \to m_\phi/2$, the red line tends to merger with the blue curve due to the contribution of three-body decay to Y_B. In other words, in the regime where $M_1 < m_\phi/2$, two-body decays dominate, and three-body decays take over when $m_\phi/2 < M_1 < m_\phi$. This also explains the features of the blue curve between the two vertical black dotted lines. Finally, we note that $M_1 \gg T_{\rm rh}$, validating the assumption of non-thermal leptogenesis.

In the right panel, we show a (m_ϕ, M_1) scan that results in $Y_B = 8.75\times10^{-12}$ (red), $Y_B = 8.75\times10^{-11}$

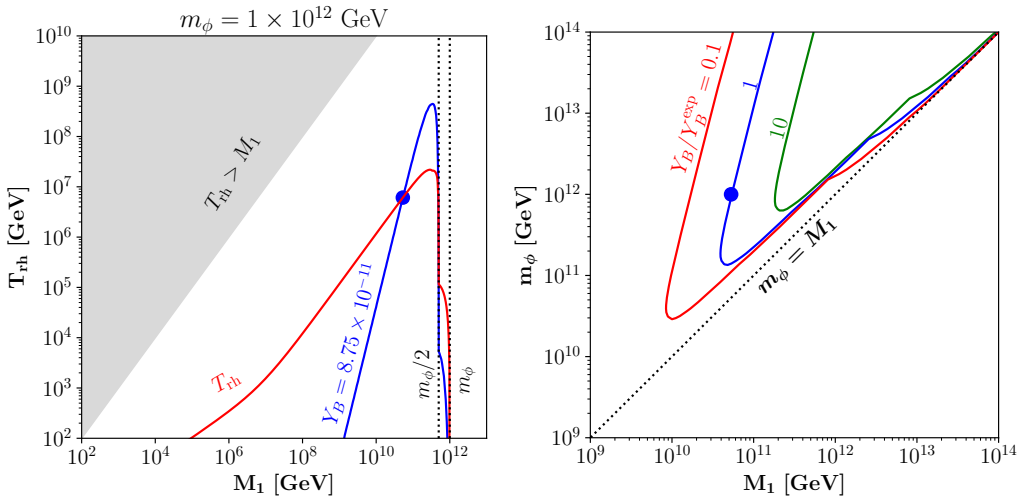

Figure 5.4: Left panel: $T_{\rm rh}$ as function of M_1 to yield $Y_B = 8.75 \times 10^{-11}$ with $m_\phi = 10^{12}$ GeV (blue line) by considering $T_{\rm rh}$ as a free parameter. The red line corresponds to the minimal reheating temperature in our scenario. Right panel: (m_ϕ, M_1) scan by assuming the minimum reheating scenario, i.e. the reheating channel also sources leptogenesis with $Y_B = 8.75 \times 10^{-12}$ (red), $Y_B = 8.75 \times 10^{-11}$ (blue) and $Y_B = 8.75 \times 10^{-10}$ (green).

(blue) and $Y_B = 8.75 \times 10^{-10}$ (green), assuming the reheating channel also accounts for leptogenesis. We note that all the curves would approach to the black dotted line with $M_1 = m_\phi$ as explained and implied by the figure in the left panel. To explain the BAU observed in our universe, the allowed parameter space is indicated by the blue curve, with the blue dot corresponding to the same point as shown in the left panel. For a fixed Y_B, in the region where $M_1 < m_\phi/2$, the inflaton mass scales as $m_\phi \propto M_1^2$, as shown in the right panel of Fig. 5.4, due to the dominance of two-body decays. We find that a lower bound on the inflaton mass around $m_\phi \gtrsim 10^{11}$GeV is required to explain the entirety of the observed baryon asymmetry, as shown in the edge of the blue line in the right panel of Fig. 5.4. This also implies the lightest right handed neutrino mass should satisfy $M_1 \gtrsim 10^{11}$GeV to give rise to the observed BAU.

We note that the lower bounds mentioned above could be relaxed if we assume that the non-thermal leptogenesis under consideration accounts for only part of the observed baryon asymmetry. For instance, m_ϕ can be as small as 10^{10} GeV if we assume that non-thermal leptogenesis contributes only 10% of the BAU, as demonstrated by the red line in the right panel of Fig. 5.4. For a much smaller inflaton mass with $m_\phi \lesssim 10^8$ GeV (corresponding to a very low reheating $T_{\rm rh} \lesssim 100$ GeV), it is very challenging to generate a sizable contribution to the observed BAU. An alternative way forward is to investigate the possibility of raising the inflationary scale, such as through large field inflation [45, 89, 206, 207], which could give rise to inflaton mass as larger as $O(10^{13})$ GeV.

Recent developments in realizing large-field inflation within the modular invariant framework are discussed in Ref. [132] for Starobinsky inflation and Refs. [179, 180] for the α-attractor scenario. In these frameworks, the reheating temperature could be higher due to an increased inflaton mass scale, potentially facilitating successful baryogenesis.

5.4 Summary and Conclusions

In this chapter, we present a minimal model that attempts to simultaneously address the lepton flavor puzzle, inflation and post-inflationary reheating based on modular symmetry. We show that all the three aspects can be achieved collectively through the modulus field, without the need to introduce any additional new physics.

In the lepton sector, we employ a Type-I seesaw modular A_4 model to explain the smallness of neutrino masses. By assigning the standard mode (SM) fields and right handed neutrinos (RHNs) different modular weights and irreducible representations, modular symmetry determines the possible forms of the Yukawa interactions. After the modulus field acquires a VEV, modular symmetry is broken, and the Yukawa coefficients become fixed. We find that the VEV $\tau_0 = -0.484747 + 0.874655i$, located around the fixed point $\omega = e^{i2\pi/3}$, can successfully reproduce SM observations in the lepton sectors as demonstrated in section 5.1.

We show that the same scalar potential that fixes the VEV of the modulus field can also account for inflation. To this end, this scalar potential must be sufficiently flat in a certain region. We consider inflation occurring around the fixed point $\tau = i$ and inflaton oscillating at $\tau = \tau_0$, which can be realized with an appropriate superpotential, as demonstrated in section 5.2. In this setup, the inflationary trajectory follows the arc of the fundamental domain, as shown in Fig. 5.1, where the special properties of modular symmetry are maximally pronounced. Consequently, the inflationary scenario is similar to the hilltop model. We find that the model can perfectly fit the CMB observations, featuring a very small tensor-to-scalar ratio $r \sim O(10^{-7})$. Additionally, the prediction for the running of the spectral index, $\alpha \sim -O(10^{-3})$, could be tested in the near future.

Any viable inflationary scenario must also explain how the Universe reheats. A novel feature of our setup is that the channels for post-inflationary reheating are automatically generated to explain the observations in the lepton sector. In particular, the expansion of the modular forms around the minimum gives rise to interactions between the inflaton and other particles, including the SM Higgs, leptons, and RHNs. After inflation, the inflaton decays through these channels, which can reheat the universe. We compute all relevant channels, including inflaton two- and three-body decays. We find that, due to the Planck-suppressed interactions, the reheating temperature tends to be low unless the inflaton mass is larger, as depicted in Fig. 5.3. The highest reheating temperature occurs when the RHN masses approach their kinematical threshold. Interestingly, we find a parameter space that yields a sufficiently high reheating temperature to preserve the successful predictions of Big Bang Nucleosynthesis (BBN). This requires the inflaton satisfy $m_\phi \gtrsim O(10^5)$ GeV.

We further explore the possibility of explaining the baryon asymmetry of the Universe (BAU) via leptogenesis in section 5.3.1. We apply the non-thermal leptogenesis mechanism, as the temperature in our framework is lower than the RHN mass, implying that the thermal production of RHNs is Boltzmann-suppressed. We find that, in order to account for the observed BAU, the inflaton and the lightest RHN masses must satisfy $m_\phi \gtrsim O(10^{11})$ GeV and $M_1 \gtrsim O(10^{11})$ GeV, as shown in Fig. 5.4. We note that the small-field hilltop inflationary model considered in the current setup cannot satisfy this condition. An interesting direction is to explore other inflationary setups, such as those presented very recently in Refs. [132, 179, 180]. Although our current setup does not fully account for the BAU, we believe that our approach provides a valuable basis for further exploration of post-inflationary cosmology within the framework of modular invariance.

CHAPTER 6

Gravitational Dark Matter Production in Supergravity α-Attractor Inflation

In this chapter we will study a different mechanism to produce dark matter (DM). This is known as the gravitational particle production (GPP), where inflation source particle production due to the time evolution of the background spacetime [58, 208].

GPP is inevitable for any degree of freedom as long as it couples to gravity. This production channel can contribute significantly to the DM abundance, and can generate subsequently DM isocurvature perturbations. For a comprehensive review, we refer to [209]. If gravity is the only interaction between DM and the Standard Model (SM) particles, DM from GPP will never be in thermal equilibrium with the rest of particles, unlike canonical thermal freeze-out mechanism. GPP has been extensively studied in the past decades, leading to a rich phenomenology for scalar and higher spin fields [208, 210–231]. Meanwhile, analytic treatments to track particle production have been developed in certain cases [232–242].

Although the precise results of GPP depend on the inflation model, some general statements can be made without specifying inflation dynamics. For a scalar field χ lighter than the inflation scale H_I, its number density spectrum will feature an infra-red (IR) divergence, which has to be regulated through a cut-off in momentum space. Its isocurvature spectrum will be almost scale-invariant, which might conflict with CMB observations. In contrast, if the field is heavier than H_I, its number density will converge without cutoff, and the isocurvature signal can be negligible.

Since gravitational interactions at sub-Planckian energies are weak, the above conclusion can be easily modified. Corrections may appear from various sources. Introducing a non-minimal coupling between DM and gravity can greatly change the efficiency of GPP. A conformally coupled scalar experiences less GPP, has no IR divergence and leaves negligible isocurvature perturbations at CMB scales, larger interaction will enhance the GPP production [214, 234, 243–246]. Introducing a direct coupling between the inflaton field and DM leads to a similar effects [247, 248]. In this chapter we would like to focus on another possibility, where such corrections comes from supergravity (SUGRA) effects.

SUGRA is a local gauge theory of supersymmetry (SUSY), which generally predicts non-renormalizable interactions between the inflaton field and DM. These interactions can play a significant role in cosmology [249–253]. The previous study of GPP in SUGRA setting focuses on the case where $m_\chi > H_I$ [254] (which comes from their inflationary model with $H_I \ll m_\phi$), and we would

like to have a comprehensive understanding of the entire parameter space. Even for light DM, SUGRA correction lifts its effective mass naturally higher than the Hubble scale. This correction has the same origin as the η-problem in SUGRA inflation research [97].

In this chapter, we focus on the α-attractor model, which is realized in SUGRA using a stabilizer field [255, 256]. This framework allows us to introduce an arbitrary SUSY breaking scale $m_{3/2}$. Even though for the canonical choice of $m_{3/2} \sim 1\,\text{TeV}$, its impact on GPP can be safely neglected, it is still interesting to investigate how a larger $m_{3/2}$ could change GPP. Compared with previous study, our model can have $m_\phi \sim H_I$, and our embedding of α-attractor model also introduces additional contributions to the (effective) mass of the DM field. We numerically calculate the number density of a scalar DM, as well as its isocurvature contribution. Compared with non-SUSY GPP, SUGRA models need a higher reheating temperature to produce the same amount of DM.

In this chapter, we use the reduced Planck mass $M_{\text{pl}} = (8\pi G)^{-1/2} = 2.44 \times 10^{18}\,\text{GeV}$, except in section 6.1.3 where the Planck units are used, i.e. $M_{\text{pl}} = 1$. This chapter is organized as follows. In section 6.1, we introduce the inflation model, the basics of GPP, and show how to embed our model in a SUGRA framework. Numerical results for GPP are presented in section 6.2 and its phenomenological consequences are discussed. Section 6.3 contains our conclusion and outlook of this work. We give a short derivation of DM relic abundance in Appendix A.8.

6.1 The Framework

6.1.1 Inflation Model

For the purpose of this chapter, its more convenient to work with conformal time τ. It is related with the cosmic time t by $dt = ad\tau$. The equation of motion of the inflaton field and the Friedmann equations of first and second kind are

$$\phi'' + 2a\mathcal{H}\phi' + a^2\frac{\partial V}{\partial \phi} = 0\,, \tag{6.1a}$$

$$\mathcal{H}^2 = \left(\frac{a'}{a}\right)^2 = \frac{1}{3M_{\text{pl}}^2}\left(\frac{\phi'^2}{2a^2} + V\right)\,, \tag{6.1b}$$

$$\frac{a''}{a} = \frac{1}{6M_{\text{pl}}^2}\left(4a^2V - \phi'^2\right)\,, \tag{6.1c}$$

where the $'$ denotes the derivative with respective to conformal time τ and $\mathcal{H}$ is the conformal Hubble parameter.

In this work, we investigate the possibility that T-mode α-attractor is the inflation model, which can be easily realized in the SUGRA context, see section 6.1.3. It has the following potential [257]

$$V_I(\phi) = V_0 \tanh^{2n}\left(\frac{\phi}{\sqrt{6\alpha}}\right)\,. \tag{6.2}$$

Here, the potential parameter α has a mass dimension 2 and controls the inflationary predictions of the model. V_0 has mass dimension 4 and is related with inflation Hubble scale. We use $n = 1$ throughout this chapter. The slow roll parameters for this model are

$$\begin{aligned}\epsilon_V &= \frac{M_{\rm pl}^2}{3\alpha}\frac{1}{\sinh^2(\phi/\sqrt{6\alpha})\cosh^2(\phi/\sqrt{6\alpha})}\,,\\ \eta_V &= \frac{M_{\rm pl}^2}{3\alpha}\frac{(1-\tanh^2(\phi/\sqrt{6\alpha}))^2 - 2\tanh^2(\phi/\sqrt{6\alpha})(1-\tanh^2(\phi/\sqrt{6\alpha}))}{\tanh^2(\phi/\sqrt{6\alpha})}\,.\end{aligned} \tag{6.3}$$

The spectral index of the scalar perturbation n_s can be given by the two slow-roll parameters at the CMB scale

$$n_s = 1 + 2\eta_* - 6\epsilon_*\,. \tag{6.4}$$

Here we denote quantities at such scale with subscript $_*$. Any viable inflation model has to give a consistent prediction on n_s with the observed value, $n_s = 0.965 \pm 0.004$ by Planck 2018 [44]. One can use n_s to compute the field value ϕ_* at the CMB scale [258]

$$\cosh^2\left(\frac{\phi_*}{\sqrt{6\alpha}}\right) = \frac{1}{2(1-n_s)}\left(1 - n_s + \frac{4}{3}\frac{M_{\rm pl}^2}{\alpha} + \sqrt{(1-n_s)^2 + \frac{8}{3}\frac{M_{\rm pl}^2}{\alpha}(1-n_s) + \frac{16}{9}\frac{M_{\rm pl}^4}{\alpha^2}}\right). \tag{6.5}$$

The potential parameter α can be expressed in terms of the tensor-to-scalar ratio r and the spectral index n_s

$$\alpha = \frac{64}{3}\frac{r}{(8(1-n_s)-r)^2 - r^2}M_{\rm pl}^2\,. \tag{6.6}$$

Currently, the BICEP/Keck 2018 results only impose an upper limit on r [51]

$$r < 0.036 \quad \text{at } 95\% \text{ C.L.}\,. \tag{6.7}$$

This can be transferred into an upper bound on $\alpha < 20\,M_{\rm pl}^2$. At last, the energy scale V_0 can be determined by the normalization of the curvature perturbation power spectrum $\mathcal{A}$ [49]

$$\mathcal{A} = (2.1 \pm 0.1)\cdot 10^{-9} = \frac{1}{24\pi^2}\,\frac{V}{M_{\rm pl}^4}\frac{1}{\epsilon_V}\bigg|_{\phi=\phi_*}\,. \tag{6.8}$$

There are two important energy scales associated with inflation, the first one is the Hubble scale during inflation

$$H_{\rm inf} \approx \sqrt{\frac{V_0}{3M_{\rm pl}^2}}\,. \tag{6.9}$$

The second one is the inflaton mass m_ϕ, which reads

$$m_\phi^2 = \frac{\partial^2 V}{\partial\phi^2}\bigg|_{\phi=0} = \frac{V_0}{3\alpha}\,. \tag{6.10}$$

The ratio between the inflation Hubble scale and inflaton mass $H_{\rm inf}^2/m_\phi^2 = \alpha/M_{\rm pl}^2$ depends on the potential parameter α. Thus, the DM field can have mass much lighter than the inflation scale

$m_\chi \ll m_\phi \sim H_I$.

The end of slow-roll inflation is marked by either one of the magnitude of slow roll parameters being unity. The field value ϕ_e at the end of inflation can be obtained through

$$2\cosh^2\left(\frac{\phi_e}{\sqrt{6\alpha}}\right) = \begin{cases} 1 + \frac{2M_{\rm pl}^2}{3\alpha} + \sqrt{1 + \frac{8M_{\rm pl}^2}{3\alpha}\left(\frac{M_{\rm pl}^2}{6\alpha} - 1\right)}, & \alpha \le \alpha_l \\ 1 + \sqrt{1 + \frac{4M_{\rm pl}^2}{3\alpha}}, & \alpha > \alpha_l \end{cases}, \tag{6.11}$$

with $\alpha_l \approx 0.17 M_{\rm pl}^2$.

6.1.2 Gravitational Particle Production

In addition to the inflaton field, we also assume there exists a spectator scalar field χ with the following action

$$S_\chi = -\frac{1}{2}\int \mathrm{d}^4x\,\sqrt{-g}\left(2\xi\chi^2 R + g^{\mu\nu}\partial_\mu\chi\partial_\nu\chi + m_\chi^2\chi^2\right), \tag{6.12}$$

where g is the determinant of $g^{\mu\nu}$ and R is the Ricci scalar. Higher order self-interactions of χ have been neglected and m_χ^2 could be a function of other fields. Here, we use the FLRW metric with conformal time.

We can rescale the field $\tilde{\chi}(\vec{r}) = a(\tau)\chi(\vec{r})$. Then, after Fourier decomposing the field $\tilde{\chi}$ through comoving momentum $\vec{k}$

$$\tilde{\chi}(\vec{k}) = \int \frac{d^3\vec{r}}{(2\pi)^3} e^{i\vec{k}\cdot\vec{r}}\tilde{\chi}(\vec{r}), \tag{6.13}$$

its equation of motion turns into the equation for the mode function $\tilde{\chi}_k = \tilde{\chi}(k)$

$$\tilde{\chi}_k'' + \omega_k^2\tilde{\chi}_k = 0, \quad \omega_k^2 = k^2 + a^2 m_{\chi,\rm eff}^2 = k^2 + a^2 m_\chi^2 - (1-6\xi)\frac{a''}{a}, \tag{6.14}$$

where $k = |\vec{k}|$ and spatial isotropy is assumed. In this work, we only consider vanishing coupling (to gravity) $\xi = 0$. When ω_k^2 varies non-adiabatically with time, the field χ can get excited and corresponding particles are produced.

The same phenomenon can also be understood in terms of the Bogoliubov coefficients. Assume that the spacetime is asymptotically flat at early and late times. The Bogoliubov coefficients describes how the orthonormal basis functions at early and late times relate to each other. The eq. (6.14) can be formulated in terms of the Bogoliubov coefficients α_k and β_k

$$\alpha_k' v_k = \frac{\omega_k'}{2\omega_k} v_k^* \beta_k, \quad \beta_k' v_k^* = \frac{\omega_k'}{2\omega_k} v_k \alpha_k, \tag{6.15}$$

with

$$v_k(\tau) = \frac{1}{\sqrt{2\omega_k}}\exp\left(-i\int^\tau \omega_k\,\mathrm{d}\tau'\right). \tag{6.16}$$

We note it is more numerically efficient to solve eqs. (6.15) instead of eqs. (6.14), except in the presence of tachyonic instability.

The comoving number density spectrum of χ field is given by

$$f_\chi(k,\tau) = |\beta_k|^2 \,, \tag{6.17}$$

and the comoving number density can be obtained from it by

$$a^3 n_\chi = \frac{1}{2\pi^2}\int \mathrm{d}k\, k^2 f_\chi(k,\tau)\,. \tag{6.18}$$

We assume that the comoving number density doesn't change after production and χ field behaves as the cold DM. The comoving energy density can be approximated as

$$a^4\rho_\chi \approx \frac{1}{2\pi^2}\int \mathrm{d}k k^2 |\beta_k|^2\omega_k\,, \tag{6.19}$$

where we only include terms up to second order in $|\beta_k|$ and ignore the terms suppressed by the Hubble parameter and Ricci scalar (which decay away quickly).

The produced χ field also generates isocurvature perturbation. The isocurvature power spectrum is defined as

$$\Delta^2_\delta(k) = \frac{1}{\rho^2}\frac{k^3}{2\pi^2}\int \mathrm{d}^3\vec{r}\, e^{-i\vec{k}\cdot\vec{r}}\,\langle\delta\hat{\rho}(0)\delta\hat{\rho}(\vec{r})\rangle\,, \tag{6.20}$$

where we have decomposed the energy density $\rho(\vec{r}) = \bar{\rho} + \delta\hat{\rho}(\vec{r})$. Their time-dependencies have been omitted. The isocurvature power spectrum can be written in terms of the mode functions [209, 213, 259]

$$\begin{aligned}\Delta^2_\delta(\eta,k) = \frac{1}{a^8\bar{\rho}^2}\frac{k^3}{(2\pi)^5}\int \mathrm{d}^3k' \Big[&|\partial\chi_{k'}|^2|\partial\chi_{|\vec{k}'-\vec{k}|}|^2 + a^4m^4|\chi_{k'}|^2|\chi_{|\vec{k}'-\vec{k}|}|^2 \\ &+ a^2m^2\left(\chi_{k'}\partial\chi^*_{k'}\chi_{|\vec{k}'-\vec{k}|}\partial\chi^*_{|\vec{k}'-\vec{k}|} + \chi^*_{k'}\partial\chi_{k'}\chi^*_{|\vec{k}'-\vec{k}|}\partial\chi_{|\vec{k}'-\vec{k}|}\right)\Big]\,.\end{aligned} \tag{6.21}$$

as well as the Bogoliubov coefficients with momenta relabeled through $(k,k',|\vec{k}'-\vec{k}|)\to(k,p,q)$ [248]

$$\Delta^2_\delta(k) = \frac{a_e^2m_\chi^2}{(a_e^4\rho)^2}\frac{2k^2}{(2\pi)^4}\int_0^\infty \mathrm{d}p\, p\int_{|k-p|}^{k+p}\mathrm{d}q\, q\left[|\beta_p|^2|\alpha_q|^2 + \mathrm{Re}\left\{\alpha_p^*\beta_p\alpha_q\beta_q^* e^{2i\Phi_p-2i\Phi_q}\right\}\right]. \tag{6.22}$$

6.1.3 SUGRA Embedment

In this section we discuss how to realize α attractor models in a SUGRA framework. Recall the scalar potential reads:

$$\begin{aligned}\sqrt{-g}\mathcal{L} &= -\mathcal{K}_{\alpha\bar{\beta}}\partial_\mu\phi^\alpha\partial^\mu\bar{\phi}^{\bar{\beta}} - V\,,\\ V &= e^{\mathcal{K}}(\mathcal{K}^{\alpha\bar{\beta}}D_\alpha\mathcal{W}\overline{D_\beta\mathcal{W}} - 3|\mathcal{W}|^2)\,,\end{aligned} \tag{6.23}$$

The factor $e^{\mathcal{K}}$ in the scalar potential leads to the so-called η problem in early studies of SUGRA inflation [97]. For any field with canonical Kähler potential $\mathcal{K} = \bar{\Phi}\Phi$, the second order derivative of

the potential:

$$\frac{\partial^2 V}{\partial\phi\partial\phi} \sim V + \text{others...} \tag{6.24}$$

leads to a $O(1)$ slow roll parameter $\eta_V = V''/V \sim 1$. This holds true for the possible inflaton field and any other fields present in the Kähler potential. In this chapter, we will assume this correction indeed exists for DM field, which means DM gets an effective mass on the order of the Hubble scale during and after inflation. As we will show in this chapter, this significantly alters the results for GPP production of DM field.

One elegant solution of the η problem is imposing a shift symmetry, which ensures that the inflaton field doesn't appear in the Kähler potential. In this way, one can realize most inflation models in [260]. To embed the aforementioned inflation model in , we use the formalism proposed in [255, 256], which can accommodate an arbitrary inflationary model with arbitrary supersymmetry (SUSY) breaking scale. Our model thus has three superfields: the inflaton superfield Φ, the stabilizer superfield S and the DM superfield χ, with the following Kähler potential $\mathcal{K}$ and superpotential $\mathcal{W}$

$$\begin{aligned}\mathcal{K}(\Phi, S, \chi) &= -\frac{1}{2}(\Phi - \bar{\Phi})^2 + S\bar{S} + \chi\bar{\chi}\,,\\ \mathcal{W}(\Phi, S, \chi) &= f(\Phi) + Sg(\Phi) + \frac{1}{2}m_\chi\chi^2\,.\end{aligned} \tag{6.25}$$

We also assume both $\mathrm{Im}(\Phi), S, \chi = 0$ during inflation as in [260]. The Kähler covariant derivative of each field reads

$$\begin{aligned}D_\Phi\mathcal{W} &= f'(\Phi) + g'(\Phi)S - (\Phi - \bar{\Phi})\mathcal{W}\,,\\ D_S\mathcal{W} &= g(\Phi) + \bar{S}\mathcal{W}\,,\\ D_\chi\mathcal{W} &= m_\chi\chi + \bar{\chi}\mathcal{W}\,.\end{aligned} \tag{6.26}$$

We set $g(\Phi) = \sqrt{3}f(\Phi)$. Up to second order in χ and ignoring the contribution from $\mathrm{Im}(\Phi)$ and S, we have from eq. (6.23)

$$V_\chi = m_\chi^2\chi\bar{\chi} - \frac{1}{2}m_\chi\bar{\chi}^2 f - \frac{1}{2}m_\chi\chi^2\bar{f} + \chi\bar{\chi}\left(f\bar{f} + f'\bar{f}'\right)\,, \tag{6.27}$$

where $f'\bar{f}' = V_I(\phi)$ is the inflaton potential and $\phi = \sqrt{2}\mathrm{Re}(\Phi)$ is the actual inflaton.

For α attractor inflation defined in eq. (6.2), the f function has the following form

$$f(\Phi) = \sqrt{3\alpha V_0}\log\left(\cosh\left(\frac{\Phi}{\sqrt{3\alpha}}\right)\right) + \frac{m_{3/2}}{\sqrt{3}}\,. \tag{6.28}$$

In the global Minkowski minimum where $\Phi = 0$, the SUSY is broken in the S direction. We have:

$$\left|D_S\mathcal{W}\right|^2 = 3|\mathcal{W}|^2 = m_{3/2}^2\,. \tag{6.29}$$

We can split the complex DM field into two real fields , $\chi = (\chi_R + i\chi_I)/\sqrt{2}$, with the following mass

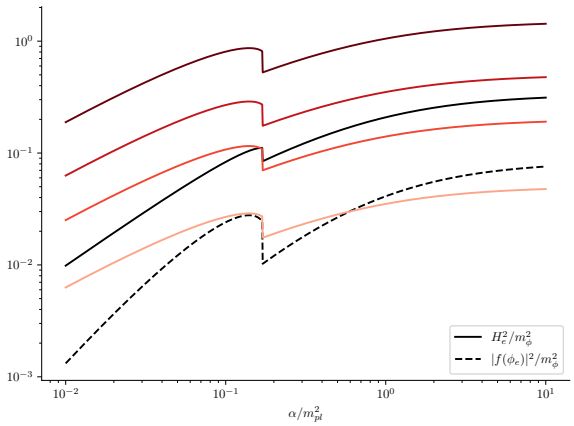

Figure 6.1: Terms in eq. (6.31) evaluated at the end of slow-roll inflation as functions of α. The colored lines, from bottom to top, are $m_\chi f(\phi_e)/m_\phi^2$ with $m_\chi/m_\phi = 0.1, 0.4, 1, 3$. The discontinuity at $\alpha = \alpha_l$ comes from eq. (6.11), as different slow roll parameters $\epsilon_V = 1$ and $\eta_V = 1$ are used on both side of a_l. This figure is simply for illustration purpose; the discontinuity plays no role in our final results.

term:

$$m_{\chi,R}^2 = m_\chi^2 + V_I + |f|^2 - m_\chi f\,, \tag{6.30a}$$
$$m_{\chi,I}^2 = m_\chi^2 + V_I + |f|^2 + m_\chi f\,, \tag{6.30b}$$

where we have used $f \in \mathbb{R}$ as only $\mathrm{Re}(\Phi)$ is non-zero during and just after inflation and there is no mixing between the real and imaginary parts. After the rescaling $\tilde{\chi}_i = a\chi_i$, their effective masses read

$$m_{\tilde{\chi},\mathrm{eff}}^2 = a^2\left(m_\chi^2 + H^2 + |f|^2 \mp m_\chi f\right). \tag{6.31}$$

Compared with the effective mass in eq. (6.14), the first distinction is that we have H^2 instead of $-a''/a^3$. This is a general feature of SUGRA correction and a result of eq. (6.24), see also [254]. As we used a different implementation of inflation to account for SUSY breaking effects, two extra terms $|f|^2$ and $m_\chi f$ arise in our calculation compared with [254]. We can roughly estimate the relative strength of the last three terms at the end of slow-roll inflation using eq. (6.11). By normalizing them to m_ϕ and taking $m_{3/2} \approx 0$, we have:

$$\begin{aligned} H_e^2 &\approx \alpha m_\phi^2 \tanh^2\left(\frac{\phi_e}{\sqrt{6\alpha}}\right), \\ |f(\phi_e)|^2 &= \alpha m_\phi^2 \cdot 3\alpha \log^2\left(\cosh\left(\frac{\phi_e}{\sqrt{6\alpha}}\right)\right), \\ m_\chi f(\phi_e) &= \alpha m_\phi^2 \cdot 3\left(\frac{m_\chi}{m_\phi}\right)\log\left(\cosh\left(\frac{\phi_e}{\sqrt{6\alpha}}\right)\right). \end{aligned} \tag{6.32}$$

When $\alpha > \alpha_l$ and $m_\chi \ll m_\phi$, H_e^2 is the dominant contribution to $m_{\tilde{\chi},\mathrm{eff}}$ among the three time-dependent

terms. Taking $\alpha = 1$ as an example, we have

$$H_e^2 \approx 0.21\alpha m_\phi^2\,, \quad \frac{|f(\phi_e)|^2}{H_e^2} \simeq 0.6, \quad \frac{m_\chi f(\phi_e)}{H_e^2} \simeq 1.7\left(\frac{m_\chi}{m_\phi}\right), \tag{6.33}$$

and the last two term are equally important to the Hubble term. However, contribution from the last term increases with decreasing α. When $\alpha < \alpha_l$, it could dominate the effective mass for a extended range of parameter space. For $\alpha = 0.01$, $H_e^2 \approx \alpha m_\phi^2$, and the ratio reads:

$$\frac{|f(\phi_e)|^2}{H_e^2} \simeq 0.14, \quad \frac{m_\chi f(\phi_e)}{H_e^2} \simeq 6.29\left(\frac{m_\chi}{m_\phi}\right), \tag{6.34}$$

In this case, as long as $m_\chi > 0.15 m_\phi$, the last term contributes most to the effective mass. This is confirmed numerically in the next section. We also want to emphasize that the estimation is without graviton mass contribution, and should be considered as conservative. Moreover, during inflation $\phi > \phi_e$, the relative contribution from $|f|^2$ and $m_\chi f$ can be even larger.

6.2 Numerical Results

In this section, we show the necessary numerical results for calculation of DM relic abundance in the current Universe. The first step is to solve the background evolution of inflaton field through eqs. (6.1). In practice, we use the slow-roll solution as initial conditions for the inflaton field. As slow-roll inflation is an attractor, the trajectory converges to the "true" one after a sufficient time.

By choosing the above conditions for the background, we also need to ensure that every mode is well inside the horizon upon simulation start and can be described by the Bunch-Davies vacuum

$$\chi_k = \frac{1}{\sqrt{2\omega_k}}\,, \ \chi_k' = \frac{-i\omega_k}{\sqrt{2\omega_k}}\,, \quad \text{or equivalently,} \quad \alpha_k = 1,\ \beta_k = 0\,, \tag{6.35}$$

where $\omega_k = \omega_k(\tau_i)$ is taken at the time of initialization τ_i and it approaches k in the infinite past $\tau_i \to -\infty$. Consequently, long wavelength modes need to be initialized early. The largest scale considered here is $k/(a_e H_e) = 10^{-2}$, and it requires initialization at ~ 10 e-folds before the end of inflation.

We show the relevant background quantities in Fig. 6.2. They are computed using the inflation potential given in eq. (6.2) with a fixed tensor to scalar ratio $r = 0.0035$ ($\alpha \approx M_{\rm pl}^2$). For a better display of data, the number of e-folds $N = \ln a(t)$, instead of the cosmic time t, is chosen as the time variable. The scale factor has been rescaled so that the scale factor at end of inflation is unity $a(t_e) \equiv 1$, which was determined by the condition that the first Hubble slow-roll parameter equals 0.1:

$$\epsilon_1 := -\frac{\dot H}{H^2} = \frac{1}{2M_{\rm pl}^2}\left(\frac{{\rm d}\phi}{{\rm d}N}\right)^2 \overset{!}{=} 0.1\,. \tag{6.36}$$

Here we use dot to denote derivative with respect to the cosmic time t and the second equality follows from the Friedmann eqs. (6.1). Thus, the number of e-folds at the end of inflation is defined as zero. The first diagram shows the evolution of the field value $\phi(N)$. It smoothly rolls down to the minimum

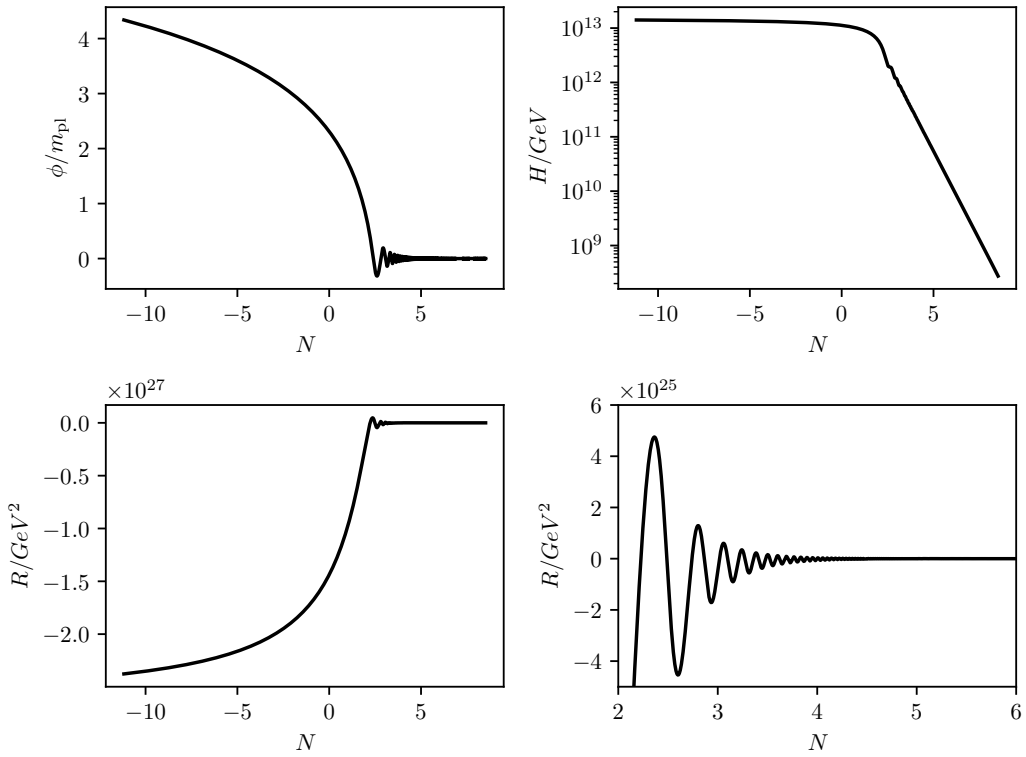

Figure 6.2: Background evolution: inflaton field value ϕ, Hubble parameter H and Ricci scalar R, with $\alpha \approx M_{\rm pl}^2$ corresponding to the tensor to scalar ratio $r = 0.0035$. The time variable has been transformed to number of e-folds $N(t) = \ln(a(t))$.

at $\phi = 0$ and starts to oscillate around it. This oscillation process induces the decrease of Hubble scale H as well as an oscillation of the Ricci scalar R. During slow roll inflation, both two quantities are more or less constants:

$$R = -6\frac{a''}{a^3} \overset{\text{SR}}{\approx} -12H^2 \approx \text{constant}\,. \tag{6.37}$$

However, the Ricci scalar oscillates around zero after inflation, while H decays exponentially and slightly oscillates. Note that the Ricci scalar R appears in the effective χ mass for non-SUGRA case in eq. (6.14), and the (square of) Hubble parameter H^2 for the SUGRA case in eq. (6.31).

Let us first consider the effective frequency squared without SUGRA correction; it takes the following form during slow-roll inflation

$$\omega_k^2 = k^2 + a^2\left(m_\chi^2 + \frac{R}{6}\right) \overset{\text{SR}}{=} k^2 + a^2\left(m_\chi^2 - \frac{2M_{\rm pl}^2}{\alpha}m_\phi^2\right)\,, \tag{6.38}$$

where the second Friedman equation in eqs. (6.37) have been used. The last equality only holds during slow-roll inflation. For light DM field, the oscillation of R leads ω_k^2 to cross zero and thus induces a tachyonic instability, especially for low momentum modes.

One can then solve the differential equation associated with ω_k to get the phase space distribution

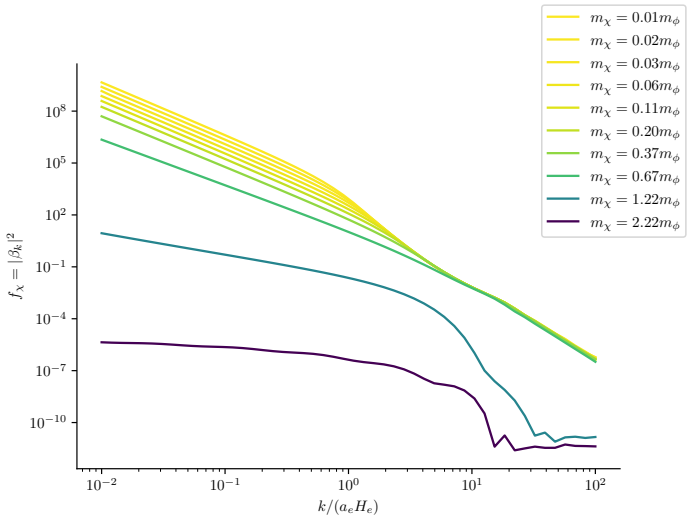

Figure 6.3: Phase space distribution of χ quanta without SUGRA correction. In the vanishing mass limit, the phase space distribution approaches $|\beta_k|^2 \propto k^{-3}$.

of the DM field. It proves to be more efficient to use eq. (6.14) due to the tachyonic instability. We show some examples with different DM mass in Fig. 6.3. For light fields, the effect of the tachyonic instability is significant, which leads to the typical scaling behavior in the low momentum region $f_\chi \propto k^3$. In contrast, for heavier DM field, f_χ approaches a constant for small momentum. The threshold DM mass is roughly the inflaton mass, as expected from eq. (6.38). Heavier DM fields are generally harder to get excited. Their f_χ are much smaller than those of light fields.

Now let us consider the GPP of DM particles with SUGRA correction. The spectra for two distinct values of $m_{3/2}$ are shown in Fig. 6.4. The most striking feature is that the spectrum has no infrared divergence. Due to the additional terms in the effective mass in eq. (6.31), the tachyonic instability doesn't exist in SUGRA case. Again, higher m_χ gives less χ particles. When $m_\chi \ll m_{3/2}$, the spectra is controlled by the inflation potential and size of $m_{3/2}$. All light fields share basically indistinguishable spectra.

It is beyond the scope of the current work to have an analytic understanding of the particle number spectra. For a qualitative understanding, the time evolution of the effective mass might give some insights. We show the effective mass of DM fields during and after inflation in Fig. 6.5. The solid and dashed lines are the effective mass of real and imaginary fields, respectively. We also plot the effective mass with $f(\phi) = 0$ to illustrate the difference from pure H^2 in effective mass as in [254]. Our estimate in eq. (6.32) is taken at time of end of slow-roll inflation, which corresponds to $N \approx 1.66$ in the plot, and agrees with numerical results. When $\phi < \phi_e$, the difference between the two cases is even more pronounced, as the extra contributions increase faster with ϕ than H^2 term. The imaginary field has higher mass during inflation and the rate of change in effective frequency is higher for $m_\chi < m_\phi$. Thus, as one can see from the Fig. 6.4, in SUGRA the imaginary part has higher production in such case. On the contrary, for $m_\chi \gtrsim m_\phi$, the real part is produced in greater amount. When $m_{3/2} \ll \alpha m_\phi / M_{\rm pl}^2$, the mass splittings prior to reheating are similar among $m_{3/2}$'s, as the first term in the f-function dominates, see eq. (6.28). Although the splitting at the end of the particle production

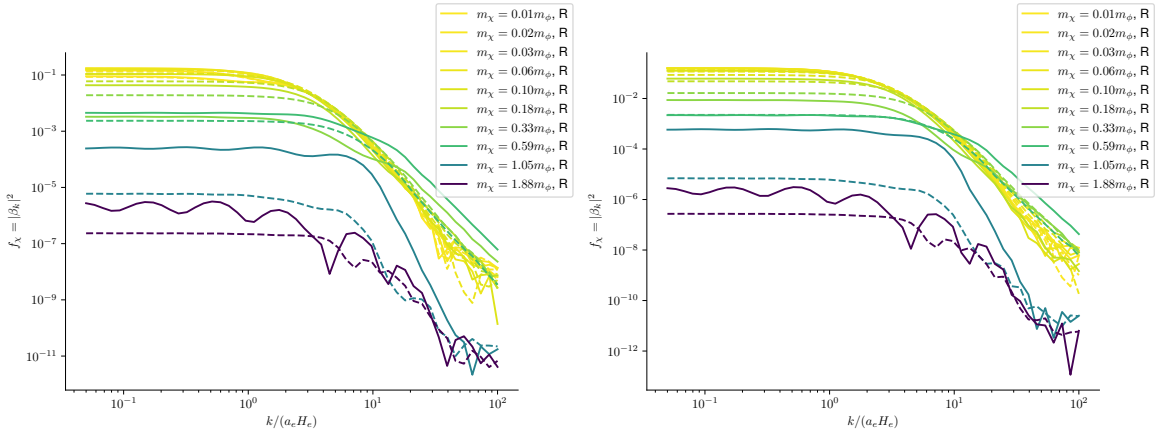

Figure 6.4: Phase space distribution of χ quanta with $m_{3/2} = 0$ (left) and $m_{3/2} = 0.1m_\phi$ (right). Dashed line represents the imaginary field and solid line the real field.

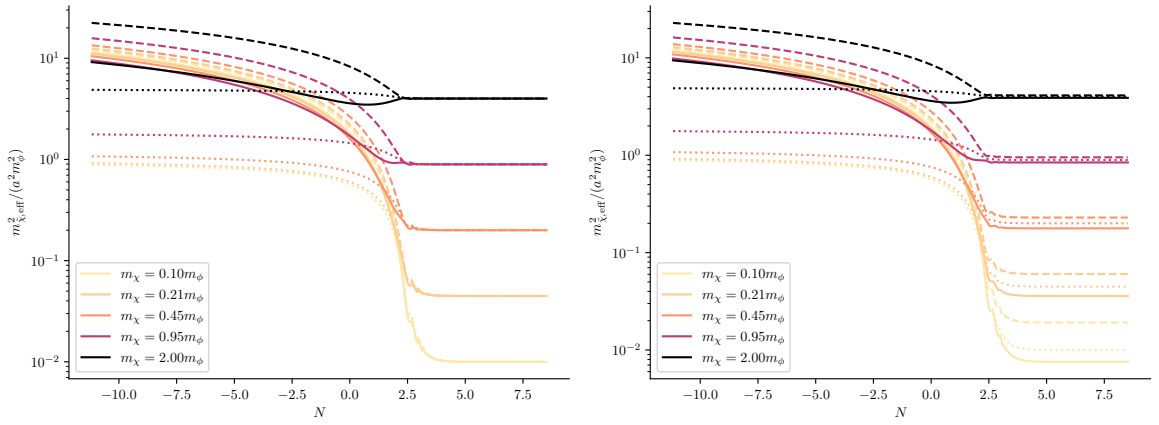

Figure 6.5: Effective mass squared in the appropriate units with $m_{3/2} = 0.0$ (left) and $m_{3/2} = 0.1m_\phi$ (right) respectively. Solid (dashed) line is for effective mass of real (imaginary) field. Dotted lines are the effective mass with $f = 0$ (which is the effective mass in [254]).

clearly depends on the gravitino mass

$$m^2_{\chi,R,I} = m^2_\chi + \frac{m^2_{3/2}}{3} \mp \frac{m_{3/2} m_\chi}{\sqrt{3}}\,, \tag{6.39}$$

the ultimate rate of change for $m^2_{\chi,\text{eff}}$ and ω^2_k are largely unaffected by it. Thus, the phase space distributions are very similar with light gravitino masses.

From the phase space distribution, the isocurvature spectrum can be calculated via eq. (6.22). It has been shown (semi-)analytically that $|\beta_k|^2 \propto k^{-3}$ (in the low momentum side) produces a nearly scale-invariant isocurvature spectrum in the low momentum side and $|\beta_k|^2 \propto$ const. gives blue-tilted spectrum [261]. In the vanishing mass limit $m_\chi \to 0$, the isocurvature spectrum indeed approaches scale invariance, see Fig. 6.6(a). This can be potentially dangerous when considering CMB isocurvature constraints [213]. In the SUGRA case, the isocurvature spectrum always holds a k^3 scaling in the low momentum limit. The spectra are shown in Fig. 6.6(b). Thus, the CMB isocurvature constraint poses no limitation on the model parameters, when SUGRA corrections are present.

We show the energy densities of DM in the current universe in Fig. 6.7. We assume that the DM particle does not interact with other (standard model) particles and their comoving number density is conserved after production. Thus, its current energy density can be expressed as $\rho_{\chi,0} \approx m_\chi n_{\chi,0}$. On the vertical axis, we use the energy density of the DM particles divided by the entropy density and reheating temperature $\rho_{\chi,0}/(s_0 T_{\text{rh}})$. This quantity is obtained from comoving number via the eq. (6.40). To get the desired relic abundance $\Omega_{\text{DM}} h^2 \approx 0.12$, we need

$$\frac{\rho_{\chi,0}}{s_0} \approx 4 \times 10^{-10}\,\text{GeV}\,. \tag{6.40}$$

This means different m_χ's will need different reheating temperature to satisfy this condition.

The phase space distribution of non-SUGRA case scales like k^{-3} in the infra-red limit. This

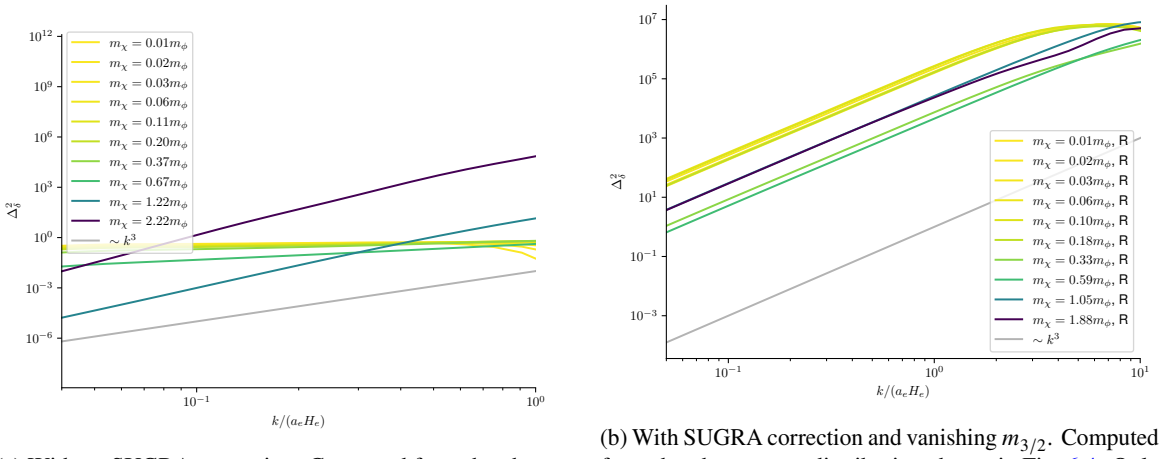

(a) Without SUGRA correction. Computed from the phase space distribution shown in Fig. 6.3.

(b) With SUGRA correction and vanishing $m_{3/2}$. Computed from the phase space distribution shown in Fig. 6.4. Only the real field contributions are shown here.

Figure 6.6: Isocurvature power spectrum calculated using eq. (6.22).

leads to an IR divergence in the total number density eq. (6.18) with $n \sim \int_0^\infty \mathrm{d}k\, k^{-1}$. To cure this divergence, one can set an IR cutoff at CMB scale, since DM perturbations larger than the horizon at recombination are just part of the background. As it is expensive to track modes across so many number of e-folds in our numerical computation, we choose to extrapolate the phase space distribution to the CMB scale. We take 60 e-folds of inflation since CMB scale. It can be shown that the final abundance is proportional to the number of e-folds, if the number of e-folds is chosen differently. The abundance without SUGRA correction can be found in Fig. 6.7. As we see, the abundance saturates at the low mass limit, as expected from the phase space distribution in Fig. 6.3. The tachyonic instability goes away with increasing m_χ, therefore, the abundance decreases rapidly.

The number density with SUGRA correction is more straightforward to compute and it is shown in Fig. 6.7 with $r = 0.0035$. When $m_\chi < m_\phi$, the abundance from GPP increases with m_χ linearly, which comes from the linear mass dependency in energy density of non-relativistic particles. The abundance then decreases exponentially when $m_\chi > m_\phi$. There is an interesting bump for small $m_{3/2}$ around $m_\chi \sim m_\phi$. This primarily comes from the real field contribution, and one can see this for $k/(a_e m_\phi) \gtrapprox 1$ also in Fig. 6.4. As one can anticipate from eq. (6.32) and Fig. 6.5, the DM abundance with $f(\Phi) \equiv 0$ (a la [254]) is more suppressed than ours, although not by much.

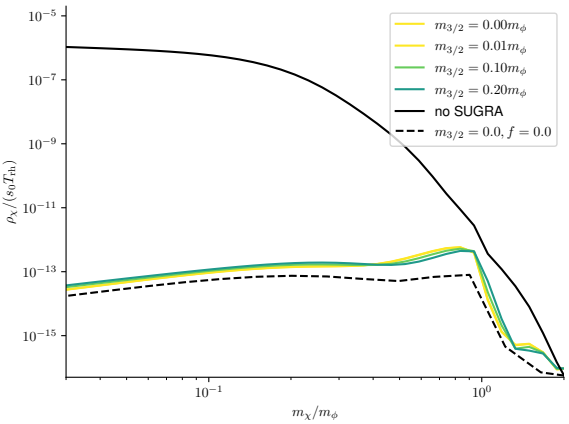

Figure 6.7: Comoving energy density of the DM field χ divided by the reheating temperature. Higher values require lower reheating temperatures. The tensor-to-scalar ratio is fixed to $r = 0.0035$. Solid black line show the abundance without SUGRA correction, while dashed shows the abundance with SUGRA correction but $f(\Phi) \equiv 0$, a la [233].

The abundances with various desired values of tensor-to-scalar ratio are plotted in Fig. 6.8. As we wish χ to be the only DM around, eq. (6.40) leads to certain reheating temperature for a set of fixed model parameters ($m_{3/2}$, m_χ and r). In SUGRA a high reheating temperature may lead to the gravitino problem [197–199]. If $m_{3/2} \approx 1$TeV, this means an upper bound on reheating temperature $T_{\rm rh} < 10^9$GeV. Our results are compatible with this bound. As implied in Fig. 6.7, required reheating temperature $T_{\rm rh}$ for all values of r goes like m_χ^{-1} for small m_χ until $m_\chi \sim m_\phi$, where the produced comoving number density drops dramatically and high reheating temperature is necessary. Effects of $m_{3/2}$ is still very minimal. Lower desired tensor-to-scalar ratio reduces the Hubble scale H_e, suppresses the GPP production and demands higher reheating temperature.

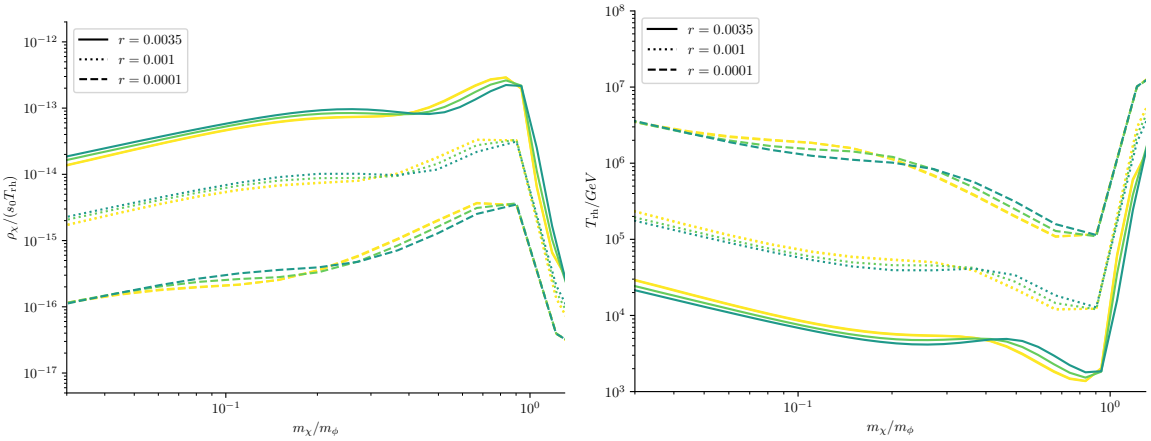

Figure 6.8: DM abundance $\rho_{\chi,0}/(s_0 T_{\rm rh})$ and required reheating temperature for χ to be the only DM. Different colors correspond to different $m_{3/2}$, c.f. Fig. 6.7.

6.3 Summary and Conclusions

In this chapter, we looked at gravitationally produced DM particles with SUGRA corrections. The α-attractor inflation model was chosen for this investigation. It is theoretically well-motivated and fits the observation well. We solve the equation governing Fourier modes of the DM field, eq. (6.14), on top of the evolving background. Then, the Bogoliubov coefficients are reconstructed and (its modulus square) can be interpreted as particle number spectrum. In the vanilla scenario without SUGRA corrections, the produced particle number decrease exponentially once the DM particles are roughly heavier than the inflaton and there is clear tachyonic instability. However, the particle production with SUGRA correction has some distinctive features. The phase space distribution shows no infra-red divergence due to the lack of tachyonic instability. Computation of the current abundance, thus, requires no cut-off. The isocurvature power spectrum is blue-titled ($\propto k^3$) and not constrained by CMB isocurvature non-detection. The required reheating temperature is shown to increase with decreasing tensor-to-scalar ratio r, and higher than non SUGRA cases. We also highlighted the difference from the usually SUGRA scenario in [254]. In particular, we find that the SUGRA suppression is still present even in models with $m_\phi \sim H_I$. Due to the additional contribution from the f-function, the GPP suppression gets reduced.

There are a couple of directions for further investigation. We focus only on the α-attractor potential with $n = 1$. One can then ask how different assumptions would change our results. The potential can be written as $V \propto |\phi|^{2n}$ near the origin. This changes the inflaton mass (there is no quadratic term in potential with $n \geq 2$) and the equation of state during the reheating phase changes. The formula (6.40) is derived assuming matter domination for reheating. Additionally, there are non-linear phenomena in the inflaton sector, which can further change the background evolution, see e.g. [262] and the review [263]. In this work, the results are all computed numerically. One might gain additional insight by deriving analytical results. How to incorporate non-minimal coupling in SUGRA setting would be an interesting direction. Introduction of a non-minimal coupling to the scalar field famously introduces massively different spectrum. It would be interesting to see such effects with SUGRA correction as well. We leave these for further works.

The χ field does not have to be the DM; instead there are several other possibilities. GPP can also be used as a portal to reheating the hidden sector [264]. GPP could also be an important channel to produce the observed baryon-asymmetry, where heavy X particles are produced gravitationally, where decay violates baryon number and CP conservation [265].

GPP can also be applied to other fields with higher spin. The spin-$1/2$ superpartner of χ field will be produced on an equal footing. As the expansion of the universe can also break SUSY characterized by the Hubble parameter [97, 187–190], the mass splitting between scalar and its fermionic superpartner becomes time dependent, which may lead to novel result. Another important example is the tensor modes (spin-2 field) in the metric perturbations which (can) corresponds to the gravitational waves. Gravitational waves are inevitably produced via the same mechanism as the scalar field: they have the same dispersion relation as massless non-minimal scalar field (at least in the non-SUGRA case). The only difference is that tensor mode has two polarizations. They would correspond to frequencies from radiation-matter equality scale $f_{\rm eq} \sim 5 \times 10^{-17}$ Hz to $f_{\rm rh} \sim 200\,{\rm Hz}\left(\frac{T_{\rm rh}}{10^9 {\rm GeV}}\right)$ [209]. As the required reheating temperature is different between SUGRA and non-SUSY case, these frequencies shifts to $\sim 1\,{\rm Hz} - 10^{-4}$Hz in our model. It is well within accessible frequency ranges of e.g. LISA. However, the energy density parameter would be $\Omega_{{\rm gw},0}h^2 \sim 10^{-15}$ below LISA sensitivity [266].

CHAPTER 7

Conclusions

The thesis contains a collection of work on the cosmology of the early universe, aiming to understand the origin of our current observable universe. Based on the cosmic microwave background (CMB), it is almost isotropic and presumably also homogeneous, contains dark matter (DM) that interacts weakly with ordinary matter, and has more baryonic matter than antibaryonic matter. We use cosmic inflation, where the universe experiences an exponential expansion, as a tool to understand the flatness of our universe, as well as the origin of DM and baryon matter asymmetry. This includes inflation model building, DM production after inflation, as well as their possible connection with supersymmetry and modular symmetry.

We first study the inflection point inflation generated by a polynomial superpotential and a canonical Kähler potential under the supergravity framework, where only one chiral superfield is needed. We find that the special form of the scalar potential limits the inflationary Hubble parameter to values $\lesssim 10^{10}$ GeV and the inflaton mass to $\lesssim 10^{11}$ GeV. We obtain analytic results for small field cases and present numerical results for large field cases. We find the tensor-to-scalar ratio $r < 10^{-8}$ is always suppressed in these models, while the running of spectral index $\alpha \approx O(-10^{-3})$ may be testable in next-generation CMB experiments. We also discuss the possible effects of SUSY breaking Polonyi term presented in the superpotential where we find a general upper bound for the SUSY breaking scale for a given value of the Hubble parameter.

As the next step, we propose new classes of inflation models based on modular symmetry, where the modulus field τ serves as the inflaton. We establish a connection between modular inflation and modular stabilization, wherein the modulus field rolls towards a fixed point along the boundary of the fundamental domain. We find the modular symmetry strongly constrains the possible shape of the potential and identifies some parameter space where the inflation predictions agree with cosmic microwave background observations. The tensor-to-scalar ratio is predicted to be smaller than 10^{-6} in our models, while the running of spectral index is of the order of 10^{-4}.

We further use modular symmetry as an organizing principle that attempts to simultaneously address the lepton flavor puzzle, inflation, and post-inflationary reheating. We demonstrate this approach using the finite modular group A_4 in the lepton sector. In this model, neutrino masses are generated via the Type-I see-saw mechanism, with modular symmetry dictating the form of the Yukawa couplings and right-handed neutrino masses. The modular field also drives inflation, and inflaton-matter interactions required for reheating naturally arise from the expansion of relevant modular forms. Although the corresponding inflaton decay rates are suppressed by the Planck scale, the reheating temperature can

still be high enough to ensure successful Big Bang nucleosynthesis. The same couplings responsible for reheating can also contribute to generating baryon asymmetry of the Universe through non-thermal leptogenesis. With the given couplings, successful leptogenesis requires the inflaton mass to be higher than 10^{13} GeV.

We also consider gravitational particle production of dark matter within a supergravity framework, utilizing the α-attractor inflation model. The particle spectrum is computed numerically, and the DM number density is obtained. We show how the DM mass, gravitino mass, and inflation model parameters modify the results, and find the reheating temperature that leads to sufficient DM production. In our setup, supergravity corrections suppress the efficiency of GPP, making the isocurvature constraint significantly weaker compared to the normal case. With tensor-to-scalar ratio ranging from $10^{-3} - 10^{-4}$ and DM mass from $10^{-2} m_\phi - m_\phi$, the required reheating temperature should be around 10^3GeV $- 10^7$GeV.

The models we have presented are only a small step towards adaquate answers to existing puzzles. An improved understanding of nature requires advances in both the theoretical and experimental sides. With more data from cosmological observations and, hopefully, collider experiments, we are awaiting the final confirmation of whether SUSY is realized in nature and other novel ideas that provide a compelling and systematic description of BSM physics.

APPENDIX A

Appendix

A.1 Relevant Modular Forms

In this section we discuss some useful modular forms which will present in our modular invariant potentials, including Dedekind eta function, Eisenstein series and j invariant. We also list some results related with our superpotentials.

- Dedekind eta function
  The Dedekind eta function is a modular function of "weight 1/2" defined as

$$\eta(\tau) = q^{1/24}\prod_{n=1}^{\infty}(1-q^n), \qquad q \equiv e^{2\pi i\tau}\,, \tag{A.1}$$

  which satisfies the identities $\eta(\tau+1) = e^{i\pi/12}\eta(\tau)$ and $\eta(-1/\tau) = \sqrt{-i\tau}\eta(\tau)$. The q-expansion of eta function is given by

$$\eta = q^{1/24}[1-q-q^2+q^5+q^7-q^{12}-q^{15}+O(q^{22})]\,. \tag{A.2}$$

  At the modular symmetry fixed points $\tau = \omega, i$, the eta function takes the following values,

$$\eta(i) = \frac{\Gamma(1/4)}{2\pi^{3/4}}\,, \quad \eta(\omega) = e^{-\frac{i\pi}{24}}\frac{3^{1/8}\,\Gamma^{3/2}(1/3)}{2\pi}\,. \tag{A.3}$$

- Eisenstein series
  The Eisenstein series $G_{2k}(\tau)$ of weight $2k$ for integer $k \geq 1$ are defined as [267]:

$$G_{2k}(\tau) = 2\zeta(2k) + 2\frac{(2\pi i)^{2k}}{(2k-1)!}\sum_{n=1}^{\infty}\sigma_{2k-1}(n)q^n\,, \tag{A.4}$$

  where $\zeta(z)$ denotes the Riemann's zeta function, and $\sigma_p(n)$ is the sum of the pth power of the divisors of n,

$$\sigma_p(n) = \sum_{d|n} d^p\,, \tag{A.5}$$

where $d|n$ is shorthand for "d divides n". The Eisenstein series $G_{2k}(\tau)$ are modular forms of weight $2k$ for any integer $k > 1$. However, $G_2(\tau)$ is not a modular form and its transformation is given by

$$G_2(\gamma\tau) = (c\tau + d)^2 G_2(\tau) - 2\pi i c(c\tau + d)\,. \tag{A.6}$$

Note the modular functions $G_2(\tau)$ and the Dedekind eta are related by

$$\frac{\partial_\tau \eta(\tau)}{\eta(\tau)} = \frac{i}{4\pi} G_2(\tau)\,. \tag{A.7}$$

The modified weight 2 Eisenstein series $\widehat{G}_2$ is defined by

$$\widehat{G}_2(\tau) = G_2(\tau) + \frac{2\pi}{i(\tau - \bar{\tau})}\,, \tag{A.8}$$

which is a non-holomorphic function but preserves modularity. Consequently $\widehat{G}_2(\tau)$ vanishes at the fixed points:

$$\widehat{G}_2(i) = \widehat{G}_2(\omega) = 0\,. \tag{A.9}$$

Sometimes it is more convenient to work with the normalized Eisenstein series $E_{2k}(\tau)$, which differ from G_{2k} in the normalization constant [267]:

$$E_{2k}(\tau) = \frac{G_{2k}(\tau)}{2\zeta(2k)}\,. \tag{A.10}$$

We provide some values of $E_{2k}(\tau)$ relevant to this paper:

$$E_2(i) = \frac{3}{\pi}\,, \qquad E_2(\omega) = \frac{2\sqrt{3}}{\pi}\,, \tag{A.11}$$

$$E_4(i) = \frac{3\Gamma^8(1/4)}{(2\pi)^6}\,, \quad E_4(\omega) = 0\,, \tag{A.12}$$

$$E_6(i) = 0\,, \qquad E_6(\omega) = \frac{6^3\Gamma^{18}(1/3)}{(2\pi)^{12}}\,. \tag{A.13}$$

As regards the derivatives of the Eisenstein series, Ramanujan-Shen's differential equation [268] is useful:

$$qE'_{2k-2} = \frac{k-1}{2\pi^2\zeta(2k-2)} \sum_{n=1}^{k-1} \zeta(2n)\zeta(2k-2n)(E_{2n}E_{2k-2n} - E_{2k})\,, \quad \text{for } k \geq 2\,, \tag{A.14}$$

where $E'_{2k-2} = \mathrm{d}E_{2k-2}/\mathrm{d}q$. The first several relations read:

$$\begin{aligned} qE'_2(q) &= \frac{1}{12}(E_2^2 - E_4)\,, \\ qE'_4(q) &= \frac{1}{3}(E_2E_4 - E_6)\,, \\ qE'_6(q) &= \frac{1}{2}(E_2E_6 - E_4^2)\,. \end{aligned} \tag{A.15}$$

Using the first identity in eq. (A.15) and $\mathrm{d}/\mathrm{d}\tau = 2\pi i q\,\mathrm{d}/\mathrm{d}q$, we find the derivative of $\widehat{G}_2$ is as follows:

$$\partial_\tau \widehat{G}_2(\tau) = \frac{i\pi^3}{18}(E_2^2 - E_4) - \frac{2\pi}{i(\tau-\bar{\tau})^2}\,, \tag{A.16}$$

and the numerical values of $\partial_\tau \widehat{G}_2(\tau)$ at the fixed points are

$$\partial_\tau \widehat{G}_2(i) = -i\frac{\Gamma^8(1/4)}{384\pi^3}\,, \quad \partial_\tau \widehat{G}_2(\omega) = 0\,. \tag{A.17}$$

The anti-holomorphic derivative of $\widehat{G}_2(\tau,\bar{\tau})$ is

$$\partial_{\bar{\tau}} \widehat{G}_2(\tau) = -\partial_\tau \overline{\widehat{G}}_2(\tau) = \frac{2\pi}{i(\tau-\bar{\tau})^2}\,, \tag{A.18}$$

the corresponding numerical values at the fixed points are

$$\begin{aligned} \partial_{\bar{\tau}} \widehat{G}_2(\tau)\Big|_{\tau=i} &= -\partial_\tau \overline{\widehat{G}}_2(\tau)\Big|_{\tau=i} = i\frac{\pi}{2}\,, \\ \partial_{\bar{\tau}} \widehat{G}_2(\tau)\Big|_{\tau=\omega} &= -\partial_\tau \overline{\widehat{G}}_2(\tau)\Big|_{\tau=\omega} = i\frac{2\pi}{3}\,. \end{aligned} \tag{A.19}$$

These relations are useful when calculating the derivatives of the scalar potential.

- Klein j-invariant function

The Klein j-invariant function is a modular form of weight zero, defined in terms of Dedekind eta function and Eisenstein series as follows [133, 137]

$$j(\tau) \equiv \frac{3^6 5^3}{\pi^{12}}\frac{G_4^3(\tau)}{\eta^{24}(\tau)} = \frac{3^6 5^3}{\pi^{12}}\frac{G_4^3(\tau)}{\Delta(\tau)}\,, \quad \Delta(\tau) \equiv \eta^{24}(\tau)\,, \tag{A.20}$$

which implies

$$j(\tau) - 1728 = \left(\frac{945}{2\pi^6}\right)^2 \left(\frac{G_6(\tau)}{\eta^{12}(\tau)}\right)^2 = \left(\frac{945}{2\pi^6}\right)^2 \frac{G_6^2(\tau)}{\Delta(\tau)}\,. \tag{A.21}$$

From eqs. (A.20, A.21), we can see that the two expressions of H function in eq. (4.6) and eq. (4.8) are equivalent. Given the identity of eq. (A.10), j and $j-1728$ can also be compactly

written as

$$j(\tau) - 1728 = \left(\frac{E_6(\tau)}{\eta^{12}(\tau)}\right)^2 , \quad j(\tau) = \left(\frac{E_4(\tau)}{\eta^8(\tau)}\right)^3 . \tag{A.22}$$

This j-function is a one-to-one map between points in the fundamental domain and the whole complex plane. At the fixed points, one has

$$j(i\infty) = +\infty , \qquad j(\omega) = 0 , \qquad j(i) = 1728 = 12^3 . \tag{A.23}$$

For convenience, the q-expansion of j-function is given by

$$\begin{aligned} j(\tau) \;=\; & 744 + \frac{1}{q} + 196884q + 21493760q^2 + 864299970q^3 + 20245856256q^4 \\ & +333202640600q^5 + 4252023300096q^6 + 44656994071935q^7 + \mathcal{O}(q^8) \end{aligned} \tag{A.24}$$

The derivatives of the j-function read as,

$$\begin{aligned} \frac{\partial j}{\partial \tau} &= -2\pi i \frac{E_6(\tau)E_4^2(\tau)}{\eta^{24}(\tau)} , \\ \frac{\partial^2 j}{\partial \tau^2} &= \frac{(2\pi)^2}{\eta^{24}(\tau)} \left[\frac{1}{6}E_2(\tau)E_4^2(\tau)E_6(\tau) - \frac{1}{2}E_4^4(\tau) - \frac{2}{3}E_6^2(\tau)E_4(\tau)\right] , \end{aligned} \tag{A.25}$$

which are useful to calculate the second derivative of scalar potential. The derivative of j-function also vanishes at the fixed points:

$$\left.\frac{\partial j}{\partial \tau}\right|_{\tau=i} = \left.\frac{\partial j}{\partial \tau}\right|_{\tau=\omega} = 0 . \tag{A.26}$$

- H function
  Using eq. (A.22), the H function in eq. (4.6) can also be written as,

$$H(\tau) = \left(\frac{E_6(\tau)}{\eta^{12}(\tau)}\right)^m \left(\frac{E_4(\tau)}{\eta^8(\tau)}\right)^n \mathcal{P}(j(\tau)) . \tag{A.27}$$

The numerical values of the H function at the fixed points are determined to be

$$\begin{aligned} H(i) &= \begin{cases} 0 & m > 0 \\ 12^n \mathcal{P}(1728) & m = 0 \end{cases} , \\ H(\omega) &= \begin{cases} 0 & n > 0 \\ i^m 2^{3m} 3^{\frac{3m}{2}} \mathcal{P}(0) & n = 0 \end{cases} . \end{aligned} \tag{A.28}$$

The derivative of the H function is found to be:

$$\partial_\tau H = -i\pi H \left(m\frac{E_4^2}{E_6} + \frac{2n}{3}\frac{E_6}{E_4} + \frac{i}{\pi}\frac{\mathrm{d}\ln\mathcal{P}}{\mathrm{d}j}\frac{\mathrm{d}j}{\mathrm{d}\tau}\right) , \tag{A.29}$$

and the corresponding numerical values at the fixed points are:

$$\begin{aligned}
\partial_\tau H(\tau)\Big|_{\tau=i} &= \begin{cases} 0 & m=0 \text{ or } m>1 \\ -i2^{2n+2}3^{2+n}\frac{\Gamma^4(1/4)}{(2\pi)^2}\mathcal{P}(1728) & m=1 \end{cases}, \\
\partial_\tau H(\tau)\Big|_{\tau=\omega} &= \begin{cases} 0 & n=0 \text{ or } n>1 \\ -i^{m+1}2^{3m+3}3^{3m/2+1}e^{i\frac{\pi}{3}}(2\pi)^{-3}\Gamma^6(1/3)\mathcal{P}(0) & n=1 \end{cases}.
\end{aligned} \tag{A.30}$$

When determining the Hessian matrix of the scalar potential, the second order derivative of the H function is needed. It is found that $\partial_\tau^2 H$ takes the following value at the fixed points:

$$\begin{aligned}
\partial_\tau^2 H(\tau)\Big|_{\tau=i} &= \begin{cases} 0 & m>2 \\ -3^{n+4}2^{5+2n}\frac{\Gamma^8(1/4)}{(2\pi)^4}\mathcal{P}(1728) & m=2 \\ 3^{n+2}2^{2n+2}\frac{\Gamma^4(1/4)}{(2\pi)^2}\mathcal{P}(1728) & m=1 \\ -2^{2n-1}3^n\frac{\Gamma^8(1/4)}{(2\pi)^4}\mathcal{P}(1728)\left(n+3^4 2^6\frac{\mathcal{P}'(1728)}{\mathcal{P}(1728)}\right) & m=0 \end{cases}, \\
\partial_\tau^2 H(\tau)\Big|_{\tau=\omega} &= \begin{cases} 0 & n=0 \text{ or } n>2 \\ -i^m e^{i\frac{2\pi}{3}}2^{3m+7}3^{\frac{3m}{2}+2}\frac{\Gamma^{12}(1/3)}{(2\pi)^6}\mathcal{P}(0) & n=2 \\ i^m e^{i\frac{\pi}{3}}2^{3m+4}3^{\frac{3}{2}m+\frac{1}{2}}\frac{\Gamma^6(1/3)}{(2\pi)^3}\mathcal{P}(0) & n=1 \end{cases}.
\end{aligned} \tag{A.31}$$

A.2 Concrete Examples of Modular Inflation

In this section we list some concrete examples where modular inflation is realized with different choices of parameters and their predictions, as shown in table A.1. All the cases share same features: The tensor to scalar ratio r is smaller than 10^{-6}, while the running of spectral index $\alpha \approx -2\xi_V^2$ is of order $O(-10^{-4})$. It is hard to detect such a small tensor to scalar ratio r but we might have enough sensitivity on α in the future CMB S4 mission and observation of 21 cm fluctuations [111–114].

A.3 A Toy Model of Dilaton Stabilization

In this thesis we have assumed that dilaton field S is stabilized while the modulus field τ remains dynamic. We would like to justify this assumption using a toy model, where stabilization of dilaton filed does not constraint the modulus potential. This toy model is inspired by the racetrack scenario, which has been used to study moduli stabilization and inflation [269–273]. Here we consider a two-component superpotential with different energy scales:

$$\mathcal{W} = \Lambda_1 \Delta(S) g(\tau) + \Lambda_2 \Omega(S) f(\tau) \tag{A.32}$$

where $g(\tau)$ and $f(\tau)$ are weight -3 modular functions, both of them can be parameterized by $H(\tau)\eta^{-6}(\tau)$ with different m, n and polynomial $\mathcal{P}(j(\tau))$. $\Delta(S)$ and $\Omega(S)$ are holomorphic functions of S. The second term $\Lambda_2\Omega(S)f(\tau)$ was used in our paper to generate the inflation potential. Λ_2 is the inflation scale and Λ_1 refers the mass scale of dilaton field, which can be much larger than the

N_e	50			
A	29.1470	24.3060	29.1495	25
β	0	0.126434	0	0.108376
γ	0	0	−0.115590	−0.016932
n_s	0.9462	0.9637	0.9643	0.9639
$\log_{10} r$	−7.39	−6.03	−6.30	−6.04
ε_V	2.5×10^{-9}	6.7×10^{-8}	3.1×10^{-8}	5.6×10^{-8}
η_V	−0.0269	−0.019	−0.018	−0.018
ξ_V^2	0.00054	0.00028	0.00035	0.00033
ϖ_V^2	-7.7×10^{-6}	-1.2×10^{-5}	-1.2×10^{-6}	-1.2×10^{-5}
N_e	55			
A	29.1470	24.3091	29.1441	25
β	0	0.126425	0	0.108152
γ	0	0	−0.115640	−0.017168
n_s	0.9510	0.9649	0.9649	0.9650
$\log_{10} r$	−7.50	−6.04	−6.60	−6.42
ε_V	1.9×10^{-9}	5.7×10^{-8}	1.6×10^{-8}	1.5×10^{-8}
η_V	−0.024	−0.018	−0.018	−0.018
ξ_V^2	0.00045	0.00021	0.00038	0.00037
ϖ_V^2	-5.9×10^{-6}	-8.6×10^{-6}	-8.5×10^{-6}	-7.8×10^{-6}
N_e	60			
A	29.1470	24.3108	29.1548	25
β	0	0.126420	0	0.108104
γ	0	0	−0.115567	−0.017219
n_s	0.9551	0.9649	0.9649	0.9654
$\log_{10} r$	−7.61	−6.09	−6.34	−6.61
ε_V	1.5×10^{-9}	5.1×10^{-8}	2.8×10^{-8}	1.54×10^{-8}
η_V	−0.0225	−0.018	−0.018	−0.017
ξ_V^2	0.00037	0.00013	0.00012	0.00033
ϖ_V^2	-4.7×10^{-6}	-5.9×10^{-6}	-5.8×10^{-6}	-5.4×10^{-6}

Table A.1: Numerical results of the slow-roll parameters $\{\varepsilon_V, \eta_V, \xi_V^2, \varpi_V^3\}$ and inflationary predictions n_s and r for various combinations of A, β and γ in the inflation potential. Notably, we highlight the results for distinguished values of A. It's worth noting that the spectral index n_s is a bit small in the cases of $\beta = \gamma = 0$, as indicated by data plotted in red.

inflation scale $\Lambda_1 \gg \Lambda_2$. Then it would be the first term dominate the potential while the second term only perturb it. One can suppose the first term determines the minimum of S. If the dilaton field is stabilized at S_0 with the following property:

$$\Delta(S_0) = \Delta_S(S_0) = 0, \quad \Omega_S(S_0) + K_S\Omega(S_0) \neq 0 \,, \tag{A.33}$$

the full potential

$$\begin{aligned} V &= e^K \Lambda_1^2 \left[K^{S\bar{S}} |\Delta_S(S) g(\tau) + K_S \Delta(S) g(\tau)|^2 + |\Delta(S)|^2 K^{\tau\bar{\tau}} D_\tau g(\tau) D_{\bar{\tau}} \overline{g(\tau)} - 3|\Delta(S) g(\tau)|^2 \right] \\ &+ e^K \Lambda_2^2 \left[K^{S\bar{S}} |\Omega_S(S) f(\tau) + K_S \Omega(S) f(\tau)|^2 + |\Omega(S)|^2 K^{\tau\bar{\tau}} D_\tau f(\tau) D_{\bar{\tau}} \overline{f(\tau)} - 3|\Omega(S) f(\tau)|^2 \right] \\ &+ \text{cross terms} \,, \end{aligned} \tag{A.34}$$

would reduce to the potential used in the paper at the minimum of S:

$$\begin{aligned} V(S_0, \tau) &= e^K \Lambda_2^2 \Big[K^{S\bar{S}} |\Omega_S(S) f(\tau) + K_S \Omega(S) f(\tau)|^2 + |\Omega(S)|^2 K^{\tau\bar{\tau}} D_\tau f(\tau) D_{\bar{\tau}} \overline{f(\tau)} \\ &\quad - 3|\Omega(S) f(\tau)|^2 \Big] \Big|_{S=S_0} \,. \end{aligned} \tag{A.35}$$

Phenomenally, this means the mass of dilaton is much larger than the energy scale of inflation. The influence of inflaton to dilaton stabilization would be suppressed by Λ_2/Λ_1.

A.4 Finite Modular Group $\Gamma_3 \cong A_4$ and Modular Forms of Level 3

The level 3 finite modular group Γ_3 is isomorphic to the A_4 group which is the even permutation group of four objects, and it can be generated by the modular generators S and T satisfying the following relations

$$S^2 = (ST)^3 = T^3 = 1 \,. \tag{A.36}$$

The $\Gamma_3 \cong A_4$ group has three singlet representations $\mathbf{1}$, $\mathbf{1}'$ and $\mathbf{1}''$, and one triplet representation $\mathbf{3}$. In the singlet representations, the generators S and T are represented by ordinary numbers. From the multiplication rules in eq. (A.36), it is straightforward to obtain the singlet representations as follows,

$$\begin{aligned} &\mathbf{1} \,:\, S = 1 \,, \qquad T = 1 \,, \\ &\mathbf{1}' \,:\, S = 1 \,, \qquad T = e^{2\pi i/3} \equiv \omega \,, \\ &\mathbf{1}'' \,:\, S = 1 \,, \qquad T = e^{4\pi i/3} = \omega^2 \,. \end{aligned} \tag{A.37}$$

For the triplet representation $\mathbf{3}$, the generators S and T are represented by

$$\mathbf{3} \,:\, S = \frac{1}{3} \begin{pmatrix} -1 & 2 & 2 \\ 2 & -1 & 2 \\ 2 & 2 & -1 \end{pmatrix}, \qquad T = \begin{pmatrix} 1 & 0 & 0 \\ 0 & \omega & 0 \\ 0 & 0 & \omega^2 \end{pmatrix} . \tag{A.38}$$

The tensor products of singlet representations are

$$\mathbf{1}' \otimes \mathbf{1}' = \mathbf{1}'' \,, \quad \mathbf{1}'' \otimes \mathbf{1}'' = \mathbf{1}' \,, \quad \mathbf{1}' \otimes \mathbf{1}'' = \mathbf{1} \,. \tag{A.39}$$

The tensor product of two A_4 triplets is

$$\mathbf{3} \otimes \mathbf{3} = \mathbf{1} \oplus \mathbf{1}' \oplus \mathbf{1}'' \oplus \mathbf{3}_S \oplus \mathbf{3}_A \,, \tag{A.40}$$

where $\mathbf{3}_S$ and $\mathbf{3}_A$ denote the symmetric and antisymmetric triplet contractions respectively. In terms of the components of the two triplets $\boldsymbol{a} = (a_1, a_2, a_3)^T$ and $\boldsymbol{b} = (b_1, b_2, b_3)^T$, we have

$$\begin{aligned}
(\boldsymbol{a} \otimes \boldsymbol{b})_{\mathbf{1}} &= a_1 b_1 + a_2 b_3 + a_3 b_2 \,, \\
(\boldsymbol{a} \otimes \boldsymbol{b})_{\mathbf{1}'} &= a_1 b_2 + a_2 b_1 + a_3 b_3 \,, \\
(\boldsymbol{a} \otimes \boldsymbol{b})_{\mathbf{1}''} &= a_1 b_3 + a_2 b_2 + a_3 b_1 \,, \\
(\boldsymbol{a} \otimes \boldsymbol{b})_{\mathbf{3}_S} = \begin{pmatrix} 2a_1 b_1 - a_2 b_3 - a_3 b_2 \\ 2a_3 b_3 - a_1 b_2 - a_2 b_1 \\ 2a_2 b_2 - a_1 b_3 - a_3 b_1 \end{pmatrix} &, \quad (\boldsymbol{a} \otimes \boldsymbol{b})_{\mathbf{3}_A} = \begin{pmatrix} a_2 b_3 - a_3 b_2 \\ a_1 b_2 - a_2 b_1 \\ a_3 b_1 - a_1 b_3 \end{pmatrix} .
\end{aligned} \tag{A.41}$$

A.4.1 Modular Forms of Level 3

The even weight modular forms of level 3 can be arranged into multiplets of A_4 up to the automorphy factor. At weight $k = 2$, there are only three linearly independent modular forms $Y_1(\tau)$, $Y_2(\tau)$ and $Y_3(\tau)$ which form a A_4 triplet $Y^{(2)}_{\mathbf{3}}(\tau) \equiv \left(Y_1(\tau), Y_2(\tau), Y_3(\tau)\right)^T$ [74]. One can express $Y_{1,2,3}(\tau)$ in terms of the product of Dedekind eta-function [274] or its derivative [74]. In practice, the first few terms of the q-expansion of $Y_{1,2,3}(\tau)$ provide sufficiently accurate approximation [74],

$$\begin{aligned}
Y_1(\tau) &= 1 + 12q + 36q^2 + 12q^3 + 84q^4 + 72q^5 + \ldots \,, \\
Y_2(\tau) &= -6q^{1/3}\left(1 + 7q + 8q^2 + 18q^3 + 14q^4 + 31q^5 + \ldots\right) \,, \\
Y_3(\tau) &= -18q^{2/3}\left(1 + 2q + 5q^2 + 4q^3 + 8q^4 + 6q^5 + \ldots\right) \,.
\end{aligned} \tag{A.42}$$

Using the tensor product decomposition in eq. (A.41), the higher weight modular forms of level 3 can be written as polynomials of $Y_1(\tau)$, $Y_2(\tau)$ and $Y_3(\tau)$. At weight 4, the tensor product of $Y^{(2)}_{\mathbf{3}} \otimes Y^{(2)}_{\mathbf{3}}$ gives rise to three linearly independent modular multiplets,

$$\begin{aligned}
Y^{(4)}_{\mathbf{1}} &= (Y^{(2)}_{\mathbf{3}} \otimes Y^{(2)}_{\mathbf{3}})_{\mathbf{1}} = Y_1^2 + 2Y_2 Y_3 \,, \\
Y^{(4)}_{\mathbf{1}'} &= (Y^{(2)}_{\mathbf{3}} \otimes Y^{(2)}_{\mathbf{3}})_{\mathbf{1}'} = Y_3^2 + 2Y_1 Y_2 \,, \\
Y^{(4)}_{\mathbf{3}} &= \frac{1}{2}(Y^{(2)}_{\mathbf{3}} \otimes Y^{(2)}_{\mathbf{3}})_{\mathbf{3}_S} = \begin{pmatrix} Y_1^2 - Y_2 Y_3 \\ Y_3^2 - Y_1 Y_2 \\ Y_2^2 - Y_1 Y_3 \end{pmatrix} .
\end{aligned} \tag{A.43}$$

The weight 6 modular forms of level 3 decompose as $\mathbf{1}\oplus\mathbf{3}\oplus\mathbf{3}$ under A_4, there are two independent triplet modular forms and they can be chosen as

$$\begin{aligned}
Y^{(6)}_{\mathbf{1}} &= \left(Y^{(2)}_{\mathbf{3}}\otimes Y^{(4)}_{\mathbf{3}}\right)_{\mathbf{1}} = Y_1^3+Y_2^3+Y_3^3-3Y_1Y_2Y_3\,,\\
Y^{(6)}_{\mathbf{3}I} &= \left(Y^{(2)}_{\mathbf{3}}\otimes Y^{(4)}_{\mathbf{1}}\right)_{\mathbf{3}} = (Y_1^2+2Y_2Y_3)\begin{pmatrix}Y_1\\Y_2\\Y_3\end{pmatrix},\\
Y^{(6)}_{\mathbf{3}II} &= \left(Y^{(2)}_{\mathbf{3}}\otimes Y^{(4)}_{\mathbf{1}'}\right)_{\mathbf{3}} = (Y_3^2+2Y_1Y_2)\begin{pmatrix}Y_3\\Y_1\\Y_2\end{pmatrix}.
\end{aligned}\tag{A.44}$$

The Dedekind eta function $\eta(\tau)$, is a modular function of "weight $1/2$" defined as

$$\eta(\tau)=q^{1/24}\prod_{n=1}^{\infty}(1-q^n),\qquad q\equiv e^{2\pi i\tau}\,,\tag{A.45}$$

which satisfies the following modular transformation identities: $\eta(\tau+1)=e^{i\pi/12}\eta(\tau)$ and $\eta(-1/\tau)=\sqrt{-i\tau}\eta(\tau)$. The q-expansion of eta function is given by

$$\eta=q^{1/24}[1-q-q^2+q^5+q^7-q^{12}-q^{15}+O(q^{22})]\,.\tag{A.46}$$

The j function is related to the Dedekind eta and its derivatives as follow,

$$j=\left(\frac{72}{\pi^2}\frac{\eta\eta''-\eta'^2}{\eta^{10}}\right)^3=\left[\frac{72}{\pi^2\eta^6}\left(\frac{\eta'}{\eta^3}\right)'\right]^3,\tag{A.47}$$

where prime denotes derivative with respect to τ.

A.5 Vacuum Structure of Modulus

In this section, we exam the properties of $\tau=\omega$ and $\tau=\tau_0$ in details. Both are minima, but they have different potential values. For convenience, we denote

$$\mathcal{P}(j(\tau))=1+\beta\left(1-\frac{j(\tau)}{1728}\right)+\gamma\left(1-\frac{j(\tau)}{1728}\right)^2\tag{A.48}$$

in eq. (5.10). For $\tau=\omega$, the potential and its first-order derivatives read

$$V(\omega)=\Lambda^4\frac{(2\pi)^{12}}{3^3\Gamma^{18}(1/3)}(A-3)|j^2(\tau_0)\mathcal{P}(0)|^2\,,\quad \partial_\tau V(\omega)=\partial_{\bar\tau}V(\omega)=0\,,\tag{A.49}$$

implying $V(\omega)$ will be positive-definite as long as $A>3$. As ω is a fix point under modular transformation, Modular symmetry ensures the first-order derivatives to vanish. The second-order

derivatives of the potential, forming the Hessian matrix, are

$$\left.\frac{\partial^2 V}{\partial \rho^2}\right|_{\tau=\omega} = \left.\frac{\partial^2 V}{\partial \theta^2}\right|_{\tau=\omega} = 2\Lambda^4 \frac{(2\pi)^{12}}{3^3\Gamma^{18}(1/3)}(A-2)\,|j^2(\tau_0)\mathcal{P}(0)|^2\,, \quad \left.\frac{\partial^2 V}{\partial\theta\partial\rho}\right|_{\tau=\omega} = 0\,. \tag{A.50}$$

Because the Hessian matrix is positive-definite, $\tau = \omega$ is a local minimum.

Unlike ω, the property at τ_0 heavily rely on the special form of $H(\tau)$. Using that $H(\tau_0) = \partial_\tau H(\tau_0) = 0$, the potential and its first-order derivatives are

$$V(\tau_0) = 0\,, \quad \partial_\tau V(\tau_0) = \partial_{\bar\tau} V(\omega) = 0\,. \tag{A.51}$$

and the second-order derivatives read

$$\left.\frac{\partial^2 V}{\partial \rho^2}\right|_{\tau=\tau_0} = \left.\frac{\partial^2 V}{\partial \theta^2}\right|_{\tau=\tau_0} = \frac{4\left|(\partial_\tau j(\tau_0))^2\mathcal{P}(j(\tau_0))\right|^2}{3\sin\big(\arg(\tau_0)\big)\left|\eta(\tau_0)\right|^{12}} > 0\,, \quad \left.\frac{\partial^2 V}{\partial\theta\partial\rho}\right|_{\tau=\tau_0} = 0\,. \tag{A.52}$$

In this case, the Hessian matrix is positive-definite when τ_0 stays in the fundamental domain. Since our potential is semi-positive, the vanishing potential at τ_0 ensures it is a global minimum.

The property at $\tau = i$ is rather non-trivial. In this paper we need i to be a saddle point, which is not a general conclusion. The Hessian matrix now depends on the parameters in $\mathcal{P}(j(\tau))$. Thus, we only show the numerical result in Fig. (5.1).

A.6 A Toy Model of Large Field Inflation

As a concrete example, we illustrate such a possibility by following the proposal in Ref. [179], where the authors showed that at large $\mathrm{Im}(\tau)$ one can have T-mode α attractor large field inflation model. At large $\mathrm{Im}(\tau)$, the squared norm of j-invariant can be approximated as

$$|j(\tau)|^2 \approx e^{4\pi\,\mathrm{Im}(\tau)}\,. \tag{A.53}$$

In Ref. [179], the authors proposed to use the following I function:

$$I(\tau,\bar\tau) = \frac{\ln\left(|j(\tau)|^2+\beta^2\right)}{\ln\beta^2}\,, \quad \left.I(\tau,\bar\tau)\right|_{\mathrm{Im}(\tau)\to\infty} \approx \frac{4\pi}{\ln\left(\beta^2\right)}\,\mathrm{Im}(\tau) \equiv c\,\mathrm{Im}(\tau)\,, \tag{A.54}$$

to construct inflationary potential as follow,

$$V(\tau,\bar\tau) = V_0\left(\frac{I(\tau,\bar\tau)-1}{I(\tau,\bar\tau)+1}\right)^2\,, \quad \left.V(\tau,\bar\tau)\right|_{\mathrm{Im}(\tau)\to\infty} \approx V_0\left(1-\frac{8}{c\,\mathrm{Im}(\tau)}+\ldots\right)\,. \tag{A.55}$$

The above potential features a plateau behavior at large $\mathrm{Im}(\tau)$. As a specific example, they considered $\beta = j(i)$, thus $I(\omega,\bar\omega) = 1$ and the potential has a Minkowski minimum at $\tau = \omega$.

To incorporate the idea of Ref. [179] into our work, a shift of potential minimum from $\tau = \omega$ to $\tau = \tau_0$ is necessary in order to be compatible with the lepton sector within our setup. We noticed that

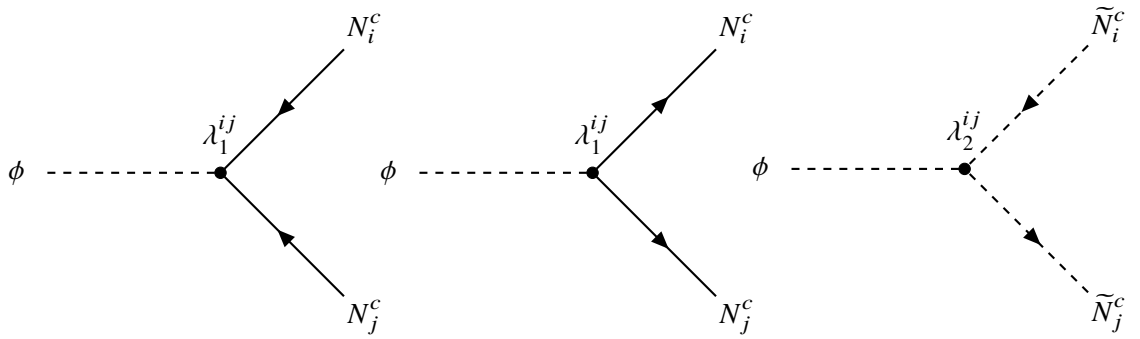

(a) $\phi \longrightarrow N_i^c\ N_j^c$ (b) $\phi \longrightarrow N_i^{c*}\ N_j^{c*}$ (c) $\phi \longrightarrow \widetilde{N}_i^c\ \widetilde{N}_j^{c*}$

Figure A.1: Feynman diagrams for inflaton two-body decay.

this can be done via a redefinition of I function:

$$I(\tau,\bar{\tau}) = \frac{\ln\left(|j(\tau)|^2+\beta^2\right)}{\ln\left(\left|j(\tau_0)\right|^2+\beta^2\right)}\,, \quad I(\tau,\bar{\tau})\Big|_{\mathrm{Im}(\tau)\to\infty} \approx \frac{4\pi}{\ln\left(\left|j(\tau_0)\right|^2+\beta^2\right)}\,\mathrm{Im}(\tau) \equiv c'\,\mathrm{Im}(\tau)\,. \tag{A.56}$$

This redefinition ensures $I(\tau_0,\bar{\tau}_0)=1$ and does not modify the expansion of I function in the limit of large $\mathrm{Im}(\tau)$. Moreover, the plateau behavior of potential in eq. (A.55) is preserved. We notice that the mass of canonically normalized infaton field $\phi=\sqrt{3/2}\ln\left[\mathrm{Im}(\tau)\right]$ decrease with increasing β. As a rough estimate, taking $V_0 \approx \left(10^{15}\ \mathrm{GeV}\right)^4$ – the typical energy scale of α attractor models, the mass of inflaton can be as large as 10^{13} GeV for $\beta=1$. This inflaton mass exceeds the lower bound 10^{11} GeV derived in our paper and successful leptogenesis could be realized.

However, the following challenge arises. As noted in Ref. [179], both $\mathrm{Re}(\tau)$ and $\mathrm{Im}(\tau)$ become dynamical fields as the system approaches the minima. This transition requires a treatment beyond our current single-field framework, which we have assumed throughout both the inflationary phase and the reheating dynamics. A similar difficulty emerges when incorporating the proposal in Ref. [17] for Starobinsky inflation. Given that the primary objective of this work is to investigate the post-inflationary single-field dynamics within the modular slow-roll inflation framework, a thorough study of multi-field effects in these large-field scenarios is an interesting direction for future research.

A.7 Inflaton Decay Rates

In this section we will present calculations about inflaton decays. As we are dealing with Majorana fermions, this calculation will be carried out in the two component notations.

A.7.1 Inflaton 2-body Decay

We consider the inflaton two body decay in the following Lagrangian:

$$\mathcal{L} = \frac{1}{2}\frac{\Lambda_N}{M_{\rm pl}}\lambda_1^{ij}\phi N_i^c N_j^c + \frac{1}{2}\frac{\Lambda_N^2}{M_{\rm pl}}\lambda_2^{ij}\phi\widetilde{N}_i^{c*}\widetilde{N}_j^c + \text{h.c.}\,, \tag{A.57}$$

where N_i^c is a Majorana particle with mass M_i and $\widetilde{N}_i^c$ is corresponding sfermion. We first consider inflaton decay to two fermions, in the two component notation, matrix element reads:

$$i\mathcal{M} = y(\vec{p}_1, s_1)^\alpha (i\frac{\Lambda_N}{M_{\rm pl}}\lambda_1^{ij}\delta_\alpha{}^\beta) y(\vec{p}_2, s_2)_\beta + x^\dagger(\vec{p}_1, s_1)_{\dot\alpha}(i\frac{\Lambda_N}{M_{\rm pl}}\lambda_1^{ij*}\delta^{\dot\alpha}{}_{\dot\beta})x^\dagger(\vec{p}_2, s_2)^{\dot\beta}\,, \tag{A.58}$$

where x, y are the two component spinor wave functions, which play the same role as u, v in four component notation. After taking hermitian conjugate and performing spin sum, we have:

$$\begin{aligned} |\mathcal{M}|^2 &= 4\left(\frac{\Lambda_N}{M_{\rm pl}}\right)^2\left(|\lambda_1^{ij}|^2 p_i\cdot p_j - \text{Re}\left[(\lambda_1^{ij})^2\right]M_i M_j\right) \\ &= 4\left(\frac{\Lambda_N}{M_{\rm pl}}\right)^2\left(|\lambda_1^{ij}|^2\frac{m_\phi^2 - (M_j^2+M_i^2)}{2} - \text{Re}\left[(\lambda_1^{ij})^2\right]M_i M_j\right), \end{aligned} \tag{A.59}$$

where M_i, M_j are mass of N_i^c, N_j^c, respectively. For inflation decay to two scalars, the matrix element is much simpler:

$$|\mathcal{M}|^2 = \left|\frac{\Lambda_N^2}{M_{\rm pl}}\lambda_2^{ij}\right|^2\,, \tag{A.60}$$

The phase space integral can be performed as usual, the total decay rates are:

$$\Gamma(\phi\to\widetilde{N}_i^c\widetilde{N}_j^{c*}) = \left|\frac{\Lambda_N^2\lambda_2^{ij}}{M_{\rm pl}}\right|^2\frac{1}{16\pi m_\phi}\sqrt{\left(1-\frac{(M_i-M_j)^2}{m_\phi^2}\right)\left(1-\frac{(M_i+M_j)^2}{m_\phi^2}\right)}, \tag{A.61}$$

for inflaton decay to two sfermions and:

$$\begin{aligned} \Gamma(\phi\to N_i^c N_j^c) = \frac{m_\phi}{8(1+\delta_{ij})\pi}\left(\frac{\Lambda_N}{M_{\rm pl}}\right)^2&\left(\left|\lambda_1^{ij}\right|^2\left(1-\frac{M_i^2+M_j^2}{m_\phi^2}\right) - 2\text{Re}[(\lambda_1^{ij})^2]\frac{M_i M_j}{m_\phi^2}\right) \\ &\times\sqrt{\left(1-\frac{(M_j-M_i)^2}{m_\phi^2}\right)\left(1-\frac{(M_j+M_i)^2}{m_\phi^2}\right)}, \end{aligned} \tag{A.62}$$

for inflaton decay to two fermions. Note δ_{ij} accounts for the effects of identical particles when $i = j$.

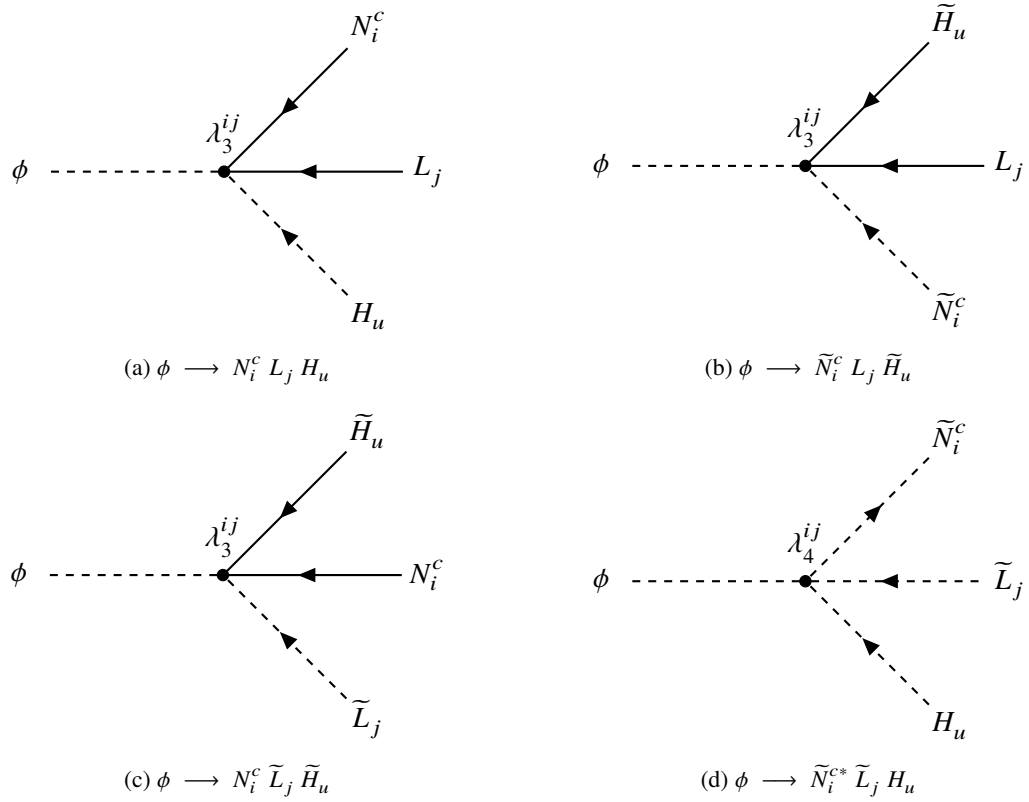

(a) $\phi \longrightarrow N_i^c\ L_j\ H_u$ (b) $\phi \longrightarrow \widetilde{N}_i^c\ L_j\ \widetilde{H}_u$

(c) $\phi \longrightarrow N_i^c\ \widetilde{L}_j\ \widetilde{H}_u$ (d) $\phi \longrightarrow \widetilde{N}_i^{c*}\ \widetilde{L}_j\ H_u$

Figure A.2: Feynman diagrams for inflaton three-body decay.

A.7.2 Inflaton 3-body Decay

For three-body decays, there are four channels as shown in Fig. (A.2(a)) -Fig. (A.2(d)). We first consider the inflaton three body decay $\phi(p) \rightarrow H(k_1)L(k_2)N^c(k_3)$, namely the process shown in Fig. (A.2(a)). The relevant Lagrangian is:

$$\mathcal{L} = \frac{\lambda_3^{ij}}{M_{\rm pl}}\phi N_i^c (L_j \cdot H_u) + h.c.\,, \tag{A.63}$$

where $L_j = \left(\nu_j\,, l_j\right)^T$, $H_u = \left(H_u^+\,, H_u^0\right)^T$ are SU(2) doublet and $(L_j \cdot H_u) = \nu_j H_u^0 - l_j H^+$.

In the following, we will neglect the Higgs and light neutrino masses, as they are much smaller compared to the inflaton mass and the right-handed neutrino mass. The spin summed, squared matrix element for a single combination ($\nu_j H_u^0$ or $l_j H^+$) reads:

$$|\mathcal{M}|^2 = \left|\frac{\lambda_3^{ij}}{M_{\rm pl}}\right|^2 4(k_2 \cdot k_3)\,, \tag{A.64}$$

With the squared matrix element, we can further compute the three-body decay rate, which is:

$$\Gamma(\phi \to N_i^c (L_j \cdot H)) \equiv \frac{1}{2\, m_\phi} \int d\Pi_3 |\mathcal{M}|^2 \,. \tag{A.65}$$

The three–body phase space integral can be further written as (see e.g. Sec. 20 of Ref. [275] or step-by-step computation in Appendix C of Ref. [276])

$$\int d\Pi_3 = \frac{m_\phi^2}{128\pi^3} \int_0^{1-\mu_N} dx_1 \int_{1-x_1-\mu_N}^{1-\frac{\mu_N}{1-x_1}} dx_2 \,, \tag{A.66}$$

where $x_i = 2E_i/m_\phi \,, i = 1, 2$, where E_1 is the energy of the Higgs boson, and E_2 is the energy of the charged lepton in the inflaton rest frame, with $\mu_N \equiv M_N^2/m_\phi^2$. We have neglected all final state masses except for that of the right-handed neutrino (RHN). Using eq. (A.66), we find that the three-body decay rate eq. (A.65) becomes

$$\Gamma(\phi \to N_i^c (L_j \cdot H)) = 2 \times \left| \frac{\lambda_3^{ij}}{M_{\rm pl}} \right|^2 \frac{m_\phi^3}{768\pi^3} \left[1 - 6\mu_N + 3\mu_N^2 + 2\mu_N^3 - 6\mu_N^2 \log(\mu_N) \right] . \tag{A.67}$$

where we use 2 to count 2 possible combinations in the $SU(2)$ contraction. We note that in the limit $\mu_N \to 1$, the rate $\Gamma_{\phi \to HLN} \to 0$, as expected, since the decay becomes kinematically blocked in this scenario.

For other channels, the procedure is similar. In particular for $\phi(p) \to \widetilde{H}(k_1) L(k_2) \widetilde{N}^c(k_3)$ (Fig. (A.2(b))), we find the squared matrix element is given by

$$|\mathcal{M}|^2 = \left| \frac{\lambda_3^{ij}}{M_{\rm pl}} \right|^2 4(k_1 \cdot k_2) \,, \tag{A.68}$$

with which corresponding decay rate is shown to be

$$\Gamma(\phi \to \widetilde{N}_i^c (L_j \cdot \widetilde{H})) = 2 \times \left| \frac{\lambda_3^{ij}}{M_{\rm pl}} \right|^2 \frac{m_\phi^3}{768\pi^3} \left[1 + 9\mu_N - 9\mu_N^2 - \mu_N^3 + 6\mu_N \log(\mu_N) + 6\mu_N^2 \log(\mu_N) \right] . \tag{A.69}$$

For $\phi(p) \to \widetilde{H}(k_1) \widetilde{L}(k_2) N^c(k_3)$ (Fig. (A.2(c))), the the squared matrix element is

$$|\mathcal{M}|^2 = \left| \frac{\lambda_3^{ij}}{M_{\rm pl}} \right|^2 4(k_1 \cdot k_3) \,, \tag{A.70}$$

and decay rate

$$\Gamma(\phi \to N_i^c (\widetilde{L}_j \cdot \widetilde{H})) = 2 \times \left| \frac{\lambda_3^{ij}}{M_{\rm pl}} \right|^2 \frac{m_\phi^3}{768\pi^3} \left[1 - 6\mu_N + 3\mu_N^2 + 2\mu_N^3 - 6\mu_N^2 \log(\mu_N) \right] . \tag{A.71}$$

Finally, for the inflaton decays into three scalars $\phi(p) \to H(k_1)\widetilde{L}(k_2)\widetilde{N}^c(k_3)$ (Fig. (A.2(d))), the squared matrix element is

$$|\mathcal{M}|^2 = \left|\frac{\lambda_4^{ij}\Lambda_N}{M_{\rm pl}}\right|^2 , \tag{A.72}$$

and decay rate reads

$$\Gamma(\phi \to \widetilde{N}_i^c(\widetilde{L}_j \cdot H)) = 2 \times \left|\frac{\lambda_4^{ij}\Lambda_N}{M_{\rm pl}}\right|^2 \times \frac{m_\phi}{512\pi^3}\left[1 - \mu_N^2 + 2\mu_N \log(\mu_N)\right] . \tag{A.73}$$

A.8 Calculation for DM Energy Density to Entropy Density Ratio

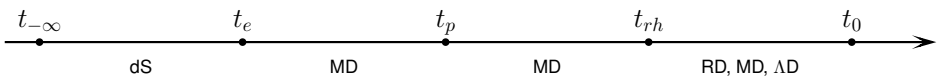

Figure A.3: Thermal history of our model. Here $t_{-\infty}$ represents the initial time in our simulation. t_e represents the time when inflation has ended and inflaton starts to oscillates around its minimum. t_p denotes the time when GPP is almost finished and $t_{\rm rh}$ denotes the time when reheating is complete. We also use t_0 to denote the current time.

In this section we briefly review the thermal history of our universe and explain how we calculate the density-to-entropy ratio explicitly. Our simulation starts when the inflaton ϕ field stays in the inflation region, which we will formally denote it by $t_{-\infty}$. At $t = t_e$ the (Hubble) slow roll conditions are broken and ϕ field starts to oscillate around its minimum. In this paper we consider the case where the oscillation part can be approximated by ϕ^2, which means the energy density of the inflaton field red-shifts as matter. This transition from de Sitter spacetime to matter-dominated space also triggers the gravitational production of the super heavy DM. Most of the super heavy DM are produced at the beginning of the oscillation part, and we assume at $t = t_p$ this production is basically complete and its energy density also red-shifts as matter. Hence we have the following identity

$$\frac{\rho_\chi(t_p)}{\rho_\phi(t_p)} = \frac{\rho_\chi(t_{\rm rh})}{\rho_\phi(t_{\rm rh})} = \frac{\rho_\chi(t_{\rm rh})}{\rho_r(t_{\rm rh})}, \tag{A.74}$$

where we have used that DM χ field redshifts in the same way as the inflaton ϕ field, and we define the reheating temperature when $\rho_\phi(t_{\rm rh}) = \rho_r(t_{\rm rh})$. Here, ρ_r denotes the energy density in radiation. After the reheating is complete, we have

$$\frac{\rho_\chi(t_{\rm rh})}{\rho_r(t_{\rm rh})} = \frac{\rho_\chi(t_0)}{\rho_r(t_0)}\frac{T_0}{T_{\rm rh}}. \tag{A.75}$$

The entropy density and energy density in today's Universe reads

$$\begin{aligned} s_0 &= g_* \frac{2\pi^2}{45} T_0^3, \\ \rho_{r,0} &= g_* \frac{\pi^2}{30} T_0^4. \end{aligned} \tag{A.76}$$

Hence, we can rewrite $\rho_{r,0} = \frac{3}{4} s T_0$ and the energy density to entropy density reads

$$\frac{\rho_\chi(t_0)}{s_0} = \frac{3}{4} T_0 \frac{\rho_\chi(t_0)}{\rho_r(t_0)} = \frac{3 m_\chi T_{\rm rh}}{4} \frac{n_\chi(t_p)}{\rho_\phi(t_p)}, \tag{A.77}$$

where we have used $\rho = mn$ for non-relativistic particles (CDM). The energy density of $\rho_\phi(t_p)$ can be connected to the energy density of inflaton at the end of inflation

$$\rho_\phi(t_p) = \rho_\phi(t_e) \left(\frac{a(t_e)}{a(t_p)} \right)^3 = 3 M_{\rm pl}^2 H^2(t_e) \left(\frac{a(t_e)}{a(t_p)} \right)^3 . \tag{A.78}$$

The finial expression reads

$$\frac{\rho_\chi(t_0)}{s_0} = \frac{m_\chi T_{\rm rh} H(t_e)}{4 M_{\rm pl}^2} \left(\frac{a^3(t_p) n_\chi(t_p)}{a^3(t_e) H^3(t_e)} \right) . \tag{A.79}$$

Current observation suggests this quantity should be equal to 4×10^{-10} GeV to contribute the full amount of DM.

Bibliography

[1] K. Kodama et al., *Observation of tau neutrino interactions*, Phys. Lett. B **504** (2001) 218, arXiv: hep-ex/0012035.

[2] S. Chatrchyan et al.,
Observation of a New Boson at a Mass of 125 GeV with the CMS Experiment at the LHC,
Phys. Lett. B **716** (2012) 30, arXiv: 1207.7235 [hep-ex].

[3] G. Aad et al., *Observation of a new particle in the search for the Standard Model Higgs boson with the ATLAS detector at the LHC*, Phys. Lett. B **716** (2012) 1,
arXiv: 1207.7214 [hep-ex].

[4] C. D. Anderson and S. H. Neddermeyer,
Cloud Chamber Observations of Cosmic Rays at 4300 Meters Elevation and Near Sea-Level,
Phys. Rev. **50** (1936) 263.

[5] J. C. Street and E. C. Stevenson, *New Evidence for the Existence of a Particle of Mass Intermediate Between the Proton and Electron*, Phys. Rev. **52** (1937) 1003.

[6] C. L. Cowan, F. Reines, F. B. Harrison, H. W. Kruse and A. D. McGuire,
Detection of the free neutrino: A Confirmation, Science **124** (1956) 103.

[7] G. Danby et al.,
Observation of High-Energy Neutrino Reactions and the Existence of Two Kinds of Neutrinos,
Phys. Rev. Lett. **9** (1962) 36.

[8] J. J. Aubert et al., *Experimental Observation of a Heavy Particle J*,
Phys. Rev. Lett. **33** (1974) 1404.

[9] J. E. Augustin et al., *Discovery of a Narrow Resonance in e^+e^- Annihilation*,
Phys. Rev. Lett. **33** (1974) 1406.

[10] M. L. Perl et al., *Evidence for Anomalous Lepton Production in e+ - e- Annihilation*,
Phys. Rev. Lett. **35** (1975) 1489.

[11] S. W. Herb et al.,
Observation of a Dimuon Resonance at 9.5-GeV in 400-GeV Proton-Nucleus Collisions,
Phys. Rev. Lett. **39** (1977) 252.

[12] R. Brandelik et al., *Evidence for Planar Events in e+ e- Annihilation at High-Energies*,
Phys. Lett. B **86** (1979) 243.

[13] D. P. Barber et al.,
Discovery of Three Jet Events and a Test of Quantum Chromodynamics at PETRA Energies,
Phys. Rev. Lett. **43** (1979) 830.

[14] C. Berger et al., *Evidence for Gluon Bremsstrahlung in e+ e- Annihilations at High-Energies*,
Phys. Lett. B **86** (1979) 418.

[15] G. Arnison et al., *Experimental Observation of Isolated Large Transverse Energy Electrons with Associated Missing Energy at* $\sqrt{s}$ = 540 *GeV*, Phys. Lett. B **122** (1983) 103.

[16] M. Banner et al., *Observation of Single Isolated Electrons of High Transverse Momentum in Events with Missing Transverse Energy at the CERN anti-p p Collider*,
Phys. Lett. B **122** (1983) 476.

[17] S. Abachi et al., *Observation of the top quark*, Phys. Rev. Lett. **74** (1995) 2632,
arXiv: hep-ex/9503003.

[18] F. Abe et al., *Observation of top quark production in* $\bar{p}p$ *collisions*,
Phys. Rev. Lett. **74** (1995) 2626, arXiv: hep-ex/9503002.

[19] A. A. Penzias and R. W. Wilson, *A Measurement of excess antenna temperature at 4080-Mc/s*,
Astrophys. J. **142** (1965) 419.

[20] V. C. Rubin and W. K. Ford Jr.,
Rotation of the Andromeda Nebula from a Spectroscopic Survey of Emission Regions,
Astrophys. J. **159** (1970) 379.

[21] A. G. Riess et al., *Observational evidence from supernovae for an accelerating universe and a cosmological constant*, Astron. J. **116** (1998) 1009, arXiv: astro-ph/9805201.

[22] Y. Fukuda et al., *Evidence for oscillation of atmospheric neutrinos*,
Phys. Rev. Lett. **81** (1998) 1562, arXiv: hep-ex/9807003.

[23] K. Eguchi et al.,
First results from KamLAND: Evidence for reactor anti-neutrino disappearance,
Phys. Rev. Lett. **90** (2003) 021802, arXiv: hep-ex/0212021.

[24] C. S. Wu, E. Ambler, R. W. Hayward, D. D. Hoppes and R. P. Hudson,
Experimental Test of Parity Conservation in β *Decay*, Phys. Rev. **105** (1957) 1413.

[25] P. A. M. Dirac, *Quantum theory of emission and absorption of radiation*,
Proc. Roy. Soc. Lond. A **114** (1927) 243.

[26] S. Tomonaga, *On a relativistically invariant formulation of the quantum theory of wave fields*,
Prog. Theor. Phys. **1** (1946) 27.

[27] H. A. Bethe, *The Electromagnetic shift of energy levels*, Phys. Rev. **72** (1947) 339.

[28] J. S. Schwinger, *Quantum electrodynamics. I A covariant formulation*,
Phys. Rev. **74** (1948) 1439, ed. by K. A. Milton.

[29] R. P. Feynman, *Space - time approach to quantum electrodynamics*,
Phys. Rev. **76** (1949) 769, ed. by L. M. Brown.

[30] F. J. Dyson, *The Radiation theories of Tomonaga, Schwinger, and Feynman*,
Phys. Rev. **75** (1949) 486.

[31] C.-N. Yang and R. L. Mills, *Conservation of Isotopic Spin and Isotopic Gauge Invariance*, Phys. Rev. **96** (1954) 191, ed. by J.-P. Hsu and D. Fine.

[32] S. L. Glashow, *Partial Symmetries of Weak Interactions*, Nucl. Phys. **22** (1961) 579.

[33] F. Englert and R. Brout, *Broken Symmetry and the Mass of Gauge Vector Mesons*, Phys. Rev. Lett. **13** (1964) 321, ed. by J. C. Taylor.

[34] P. W. Higgs, *Broken Symmetries and the Masses of Gauge Bosons*, Phys. Rev. Lett. **13** (1964) 508, ed. by J. C. Taylor.

[35] G. S. Guralnik, C. R. Hagen and T. W. B. Kibble, *Global Conservation Laws and Massless Particles*, Phys. Rev. Lett. **13** (1964) 585, ed. by J. C. Taylor.

[36] S. Weinberg, *A Model of Leptons*, Phys. Rev. Lett. **19** (1967) 1264.

[37] A. Salam, *Weak and Electromagnetic Interactions*, Conf. Proc. C **680519** (1968) 367.

[38] M. Gell-Mann, *A Schematic Model of Baryons and Mesons*, Phys. Lett. **8** (1964) 214.

[39] G. Zweig, *An SU(3) model for strong interaction symmetry and its breaking. Version 1*, (1964).

[40] G. 't Hooft, *Renormalization of Massless Yang-Mills Fields*, Nucl. Phys. B **33** (1971) 173.

[41] D. J. Gross and F. Wilczek, *Ultraviolet Behavior of Nonabelian Gauge Theories*, Phys. Rev. Lett. **30** (1973) 1343, ed. by J. C. Taylor.

[42] H. D. Politzer, *Reliable Perturbative Results for Strong Interactions?*, Phys. Rev. Lett. **30** (1973) 1346, ed. by J. C. Taylor.

[43] B. P. Abbott et al., *Observation of Gravitational Waves from a Binary Black Hole Merger*, Phys. Rev. Lett. **116** (2016) 061102, arXiv: 1602.03837 [gr-qc].

[44] N. Aghanim et al., *Planck 2018 results. VI. Cosmological parameters*, Astron. Astrophys. **641** (2020) A6, [Erratum: Astron.Astrophys. 652, C4 (2021)], arXiv: 1807.06209 [astro-ph.CO].

[45] A. A. Starobinsky, *A New Type of Isotropic Cosmological Models Without Singularity*, Phys. Lett. B **91** (1980) 99, ed. by I. M. Khalatnikov and V. P. Mineev.

[46] A. H. Guth, *The Inflationary Universe: A Possible Solution to the Horizon and Flatness Problems*, Phys. Rev. D **23** (1981) 347, ed. by L.-Z. Fang and R. Ruffini.

[47] A. D. Linde, *A New Inflationary Universe Scenario: A Possible Solution of the Horizon, Flatness, Homogeneity, Isotropy and Primordial Monopole Problems*, Phys. Lett. B **108** (1982) 389, ed. by L.-Z. Fang and R. Ruffini.

[48] A. Albrecht and P. J. Steinhardt, *Cosmology for Grand Unified Theories with Radiatively Induced Symmetry Breaking*, Phys. Rev. Lett. **48** (1982) 1220, ed. by L.-Z. Fang and R. Ruffini.

[49] Y. Akrami et al., *Planck 2018 results. X. Constraints on inflation*, Astron. Astrophys. **641** (2020) A10, arXiv: 1807.06211 [astro-ph.CO].

[50] R. K. Sachs and A. M. Wolfe,
Perturbations of a cosmological model and angular variations of the microwave background,
Astrophys. J. **147** (1967) 73.

[51] P. A. R. Ade et al., *Improved Constraints on Primordial Gravitational Waves using Planck, WMAP, and BICEP/Keck Observations through the 2018 Observing Season*,
Phys. Rev. Lett. **127** (2021) 151301, arXiv: 2110.00483 [astro-ph.CO].

[52] A. R. Liddle and S. M. Leach,
How long before the end of inflation were observable perturbations produced?,
Phys. Rev. D **68** (2003) 103503, arXiv: astro-ph/0305263.

[53] J. Martin and C. Ringeval, *First CMB Constraints on the Inflationary Reheating Temperature*,
Phys. Rev. D **82** (2010) 023511, arXiv: 1004.5525 [astro-ph.CO].

[54] E. Calabrese et al.,
The Atacama Cosmology Telescope: DR6 Constraints on Extended Cosmological Models,
(2025), arXiv: 2503.14454 [astro-ph.CO].

[55] M. S. Turner, *Coherent Scalar Field Oscillations in an Expanding Universe*,
Phys. Rev. D **28** (1983) 1243.

[56] K. C. Freeman, *On the disks of spiral and SO Galaxies*, Astrophys. J. **160** (1970) 811.

[57] T. S. van Albada, J. N. Bahcall, K. Begeman and R. Sancisi,
Distribution of dark matter in the spiral galaxy NGC 3198.,
Astrophysical Journal **295** (1985) 305.

[58] D. J. H. Chung, E. W. Kolb and A. Riotto, *Superheavy dark matter*,
Phys. Rev. D **59** (1998) 023501, arXiv: hep-ph/9802238.

[59] I. Esteban et al., *NuFit-6.0: Updated global analysis of three-flavor neutrino oscillations*,
JHEP **12** (2024) 216, arXiv: 2410.05380 [hep-ph].

[60] S. Navas et al., *Review of particle physics*, Phys. Rev. D **110** (2024) 030001.

[61] A. D. Sakharov,
Violation of CP Invariance, C asymmetry, and baryon asymmetry of the universe,
Pisma Zh. Eksp. Teor. Fiz. **5** (1967) 32.

[62] G. 't Hooft, *Computation of the Quantum Effects Due to a Four-Dimensional Pseudoparticle*,
Phys. Rev. D **14** (1976) 3432, ed. by M. A. Shifman, [Erratum: Phys.Rev.D 18, 2199 (1978)].

[63] S. Dimopoulos and L. Susskind, *On the Baryon Number of the Universe*,
Phys. Rev. D **18** (1978) 4500.

[64] N. S. Manton, *Topology in the Weinberg-Salam Theory*, Phys. Rev. D **28** (1983) 2019.

[65] K. Kajantie, M. Laine, K. Rummukainen and M. E. Shaposhnikov,
Is there a hot electroweak phase transition at $m_H \gtrsim m_W$?, Phys. Rev. Lett. **77** (1996) 2887,
arXiv: hep-ph/9605288.

[66] M. Drees, R. Godbole and P. Roy, *Theory and phenomenology of sparticles: An account of four-dimensional N=1 supersymmetry in high energy physics*, 2004.

[67] S. R. Coleman and J. Mandula, *All Possible Symmetries of the S Matrix*,
Phys. Rev. **159** (1967) 1251, ed. by A. Zichichi.

[68] Y. A. Golfand and E. P. Likhtman,
Extension of the Algebra of Poincare Group Generators and Violation of p Invariance,
JETP Lett. **13** (1971) 323, ed. by A. Salam and E. Sezgin.

[69] R. Haag, J. T. Lopuszanski and M. Sohnius,
All Possible Generators of Supersymmetries of the s Matrix, Nucl. Phys. B **88** (1975) 257.

[70] L. O'Raifeartaigh, *Spontaneous Symmetry Breaking for Chiral Scalar Superfields*,
Nucl. Phys. B **96** (1975) 331.

[71] D. Z. Freedman and A. Van Proeyen, *Supergravity*,
Cambridge, UK: Cambridge Univ. Press, 2012, ISBN: 978-1-139-36806-3.

[72] J. Wess and J. Bagger, *Supersymmetry and supergravity*,
Princeton, NJ, USA: Princeton University Press, 1992, ISBN: 978-0-691-02530-8.

[73] J. Polonyi, *Generalization of the Massive Scalar Multiplet Coupling to the Supergravity*,
(1977).

[74] F. Feruglio, "Are neutrino masses modular forms?",
From My Vast Repertoire ...: Guido Altarelli's Legacy, ed. by A. Levy, S. Forte and G. Ridolfi,
2019 227, arXiv: 1706.08749 [hep-ph].

[75] K. Enqvist, A. Mazumdar and P. Stephens, *Inflection point inflation within supersymmetry*,
JCAP **06** (2010) 020, arXiv: 1004.3724 [hep-ph].

[76] A. Mazumdar, S. Nadathur and P. Stephens, *Inflation with large supergravity corrections*,
Phys. Rev. D **85** (2012) 045001, arXiv: 1105.0430 [hep-th].

[77] S. Hotchkiss, A. Mazumdar and S. Nadathur,
Inflection point inflation: WMAP constraints and a solution to the fine-tuning problem,
JCAP **06** (2011) 002, arXiv: 1101.6046 [astro-ph.CO].

[78] H.-Y. Chang and R. J. Scherrer, *Inflection Point Quintessence*,
Phys. Rev. D **88** (2013) 083003, arXiv: 1306.4662 [astro-ph.CO].

[79] J. Martin, C. Ringeval and V. Vennin, *Encyclopædia Inflationaris: Opiparous Edition*,
Phys. Dark Univ. **5-6** (2014) 75, arXiv: 1303.3787 [astro-ph.CO].

[80] T.-J. Gao and Z.-K. Guo, *Inflection point inflation and dark energy in supergravity*,
Phys. Rev. D **91** (2015) 123502, arXiv: 1503.05643 [hep-th].

[81] N. Okada and D. Raut, *Inflection-point Higgs Inflation*, Phys. Rev. D **95** (2017) 035035,
arXiv: 1610.09362 [hep-ph].

[82] T.-J. Gao, W.-T. Xu and X.-Y. Yang, *Inflection point in running kinetic term inflation*,
Mod. Phys. Lett. A **32** (2017) 1750072, arXiv: 1606.05951 [hep-ph].

[83] S.-M. Choi and H. M. Lee, *Inflection point inflation and reheating*,
Eur. Phys. J. C **76** (2016) 303, arXiv: 1601.05979 [hep-ph].

[84] K. Dimopoulos, C. Owen and A. Racioppi, *Loop inflection-point inflation*,
Astropart. Phys. **103** (2018) 16, arXiv: 1706.09735 [hep-ph].

[85] N. Musoke and R. Easther, *Expectations for Inflationary Observables: Simple or Natural?*,
JCAP **12** (2017) 032, arXiv: 1709.01192 [astro-ph.CO].

[86] N. Okada, S. Okada and D. Raut,
Inflection-point inflation in hyper-charge oriented U(1)$_X$ model,
Phys. Rev. D **95** (2017) 055030, arXiv: 1702.02938 [hep-ph].

[87] C. Pallis, *Inflection-point sgoldstino inflation in no-scale supergravity*,
Phys. Lett. B **843** (2023) 138018, arXiv: 2302.12214 [hep-ph].

[88] M. Drees and Y. Xu,
Small field polynomial inflation: reheating, radiative stability and lower bound,
JCAP **09** (2021) 012, arXiv: 2104.03977 [hep-ph].

[89] M. Drees and Y. Xu,
Large field polynomial inflation: parameter space, predictions and (double) eternal nature,
JCAP **12** (2022) 005, arXiv: 2209.07545 [astro-ph.CO].

[90] M. Drees and Y. Xu, *Parameter space of leptogenesis in polynomial inflation*,
JCAP **04** (2024) 036, arXiv: 2401.02485 [hep-ph].

[91] N. Bernal, J. Harz, M. A. Mojahed and Y. Xu,
Graviton- and inflaton-mediated dark matter production after large field polynomial inflation,
Phys. Rev. D **111** (2025) 043517, arXiv: 2406.19447 [hep-ph].

[92] M. Drees and C. Wang, *Inflaton Self Resonance, Oscillons, and Gravitational Waves in Small Field Polynomial Inflation*, (2025), arXiv: 2501.13811 [astro-ph.CO].

[93] D. V. Nanopoulos, K. A. Olive, M. Srednicki and K. Tamvakis,
Primordial Inflation in Simple Supergravity, Phys. Lett. B **123** (1983) 41.

[94] B. A. Ovrut and P. J. Steinhardt, *Supersymmetry and Inflation: A New Approach*,
Phys. Lett. B **133** (1983) 161.

[95] R. Holman, P. Ramond and G. G. Ross, *Supersymmetric Inflationary Cosmology*,
Phys. Lett. B **137** (1984) 343.

[96] F. C. Adams, J. R. Bond, K. Freese, J. A. Frieman and A. V. Olinto, *Natural inflation: Particle physics models, power law spectra for large scale structure, and constraints from COBE*,
Phys. Rev. D **47** (1993) 426, arXiv: hep-ph/9207245.

[97] E. J. Copeland, A. R. Liddle, D. H. Lyth, E. D. Stewart and D. Wands,
False vacuum inflation with Einstein gravity, Phys. Rev. D **49** (1994) 6410,
arXiv: astro-ph/9401011.

[98] K. Kumekawa, T. Moroi and T. Yanagida,
Flat potential for inflaton with a discrete R invariance in supergravity,
Prog. Theor. Phys. **92** (1994) 437, arXiv: hep-ph/9405337.

[99] K. .-. Izawa and T. Yanagida, *Natural new inflation in broken supergravity*,
Phys. Lett. B **393** (1997) 331, arXiv: hep-ph/9608359.

[100] A. D. Linde and A. Riotto, *Hybrid inflation in supergravity*, Phys. Rev. D **56** (1997) R1841,
arXiv: hep-ph/9703209.

[101] P. Binetruy, G. Dvali, R. Kallosh and A. Van Proeyen,
Fayet-Iliopoulos terms in supergravity and cosmology, Class. Quant. Grav. **21** (2004) 3137,
arXiv: hep-th/0402046.

[102] R. Allahverdi, K. Enqvist, J. Garcia-Bellido, A. Jokinen and A. Mazumdar, *MSSM flat direction inflation: Slow roll, stability, fine tunning and reheating*, JCAP **06** (2007) 019, arXiv: hep-ph/0610134.

[103] I. Ben-Dayan, R. Brustein and S. P. de Alwis, *Models of Modular Inflation and Their Phenomenological Consequences*, JCAP **07** (2008) 011, arXiv: 0802.3160 [hep-th].

[104] J. Ellis, D. V. Nanopoulos and K. A. Olive, *No-Scale Supergravity Realization of the Starobinsky Model of Inflation*, Phys. Rev. Lett. **111** (2013) 111301, [Erratum: Phys.Rev.Lett. 111, 129902 (2013)], arXiv: 1305.1247 [hep-th].

[105] J. Ellis, D. V. Nanopoulos and K. A. Olive, *Starobinsky-like Inflationary Models as Avatars of No-Scale Supergravity*, JCAP **10** (2013) 009, arXiv: 1307.3537 [hep-th].

[106] S. Ferrara, R. Kallosh, A. Linde and M. Porrati, *Minimal Supergravity Models of Inflation*, Phys. Rev. D **88** (2013) 085038, arXiv: 1307.7696 [hep-th].

[107] R. Kallosh, A. Linde and D. Roest, *Large field inflation and double α-attractors*, JHEP **08** (2014) 052, arXiv: 1405.3646 [hep-th].

[108] S. V. Ketov and T. Terada, *Inflation in supergravity with a single chiral superfield*, Phys. Lett. B **736** (2014) 272, arXiv: 1406.0252 [hep-th].

[109] J. J. M. Carrasco, R. Kallosh and A. Linde, *α-Attractors: Planck, LHC and Dark Energy*, JHEP **10** (2015) 147, arXiv: 1506.01708 [hep-th].

[110] M. C. Romao and S. F. King, *Starobinsky-like inflation in no-scale supergravity Wess-Zumino model with Polonyi term*, JHEP **07** (2017) 033, arXiv: 1703.08333 [hep-ph].

[111] K. Kohri, Y. Oyama, T. Sekiguchi and T. Takahashi, *Precise Measurements of Primordial Power Spectrum with 21 cm Fluctuations*, JCAP **10** (2013) 065, arXiv: 1303.1688 [astro-ph.CO].

[112] K. N. Abazajian et al., *CMB-S4 Science Book, First Edition*, (2016), arXiv: 1610.02743 [astro-ph.CO].

[113] J. B. Muñoz, E. D. Kovetz, A. Raccanelli, M. Kamionkowski and J. Silk, *Towards a measurement of the spectral runnings*, JCAP **05** (2017) 032, arXiv: 1611.05883 [astro-ph.CO].

[114] T. Modak, T. Plehn, L. Röver and B. M. Schäfer, *Probing the Inflaton Potential with SKA*, SciPost Phys. Core **5** (2022) 037, arXiv: 2112.09148 [astro-ph.CO].

[115] R. Easther, B. Bahr-Kalus and D. Parkinson, *Running primordial perturbations: Inflationary dynamics and observational constraints*, Phys. Rev. D **106** (2022) L061301, arXiv: 2112.10922 [astro-ph.CO].

[116] B. Bahr-Kalus, D. Parkinson and R. Easther, *Constraining cosmic inflation with observations: Prospects for 2030*, Mon. Not. Roy. Astron. Soc. **520** (2023) 2405, arXiv: 2212.04115 [astro-ph.CO].

[117] R. Kallosh and A. D. Linde, *Landscape, the scale of SUSY breaking, and inflation*, JHEP **12** (2004) 004, arXiv: hep-th/0411011.

[118] J. Polchinski, *String theory. Vol. 1: An introduction to the bosonic string*, Cambridge Monographs on Mathematical Physics, Cambridge University Press, 2007, ISBN: 978-0-511-25227-3.

[119] K. Becker, M. Becker and J. H. Schwarz, *String theory and M-theory: A modern introduction*, Cambridge University Press, 2006, ISBN: 978-0-511-25486-4.

[120] L. E. Ibanez and A. M. Uranga, *String theory and particle physics: An introduction to string phenomenology*, Cambridge University Press, 2012, ISBN: 978-0-521-51752-2.

[121] T. Kobayashi and M. Tanimoto, "Modular flavor symmetric models", 2023, arXiv: 2307.03384 [hep-ph].

[122] G.-J. Ding and S. F. King, *Neutrino mass and mixing with modular symmetry*, Rept. Prog. Phys. **87** (2024) 084201, arXiv: 2311.09282 [hep-ph].

[123] M. Cicoli et al., *String cosmology: From the early universe to today*, Phys. Rept. **1059** (2024) 1, arXiv: 2303.04819 [hep-th].

[124] M. Badziak and M. Olechowski, *Volume modulus inflation and a low scale of SUSY breaking*, JCAP **07** (2008) 021, arXiv: 0802.1014 [hep-th].

[125] L. Covi et al., *Constraints on modular inflation in supergravity and string theory*, JHEP **08** (2008) 055, arXiv: 0805.3290 [hep-th].

[126] T. Kobayashi, D. Nitta and Y. Urakawa, *Modular invariant inflation*, JCAP **08** (2016) 014, arXiv: 1604.02995 [hep-th].

[127] Y. Abe, T. Higaki, F. Kaneko, T. Kobayashi and H. Otsuka, *Moduli inflation from modular flavor symmetries*, JHEP **06** (2023) 187, arXiv: 2303.02947 [hep-ph].

[128] D. Frolovsky and S. V. Ketov, *Dilaton–Axion modular inflation in supergravity*, Int. J. Mod. Phys. D (2024) 2340008, arXiv: 2403.02125 [hep-th].

[129] R. Schimmrigk, *Automorphic inflation*, Phys. Lett. B **748** (2015) 376, arXiv: 1412.8537 [hep-th].

[130] R. Schimmrigk, *A General Framework of Automorphic Inflation*, JHEP **05** (2016) 140, arXiv: 1512.09082 [hep-th].

[131] R. Schimmrigk, *Modular Inflation Observables and j-Inflation Phenomenology*, JHEP **09** (2017) 043, arXiv: 1612.09559 [hep-th].

[132] G. F. Casas and L. E. Ibáñez, *Modular Invariant Starobinsky Inflation and the Species Scale*, (2024), arXiv: 2407.12081 [hep-th].

[133] M. Cvetic, A. Font, L. E. Ibanez, D. Lust and F. Quevedo, *Target space duality, supersymmetry breaking and the stability of classical string vacua*, Nucl. Phys. B **361** (1991) 194.

[134] T. Kobayashi, Y. Shimizu, K. Takagi, M. Tanimoto and T. H. Tatsuishi, *A_4 lepton flavor model and modulus stabilization from S_4 modular symmetry*, Phys. Rev. D **100** (2019) 115045, [Erratum: Phys.Rev.D 101, 039904 (2020)], arXiv: 1909.05139 [hep-ph].

[135] T. Kobayashi et al., *CP violation in modular invariant flavor models*, Phys. Rev. D **101** (2020) 055046, arXiv: 1910.11553 [hep-ph].

[136] K. Ishiguro, T. Kobayashi and H. Otsuka, *Landscape of Modular Symmetric Flavor Models*, JHEP **03** (2021) 161, arXiv: 2011.09154 [hep-ph].

[137] P. P. Novichkov, J. T. Penedo and S. T. Petcov, *Modular flavour symmetries and modulus stabilisation*, JHEP **03** (2022) 149, arXiv: 2201.02020 [hep-ph].

[138] J. M. Leedom, N. Righi and A. Westphal, *Heterotic de Sitter beyond modular symmetry*, JHEP **02** (2023) 209, arXiv: 2212.03876 [hep-th].

[139] V. Knapp-Perez, X.-G. Liu, H. P. Nilles, S. Ramos-Sanchez and M. Ratz, *Matter matters in moduli fixing and modular flavor symmetries*, Phys. Lett. B **844** (2023) 138106, arXiv: 2304.14437 [hep-th].

[140] S. F. King and X. Wang, *Modulus stabilisation in the multiple-modulus framework*, (2023), arXiv: 2310.10369 [hep-ph].

[141] T. Kobayashi, K. Nasu, R. Sakuma and Y. Yamada, *Radiative correction on moduli stabilization in modular flavor symmetric models*, Phys. Rev. D **108** (2023) 115038, arXiv: 2310.15604 [hep-ph].

[142] T. Higaki, J. Kawamura and T. Kobayashi, *Finite modular axion and radiative moduli stabilization*, JHEP **04** (2024) 147, arXiv: 2402.02071 [hep-ph].

[143] F. Feruglio, V. Gherardi, A. Romanino and A. Titov, *Modular invariant dynamics and fermion mass hierarchies around $\tau = i$*, JHEP **05** (2021) 242, arXiv: 2101.08718 [hep-ph].

[144] P. P. Novichkov, J. T. Penedo and S. T. Petcov, *Fermion mass hierarchies, large lepton mixing and residual modular symmetries*, JHEP **04** (2021) 206, arXiv: 2102.07488 [hep-ph].

[145] S. T. Petcov and M. Tanimoto, *A_4 modular flavour model of quark mass hierarchies close to the fixed point $\tau = \omega$*, Eur. Phys. J. C **83** (2023) 579, arXiv: 2212.13336 [hep-ph].

[146] S. Kikuchi, T. Kobayashi, K. Nasu, S. Takada and H. Uchida, *Quark hierarchical structures in modular symmetric flavor models at level 6*, Phys. Rev. D **107** (2023) 055014, arXiv: 2301.03737 [hep-ph].

[147] Y. Abe, T. Higaki, J. Kawamura and T. Kobayashi, *Quark masses and CKM hierarchies from S_4' modular flavor symmetry*, Eur. Phys. J. C **83** (2023) 1140, arXiv: 2301.07439 [hep-ph].

[148] S. Kikuchi, T. Kobayashi, K. Nasu, S. Takada and H. Uchida,
Quark mass hierarchies and CP violation in $A_4 \times A_4 \times A_4$ modular symmetric flavor models,
JHEP **07** (2023) 134, arXiv: 2302.03326 [hep-ph].

[149] Y. Abe, T. Higaki, J. Kawamura and T. Kobayashi,
Quark and lepton hierarchies from S4' modular flavor symmetry,
Phys. Lett. B **842** (2023) 137977, arXiv: 2302.11183 [hep-ph].

[150] S. T. Petcov and M. Tanimoto,
A_4 modular flavour model of quark mass hierarchies close to the fixed point $\tau = i\infty$,
JHEP **08** (2023) 086, arXiv: 2306.05730 [hep-ph].

[151] Y. Abe, T. Higaki, J. Kawamura and T. Kobayashi,
Fermion hierarchies in SU(5) grand unification from Γ_6' modular flavor symmetry,
JHEP **08** (2023) 097, arXiv: 2307.01419 [hep-ph].

[152] I. de Medeiros Varzielas, M. Levy, J. T. Penedo and S. T. Petcov,
Quarks at the modular S_4 cusp, JHEP **09** (2023) 196, arXiv: 2307.14410 [hep-ph].

[153] G.-J. Ding, F. Feruglio and X.-G. Liu,
Universal predictions of Siegel modular invariant theories near the fixed points,
JHEP **05** (2024) 052, arXiv: 2402.14915 [hep-ph].

[154] S. H. Shenker, "The Strength of nonperturbative effects in string theory",
Cargese Study Institute: Random Surfaces, Quantum Gravity and Strings, 1990 809.

[155] J. A. Casas, *The generalized dilaton supersymmetry breaking scenario*,
Phys. Lett. B **384** (1996) 103, arXiv: hep-th/9605180.

[156] T. Higaki, Y. Kawamura, T. Kobayashi and H. Nakano,
Non-perturbative Kähler potential, dilaton stabilization and Fayet–Iliopoulos term,
Phys. Lett. B **582** (2004) 257, arXiv: hep-ph/0311315.

[157] M. Dine, R. Rohm, N. Seiberg and E. Witten, *Gluino Condensation in Superstring Models*,
Phys. Lett. B **156** (1985) 55.

[158] A. D. Linde and A. Westphal, *Accidental Inflation in String Theory*, JCAP **03** (2008) 005,
arXiv: 0712.1610 [hep-th].

[159] W. H. Kinney, *Horizon crossing and inflation with large eta*, Phys. Rev. D **72** (2005) 023515,
arXiv: gr-qc/0503017.

[160] J. Martin, H. Motohashi and T. Suyama,
Ultra Slow-Roll Inflation and the non-Gaussianity Consistency Relation,
Phys. Rev. D **87** (2013) 023514, arXiv: 1211.0083 [astro-ph.CO].

[161] K. Dimopoulos, *Ultra slow-roll inflation demystified*, Phys. Lett. B **775** (2017) 262,
arXiv: 1707.05644 [hep-ph].

[162] M. H. Namjoo, H. Firouzjahi and M. Sasaki,
Violation of non-Gaussianity consistency relation in a single field inflationary model,
EPL **101** (2013) 39001, arXiv: 1210.3692 [astro-ph.CO].

[163] S. Mooij and G. A. Palma, *Consistently violating the non-Gaussian consistency relation*,
JCAP **11** (2015) 025, arXiv: 1502.03458 [astro-ph.CO].

[164] C. Germani and T. Prokopec, *On primordial black holes from an inflection point*, Phys. Dark Univ. **18** (2017) 6, arXiv: 1706.04226 [astro-ph.CO].

[165] M. Kawasaki, K. Kohri and N. Sugiyama, *MeV scale reheating temperature and thermalization of neutrino background*, Phys. Rev. D **62** (2000) 023506, arXiv: astro-ph/0002127.

[166] S. Hannestad, *What is the lowest possible reheating temperature?*, Phys. Rev. D **70** (2004) 043506, arXiv: astro-ph/0403291.

[167] P. F. de Salas et al., *Bounds on very low reheating scenarios after Planck*, Phys. Rev. D **92** (2015) 123534, arXiv: 1511.00672 [astro-ph.CO].

[168] T. Hasegawa et al., *MeV-scale reheating temperature and thermalization of oscillating neutrinos by radiative and hadronic decays of massive particles*, JCAP **12** (2019) 012, arXiv: 1908.10189 [hep-ph].

[169] G.-J. Ding, S.-Y. Jiang and W. Zhao, *Modular invariant slow roll inflation*, JCAP **10** (2024) 016, arXiv: 2405.06497 [hep-ph].

[170] F. Feruglio, *Universal Predictions of Modular Invariant Flavor Models near the Self-Dual Point*, Phys. Rev. Lett. **130** (2023) 101801, arXiv: 2211.00659 [hep-ph].

[171] F. Feruglio, *Fermion masses, critical behavior and universality*, JHEP **03** (2023) 236, arXiv: 2302.11580 [hep-ph].

[172] G. Lazarides and Q. Shafi, *Origin of matter in the inflationary cosmology*, Phys. Lett. B **258** (1991) 305.

[173] T. Asaka, K. Hamaguchi, M. Kawasaki and T. Yanagida, *Leptogenesis in inflaton decay*, Phys. Lett. B **464** (1999) 12, arXiv: hep-ph/9906366.

[174] T. Asaka, K. Hamaguchi, M. Kawasaki and T. Yanagida, *Leptogenesis in inflationary universe*, Phys. Rev. D **61** (2000) 083512, arXiv: hep-ph/9907559.

[175] V. N. Senoguz and Q. Shafi, *GUT scale inflation, nonthermal leptogenesis, and atmospheric neutrino oscillations*, Phys. Lett. B **582** (2004) 6, arXiv: hep-ph/0309134.

[176] F. Hahn-Woernle and M. Plumacher, *Effects of reheating on leptogenesis*, Nucl. Phys. B **806** (2009) 68, arXiv: 0801.3972 [hep-ph].

[177] S. Antusch, J. P. Baumann, V. F. Domcke and P. M. Kostka, *Sneutrino Hybrid Inflation and Nonthermal Leptogenesis*, JCAP **10** (2010) 006, arXiv: 1007.0708 [hep-ph].

[178] K. Abazajian et al., *CMB-S4 Science Case, Reference Design, and Project Plan*, (2019), arXiv: 1907.04473 [astro-ph.IM].

[179] R. Kallosh and A. Linde, $SL(2,\mathbb{Z})$ *Cosmological Attractors*, (2024), arXiv: 2408.05203 [hep-th].

[180] R. Kallosh and A. Linde, *Landscape of Modular Cosmology*, (2024), arXiv: 2411.07552 [hep-th].

[181] L. Kofman, A. D. Linde and A. A. Starobinsky, *Reheating after inflation*, Phys. Rev. Lett. **73** (1994) 3195, arXiv: hep-th/9405187.

[182] R. Allahverdi, R. Brandenberger, F.-Y. Cyr-Racine and A. Mazumdar, *Reheating in Inflationary Cosmology: Theory and Applications*, Ann. Rev. Nucl. Part. Sci. **60** (2010) 27, arXiv: 1001.2600 [hep-th].

[183] M. A. Amin, M. P. Hertzberg, D. I. Kaiser and J. Karouby, *Nonperturbative Dynamics Of Reheating After Inflation: A Review*, Int. J. Mod. Phys. D **24** (2014) 1530003, arXiv: 1410.3808 [hep-ph].

[184] K. D. Lozanov, *Lectures on Reheating after Inflation*, (2019), arXiv: 1907.04402 [astro-ph.CO].

[185] G. F. Giudice, E. W. Kolb and A. Riotto, *Largest temperature of the radiation era and its cosmological implications*, Phys. Rev. D **64** (2001) 023508, arXiv: hep-ph/0005123.

[186] C. Cosme, F. Costa and O. Lebedev, *Temperature evolution in the Early Universe and freeze-in at stronger coupling*, JCAP **06** (2024) 031, arXiv: 2402.04743 [hep-ph].

[187] M. Dine, W. Fischler and D. Nemeschansky, *Solution of the Entropy Crisis of Supersymmetric Theories*, Phys. Lett. B **136** (1984) 169.

[188] O. Bertolami and G. G. Ross, *Inflation as a Cure for the Cosmological Problems of Superstring Models With Intermediate Scale Breaking*, Phys. Lett. B **183** (1987) 163.

[189] G. R. Dvali, *Inflation versus the cosmological moduli problem*, (1995), arXiv: hep-ph/9503259.

[190] M. Dine, L. Randall and S. D. Thomas, *Supersymmetry breaking in the early universe*, Phys. Rev. Lett. **75** (1995) 398, arXiv: hep-ph/9503303.

[191] R. Allahverdi and M. Drees, *Leptogenesis from a sneutrino condensate revisited*, Phys. Rev. D **69** (2004) 103522, arXiv: hep-ph/0401054.

[192] A. Dedes, H. E. Haber and J. Rosiek, *Seesaw mechanism in the sneutrino sector and its consequences*, JHEP **11** (2007) 059, arXiv: 0707.3718 [hep-ph].

[193] H. K. Dreiner, H. E. Haber and S. P. Martin, *Two-component spinor techniques and Feynman rules for quantum field theory and supersymmetry*, Phys. Rept. **494** (2010) 1, arXiv: 0812.1594 [hep-ph].

[194] W. Buchmuller, P. Di Bari and M. Plumacher, *Leptogenesis for pedestrians*, Annals Phys. **315** (2005) 305, arXiv: hep-ph/0401240.

[195] C. S. Fong, E. Nardi and A. Riotto, *Leptogenesis in the Universe*, Adv. High Energy Phys. **2012** (2012) 158303, arXiv: 1301.3062 [hep-ph].

[196] M. Fukugita and T. Yanagida, *Baryogenesis Without Grand Unification*, Phys. Lett. B **174** (1986) 45.

[197] M. Y. Khlopov and A. D. Linde, *Is It Easy to Save the Gravitino?*, Phys. Lett. B **138** (1984) 265.

[198] J. R. Ellis, J. E. Kim and D. V. Nanopoulos, *Cosmological Gravitino Regeneration and Decay*, Phys. Lett. B **145** (1984) 181.

[199] M. Kawasaki and T. Moroi,
Gravitino production in the inflationary universe and the effects on big bang nucleosynthesis, Prog. Theor. Phys. **93** (1995) 879, arXiv: hep-ph/9403364.

[200] M. Fujii, K. Hamaguchi and T. Yanagida,
Leptogenesis with almost degenerate majorana neutrinos, Phys. Rev. D **65** (2002) 115012, arXiv: hep-ph/0202210.

[201] S. Y. Khlebnikov and M. E. Shaposhnikov,
The Statistical Theory of Anomalous Fermion Number Nonconservation,
Nucl. Phys. B **308** (1988) 885.

[202] J. A. Harvey and M. S. Turner, *Cosmological baryon and lepton number in the presence of electroweak fermion number violation*, Phys. Rev. D **42** (1990) 3344.

[203] A. Pilaftsis and T. E. J. Underwood, *Resonant leptogenesis*, Nucl. Phys. B **692** (2004) 303, arXiv: hep-ph/0309342.

[204] E. W. Kolb, *The Early Universe*, vol. 69, Taylor and Francis, 2019, ISBN: 978-0-429-49286-0.

[205] B. D. Fields, K. A. Olive, T.-H. Yeh and C. Young, *Big-Bang Nucleosynthesis after Planck*, JCAP **03** (2020) 010, [Erratum: JCAP 11, E02 (2020)],
arXiv: 1912.01132 [astro-ph.CO].

[206] R. Kallosh and A. Linde, *Universality Class in Conformal Inflation*, JCAP **07** (2013) 002, arXiv: 1306.5220 [hep-th].

[207] R. Kallosh and A. Linde, *Non-minimal Inflationary Attractors*, JCAP **10** (2013) 033, arXiv: 1307.7938 [hep-th].

[208] D. H. Lyth and D. Roberts, *Cosmological consequences of particle creation during inflation*, Phys. Rev. D **57** (1998) 7120, arXiv: hep-ph/9609441.

[209] E. W. Kolb and A. J. Long,
Cosmological gravitational particle production and its implications for cosmological relics, (2023), arXiv: 2312.09042 [astro-ph.CO].

[210] D. J. H. Chung, E. W. Kolb and A. Riotto, *Nonthermal supermassive dark matter*, Phys. Rev. Lett. **81** (1998) 4048, arXiv: hep-ph/9805473.

[211] E. W. Kolb, D. J. H. Chung and A. Riotto, *WIMPzillas!*,
AIP Conf. Proc. **484** (1999) 91, ed. by H. Falomir, R. E. Gamboa Saravi and F. A. Schaposnik, arXiv: hep-ph/9810361.

[212] V. Mukhanov, *Physical Foundations of Cosmology*,
Oxford: Cambridge University Press, 2005, ISBN: 978-0-521-56398-7.

[213] S. Ling and A. J. Long, *Superheavy scalar dark matter from gravitational particle production in α-attractor models of inflation*, Phys. Rev. D **103** (2021) 103532,
arXiv: 2101.11621 [astro-ph.CO].

[214] M. A. G. Garcia, M. Pierre and S. Verner,
New window into gravitationally produced scalar dark matter,
Phys. Rev. D **108** (2023) 115024, arXiv: 2305.14446 [hep-ph].

[215] V. Kuzmin and I. Tkachev, *Matter creation via vacuum fluctuations in the early universe and observed ultrahigh-energy cosmic ray events*, Phys. Rev. D **59** (1999) 123006,
arXiv: hep-ph/9809547.

[216] D. J. H. Chung, L. L. Everett, H. Yoo and P. Zhou,
Gravitational Fermion Production in Inflationary Cosmology, Phys. Lett. B **712** (2012) 147,
arXiv: 1109.2524 [astro-ph.CO].

[217] P. W. Graham, J. Mardon and S. Rajendran,
Vector Dark Matter from Inflationary Fluctuations, Phys. Rev. D **93** (2016) 103520,
arXiv: 1504.02102 [hep-ph].

[218] A. Ahmed, B. Grzadkowski and A. Socha, *Gravitational production of vector dark matter*,
JHEP **08** (2020) 059, arXiv: 2005.01766 [hep-ph].

[219] E. W. Kolb and A. J. Long,
Completely dark photons from gravitational particle production during the inflationary era,
JHEP **03** (2021) 283, arXiv: 2009.03828 [astro-ph.CO].

[220] M. Gorghetto, E. Hardy, J. March-Russell, N. Song and S. M. West,
Dark photon stars: formation and role as dark matter substructure, JCAP **08** (2022) 018,
arXiv: 2203.10100 [hep-ph].

[221] J. A. R. Cembranos, L. J. Garay, Á. Parra-López and J. M. Sánchez Velázquez,
Vector dark matter production during inflation and reheating, JCAP **02** (2024) 013,
arXiv: 2310.07515 [gr-qc].

[222] O. Özsoy and G. Tasinato,
Vector dark matter, inflation, and non-minimal couplings with gravity, JCAP **06** (2024) 003,
arXiv: 2310.03862 [astro-ph.CO].

[223] F. Hasegawa, K. Mukaida, K. Nakayama, T. Terada and Y. Yamada,
Gravitino Problem in Minimal Supergravity Inflation, Phys. Lett. B **767** (2017) 392,
arXiv: 1701.03106 [hep-ph].

[224] R. Kallosh, L. Kofman, A. D. Linde and A. Van Proeyen, *Gravitino production after inflation*,
Phys. Rev. D **61** (2000) 103503, arXiv: hep-th/9907124.

[225] I. Antoniadis, K. Benakli and W. Ke, *Salvage of too slow gravitinos*, JHEP **11** (2021) 063,
arXiv: 2105.03784 [hep-th].

[226] K. Kaneta, W. Ke, Y. Mambrini, K. A. Olive and S. Verner,
Gravitational production of spin-3/2 particles during reheating,
Phys. Rev. D **108** (2023) 115027, arXiv: 2309.15146 [hep-ph].

[227] G. Casagrande, E. Dudas and M. Peloso,
On energy and particle production in cosmology: the particular case of the gravitino,
JHEP **06** (2024) 003, arXiv: 2310.14964 [hep-th].

[228] E. W. Kolb, S. Ling, A. J. Long and R. A. Rosen,
Cosmological gravitational particle production of massive spin-2 particles,
JHEP **05** (2023) 181, arXiv: 2302.04390 [astro-ph.CO].

[229] H. P. Nilles, M. Peloso and L. Sorbo, *Nonthermal production of gravitinos and inflatinos*,
Phys. Rev. Lett. **87** (2001) 051302, arXiv: hep-ph/0102264.

[230] H. P. Nilles, M. Peloso and L. Sorbo, *Coupled fields in external background with application to nonthermal production of gravitinos*, JHEP **04** (2001) 004, arXiv: hep-th/0103202.

[231] R. Zhang and S. Zheng, *Gravitational dark matter from minimal preheating*,
Journal of High Energy Physics **2024** (2024), ISSN: 1029-8479,
URL: http://dx.doi.org/10.1007/JHEP02(2024)061.

[232] D. J. H. Chung, *Classical Inflation Field Induced Creation of Superheavy Dark Matter*,
Phys. Rev. D **67** (2003) 083514, arXiv: hep-ph/9809489.

[233] Y. Ema, K. Nakayama and Y. Tang, *Production of Purely Gravitational Dark Matter*,
JHEP **09** (2018) 135, arXiv: 1804.07471 [hep-ph].

[234] J. A. R. Cembranos, L. J. Garay and J. M. Sánchez Velázquez,
Gravitational production of scalar dark matter, JHEP **06** (2020) 084,
arXiv: 1910.13937 [hep-ph].

[235] S. Enomoto and T. Matsuda, *The exact WKB for cosmological particle production*,
JHEP **03** (2021) 090, arXiv: 2010.14835 [hep-ph].

[236] E. E. Basso and D. J. H. Chung,
Computation of gravitational particle production using adiabatic invariants,
JHEP **11** (2021) 146, arXiv: 2108.01653 [hep-ph].

[237] S. Hashiba and Y. Yamada,
Stokes phenomenon and gravitational particle production — How to evaluate it in practice,
JCAP **05** (2021) 022, arXiv: 2101.07634 [hep-th].

[238] E. Basso, D. J. H. Chung, E. W. Kolb and A. J. Long,
Quantum interference in gravitational particle production, JHEP **12** (2022) 108,
arXiv: 2209.01713 [gr-qc].

[239] K. Kaneta, S. M. Lee and K.-y. Oda,
Boltzmann or Bogoliubov? Approaches compared in gravitational particle production,
JCAP **09** (2022) 018, arXiv: 2206.10929 [astro-ph.CO].

[240] D. Racco, S. Verner and W. Xue,
Gravitational production of heavy particles during and after inflation, JHEP **09** (2024) 129,
arXiv: 2405.13883 [hep-ph].

[241] S. Verner, *Nonminimal Superheavy Dark Matter*, (2024), arXiv: 2408.11889 [hep-ph].

[242] L. Jenks, E. W. Kolb and K. Thyme, *Gravitational Particle Production of Scalars: Analytic and Numerical Approaches Including Early Reheating*, (2024),
arXiv: 2410.03938 [hep-ph].

[243] T. Markkanen and S. Nurmi, *Dark matter from gravitational particle production at reheating*,
JCAP **02** (2017) 008, arXiv: 1512.07288 [astro-ph.CO].

[244] M. Fairbairn, K. Kainulainen, T. Markkanen and S. Nurmi,
Despicable Dark Relics: generated by gravity with unconstrained masses,
JCAP **04** (2019) 005, arXiv: 1808.08236 [astro-ph.CO].

[245] S. Clery, Y. Mambrini, K. A. Olive, A. Shkerin and S. Verner,
Gravitational portals with nonminimal couplings, Phys. Rev. D **105** (2022) 095042,
arXiv: 2203.02004 [hep-ph].

[246] Z. Yu, C. Fu and Z.-K. Guo,
Particle production during inflation with a nonminimally coupled spectator scalar field,
Phys. Rev. D **108** (2023) 123509, arXiv: 2307.03120 [gr-qc].

[247] M. A. G. Garcia, M. Pierre and S. Verner,
Scalar dark matter production from preheating and structure formation constraints,
Phys. Rev. D **107** (2023) 043530, arXiv: 2206.08940 [hep-ph].

[248] M. A. G. Garcia, M. Pierre and S. Verner,
Isocurvature constraints on scalar dark matter production from the inflaton,
Phys. Rev. D **107** (2023) 123508, arXiv: 2303.07359 [hep-ph].

[249] M. Endo, M. Kawasaki, F. Takahashi and T. T. Yanagida,
Inflaton decay through supergravity effects, Phys. Lett. B **642** (2006) 518,
arXiv: hep-ph/0607170.

[250] M. Endo, F. Takahashi and T. T. Yanagida,
Spontaneous Non-thermal Leptogenesis in High-scale Inflation Models,
Phys. Rev. D **74** (2006) 123523, arXiv: hep-ph/0611055.

[251] M. Endo, F. Takahashi and T. T. Yanagida, *Inflaton Decay in Supergravity*,
Phys. Rev. D **76** (2007) 083509, arXiv: 0706.0986 [hep-ph].

[252] S. Enomoto, S. Iida, N. Maekawa and T. Matsuda, *Beauty is more attractive: particle production and moduli trapping with higher dimensional interaction*, JHEP **01** (2014) 141,
arXiv: 1310.4751 [hep-ph].

[253] Y. Ema, M. A. G. Garcia, W. Ke, K. A. Olive and S. Verner,
Inflaton Decay in No-Scale Supergravity and Starobinsky-like Models,
Universe **10** (2024) 239, arXiv: 2404.14545 [hep-ph].

[254] K. Nakayama, *A Note on Gravitational Particle Production in Supergravity*,
Phys. Lett. B **797** (2019) 134857, arXiv: 1905.09143 [hep-ph].

[255] G. Dall'Agata and F. Zwirner, *On sgoldstino-less supergravity models of inflation*,
JHEP **12** (2014) 172, arXiv: 1411.2605 [hep-th].

[256] R. Kallosh, A. Linde and M. Scalisi, *Inflation, de Sitter Landscape and Super-Higgs effect*,
JHEP **03** (2015) 111, arXiv: 1411.5671 [hep-th].

[257] R. Kallosh, A. Linde and D. Roest, *Superconformal Inflationary α-Attractors*,
JHEP **11** (2013) 198, arXiv: 1311.0472 [hep-th].

[258] G. Germán, *On the α-attractor T-models*,
Journal of Cosmology and Astroparticle Physics **2021** (2021) 017, ISSN: 1475-7516,
URL: http://dx.doi.org/10.1088/1475-7516/2021/09/017.

[259] D. J. H. Chung, E. W. Kolb, A. Riotto and L. Senatore,
Isocurvature constraints on gravitationally produced superheavy dark matter,
Physical Review D **72** (2005), ISSN: 1550-2368,
URL: http://dx.doi.org/10.1103/PhysRevD.72.023511.

[260] R. Kallosh, A. Linde and T. Rube, *General inflaton potentials in supergravity*,
Phys. Rev. D **83** (2011) 043507, arXiv: 1011.5945 [hep-th].

[261] E. W. Kolb, A. J. Long, E. McDonough and G. Payeur,
Completely dark matter from rapid-turn multifield inflation,
Journal of High Energy Physics **2023** (2023), ISSN: 1029-8479,
URL: http://dx.doi.org/10.1007/JHEP02(2023)181.

[262] K. D. Lozanov and M. A. Amin,
Self-Resonance after Inflation: Oscillons, Transients and Radiation Domination,
Physical Review D **97** (2018) 023533, ISSN: 2470-0010, 2470-0029, arXiv: 1710.06851,
(visited on 03/12/2021).

[263] M. A. Amin, M. P. Hertzberg, D. I. Kaiser and J. Karouby,
Nonperturbative Dynamics Of Reheating After Inflation: A Review,
International Journal of Modern Physics D **24** (2015) 1530003, ISSN: 0218-2718, 1793-6594,
arXiv: 1410.3808, (visited on 06/12/2021).

[264] B. Barman, S. Cléry, R. T. Co, Y. Mambrini and K. A. Olive,
Gravity as a portal to reheating, leptogenesis and dark matter,
Journal of High Energy Physics **2022** (2022), ISSN: 1029-8479,
URL: http://dx.doi.org/10.1007/JHEP12(2022)072.

[265] M. M. Flores and Y. F. Perez-Gonzalez,
On the Role of Cosmological Gravitational Particle Production in Baryogenesis, 2024,
arXiv: 2404.06530 [hep-ph], URL: https://arxiv.org/abs/2404.06530.

[266] C. J. Moore, R. H. Cole and C. P. L. Berry, *Gravitational-wave sensitivity curves*,
Classical and Quantum Gravity **32** (2014) 015014, ISSN: 1361-6382,
URL: http://dx.doi.org/10.1088/0264-9381/32/1/015014.

[267] E. D'Hoker and J. Kaidi, *Lectures on modular forms and strings*, (2022),
arXiv: 2208.07242 [hep-th].

[268] M. Kobayashi, *Ramanujan–Shen's differential equations for Eisenstein series of level 2*,
Research in Number Theory **10** (2024) 41, arXiv: 2307.15206.

[269] N. V. Krasnikov, *On Supersymmetry Breaking in Superstring Theories*,
Phys. Lett. B **193** (1987) 37.

[270] T. Banks, M. Berkooz, S. H. Shenker, G. W. Moore and P. J. Steinhardt, *Modular cosmology*,
Phys. Rev. D **52** (1995) 3548, arXiv: hep-th/9503114.

[271] T. Barreiro, B. de Carlos and E. J. Copeland, *Stabilizing the dilaton in superstring cosmology*,
Phys. Rev. D **58** (1998) 083513, arXiv: hep-th/9805005.

[272] J. J. Blanco-Pillado et al., *Racetrack inflation*, JHEP **11** (2004) 063,
arXiv: hep-th/0406230.

[273] J. J. Blanco-Pillado et al., *Inflating in a better racetrack*, JHEP **09** (2006) 002, arXiv: hep-th/0603129.

[274] X.-G. Liu and G.-J. Ding, *Neutrino Masses and Mixing from Double Covering of Finite Modular Groups*, JHEP **08** (2019) 134, arXiv: 1907.01488 [hep-ph].

[275] M. D. Schwartz, *Quantum Field Theory and the Standard Model*, Cambridge University Press, 2014, ISBN: 978-1-107-03473-0.

[276] Y. Xu, *Polynomial Inflation and Its Aftermath*, PhD thesis: U. Bonn (main), 2022.

List of Figures

List of Tables